Advancements in Purification Process Development for a Therapeutic Replication-Competent Enveloped Virus Particle

Zur Erlangung des akademischen Grades eines

DOKTORS DER INGENIEURWISSENSCHAFTEN (DR.-ING.)

von der KIT-Fakultät für Chemieingenieurwesen und Verfahrenstechnik des Karlsruher Instituts für Technologie (KIT)
genehmigte

DISSERTATION

von

M.Sc. Adrian Moritz Schimek
aus Filderstadt

Tag der mündlichen Prüfung:	17. Dezember 2025
Erstgutachter:	Prof. Dr. Jürgen Hubbuch
Zweitgutachter:	Prof. Dr. Michael Wolff

Danksagung

An dieser Stelle möchte ich meine aufrichtige Dankbarkeit gegenüber all jenen ausdrücken, die mich während der vergangenen Jahre begleitet haben und deren fachliche und persönliche Unterstützung wesentlich zum Gelingen dieser Arbeit beigetragen haben. An erster Stelle möchte ich mich bei Prof. Dr. Jürgen Hubbuch für die fachliche Betreuung, die wertvollen Anregungen und die kontinuierliche Förderung danken. Ebenso möchte ich meinen Dank an Prof. Dr. Michael Wolff als Zweitgutachter aussprechen.

Diese Dissertation entstand im Rahmen einer Direktkooperation zwischen dem Karlsruher Institut für Technologie (KIT) und der ViraTherapeutics GmbH, einem Unternehmen der Boehringer Ingelheim Gruppe. Die Zusammenarbeit war für mich nicht nur fachlich bereichernd, sondern hat meinen Blick für praxisnahe Fragestellungen geschärft und mir Einblicke in industrielle Entwicklungsprozesse ermöglicht. Für die Ermöglichung dieser Industriepromotion und das Vertrauen in mich danke ich Dr. Knut Elbers und Dr. Lisa Egerer. Den Kolleginnen und Kollegen bei ViraTherapeutics danke ich für ihre Offenheit, ihre Hilfsbereitschaft und den regen fachlichen Austausch. Mein besonderer Dank gilt Dr. Judy Ng für zahlreiche konstruktive Diskussionen und ihre unermüdliche fachliche wie persönliche Unterstützung. Ebenso danke ich Dr. Michaela Smolle für inspirierende Impulse und Ioannes Basbas für seine Hilfe bei der Methodenentwicklung. Ich wünsche Ioannes Basbas alles Gute und viel Erfolg bei seiner eigenen Doktorarbeit. Dem gesamten Team möchte ich für die vertrauensvolle und angenehme Arbeitsatmosphäre danken, die diese Zeit für mich besonders gemacht hat.

Mein Dank gilt auch den Kolleginnen und Kollegen bei Boehringer Ingelheim, die mich durch intensiven Austausch begleitet und unterstützt haben: Dr. Federico Will (geb. Rischawy), Dr. David Saleh, Dr. Marija Brgles und Dr. Rudger Heß. Mit großer Wertschätzung danke ich auch allen Mitautoren der im Rahmen dieser Dissertation entstandenen Publikationen für die stets produktive, vertrauensvolle und inspirierende Zusammenarbeit.

Schließlich gilt mein tiefster Dank meiner Familie. Ohne ihre Geduld und uneingeschränkte Unterstützung wäre diese Dissertation nicht möglich gewesen. Sie haben mir in allen Phasen dieses Weges den nötigen Rückhalt gegeben – in Momenten des Zweifelns ebenso wie in Zeiten des Fortschritts – und mir die Kraft verliehen, Herausforderungen zu meistern, Rückschläge einzuordnen und diesen Weg bis zum Ende zu gehen.

Zusammenfassung

Fortschritte bei der Entwicklung eines Reinigungsverfahrens für ein therapeutisches replikationskompetentes umhülltes Viruspartikel

Replikationskompetente behüllte Viren sind vielversprechend für den Einsatz in der onkolytischen Virotherapie und als Vektor für Krebsimpfstoffe. Sie verfügen den Wirtszellen-Spezifität und bieten in ihrem Genom Platz für therapeutisches Genmaterial. Ihre Lipidhülle und ihre Größe machen diese Viruspartikel (VP) jedoch empfindlich gegenüber Umweltfaktoren wie pH-Wert, Temperatur und Scherkräften. Dies macht milde und optimierte Bioprozesse erforderlich, um die Partikelintegrität und dadurch die Infektiosität während der Herstellung zu bewahren. Hohe Konzentrationen infektiöser und replikationskompetenter Partikel sind erforderlich, um die gewünschte therapeutische Wirkung auf Tumorzellen zu erzielen. Obwohl neue analytische und präparative Methoden, angepasst für die Anwendung von VP etabliert wurden, gibt es immer noch Wissenslücken und Herausforderungen. Das Wissen über die Bioprozesse wird durch iterative Experimente gesammelt, wodurch Prozesserfahrung aufgebaut wird. Bei VP ist die Übertragbarkeit zwischen Virusstämmen jedoch schwierig, so dass der Wissensgewinn in diesem neuen Bereich kleinteilig ist. Die Auswirkungen von Bioprozessschritten auf die Integrität verschiedener Virusstämme sind komplex und nicht gut verstanden. Außerdem wird die Prozessentwicklung durch den Mangel an schnellen und zuverlässigen Analysemethoden, die eine effiziente Charakterisierung der Prozessschritte ermöglichen, behindert. Dies verhindert technologischen Fortschritt, wie z. B. die mechanistische Modellierung, die eine zuverlässige, tiefgehende Charakterisierung der Prozessschritte erfordert. In dieser Dissertation wird der aktuelle Stand der präparativen Aufreinigungsmethoden für umhüllte VP zusammengefasst und anschließend Forschungsfortschritte für identifizierte Herausforderungen bei der Partikelquantifizierung und chromatographischen Reinigung vorgestellt.

Zunächst bietet ein umfassendes Literatur Review einen Einblick in die Reinigungsprozesse replikationskompetenter umhüllter VP und unterstreicht die Wichtigkeit der Erhaltung ihrer Integrität für sichere und effektive therapeutische Anwendungen. Umhüllte VP bieten Vorteile wie große Genkapazität und Wirtszellen-Spezifität, sind jedoch empfindlich gegenüber Umweltfaktoren was erhebliche Herausforderungen im Bioprozess mit sich bringt. Die Heterogenität der Partikel erschwert die Entwicklung eines universellen Plattformprozesses und erfordert häufig eine *de novo* Prozessentwicklung für unterschiedliche Virusstämme. In diesem Review werden Reinigunsverfahren hinsichtlich ihres Einflusses auf die Partikelintegrität bewertet, angefangen bei der Zellernte über Zentrifugations- und chromatographische Techniken bis hin zur sterilen Filtration und Lagerung. Ein Schwerpunkt liegt auf Chromatographieschritten, in dem herkömmliche und neu angepasste stationäre Phasen verglichen werden. Konvektiv betriebene Phasen wie Membranadsorber und Monolithen sind für große VP vorteilhaft, da sie keine diffusionalen Einschränkungen aufweisen. Ihr hoher Stoffübergang und niedriger Rückdruck ermöglichen hohe Flussraten ohne Reduktion der Bindungskapazität. Vor- und Nachteile sowie bestehende Wissenslücken in der VP-Reinigung werden beschrieben, ebenso wie analytische Lücken, die eine effiziente Bewertung der Partikelqualität und -quantität, und damit die Optimierung der Bioprozessschritte behindern.

Die Dissertation geht in Forschungsartikel über, die Fortschritte bei analytischen und präparativen Methoden darstellen. Dabei kam ein modifiziertes Vesicular Stomatitis Virus (VSV) zum Einsatz. VSV ist ein patronen- (engl. "bullet-") förmiges, umhülltes VP mit Abmessungen von ~70 nm×~200 nm. Die entwickelte analytische Methode adressiert den Bedarf an schneller und präziser VP-Quantifizierung, um Massenbilanzen zur Evaluierung von Prozessschritten zu ermöglichen. Vorgestellt wird eine markierungsfreie Methode, basierend auf Hochleistungsflüssigkeitschromatographie (engl. "high performance liquid chromatography", HPLC) und Größenausschlusschromatografie (engl. "size exclusion chromatography", SEC), gekoppelt mit UV-Detektion für die Partikelquantifizierung. Das Setup ist ergänzt durch einen Mehrwinkel-Lichtstreuungsdetektor (engl. "multi-angle light scattering", MALS) zur Partikelcharakterisierung welcher zusätzliche Informationen wie Partikelgröße liefert. Die Methode wurde hinsichtlich einer hohen Rückgewinnungsrate der VP von der SEC Säule und dem HPLC System optimiert, um somit Robustheit und Zuverlässigkeit zu garantieren. Der SEC Auschlusspeak wurde mittels offline Analysen und online UV-Detektion als Viruspeak identifiziert, was sich in einem konsistenten UV 260 nm/UV 280 nm-Verhältnis zeigte. Die Methode zeigte hohe Präzision und Robustheit mit einer Reproduzierbarkeitsabweichung von unter 1 % und einer Präzisionsabweichung von unter 3 %. Der lineare Quantifizierungsbereich erstreckt sich von 7.1×10^8 bis 1.7×10^{11} $\frac{\text{VPs}}{\text{mL}}$, mit einem Detektionslimit (engl. "limit of detection", LOD) von 7.7×10^7 $\frac{\text{VPs}}{\text{mL}}$ und einer unteren Bestimmungsgrenze (engl. "lower limit of quantification", LLOQ) von 4.2×10^8 $\frac{\text{VPs}}{\text{mL}}$. Die Quantifizierung erwies sich als unabhängig von der unterschiedlichen Zusammensetzung der Probenmatrix durch die Reinigungsstufen. Während die Methode die Gesamtzahl der VP quantifiziert und eine orthogonal quantifiziertes Referenzmaterial benötigt, liefert sie Ergebnisse am selben Tag mit minimalem Arbeitsaufwand und ermöglicht schnelle Entscheidungen in VP-Reinigungsprozessen. Eine Anwendung für eine Massenbilanz des Chromatographieschrittes eines modifizierten VSV belegte ihre Eignung für Prozesscharakterisierungen und Entwicklung mechanistischer Prozessmodelle.

Die anschließende Studie untersuchte spezifisch das Verhalten des modifizierten VSV in einem chromatographischen Reinigungsschritt. Bei der Charakterisierung des Capture-Schrittes mittels einem Kationaustauschchromatografen (engl. "cation exchange chromatography", CEX) bei Verwendung eines Monolithen wurde ein unerwartetes fluiddynamisches Phänomen festgestellt. Es resultierte in einem Tailing-Effekt und der Trennung von Subpopulationen, welche sich nicht durch gängige chromatographische Prinzipien erklären ließen. Das Phänomen wurde als konvektiver Einschluss (engl. "convective entrapment", CE) identifiziert, ein Effekt, bei dem große Biomoleküle vorübergehend in Engstellen der stationären Phase eingeschlossen werden. Partikel werden durch Advektion in diese Engstellen gedrückt und können nur durch Diffusion zurück in den Hauptströmungspfad gelangen. Frühere Studien zeigten diesen Effekt bei großen Biomolekülen mit der Auswirkungen von Ertragsverlusten und Verzögerungen in der Elution. Jedoch wurde dieser Effekt in konventionellen mechanistischen Chromatographiemodellen bisher nicht berücksichtigt. Im vorgestellten mechanistischen Modell wird der CE-Effekt mithilfe der Langmuir-Isotherme abgebildet und damit als eigenes Bindungsmodalität, zusätzlich zur elektrostatischen Wechselwirkung nach dem sterisches Massenwirkungsmodell (engl. "steric mass action", SMA), beschrieben. Simulationen zeigten, dass hauptsächlich eine Subpopulation für das Tailing verantwortlich ist und eine stärkere Retention dem CE zuzuschreiben ist. Das Modell ermöglichte ein besseres Verständnis des präparativen Virusreinigungsprozesses, ist jedoch ohne weitere Entwicklung in seiner Anwendung eingeschränkt. Tailing durch den CE-Effekt ist bei charakteristischen Flussraten in allen Maßstäben zu erwarten, weshalb Ertragsverluste evaluiert und potenzielle Anpassungen der cleaning in place (CIP)-Protokolle geprüft werden sollten. Niedrige Flussraten oder Flusspausen können die Freisetzung der Partikel begünstigen.

Zusammenfassend wurde der aktuelle Stand der Reinigungsmethoden für umhüllte VP evaluiert und Fortschritte in der VP-Prozessentwicklung vorgestellt. Das Literatur Review schafft eine Grundlage über den aktuellen Wissensstand und die Herausforderungen von VP-Bioprozessen, insbesondere hinsichtlich der Auswirkungen auf die virale Integrität. Es werden analytische Lücken identifiziert, welche schnelle Prozessentwicklungsiterationen verhindern. Eine dieser Lücken wird durch die Entwicklung einer Quantifizierungsmethode geschlossen, die schnelle und zuverlässige Ergebnisse liefert und die Charakterisierung von Prozessen ermöglicht. Die eingehende Charakterisierung eines präparativen Monolith-Chromatographieschrittes zeigte einen Mangel an Prozessverständnis, der sich in einem nicht erwarteten Tailing-Effekt manifestierte. Das strömungsdynamische Phänomen des convective entrapment wurde zum ersten Mal mit einem mechanistischen Modell dargestellt, das die Bewertung seiner Auswirkungen durch Simulationen ermöglicht. Weitere Studien könnten das mechanistische Modell verbessern, um *in silico* Optimierungen und eine robuste Herstellung von umhüllten VP zu ermöglichen.

Abstract

Replication-competent enveloped viruses show promise for use in oncolytic virotherapy and as vector for cancer vaccines. They confer host cell target specificity, and provide large capacity in their genome to carry therapeutic cargos. However, their lipid envelope and size renders these virus particles (VPs) sensitive against environmental factors such as pH, temperature and shear forces. This necessitates mild and optimized bioprocesses to maintain particle integrity and preserve infectivity during manufacturing. High concentrations of infectious and replication-competent particles are needed to achieve the desired therapeutic effect on tumor cells. Although new analytical and preparative methods have been tailored and established for VP applications, gaps and challenges prevail. Bioprocessing knowledge accumulates through iterative experiments, generating process experience. However, for VPs the transferability between virus strains is difficult and thus knowledge gain in this new field is cumbersome. E.g., the effects of bioprocessing steps on the integrity of various virus strains are complex and not well understood. Also, process development is constricted due to the lack of fast and reliable analytical methods capable of efficient evaluation of process steps. This hinders technological progress such as mechanistic modeling which requires reliable in-depth characterization of process steps. This doctoral thesis synthesizes the current state of preparative processing methods for enveloped VPs and subsequently presents research advancements for identified challenges in particle quantification and chromatographic purification.

First, a comprehensive literature review examines the purification processes for replication-competent enveloped VPs, emphasizing the importance of maintaining their integrity for safe and effective therapeutic applications. Enveloped VPs offer substantial advantages, including large gene insert capacities and target specificity, however their inherent sensitivity to environmental factors presents significant bioprocessing challenges which needs to be considered. Further, particle heterogeneity hinders the development of a broadly applicable platform process, often necessitating *de novo* process development for different virus strains. In this review purification process technologies are evaluated for their influence on particle integrity, including cell-culture harvest, centrifugation and chromatographic techniques, sterile filtration and storage considerations. A focus is set on chromatography steps in which conventional and new, tailored stationary phases are compared. Convective-driven stationary phases like membrane adsorbers and monoliths are beneficial for large VPs due to the lack of diffusional limitations. A key benefit is their ability to facilitate high mass transfer rates and low back pressure, enabling high flow rates without compromising binding capacity. The review describes individual process steps and identifies knowledge gaps and challenges in VP purification. One of them being an analytical gap which hinder the efficient characterization of VP process steps due to lack of efficient and robust analytical methods. Slow and low throughput methods are typically used which slow down process development.

The thesis progresses into research articles which constitute advancements in analytical and preparative methods. A modified vesicular stomatitis virus (VSV) was utilized in the studies. VSV is a bullet-shaped enveloped VP, of ~70 nm × ~200 nm in size. The analytical method developed in this

thesis addresses the need for a rapid and precise VP quantification to facilitate mass balance calculations to evaluate and characterize process steps. A label-free high performance liquid chromatography (HPLC)-based method is presented utilizing size exclusion chromatography (SEC) coupled with UV for particle quantification. This setup integrates a multi-angle light scattering (MALS) detector for particle characterization, providing additional information such as particle size. The method was optimized to achieve high VP recovery from the SEC column and HPLC system to establish a robust and reliable method. The SEC exclusion peak was confirmed to be the virus peak through offline analytical methods and online UV detection, resulting in a consistent UV 260 nm to UV 280 nm ratio. The method demonstrated high precision and robustness, with repeatability variation of less than 1 % and intermediate precision deviation of less than 3 %. The linear quantification range spans 7.1×10^8 to 1.7×10^{11} $\frac{\text{VPs}}{\text{mL}}$, with a limit of detection (LOD) of 7.7×10^7 $\frac{\text{VPs}}{\text{mL}}$ and lower limit of quantification (LLOQ) of 4.2×10^8 $\frac{\text{VPs}}{\text{mL}}$. The quantification method proved to be independent by variations in process sample matrices from different purification processing steps. While the method quantifies total VPs and requires an orthogonally quantified reference material, it delivers same-day results with minimal hands-on time, enabling fast process evaluation and thus fast decisions in VP purification processes and development. It further facilitates in-depth process characterizations and mass balance calculations as shown for a cation exchange chromatography (CEX) step of the VSV purification. This enables the development of mechanistic process models for which process understanding and characterization is needed.

In the next presented study, the chromatographic behavior of modified VSV particles on a CEX purification step is investigated and mechanistic model developed. During the characterization of the CEX monolith capture step, an unexpected fluid-dynamic phenomenon was observed. It resulted in a tailing effect and subpopulation separation that could not be explained by anticipated chromatographic behaviors. The phenomenon was identified as convective entrapment (CE), an effect where large biomolecules are temporarily restricted in the resin's constriction sites. Particles are pushed into these narrow sites by advection and can only be released by diffusing back through the opening, relying on chance to take a different flow path. Previous research has demonstrated this effect for large biomolecules, impacting recovery and leading to peak delays or tailing, but it has not been accounted for in chromatographic mechanistic models. In the presented model the CE effect is implemented by the Langmuir isotherm. This approximation represents CE as a binding modality, additionally to electrostatic interaction modeled by a steric mass action model (SMA) isotherm. The simulations showed that a subpopulation was primarily responsible for the tailing, with a stronger retention attributed to the CE. The model supports knowledge gain for the preparative virus purification run, however it is limited in its application scope (e.g., a fixed flow rate is used) without further development. Tailing effects due to CE are expected across all scales at characteristic flow rates, necessitating evaluation of recovery losses and potential adjustments of cleaning in place (CIP) steps. Low flow rate steps or flow rate pauses can facilitate particle release.

In summary, the current state of purification methods for enveloped VPs was assessed, and advancements in VP process development were discussed. The literature review establishes a baseline of current knowledge and challenges in bioprocessing, especially regarding the impact on viral integrity. Analytical gaps are identified which prevent fast process development iterations. This gap is addressed by the development of a quantification method which provides fast and reliable results and enables process characterizations. The in-depth characterization of a preparative monolith chromatography step revealed a lack of process understanding which was manifested in a tailing effect not anticipated. The fluid dynamic phenomenon of convective entrapment was represented for the first in a mechanis-

tic model, enabling evaluation of its impact through simulations. Further studies could advance the mechanistic model to enable *in silico* optimizations and a robust manufacturing of enveloped VPs.

Contents

List of Figures

List of Tables

List of Abbreviations

Please note that chapter 3 includes its own, extended list of abbreviations at the end of that chapter.

AAV	adeno-associated virus
AEX	anion exchange chromatography
BE-mode	bind-and-elute mode
BHK	baby hamster kidney
CE	convective entrapment
CEX	cation exchange chromatography
cGE	capillary gel electrophoresis
CIP	cleaning in place
cryo-EM	cryogenic electron microscopy
DIP	defective interfering particles
DMSO	dimethyl sulfoxide
DNA	deoxyribonucleic acid
EDM	equilibrium dispersive model
ELISA	enzyme-linked immunosorbent assay
EM	electron microscopy
EV	extracellular vesicle
FFF	field flow fractionation
FLR	fluorescence
FT-cycle	freeze thaw cycle
FT-mode	flow-through mode
hcDNA	host cell deoxyribonucleic acid (DNA)
hcP	host cell protein
HIC	hydrophobic interaction chromatography
HPLC	high performance liquid chromatography
IEP	isoelectric point
IEX	ion exchange chromatography
IFN	interferon type I
IPC	in-process control
IU	infectious unit
LC	liquid chromatography
LCMV	lymphocytic choriomeningitis virus
LLOQ	lower limit of quantification
LOD	limit of detection
LS	light scattering

MALS	multi-angle light scattering
MLP	monolith-like particle
MOI	multiplicity of infection
mRNA	messenger ribonucleic acid (RNA)
MS	mass spectrometry
ns-EM	negative staining electron microscopy
OC	open circular
OV	oncolytic virus
P:IU	particles-to-infectious unit
PCR	polymerase chain reaction
pDNA	plasmid DNA
PEEK	polyether ether ketone
PP	polypropylene
qPCR	quantitative polymerase chain reaction
RAM	restricted-access-medium
RI	refractive index
RNA	ribonucleic acid
RP	reverse phase chromatography
SEC	size exclusion chromatography
SMA	steric mass action model
SXC	steric exclusion chromatography
$TCID_{50}$	tissue culture infectious dose 50
UF/DF	ultrafiltration/ diafiltration
UV	ultraviolet
VLP	virus-like-particle
VP	virus particle
VSV	vesicular stomatitis virus
VSV-GP	modified VSV, pseudotyped using the lymphocytic choriomeningitis virus (LCMV) glycoprotein

List of Symbols

Λ	Total ionic exchange capacity	[M]
ε	Total porosity	-
λ	Wavelength	[m]
μ	Dynamic viscosity	[Pa s]
ν	Characteristic charge	-
σ	Shielding	-
A	Cross-section area	[m^2]
c	Interstitial mobile phase concentration	[M]
c_p	Pore phase concentration	[M]
c_0	Counterion concentration	[M]
D	Particle diffusion coefficient	[$m^2\ s^{-1}$]
D_{app}	Lumped, apparent dispersion coefficient	[$m^2\ s^{-1}$]
D_{ax}	Axial dispersion coefficient	[$m^2\ s^{-1}$]
d	Diameter	[m]
d_b	Bioparticle diameter	[m]
d_c	Diameter of constriction site	[m]
d_p	Mean channel diameter	[m]
I	Intensity of light	[$W\ m^{-2}$]
$_{i,j}$	Component subscript indices	
K_{eq}	Equilibrium coefficient	-
k_{ads}	Adsorption coefficient	[$m^3\ s\ g^{-1}$]
k_{des}	Desorption coefficient	[$m^3\ s\ g^{-1}$]
k_{kin}	Kinetic parameter	[$s\ M^{\nu}$]
k_p	Association constant	[$m\ s^{-1}$]
L	Length	[m]
L_{Col}	Column length	[m]
L_c	Characteristic path length	[m]
N_{comp}	Number of components	-
P	Solute	
P_{ads}	Amount of adsorbed solute	[mol]
Pe	Peclet number	-
p	Pressure	[Pa]
Q	Volumetric flow rate	[$m^3\ s^{-1}$]
q	Concentration bound to the stationary phase	[$mol\ m^{-3}$]
q_{max}	Saturation capacity of the stationary phase for all components	[$mol\ m^{-3}$]

$\bar{q}_\mathrm{s}$	Counterions on available binding sites	$[\mathrm{mol\,m^{-3}}]$
r	Radius	[m]
S	Amount of counterions	[mol]
t	Time coordinate	[s]
u	Interstitial velocity, local average mobile phase velocity	$[\mathrm{m\,s^{-1}}]$
u_s	Superficial velocity, empty conduit velocity	$[\mathrm{m\,s^{-1}}]$
u_c	Flow velocity through constriction sites	$[\mathrm{m\,s^{-1}}]$
x	Spatial coordinate	[m]
z	Effective binding charge number	-

1 Introduction

Virus particles (VPs) are host-dependent, passive entities whose primary aim is to spread progeny through replication in hosts. They are remarkably abundant, with billions of particles encountered daily by every living organism [1]. In its evolution, the humankind had to deal with the pathogenic threat by viruses since its beginning [2]. Viruses are extremely adaptable, evolving rapidly to adapt to their host and environment [3]. Numerous viral variations have resulted from this evolutionary advantage, many of which have distinct and specialized characteristics like host and target cell specificity or host immune evasion tactics.

Modern science has leveraged the unique properties of viruses for biotechnological and medicinal applications. Virus-derived nanoparticles are being studied and used as therapeutic, preventive, and diagnostic tools [4]. For centuries, both inactivated and attenuated viruses have been employed as vaccines. Vaccine designs based on non-infectious, antigen-presenting virus-like-particles (VLPs) have emerged in recent decades due to fundamental research breakthroughs in immunology, synthetic biology, DNA sequencing methods and genetic engineering. The same technological progress has led to new therapeutic applications of replication-incompetent and also -competent VPs for the treatment of cancer and genetic diseases. Significant progress has been observed for oncolytic virus (OV) treatments [5] and gene therapies [6] as observed by the increasing amount of clinical trials and approvals in those fields.

Despite this progress, developing viral production processes remains laborious. The requirements for virus processes differ from those of conventional, small biopharmaceutical products due to the size and fragility of VPs. Because of the diverse morphologies and properties of virus species and strains, a universal platform process for all viruses does not exist. Conventional methods must be adapted, or new methods developed and tested. A common lack of comprehensive knowledge in VP purification means methods are often tested and optimized through empirical iterations. Evaluating each iteration is cumbersome due to the limited availability of process analytical technology tools for viral vectors [7, 8] and the inability of online detectors to provide qualitative process performance information. Typically, offline analytical methods are required, which are time-consuming, have low throughput, and are imprecise; making rapid process development iterations difficult. The heterogeneity of VP populations and their dependency on upstream parameters further complicate analytical and preparative method development and evaluation.

Even though the utilized VPs and corresponding medicinal applications vary widely, similar preparative and analytical methods are employed, leading to comparable challenges. These methods, and thus the challenges, can be transferred amongst different VPs to some extent, especially when morphological properties are similar. However, enveloped VPs are particularly delicate. The lipid bilayer envelope is vulnerable to environmental factors such as pH, elevated temperatures, and shear stress. Osmolarity, ionic strength, solvents, detergents, and excipients might additionally reduce viral activity. Additionally, oncolytic applications have the highest particle quality requirements because replication competency is necessary for the therapeutic effect. Therefore, this work focuses

on replication-competent enveloped VPs. It establishes a baseline of current knowledge and best practices for the preparative purification process of replication-competent enveloped VPs and offers novel approaches to identified challenges using a modified vesicular stomatitis virus (VSV) intended for oncolytic therapy.

Due to the specific requirements of VPs new and tailored processing methods have been developed and established in the industry to support the new therapeutical field. However, a platform process is not feasible due to the heterogeneity of VPs between strains, which complicates bioprocess development. Further, the impact of processing steps on VP is often unknown which is particularly important for labile enveloped VPs. To evaluate current knowledge of processing impact on VPs, the *status quo* is described in a comprehensive literature review in chapter 3, covering everything from cell culture harvest to formulation. Conventional biopharmaceutical and new, VP methods are assessed regarding their impact on viral integrity, and an overview of relevant analytical methods for bioprocessing is included. Iterative bioprocess development depends on efficient analytical methods for characterizing process samples. For VPs, a comprehensive and timely set of analytical methods is typically required to thoroughly assess a sample and thus derive process implications. Additionally, many methods are limited by low throughput, slow result turnaround, imprecision, or the requirement for specialized equipment. A tailored and validated quantification method for process development which would also enable mechanistic model development was lacking for VSV. To address this gap, chapter 4 presents the development and validation of a quantification method based on widely available HPLC device with ultraviolet (UV) detection, enabling high-precision quantification with minimal labor. The quantification method facilitated the in-depth characterization of process steps required to establish a mechanistic model as presented in chapter 5. The characterization of the CEX capture step of an enveloped VP revealed an unexpected tailing effect. This effect was most likely due to CE, which was incorporated into a mechanistic model that successfully described the purification process. The process characterization during model development, together with the model simulations, has improved the process understanding of monoliths and provided insights for future applications of chromatographic monoliths.

In the following sections, VPs for medicinal applications, their properties, analytical characterization, and preparative process are introduced. The focus is set on materials and methods utilized in later chapters, such as VSV particles, HPLC-derived analytical methods, and monolithic chromatography material. A fundamental introduction for mechanistic modeling of chromatography steps, used for *in silico* representation, is provided. The introductory sections, section 1.2 to section 1.4, are partially based on the published literature review [9], presented in chapter 3. Topics covered in the review are introduced but not extensively elaborated upon. In relevant sections, the reader is directed to chapter 3 for further information.

1.1 Virus Based Vaccines and Therapies

Viruses and modified VPs in various formats are used in medicine to prevent and treat viral diseases, cancers, and genetic disorders. An overview of VP types and their applications is provided in Table 1.1. Vaccines are designed to stimulate the immune system to recognize and combat pathogens, such as viruses. Conventional viral vaccines use viruses attenuated by passage through different animal species, as well as chemically inactivated pathogenic viral particles or viral subunits. Modern vaccination strategies utilize VLPs as vectors displaying a variety of antigens [10]. VLPs lack viral genetic

Table 1.1: Overview of VPs and derived particle types researched for medicinal interventions

Applications	Virus particle type				
	Replication-competent VPs		**Replication-incompetent VPs**		**VPs deficient of viral genes**
	Non-pathogenic VPs	Live attenuated VPs	Replication-defective VPs	Inactivated VPs	VLPs
Viral diseases	Vaccines [14]	Vaccines	Vaccines [15]	Vaccines	Vaccines
Oncology	Oncolytic treatments and therapeutic cancer vaccines [15]				Preventive and therapeutic cancer vaccines [16]
Genetic disorders			Gene therapies		

material and are thus non-infectious. Vaccines that prevent oncovirus infections, and consequently infection-related cancers, are considered (preventive) cancer vaccines because they eliminate the underlying factor of tumor formation. Therapeutic cancer vaccines, on the other hand, are designed to treat existing cancers through immunostimulation. These vaccines expose the immune system to cancer-specific antigens, helping it target and eliminate cancer cells. The therapeutic goal is to induce tumor regression, eliminate residual tumor cells after surgery, and establish long-term immunity. Tumor antigens are either introduced into patients as peptides or transferred via vectors as genes encoding antigens [11]. VLPs and replication-competent VPs lacking pathogenicity are used as vectors. The latter is preferred if the virus itself exhibits oncolytic properties. The antitumoral effect of these viruses is then enhanced by combining them with immunostimulatory genes, engineering a therapeutic cancer vaccine [12].

Gene therapies, particularly those targeting monogenic inherited disorders, use vectors to deliver a functional copy or modification of a mutated gene into cells. However, the first generation of gene therapy viral vectors revealed severe carcinogenic side effects, including lethal outcomes, due to replicating VPs. In response, newer generations of viral vectors have been developed to be replication-incompetent, with strategies to prevent the regain of replication competency, thereby enhancing safety [13]. OVs, which may also be considered gene therapies, introduce viral genes and payloads specifically into tumors. Unlike most gene therapies that aim for a one-time treatment of genetic diseases using replication-incompetent viruses, OVs require replication competency and may be applied multiple times. The replication cycle enables their lytic activity and payload expression, thus facilitating their therapeutic function.

1.1.1 Oncolytic Virus (OV) Therapeutics

OVs represent a promising approach in cancer therapy, leveraging the unique properties of viruses to target and destroy cancer cells. These viruses exhibit naturally occurring or engineered specificity for cancer cells, ensuring that cancer cells are preferentially infected while normal, healthy cells are spared. Viral replication within the cancer cells eventually leads to their destruction by host cell shut-off and hijacking the cell's metabolism for virus progeny and through virus-induced cell lysis, resulting in cell death. The release of viral progeny can lead to multiple rounds of infection within the tumor and may also reach metastases. Cell lysis and the release of cellular components can modulate the tumor microenvironment to a pro-inflammatory state, stimulating the body's immune system to recognize and attack the tumor. This effect can be enhanced by introducing transgenes into the viruses, which express immunomodulatory agents within the tumor cells. This

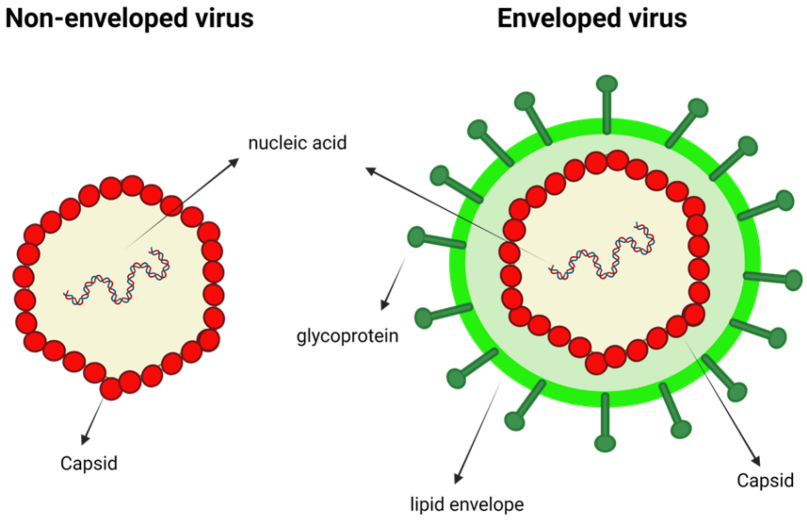

Figure 1.1: Generalized schematics of non-enveloped and enveloped VPs showing structural differences. Sourced from [20] under Creative Commons Attribution 4.0 International (CC BY 4.0) license (`https://creativecommons.org/licenses/by/4.0/`).

cancer vaccine setting enhances the overall efficacy of the treatment, potentially leading to long-term cancer remission [17]. Payload expression is limited in timing, duration, and localization due to its dependence on virus replication. The specificity of viral infection and the limited localization of expressed antitumor agents reduce unnecessary exposure of healthy tissue and systemic toxicity, as seen in conventional chemotherapy. However, these limitations might be too stringent for effective treatment. Administering OVs alongside other therapeutics in combination drug approaches can overcome these limitations. Examples of complementary drugs include immune checkpoint inhibitors and prodrugs when the prodrug-converting enzyme is introduced as a viral payload [18]. Tumor specificity of OVs and their limited ability to replicate in normal, healthy cells can originate from the virus's natural tropism for factors overexpressed or suppressed in tumor cells. Various strategies are also utilized in OV development to engineer specificity: alteration of surface glycoproteins; deleting viral genes required for replication in healthy, non-dividing cells; exploiting defects in antiviral cell response pathways; and using tumor-specific promoters for viral gene expression. These strategies have led to generally safe applications with a low toxicity profile [19]. Advances in safety and efficacy have broadened the potential applications of OVs, as evidenced by over 100 ongoing clinical trials as of February 2025 [see chapter 3].

Virus strains studied for oncolytic applications include non-enveloped viruses (e.g., Adenovirus, Reoviruses) as well as enveloped VPs (e.g., HSV, Vaccinia, VSV) [21], with the latter being the majority tested in clinical trials [see chapter 3]. Enveloped VPs have an additional lipid membrane as their outermost layer and are generally larger, thus providing higher gene insert capacities. Structural differences are schematically shown in Figure 1.1. The lipid membrane is derived from the host cell, making its composition and properties dependent on the host cell state and culture conditions. Glycoproteins embedded in the lipid membrane facilitate cell recognition, attachment, and entry, initiating the infectious cycle. Through additions, alterations, and exchanges of glycoproteins, such as pseudotyping, the tropism of VPs can be modified to tailor their specificity to the therapeutic target. The integrity of glycoproteins on the viral surface, as well as the entire structure of the VP, needs to remain intact from viral release until the infection of another cell to continue the infectious cycle. In

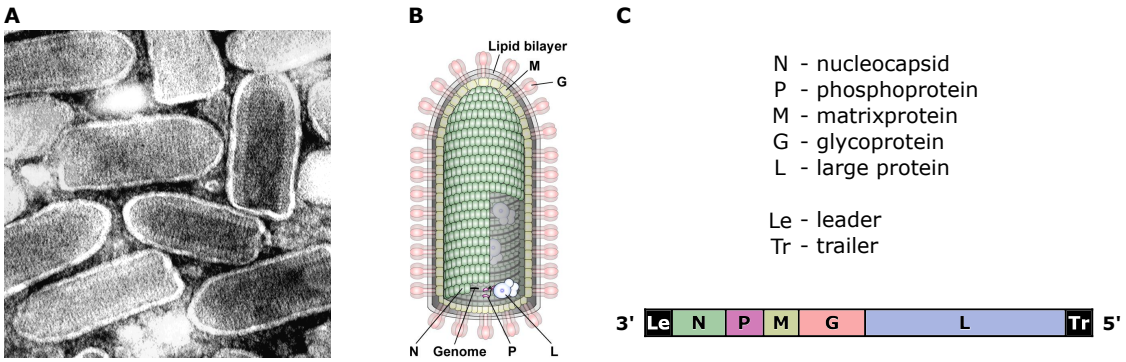

Figure 1.2: VSV particle images and genome structure. (A) Negative staining electron microscopy (ns-EM) picture of VSV, magnification approx. 40.000x, cropped micrograph from F.A. Murphy, University of Texas Medical Branch, Galveston, Texas [22]. (B) Schematic VSV, adapted from [23] under Creative Commons Attribution 4.0 International (CC BY 4.0) license (`https://creativecommons.org/licenses/by/4.0/`). (C) Genomic structure with approximated gene lengths.

the case of virus manufacturing for therapeutic applications, this time frame includes the production of viral progeny in a cell culture and its subsequent purification, formulation, and storage, typically in a frozen state. Afterward, the VP must remain stable during thawing, potential dilution, and patient administration until a new host cell is targeted within the patient.

Enveloped OVs Enveloped VPs offer advantages for research and therapy due to their size and structure; however, these same viral properties present challenges for production processes. The non-rigid envelope and size of enveloped VPs provide large gene insert capacities, offering researchers room for transgenes and flexibility in gene design. Depending on the location and modification, tags can be added to structural viral proteins, and proteins to be expressed separately can be introduced. Glycoproteins on the particle surface can be modified or exchanged with foreign glycoproteins, resulting in a pseudotyped VP with altered tropism. Enveloped VPs bud and thus derive their lipid membrane from cellular membranes. Present cellular membrane proteins and expressed viral proteins can be incorporated into the viral envelope. In the case of non-enveloped VPs, the capsid structure is rigid, and modifications may impair its structural integrity. Tropism changes are possible; however, they require more sophisticated methods.

As described, the size and lipid envelope of enveloped VPs are key properties offering advantages for therapeutic applications. At the same time, the lipid envelope renders the whole VP sensitive to its local environment. Mechanical, chemical, and thermal stress can quickly disrupt the envelope or the membrane proteins it contains, thus inactivating the VP. This necessitates the application of relatively mild processing conditions to maintain viral integrity and infectious VPs for an effective drug substance.

1.1.2 Vesicular Stomatitis Virus (VSV)

In this work, a modified yet infectious version of the VSV Indiana strain was utilized. VSV belongs to the Rhabdoviridae family and is a non-segmented, negative-strand RNA virus [24]. It has been extensively studied in the past as a model virus for RNA viruses [25] due to its highly efficient and

rapid replication cycle, simple structure, and error-prone polymerase [24, 25]. Viral progeny of VSV appear 2 to 10 h after infection in baby hamster kidney (BHK) cells [26]. VSV induces apoptosis, leading to programmed cell death upon infection [27, 28].

VSV Structure Native VSV particles are bullet-shaped, with a cylindrical end on one side and a narrowing, pointed opposite side, as depicted in Figure 1.2 A and B. Wild-type particles are approximately 70 nm in diameter and 200 nm in length [24]. The viral genome of VSV comprises approximately 11 kb and encodes five structural viral proteins, as shown in Figure 1.2 C. It is encapsidated with nucleoproteins (N) to form a helical nucleocapsid structure. This is covered by a layer of matrix proteins (M), which is further encased by the lipid bilayer envelope spiked with glycoproteins (G). Associated with the N-RNA complex are polymerase ('large') proteins and their cofactor phosphoproteins [29].

Oncolytic Activity of VSV Wild-type VSV exhibits an inherent oncolytic effect due to its ability to efficiently replicate in malignant cells, thereby inducing cell death in tumors. The selectivity for malignant cells does not arise from the specific targeting of certain cells; rather, it is due to the favorable conditions for VSV replication present in many malignant cell types. Most tumor cells have a defective interferon type I (IFN) response or lack a IFN response entirely. Additionally, abnormal messenger RNA (mRNA) translation in malignant cells promotes VSV replication. In contrast, healthy cells inhibit viral replication due to their IFN response, which enables an antiviral state [30].

Pseudotyping of VSV Although VSV infection typically causes non-lethal fever and blister-like lesions in natural hosts, neurotoxicity has been observed in rodents, and there is one known case of induced encephalitis in humans [31]. Replacing the VSV glycoprotein with a glycoprotein from another virus (pseudotyping) has been shown to reduce or completely abolish neurotoxicity, as seen with Ebola and Lassa fever glycoproteins [32]. In this study, a VSV variant pseudotyped with the glycoprotein from lymphocytic choriomeningitis virus (LCMV), termed VSV-GP, was used. This modification confers cell specificity to VSV infection and abolishes neurotoxicity while retaining tropism for malignant cells. Preclinical studies demonstrated that VSV-GP could be safely inoculated into rodent brains at high dosages, unlike wild-type VSV [33]. Furthermore, the glycoprotein of LCMV does not lead to the rapid induction of neutralizing antibodies, as observed with wild-type VSV, enabling repeated application of VSV-GP. Additionally, replication competency is sustained, which is required for the induction of cell death in malignant cells [33, 34, 35].

Known particle heterogeneity Enveloped VP populations exhibit significant heterogeneity in morphology, size, protein composition, and genomic content, all of which directly influence their functionality. This variability arises from differences in host-cell membrane incorporation, viral assembly mechanisms, and environmental influences, such as those encountered during cell culture and bioprocessing. In contrast, non-enveloped viruses tend to be morphologically uniform, as their highly structured protein capsid provides a more rigid and consistent framework for particle formation. The diversity of enveloped viruses is further shaped by cellular factors, including lipid composition and glycoprotein distribution, leading to complex interactions that affect infectivity and immune recognition. Additionally, external conditions, such as temperature fluctuations and purification processes, can further contribute to population heterogeneity, highlighting the sensitive nature of enveloped VPs compared to their non-enveloped counterparts.

Defective interfering particless (DIPs) are VPs with mutations such as genomic deletions or partial genomes. They arise due to errors in replication or recombination and cannot replicate on their own. They require a helper virus, a fully functional virus, to coinfect a cell and provide the missing factors needed for replication. DIPs interfere with the replication of their parent virus by competing for resources within the cell, often reducing the overall viral load and altering disease progression. They have been observed in various RNA viruses, including the influenza virus, VSV, and the measles virus [36]. In cell cultures, DIPs occur in high numbers if a high multiplicity of infection (MOI) is used for infection, resulting in a higher probability of coinfections of DIPs and functional VPs. DIPs can become the dominant species; however, they can also drive viral evolution, leading to DIP-resistant species [24]. DIPs impair the production of infectious VPs in cell culture and reduce capacity in purification processes for infectious VPs. They should thus be prevented and minimized for an efficient production process.

The particles-to-infectious unit (P:IU) ratio, which indicates the number of total VPs in a VP preparation per infectious unit (IU), is generally well above 1, signifying a low proportion of infectious particles compared to total VPs [1]. DIPs increase this ratio, as do other non-infectious VPs, such as malformed and defective particles, which may arise during the cell culture stage depending on the culture conditions [37, 38], or during purification [39].

The incorporation of transgenes into the VSV genome has been shown to yield replication-competent VPs with little or no attenuation. Reporter genes, such as fluorescent tags, have been successfully added to viral proteins without compromising viral function [40]. Transgenes encoding immunomodulatory proteins have been inserted into intergenic regions, allowing for transcription and expression within infected cells [32]. The viral nucleocapsid, which encapsulates the genomic RNA, forms a rigid helical structure with fixed angular parameters, contributing to the virus's characteristic morphology and stability. The highly ordered interactions between structural proteins result in a consistent VP diameter of approximately 70 nm [29]. Modifications affecting genome length impact the length of VPs, while the width of particles remains the same [41].

1.2 Analytical Characterization of Enveloped Viral Particles

An analytical panel to evaluate the quality attributes of VP preparations typically comprises methods related to general quality, safety, strength, identity, purity, process-related impurities, and potency [42]. This extensive panel is necessary to encompass all aspects of the complex VP integrity and structure, which is a combination of nucleic acids, proteins, and, in the case of enveloped VPs, lipids.

Structural VP characteristics can be assessed using electron microscopy (EM) techniques, such as cryogenic electron microscopy (cryo-EM) and ns-EM. The latter method is also regarded as the current benchmark for quantification purposes [43]. The composition of VPs can be evaluated by methods that identify viral proteins, such as mass spectrometry (MS) and Western blotting. Advancements in adapting flow cytometers for virus detection have led to the development of flow virometry, a technique that enables the analysis of viral particles at the single particle level. Through labeling techniques, surface structure and composition are analyzed, facilitating the quantification of VPs as well as certain impurities [44]. Other well-established methods for purity analysis include conventional enzyme-linked immunosorbent assay (ELISA) and polymerase chain reaction (PCR)-based methods for host cell protein (hcP) and host cell DNA (hcDNA) quantification. Aggregation of viral particles can be assessed by DLS [45] or NTA [46], both of which are used for stability and formulation

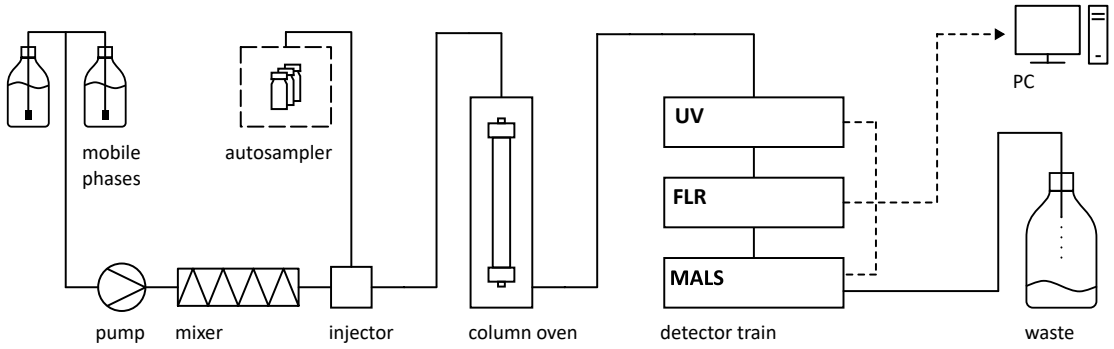

Figure 1.3: Simplified schematic of an HPLC device.

studies. The analysis of particulate impurities within the same size range as VPs and VLPs is more challenging, if not impossible. If different surface properties can be labeled, flow virometry can be used to differentiate between particle populations [47]. However, some populations, such as defective VPs and extracellular vesicles (EVs), can exhibit the same surface markers, making staining strategies important [48]. EM methods, such as ns-EM and cryo-EM, can provide images of the VPs, enabling the evaluation of structural integrity and quantification. Although regarded as the current gold standard for quantification, the influences of sample preparation must be considered. Moreover, EM methods are expensive, labor-intensive, and low-throughput. Additionally, EVs can only be distinguished if distinct shape differences are present [48].

1.2.1 HPLC-based Virus Particle Characterization

High performance liquid chromatography (HPLC) devices offer a modular and automated analytical platform for developing and establishing various analytical methods. Thanks to the platform's flexibility, these methods can be tailored to specific analytes and attributes for evaluation. Figure 1.3 provides a schematic of an HPLC device, illustrating its modular design with application-dependent options for the chromatographic column and detector modules in the detector train. HPLC applications typically involve chromatographic separation followed by the detection of the target analyte. The HPLC does sample management, solvent management and mixing, and enables the use of various detectors. Due to the pressurized and constant solvent flow, analyte separations in HPLCs are generally reliable. These devices are widely used in biopharmaceutical labs and are readily available, with experienced analytical staff usually present [49]. When equipped with an autosampler module and properly set up, the device can autonomously process many samples sequentially, limited only by the sample stability within the autosampler environment.

HPLC-based analytical characterization methods for VPs employ various strategies for separation and detection, depending on the specific analyte preparation and related challenges and requirements. The chromatographic separation should isolate the analyte from impurities that could impair detector signals. Separation methods might resolve different VP populations, allowing for individual analysis.

Table 1.2 provides an overview of published quantification methods for enveloped and non-enveloped VPs and VLPs established on HPLC devices. A variety of separation principles — reverse phase

chromatography (RP), anion exchange chromatography (AEX), SEC, and affinity chromatography — as well as a variety of detectors — UV, fluorescence (FLR), MALS — are used. Target analytes for quantification include whole VPs and VLPs, as well as viral proteins, for which a correlation factor (viral protein per VP or VLP) is used to determine the VP or VLP count.

Table 1.2: Overview of HPLC-based quantification methods of VPs, VLPs and viral proteins. Abbreviations: HA - hemagglutinin protein, LC - Liquid Chomatogrpahy, Lin. - Linearity, Prep - Preparation, Ref - Reference, SRID - single radial immunodiffusion, ex. - excitation, em. - emmission, inact. - inactivated, n.a. - not applied, n.e.r. - not explicitely reported. Manufacturer information: ATCC (Wesel, Germany), Millipore (Billerica, MA, USA), Sigma (St. Louis, MO, USA).

Virus/ Analyte	Sample Prep./ Labeling	LC	Detector	Limits/ Linearity	Reference virus preparation	Recovery/ Accuracy	Precision	other validation
Influenza, HA [50]	Protein solubilization, trypsin digestion, stabilization	RP	UV (215 nm)	LOD: n.e.r. Lin.: 8 to 62 $\frac{\mu g}{mL}$ HA	Sucrose-gradient purified, inact., SRID quantified	n.e.r.	RSD $\leq$ 7%	Transferability to other strains and production methods shown
Influenza, HA [51]	Protein solubilization, trypsin digestion, stabilization	RP	FLR (ex. 290 nm, em. 335 nm)	LOD: n.e.r. Lin.: 15.6 to 156 $\frac{\mu g}{mL}$ HA [a]	Sucrose-gradient purified, inact., SRID quantified	n.e.r.	n.e.r.	n.a.
Influenza, HA [52]	DTT reduction, stabilization by Tween (Sigma)	RP	FLR (ex 280 nm, em 335 nm)	LOD[b]: 0.25 to 1.0 $\frac{\mu g}{mL}$ LOQ[b]: 0.75 to 3.0 $\frac{\mu g}{mL}$ Lin.: 2.5 to 100 $\frac{\mu g}{mL}$ HA	Vaccine production bulk material, SRID quantified	RSD <10% compared to SRID	Repeatabiltiy RSD = 0.82%, intermediate precision RSD = 2.48%	n.a.
Chikungunya VLP, viral proteins [53]	Solubilization and stabilization of proteins by Zwittergent 3-12 (Millipore)	RP	FLR (ex. 280 nm, em. 350 nm)	LOD: n.e.r. Lin.: 5.1 to 120 $\frac{\mu g}{mL}$	n.e.r.	Recovery of structural proteins in relation to capsid protein: 96 to 106%	Peak area repeatability RSD <1.1% Intermediate precision RSD = 12%	Protein identification by SDS-PAGE and subsequent MALDI-ToF MS
Adenovirus type 5 [54]	n.a.	AEX	UV (260 nm)	LOD: n.e.r. Lin.: 2×10^{11} $\frac{VPs}{mL}$	CsCl purified, UV quantified in presence of SDS	n.e.r.	RSD: $\leq$ 5 to10%	Elution peak evaluation by UV and HPLC-SEC cross-analysis
Murine leukemia virus [55]	Nuclease treatment and concentration	AEX	UV (260 nm)	LOD: 4.7×10^{8} $\frac{VPs}{mL}$ Lin.: 3×10^{9} to 1×10^{11} $\frac{VPs}{mL}$	Sucrose cushion and SEC purified, nsEM-quantified	n.e.r.	Intraday precision RSD < 5%, Inter-day precision RSD < 10%	n.a.
Baculovirus [56]	SYBR Green I nucleic acid dye, incubation 2 h at 37 °C	AEX	FLR (ex. 479 nm, em. 520 nm)	LOD: 3×10^{7} $\frac{VPs}{mL}$ Lin.: 1×10^{8} to 5×10^{10} $\frac{VPs}{mL}$	Sucrose cushion purified BV, flow cytometer quantification	Spike accuracy: 78 to101%	intra-assay precision <10%, inter-assay precision <10%	Validation of incubation robustness and method specificity; peak identity confirmed by Western blot
Influenza [57]	n.a.	AEX	FLR (ex. 290 nm, em. 335 nm)	LOD: 2×10^{8} to 4×10^{9} $\frac{VPs}{mL}$ Lin.: 1×10^{9} to 1×10^{11} $\frac{VPs}{mL}$	Sucrose cushion purified, nsEM-quantified	n.e.r.	Intra-assay precision RSD <5-10%, Intermediate precision RSD <10-20%	Validation of specificity; method transferability for strains evaluated

continued on next page

Table1.2 – *continued from previous page*

Virus/ Analyte	Sample Prep./ Labeling	LC	Detector	Limits/ Linearity	Reference virus preparation	Recovery/ Accuracy	Precision	other validation
AAV, full/ empty capsids [58]	n.a.	AEX	FLR (ex. 280 nm, em. 348 nm)	LOD: n.e.r. Lin.: 5×10^{10} to 3×10^{13} $\frac{\text{VPs}}{\text{mL}}$	commercial AAV serotypes + CsCl gradient purified AAV serotypes	n.e.r.	only relative quantification (empty/full-ratio) was characterized	robustness regarding temperature, flow rate, pH; transferability incl. optimization for: AAV 1-3, 6, 8, 9
Reovirus [59]	n.a.	AEX	UV (260 nm)	LOD: 2.14×10^{11} $\frac{\text{VPs}}{\text{mL}}$ Lin.: 3×10^{11} to 2×10^{12} $\frac{\text{VPs}}{\text{mL}}$	chromatographic purification, UV quantified	Accuracy: 87 to100%	Intraday: RSD < 10%, interday: RSD < 15%	Specificity
Lentivirus vector [60]	n.a.	AEX	FLR (ex 290 nm, em 335 nm)	LOD: n.e.r. Lin.: 3×10^{8} to 1×10^{10} $\frac{\text{VPs}}{\text{mL}}$	n.e.r.	RSD compared to ELISA = 5.0%	Intra-assay: RSD < 5%, inter-assay: RSD < 5%	Peak identity confirmed by western blot
HIV VLP [61]	n.a.	SEC	UV (280 nm)	LOD: 7×10^{9} VP/mL Lin.: 2×10^{10} to 7×10^{10} $\frac{\text{VPs}}{\text{mL}}$	Density gradient or AEX-purified VLPs, NTA-quantified	n.e.r.	RSD <15%	Robustness against sample matrix variation and hcDNA
HIV VLP [61]	n.a.	SEC	MALS	LOD[c]: 6×10^{9} VP/mL Lin.: [c] 2×10^{10} to 7×10^{10} $\frac{\text{VPs}}{\text{mL}}$		n.e.r.	RSD <10%	
FMDV [62]	Nuclease treatment, VP recovery from emulsions	SEC	UV (254 nm)	LOD: 0.6 $\frac{\mu\text{g}}{\text{mL}}$	Nuclease treatment, buffer exchange	Spiking accuracy: within specified range (85 to 115%)	Intra-assay repeatability <10%, intermediate precision <10%	Linearity for typical PD samples
AAV, full/ empty capsids [63]	n.a.	Affinity	FLR (ex. 280 nm, em. 330 nm) UV[d]	LOD: n.e.r. LOQ: 6.1×10^{9} $\frac{\text{VPs}}{\text{mL}}$ Lin.: 7×10^{11} to 7×10^{12} $\frac{\text{VPs}}{\text{mL}}$	Chromatographic purification, SEC-MALS characterization	RMSE = 4.3%	RSD = 1.2%	Transferability evaluated, re-calibration for other strains needed
Adenovirus [64]	Nuclease treatmentment, dilution to 1×10^{11} $\frac{\text{VPs}}{\text{mL}}$	cGE	UV (214 nm)	LOD: n.e.r. Lin.: 5×10^{10} to 2×10^{11} $\frac{\text{VPs}}{\text{mL}}$	commercial Ad5 reference (ATCC)	Spiking accuracy: 95–110%	Repeatability: RSD <5%, intermediate precision: RSD <10%	Transferability evaluated; robustness shown

[a] Assuming the same mass-to-concentration calculation as in earlier publication of the same group [50].
[b] Depending on strain.
[c] Absolute MALS quantification numbers deviate by 0.5 logs.
[d] UV 260/280 for empty/full-ratio determination required to apply a full capsids dependent correction factor.

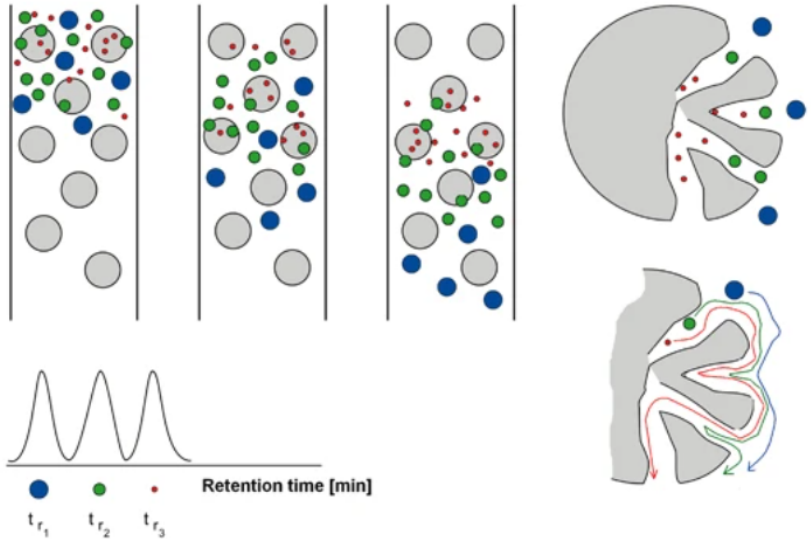

Figure 1.4: Schematic of SEC separation principle. Larger molecules are excluded from entering the pores and travel faster, while smaller molecules diffuse into the pores and experience a longer retention time, leading to separation. Figure sourced from [68], reproduced with permission from Springer Nature.

Reverse phase chromatography (RP) RP chromatography separates analytes based on their hydrophobicity in a polar environment. Organic solvents mixed with water are used as the mobile phase. This mobile phase compromises viral integrity, making RP chromatography unsuitable for characterizing whole VPs. Instead, RP is applied to quantify and characterize individual viral proteins. Viral proteins are solubilized and stabilized using agents such as detergents. The viral protein count per VP/VLP must be constant and known to derive a VP/VLP quantification. Separated viral proteins can be further characterized using methods such as MS and Western Blotting to identify proteins and characterize glycoprotein patterns.

Ion exchange chromatography (IEX) Enveloped VPs typically have an acidic Isoelectric point (IEP); however, the IEP cannot be accurately predicted or determined due to the heterogeneity of lipids and glycoproteins [65]. The resulting net negative charge at neutral pH can be utilized by binding to an AEX column. Analytical ion exchange chromatography (IEX) uses the bind-and-elute mode (BE-mode) in which analytes elute in order of their charge in an aqueous mobile phase. Typically, an increasing salt gradient is applied, leading to salt ions displacing bound analytes. However, reports show a strong binding of enveloped VPs, which are only eluted during CIP steps [38, 66].

Sufficiently high and robust recoveries are necessary for quantification purposes [67]; however, recoveries are rarely checked in evaluated publications. When checked, accuracy is evaluated by spiking studies, and statements about the recovery are concluded. Furthermore, binding of VPs to the stationary phase might impact viral integrity. This could affect the analytical result and is therefore not preferred for whole particle characterizations.

Size exclusion chromatography (SEC) In SEC, analytes are separated based on their hydrodynamic size without binding to the stationary phase. The separation principle is shown for analytes of three sizes in Figure 1.4, resulting in three retention times. Analytes diffuse in and out of the pores of

the stationary phase. Smaller analytes can access a larger pore volume, taking longer to diffuse out, which results in a retention effect. Consequently, larger analytes elute first. If nonspecific binding occurs, the separation and recovery of analytes might be compromised. The mobile phase should be designed to counteract these effects. SEC is considered a mild processing step due to the absence of interactions (ideally) and typically low flow rates. For preparative processes, this results in significant drawbacks, such as long processing times and low processable feed volumes. For analytical purposes, SEC separates VPs and VLPs from smaller impurities and enables comprehensive particle characterization. Most VPs, especially enveloped VPs, are larger than the mean pore diameter of analytical SEC columns and are thus excluded from diffusional pores. This size-based separation of VPs is not selective, and similarly sized impurities can be co-purified, potentially affecting detector signals later. Therefore, the purity and identity of the peak must be evaluated using online detectors or validated through orthogonal methods.

Other separation principles, such as capillary gel electrophoresis (cGE) and affinity chromatography are used, but not widely applied. CGE requires specialized equipment and its limited sample capacity results in a low sensitivity. Affinity chromatography is available only for a limited number of virus species, and identifying or developing new affinity targets is cumbersome.

High performance liquid chromatography (HPLC) detectors As shown in the HPLC schematic (Figure 1.3), multiple detectors can be used in the detector train, and different detectors are utilized depending on the application [69].

Ultraviolet (UV) UV detectors are the most widely used sensors in HPLC devices within biopharmaceutical laboratories. The UV detector provides absorption data for specific wavelengths or the entire UV spectrum. For particles such as VPs and VLPs, UV absorption is affected by light scattering effects. Therefore, the Lambert-Beer correlation of the UV extinction coefficient is not applicable for particle quantification. The measured UV signal for these particles is the light extinction, which is the sum of absorption and scattering effects at the specific wavelengths analyzed [70].

For spherical particles that are sufficiently small compared to the incident wavelength ($r \ll \lambda_0$), the Rayleigh approximation can be used to calculate a scattering correction factor [70, 71, 72]. This approximation correlates the intensity of scattered light with the wavelength, given by $I_{scattered} \propto \lambda^4$. Therefore, if a UV spectrum is acquired, wavelengths where only scattering effects occur can be used to estimate scattering effects at wavelengths of interest. Porterfield *et al.* demonstrate this approach for quantifying brom mosaic plant VPs, which are spherical, non-enveloped particles with a radius of 14 nm [70]. The Rayleigh approximation is only valid for particles that are sufficiently small compared to the wavelength ($r \ll \lambda_0$). For larger particles, such as most enveloped VPs, the Mie theory may be applied for UV excitation. However, Mie theory exhibits greater mathematical complexity and is limited to spherical particle geometries. Heterogeneity within enveloped VP preparations and the lack of suitable validation methods further hinder the application of a correction factor for enveloped VPs.

A linear correlation is still observed for VPs of various sizes, both with [50, 55, 60] and without envelope VPs [49, 54, 59, 62, 64]. These studies demonstrate a linear impact of the additional scattering effect depending on VP count. The observed linearity indicates that non-linear effects of light scattering (LS), described by the second virial coefficient A_2, are sufficiently small to be negligible within the concentration ranges studied. Either optimized buffer systems result in non-existent

particle-particle interaction, or particle concentrations are sufficiently low, likely due to dilution effects in chromatographic systems. Higher concentration ranges of VPs are not evaluated due to the lack of highly concentrated samples.

Fluorescence (FLR) FLR detectors measure the light emission of excited fluorophores. The intrinsic fluorescence of VPs originates from aromatic amino acids in proteins, most notably tryptophan. The fluorescence of membranes, carbohydrates, and DNA is essentially non-existent or too weak to be significant [73]. In comparison to UV, FLR detection of VPs and proteins achieves higher sensitivity, as observed by a general comparison of HPLC-based quantification methods in Table 1.2 and evaluated by several studies [52, 60]. However, the emission of fluorophores is influenced by the local environment, such as pH, polarity, and neighboring molecules, in complex and combined effects [74]. Consequently, VP heterogeneity, batch-to-batch variations due to upstream changes, and sample matrix alterations can impact the measured fluorescence emission per particle. For the precise quantification of adeno-associated viruses (AAVs) by FLR, a UV-based correction factor for the empty/full ratio of particles must be implemented [63]. Nevertheless, quantification capabilities of virus process samples at different stages have been demonstrated, with sufficient precision achieved in comparison to applied orthogonal quantification methods [52, 60]. Fluorescence labels, such as nucleic acid dyes, can further increase quantification sensitivity [56], but they also increase the method's complexity and thus the potential for errors and validation effort [75].

Multi-angle light scattering (MALS) MALS detectors are sensitive and powerful tools for characterizing macromolecules in terms of size, morphology, and concentration [76, 77]. VPs and VLPs typically fall well within the applicable size range, and MALS has been used for various characterization and quantification purposes [61, 78]. MALS detectors can be used in batch mode as well as in-line in preparative and analytical liquid chromatography (LC) systems, such as in an HPLC system combined with SEC or IEX as separation methods. However, a fair amount of pre-knowledge about the particles is required, which is not always available or feasible to determine for VPs due to the lack of well-characterized reference standards. In the case of non-enveloped and spherical VPs, parameters such as the refractive index and its increment can often be estimated [79]. For enveloped VPs, their heterogeneity, lipid content, and non-spherical and non-rigid morphology make estimations difficult. Estimations and models applied in MALS and LS calculations can be a source of error, as observed for the quantification of VLPs containing a lipid membrane [61]. For the same reasons, quantification via a refractive index (RI) detector is unfeasible.

1.2.2 Non-specific interactions of VPs in HPLC systems

VPs, as well as other large biomolecules, adhere non-specifically to various surfaces, mostly through electrostatic and hydrophobic interactions [80]. Both interaction types are facilitated by the presence of corresponding residues on biomolecules and surfaces and are influenced by environmental conditions. bear charged surface patches due to ionizable amino acid residues of surface proteins and, in the case of enveloped viruses, phospholipids containing carboxyl and amino groups, which protonate or deprotonate depending on the surrounding pH and ions [81, 82, 83]. At physiological pH, VPs typically have a net negative charge; however, positive patches remain [84]. The negatively charged nucleic acid core might also contribute to the overall negative net charge [81].

Metal surfaces typically consist of oxidized metal ions covered by hydroxyl groups in aqueous environments [85, 86]. Depending on pH and ionic strength, these metal surfaces typically carry a positive charge, promoting the adsorption of negative charged biomolecules [87, 88]. Electrostatic adsorption is also observed for borosilicate glass vials [89].

Hydrophobic attraction effects arise from minimizing the interfacial area between water and apolar surfaces, which is thermodynamically favorable. The proximity of two apolar areas reduces the water contact area between them, creating a local attraction effect [90]. Non-polar residues of amino acids exposed to the surrounding environment, the complex interplay between proteinaceous hydrophobic patches, which might or might not be hidden, and surrounding chemical environmental impacts such as kosmotropic effects strengthen hydrophobic interactions [90]. Hydrophobic interactions are reported for materials commonly used in biopharmaceutical processes and analytical methods [91] such as polypropylene (PP) [92], polyether ether ketone (PEEK) [93] and other polymers [94] and to a lesser extent glass surfaces [89, 92].

Adsorption can lead to recovery losses and molecular alterations, such as aggregation and denaturation [95]. Hydrophobic interaction might result in greater denaturation of biomolecules due to the unfolding of proteins to expose hydrophobic patches. In the case of VPs, this can lead to a loss of viral integrity and thus a loss of infectious particles. However, VPs also utilize non-specific interactions, such as with cellular lipid membranes, to initiate infection. For example, VSV uses electrostatic interaction for cell adhesion [96].

For analytical purposes, especially quantification approaches, recovery losses and analyte alterations that impede results must be minimized [97]. While buffer optimization aims to reduce non-specific binding on wettable parts of LC systems and secondary interactions within the column [98], the stability of sample storage, usually in glass or polymer vials at room temperature or in a cooled environment, is not addressed. The addition of additives into the samples, such as BSA and Tween, is commonly used [99, 100]. BSA acts as a universal suppressor of non-specific binding due to its ubiquitous adhesion to surfaces, thus shielding interaction sites [99]. Arginine has been used to suppress hydrophobic interactions through its affinity for the aromatic rings of amino acids, thereby successfully shielding against non-specific interactions [101].

1.3 Purification Process of Viral Particles

Contemporary, scalable purification processes for VLPs and VPs typically rely on a combination of chromatography and filtration steps, excluding the difficult-to-scale centrifugation steps [102, 103]. Detailed descriptions of the purification scheme and individual steps can be found in chapter 3. In brief, a generalized scheme consists of:

from USP: Cell culture bulk

1. Initial treatment as required:
   Cell disruption, Viral release, Nuclease treatment
2. Clarification
3. Capture
4. Polishing

5. Buffer exchange
6. If applicable: sterile filtration

to Fill & Finish: Drug substance

Cell disruption may be necessary for the release of intracellular VPs, common e.g. in poxviruses [104]. Techniques like freeze-thawing and sonication can disrupt cells to release VPs, but they also significantly increase impurity levels and may compromise viral integrity [105]. can adhere strongly to cellular components, and the addition of salts can reduce electrostatic interactions, facilitating their release for further processing [106]. Nuclease treatment enzymatically digests nucleic acid chains, reducing solution viscosity and aiding separation. This treatment can be repeated or applied at later purification stages, such as post-clarification [107]. During clarification, a coarse filter removes large particulate impurities like cell debris [108]. At the laboratory scale, low-speed centrifugation and two-step clarification may be employed [107]. For the capture step, bind-and-elute chromatography offers apparent advantages [109], effectively depleting impurities in the flow-through mode (FT-mode) while reducing processing volume. Further polishing reduces impurities, often using FT-mode chromatography such as SEC or filtration techniques like ultrafiltration/ diafiltration (UF/DF). These methods also facilitate simultaneous buffer exchange, allowing viral particles to be re-buffered into the formulation buffer.

During processing, the sensitivity of viral particles to environmental factors must be considered, particularly for enveloped particles, which are susceptible to inactivation from e.g. mechanical, thermal, and pH stress [105, 110, 111]. To minimize shear stress and accommodate the large size of viral particles, tailored methods such as low shear stress pumps or chromatographic stationary phases without diffusional limitations are employed.

1.4 Chromatographic Purification of Virus Particles

The size of VPs limits their diffusional mobility and accessibility to porous volumes, especially in the case of large enveloped VPs. Chromatographic methods and stationary phases are therefore tailored to utilize convection-driven media. These media are not limited by mass transfer rates, which are diffusion-dependent; instead, the convective flow facilitates the direct transport of VPs to the media surface. This enables faster processing flow rates, which is beneficial for the typically high volumetric VP preparations at the harvest stage. Examples of convection-driven media include membranes and monoliths, based on polymers, as stationary phases. Both are commonly chemically modified for application in various interaction types, such as affinity, hydrophobic interaction chromatography (HIC), IEX, and steric exclusion chromatography (SXC), for VP purification.

The size difference and limited diffusion of VPs can also be exploited by their exclusion from diffusional pores in SEC columns or restricted-access-media (RAM). RAM have a core-shell structure in which the shell sterically excludes particulates from the core, which provides binding sites for smaller impurities. Conventional, as well as VP-tailored chromatographic methods, are elaborated in depth in chapter 3.

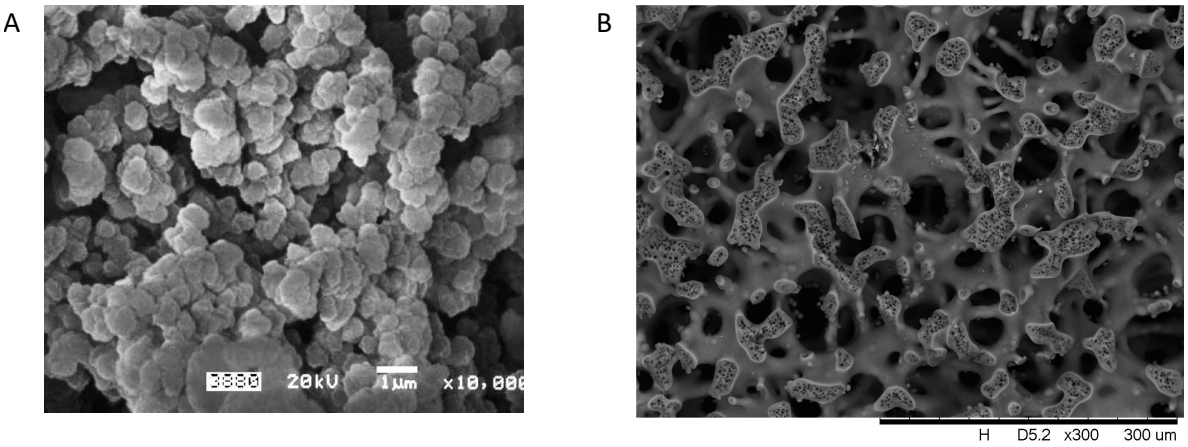

Figure 1.5: (A) EM picture of a polymer-based monolith, reprinted from with permission from Elsevier [112] (B) EM picture of a silica-based monolith, sourced from [113] under Creative Commons Attribution 4.0 International (CC BY 4.0) license (`https://creativecommons.org/licenses/by/4.0/`)

1.4.1 Monolith Adsorbers

Monoliths are advanced chromatographic stationary phases consisting of a single piece of highly porous material. They are categorized into two types: organic polymer-based and inorganic silica-based monoliths. Polymer monoliths are produced through a polymerization process, resulting in a globule-like structure with an interconnected network of convective flow channels as shown in the EM picture in Figure 1.5. In contrast, silica monoliths are created via a multistep sol-gel process, forming a bi-continuous skeleton with a hierarchical pore structure, including macropores and mesopores. Polymer monoliths are well-suited for separating large macromolecules such as proteins, viruses, and nucleic acids, while silica monoliths are more appropriate for small to medium-sized biomolecules and lower molecular weight compounds. [114, 115, 116]

Monoliths made from organic polymers, such as methacrylate, acrylamide, or styrene, are prepared as a single piece of highly porous material [115, 117]. Their manufacturing often involves a single-step molding process, typically based on thermally or radiation-initiated free-radical cross-linking polymerization reactions of monomers in the presence of porogenic solvents [118, 119]. This process is usually carried out directly within the chromatography column or mold. The bulk polymerization determines the structure of the resulting monolith, including its porosity, pore size, and pore size distribution, which are largely influenced by factors such as monomer composition, porogen content, and polymerization temperature [120, 121]. Polymeric monoliths have morphologies described as a globule-like, 3D adhered backbone, or as a 3D grid structure formed by agglomerated particles. After polymerization, the porogenic solvents and other soluble compounds are washed out. Functional groups can be introduced during the polymerization process through co-polymerization, or they can be grafted onto the pore surface after the basic structure is formed.

Monolithic columns offer significant benefits for purifying large particulates, such as VPs, due to their unique structural and hydrodynamic characteristics. Unlike traditional particle-based columns, where mass transfer is hindered by slow diffusion into pores, monoliths provide an interconnected network of large channels or macropores, ranging from 1 to 6 µm in mean diameter [122, 123]. This design promotes convective mass transport, allowing the mobile phase to flow directly through these

channels, delivering molecules to binding sites via bulk flow rather than diffusion. This results in dynamic binding capacity independent of flow rates. The high porosity of monoliths, up to 90 %, results in a low pressure drop, enabling high flow and thus rapid processing of large sample volumes [117]. Polymeric monoliths are mechanical and chemical stable to withstand harsh CIP solutions required for sanitization of active VP material [124].

Due to the polymerization of monoliths in their final form, monolith chromatography columns have to be prefabricated by the manufacturer and thus are limited in customer adjustability. The polymerization process also restricts the achievable thickness of the monolith geometry due to tight temperature controls required for a homogeneous pore size distribution. Therefore, hollow cylindrical monoliths utilizing an inward radial flow pattern are used, particularly for large scale applications [117]. The flow distribution in the column housing, the outer annulus volume before entering the monolith cylinder, and within the cylinder core is non-uniform along the cylinder's length. This non-uniformity leads to dispersion effects and peak tailing [122]. Another tailing effect observed in monoliths is caused by CE which can occur for large particles [125].

Convective entrapment (CE) CE refers to the retention of large particles in chromatographic stationary phases due to hydrodynamic effects and constraining channels, independent of resin interaction [125]. This effect is mainly observed with large bioparticles, such as open circular (OC) plasmid DNA (pDNA) [126, 127] and viruses [125]. The phenomenon occurs when particles are carried by the mobile phase into narrowing channels or constricted areas within the stationary phase that are too small for the particles to pass through. The dominant convective flow traps the particles at the constriction, and escape primarily depends on diffusion back into the flow path. The extent of CE is significantly influenced by several factors: Flow rate, where higher flow rates lead to more pronounced entrapment because convection into the constriction is high relative to diffusive escape, while decreasing the flow rate can facilitate diffusion and elution of trapped particles. Bioparticle size and shape are critical, as larger particles are more susceptible, and the OC isoform of pDNA is particularly prone due to its larger, more open structure compared to the supercoiled or linear forms. The stationary phase structure and void space size play a major role; entrapment occurs in materials with pores or channels that contain restrictions comparable in size to the bioparticle, including monoliths and perfusive resins, but also bead-based stationary phases if the interstitial space is small enough relative to the particle [127]. In case of OC pDNA, a sufficient recovery of ~15 kbp OC pDNA on monoliths requires channels of at least 4 µm.

Advection is the movement of a mass in a fluid, such as a particle in liquid, due to its surrounding fluid movement by e.g., convection. The balance between advective transport and diffusive motion of a particle is quantitatively described by the dimensionless Peclet number (Pe). In terms of entrapment, Pe is descriptive of predominant effects, with $Pe \gg 1$ indicating convection dominates and entrapment is expected, while $Pe \ll 1$ indicates the diffusion is sufficient for immediate escape of particles. The Peclet number in the context of CE can be defined as

$$Pe = \frac{\text{advective transport rate}}{\text{diffusive transport rate}} \equiv \frac{u_c L_c}{D}, \tag{1.1}$$

in which u_c is the flow velocity through the constriction, L_c is the characteristic diffusion path length the particle has to cover to diffuse out of the constriction site and D is the particle diffusion coefficient [125].

Using the Hagen-Poiseuille equation

$$Q = \frac{\pi \Delta p r^4}{8 \mu L}, \tag{1.2}$$

describing the volumetric flow Q in a cylindrical tube with radius r and the pressure difference Δp over the tube length L for a fluid with the dynamic viscosity μ, and inserting the alternative equation for Q using the tube's cross-section area A and the interstitial flow velocity u,

$$Q = uA = u\pi r^2, \tag{1.3}$$

results in:

$$u = \frac{\Delta p r^2}{8 \mu L} = \frac{\Delta p d^2}{32 \mu L}, \tag{1.4}$$

and hence the proportionality:

$$u \propto d^2, \quad \text{for } \Delta p = \text{constant}. \tag{1.5}$$

Setting up proportionalities for the constriction flow velocity u_c and the interstitial flow velocity u

$$u_c \propto d_c^2, \tag{1.6}$$

$$u = \frac{u_s}{\varepsilon} \propto d_p^2. \tag{1.7}$$

for which d_c is the diameter of the constriction site, u_s is the superficial flow velocity, ε the monolith porosity and d_p is the mean monolith channel diameter. Taking the ratio of both

$$\frac{u_c}{u} \approx \frac{d_c^2}{d_p^2}, \tag{1.8}$$

results in:

$$u_\mathrm{c} \approx \frac{u_\mathrm{s}}{\varepsilon} \left(\frac{d_\mathrm{c}}{d_\mathrm{p}} \right)^2. \tag{1.9}$$

Using Equation 1.9, an estimation of the Peclet magnitude can be derived utilizing following approximations: The diameter of constriction sites equals the bioparticle diameter ($d_\mathrm{c} = d_\mathrm{b}$), the characteristic diffusion path length equals the mean channel diameter ($L_\mathrm{c} = d_\mathrm{p}$).

$$Pe \approx \frac{u_\mathrm{s} d_\mathrm{b}^2}{\varepsilon D d_\mathrm{p}}. \tag{1.10}$$

1.5 Mechanistic Modeling of Chromatographic Monoliths

Mechanistic models of liquid chromatography system are *in silico* representations of physicochemical phenomena occurring in the chromatography column. It includes fluid dynamics, mass transfer phenomena, and adsorption thermodynamics. It's beneficial use for biopharmaceutical process science was shown for process optimization [128], robustness analysis [129], root-cause investigation [130] and scale-up [131]. The development and calibration of a mechanistic model necessitates a detailed consideration and representation of the actual physical and chemical phenomena within the process, thereby providing a deep understanding. The gain of process knowledge is a key driver for utilizing mechanistic modeling in areas like process optimization, characterization, and control [132].

In the following the focus is set on monolithic columns which are commonly applied in virus-based processes and utilized in chapter 5. Polymer-based monoliths are comprised of convective channels enabling a high mass transfer and are thus suitable for high volumetric flows as applied in VP purification processes [122, 133]. On the contrary, silica-based monoliths have a bimodal pore distribution including diffusional pores inaccessible for VPs [134]. Silica-based monoliths are thus not suitable for VPs purification and disregarded in the following.

1.5.1 Transport Model

Transport models in liquid chromatography describe the transport of solutes such as proteins or VPs in the mobile phase through a stationary phase. The typical chromatography column is a cylindrical volume of length L_{Col} which contains the porous stationary phase with its total porosity ε. The mobile phase is introduced in axial direction at the coordinate $x = 0$ by an external forced convection with the superficial flow velocity u_{s}, resulting in advection of all containing solutes $i \in [0, N_{\mathrm{comp}} - 1]$, with N_{comp} being the number of components considered in the model. In an ideal axial column, the flow is independent of the cross-sectional position. The solute transport can thus be described in a 2-dimensional space only depending on one spatial dimension in the column $x \in [0, L_{\mathrm{Col}}]$ and the time $t \in [0, T]$. Thereof the following equations are derived. The transport phenomena in a chromatography column are convection, dispersion effects and film mass transfers. Mass transfer resistance leads to peak broadening effects and delays the solutes' interaction with the stationary phase. In case of an ideal polymeric monolith, occurring phenomena are reduced as shown in Figure 1.6. The porosity of monoliths is composed of only convective flow through channels so that internal mass transfer resistances, except for the binding kinetics, are not existing. The external mass transfer describes the resistance of mass transfer between the mobile phase and the stagnant boundary layer surrounding the stationary phase. Monoliths are typically used for rapid flow rates due to their convection-driven structure. High convection decreases the thickness of the boundary layer, thereby reducing the mass transfer resistance associated with it. Studies examining different flow rates have shown that adsorption is independent of these rates, indicating that the external mass transfer rate is fast enough to be negligible [122, 135]. This is considered in the following, simplified transport model.

Equilibrium dispersive model (EDM) The equilibrium dispersive model (EDM) is a simplified transport model which originally lumps together all peak broadening effects (mass transfer resistances

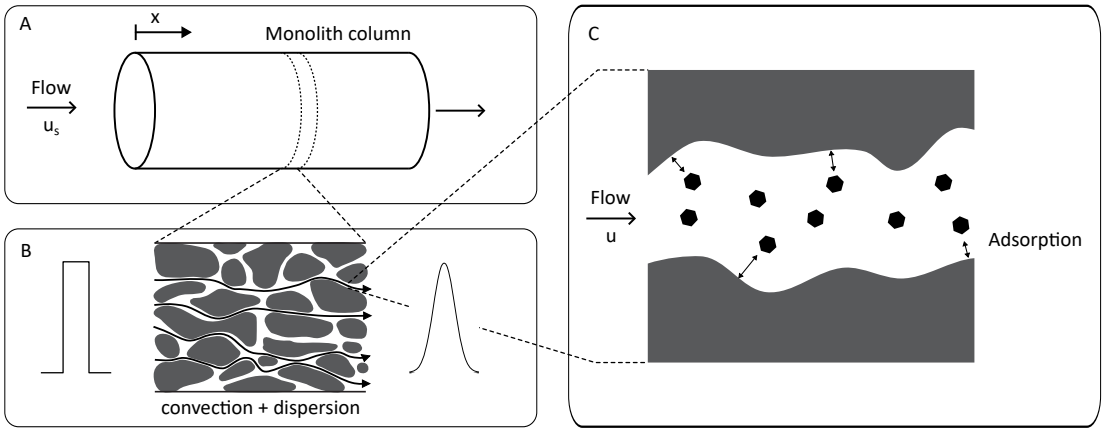

Figure 1.6: Illustrated mass transfer phenomena in an axial monolithic liquid chromatography column. (A) The mobile phase is introduced in the column at the column coordinate $x = 0$ by a forced convection with the superficial flow velocity u_s, resulting in advection of all containing solutes. (B) Convection pushes the mobile phase through the interstitial volume of the column. Axial dispersion effects such as eddy dispersion and flow distribution in the column housing result in peak broadening of rectangular applied peaks to Gaussian forms. (C) Depiction of the mass transfer of solutes to the stationary phase only influenced by adsorption kinetics due to high mass transfer rates in monoliths [122, 135].

and dispersion effects) occurring within the chromatography column into D_{app} [136]. This enables a direct linking of the adsorption model $\frac{\partial q}{\partial t}(x,t)$ to the transport model as shown in Equation 1.11. As elaborated in the previous paragraph, the influence of mass transfer resistances can be neglected, so, D_{app} can be replaced by D_{ax}, only accounting for eddy dispersion and longitudinal diffusion. Generally, the influence of band broadening effects of the monolith resin is low and outweighed by broadening effects introduced by the column housing, flow distribution and the chromatographic system [135].

$$\frac{\partial c_i\,(x,t)}{\partial t} = \underbrace{-u\,(t)\,\frac{\partial c_i\,(x,t)}{\partial x}}_{\text{Convection}} + \underbrace{D_{\text{ax}}\frac{\partial^2 c_i\,(x,t)}{\partial x^2}}_{\text{Dispersion}} - \underbrace{\frac{1-\varepsilon}{\varepsilon}\frac{\partial q_i\,(x,t)}{\partial t}}_{\text{Adsorption}} \tag{1.11}$$

The convection term represents the axial transport of applied solutes over the column driven by external forces. Convection in chromatography is applied by an external mass force described by the interstitial fluid velocity u, calculated by $u = \frac{u_s}{\varepsilon}$.

The model incorporates Danckwerts boundary conditions at both the inlet $x = 0$ and outlet $x = L_{\text{Col}}$. Equation 1.12 describes the inflow in which $c_{\text{in},i}$ is the administered concentration of component i. Equation 1.13 describes the outflow in which a zero concentration gradient is assumed.

$$\frac{\partial c_i\,(x=0,t)}{\partial x} = \frac{u\,(t)}{D_{\text{ax}}}\left(c_i\,(x=0,t) - c_{\text{in},i}\,(t)\right), \qquad \text{for } t > 0 \tag{1.12}$$

$$\frac{\partial c_i\,(x=L_{\text{Col}},t)}{\partial x} = 0\,, \qquad \text{for } t > 0 \tag{1.13}$$

Radial flow Temperature control constraints during the polymerization of polymer monoliths restrict the maximum thickness of cast monoliths in the manufacturing. Monolith columns of greater scale than small scale are thus cast as hollow tubes, enabling temperature and thus channel size control [117]. The typically inward directed, radial flow within the cylinders leads to an increase of flow velocity following the radial coordinate [128]. This effect is minimized in large-scale columns in which the outer and inner diameter of the monolith cylinders are sufficiently large and their difference sufficiently low. Furthermore, in polymer-based monoliths without diffusional pores, mass transfer was shown to be very fast and independent of flow velocity. Dispersion effects in monoliths are generally low and peak broadening effects are dominated by extra-column effects, in specific the distribution of flow along the longitudinal length of the cylindric stationary phase leads to a peak broadening [122]. It can therefore be sufficient to approximate an average velocity within the cylinder and regard the stationary phase as an axial flown through column [122].

1.5.2 Binding Models

The solutes' interaction with the stationary phase, in specific the adsorption and desorption, is described by a binding model. Depending on interaction type and level of detail various models exist taking into account local environment factors manipulating the interaction such as pH or counter-ion concentration.

Langmuir model The Langmuir isotherm is an early and simple adsorption model, formulated initially for gas molecule adsorption on a solid surface by Langmuir in 1916 [137]. An ideal solution is regarded in which a solute P adsorbs to a surface with the rate k_{ads}. Adsorbed solutes build a monolayer without solute-solute interaction. The desorption of adsorbed solutes, P_{ads} follows the rate k_{des}. The equilibration, shown in Equation 1.14 is not influenced by solvent effects [138].

$$\text{P} \underset{k_{\text{des}}}{\overset{k_{\text{ads}}}{\rightleftharpoons}} \text{P}_{\text{ads}} \tag{1.14}$$

The rate of adsorption and desorption of each component i is equal at equilibriums stage. Adsorption is proportional to the component concentration in the mobile phase, c_i and free binding sites, $\bar{q}$. Desorption is proportional to the bound amount of the component i, q_i, resulting in equation

$$k_{\text{des},i}\, q_i(x,t) = k_{\text{ads},i}\, \bar{q}\, c_i(x,t)\,. \tag{1.15}$$

Utilizing $K_{\text{eq}} = \frac{k_{\text{ads},i}}{k_{\text{des},i}}$ and $\bar{q} = q_{\max} - \sum_j^n q_j(x,t)$, and assuming an equal saturation capacity q_{max} for all components, the competitive Langmuir isotherm [138, 139] is

$$\frac{q_i\,(x,t)}{q_{\max}} = \frac{K_{\text{eq},i}\, c_i\,(x,t)}{1 + \sum_j^n K_{\text{eq},j}\, c_j\,(x,t)}\,. \tag{1.16}$$

A first-order kinetic is commonly applied to describe the saturation dependency of the adsorption process [138, 140]. A multi-component form is shown in equation Equation 1.17.

$$\frac{\partial q_i\,(x,t)}{\partial t} = k_{ads,i}\; c_i \left(q_{\max} - \sum_{j=1}^{N_{\text{comp}}} q_j\,(x,t) \right) - k_{des,i}\; q_i\,(x,t) \qquad i = 1,\ldots,N_{\text{comp}} \tag{1.17}$$

N_{comp} in this case is the number of protein/ particle components. This form of Langmuir does not consider the influence of counterions. An extension for counterion dependency of the equilibrium rates to enable the application for IEX columns has been developed [141].

Steric Mass Action (SMA) isotherm The SMA isotherm, introduced by Brooks and Cramer in 1992, describes the interaction of solutes and counter-ions of a IEX system. The interaction is described as a stoichiometric exchange of ions on the surface of the stationary phase reaching an equilibrium [142]. The equilibrium equation is

$$\mathrm{P} + \nu_{\mathrm{p}}\,\mathrm{S}_{\mathrm{ads}} \underset{k_{\mathrm{des}}}{\overset{k_{\mathrm{ads}}}{\rightleftharpoons}} \mathrm{P}_{\mathrm{ads}} + \nu_{\mathrm{p}}\,\mathrm{S}\,, \tag{1.18}$$

in which a solute P, such as a protein, displaces the amount ν_{p} salt ions ($\mathrm{S}_{\mathrm{ads}}$), which are adsorbed to oppositely charged ligands on the stationary phase surface. The solute becomes bound on the resins surface ($\mathrm{P}_{\mathrm{ads}}$), and salt ions are released into the mobile phase (S). ν_{p} is the stoichiometric coefficient of solute P, derived from the effective binding charge number of the solute z_{p} and the counter-ion z_{s}: $\nu_{\mathrm{p}} = \frac{z_{\mathrm{p}}}{z_{\mathrm{s}}}$ [143].

In an aqueous environment such as IEX and when neglecting differences in electrochemical potentials of individual components, the change of bound solute can be described by an adsorption and desorption rate term using molar concentrations:

$$\frac{\partial q_i\,(x,t)}{\partial t} = k_{\mathrm{ads},i}\;\bar{q}_{\mathrm{s}}^{\,\nu_i}\,(x,t)\;\; c_{\mathrm{p},i}\,(x,t) - k_{\mathrm{des},i}\;q_i\,(x,t)\;\; c_0^{\,\nu_i}\,(x,t)\;, \tag{1.19}$$

in which q_i denotes the bound solute, $\bar{q}_{\mathrm{s}}$ the amount of counterions on available binding sites, $c_{\mathrm{p},i}$ the concentration of component i in the stagnant volume which equals c_i for ideal monoliths at fast flow rates, and c_0 concentration of counterions in the mobile phase.

The electrochemical neutrality on the stationary phase surface dictates

$$\bar{q}_{\mathrm{s}}\,(x,t) = \Lambda - \sum_{i=1}^{n} (\nu_i + \sigma_i)\; q_i\,(x,t) \tag{1.20}$$

in which the total amount of binding sites is represented as the total ionic capacity, Λ. Bound solutes q_i occupy binding sites characterized by their stoichiometric coefficient ν_i and their shielding coefficient σ_i. The latter represents unavailable binding sites due to steric hindrance of bound solutes. Equation 1.20 into Equation 1.19 results in:

$$\frac{\partial \mathrm{q}_i^{\mathrm{SMA}}(x,t)}{\partial t} = k_{\mathrm{ads},i}\, c_{\mathrm{p},i} \left(\Lambda - \sum_{j=1}^{N_{\mathrm{comp}}-1} \left(\nu_j + \sigma_j\right)\, q_j^{\mathrm{SMA}}(x,t) \right)^{\nu_i} - k_{\mathrm{des},i}\, \mathrm{q}_i^{\mathrm{SMA}}(x,t)\, c_0^{\nu_i}(x,t)$$
$$\left(i = 1, \ldots, N_{\mathrm{comp}} - 1\right) \quad (1.21)$$

Utilizing the definitions for the equilibriums and kinetic coefficient,

$$K_{\mathrm{eq},i} = \frac{k_{\mathrm{ads},i}}{k_{\mathrm{des},i}} \quad (1.22)$$

$$k_{\mathrm{kin},i} = \frac{1}{k_{\mathrm{des},i}} \quad (1.23)$$

the kinetic form of the SMA isotherm is derived:

$$\frac{\partial \mathrm{q}_i^{\mathrm{SMA}}(x,t)}{\partial t} = \frac{1}{k_{\mathrm{kin},i}} \left(K_{\mathrm{eq},i}\, c_{\mathrm{p},i} \left(\Lambda - \sum_{j=1}^{N_{\mathrm{comp}}-1} \left(\nu_j + \sigma_j\right)\, q_j^{\mathrm{SMA}}(x,t) \right)^{\nu_i} - \mathrm{q}_i^{\mathrm{SMA}}(x,t)\, c_0^{\nu_i}(x,t) \right)$$
$$\left(i = 1, \ldots, N_{\mathrm{comp}} - 1\right) \quad (1.24)$$

References

[1] S. J. Flint, V. R. Racaniello, G. F. Rall, T. Hatziioannou, and A. M. Skalka. *Principles of Virology*. The Biomedical & Life Sciences Collection. ASM Press, 2020. DOI: 10.69645/wmlg1047.

[2] J. Lederberg. "Pandemic as a Natural Evolutionary Phenomenon". In: *Social Research* 55.3 (1988), pp. 343–359. URL: https://www.jstor.org/stable/40970507 (visited on 04/26/2025).

[3] S. Manrubia and E. Lazaro. "Viral Evolution". In: *Physics of Life Reviews* 3.2 (June 2006), pp. 65–92. DOI: 10.1016/j.plrev.2005.11.002.

[4] X. Sun, T. Tian, Y. Lian, and Z. Cui. "Current Advances in Viral Nanoparticles for Biomedicine". In: *ACS Nano* 18.50 (Dec. 17, 2024), pp. 33827–33863. DOI: 10.1021/acsnano.4c13146.

[5] E. Stavrakaki, A. Everts, B. G. Van Den Hoogen, and M. L. Lamfers. "The 16th International Oncolytic Virus Conference: Advancing Oncolytic Virotherapy by Balancing Anti-Tumor and Anti-Viral Immunity". In: *Molecular Therapy Oncology* 33.1 (Mar. 2025), p. 200950. DOI: 10.1016/j.omton.2025.200950.

[6] F. Arabi, V. Mansouri, and N. Ahmadbeigi. "Gene Therapy Clinical Trials, Where Do We Go? An Overview". In: *Biomedicine & Pharmacotherapy* 153 (Sept. 2022), p. 113324. DOI: 10.1016/j.biopha.2022.113324.

[7] T. Matos, D. Hoying, A. Kristopeit, M. Wenger, and J. Joyce. "Continuous Multi-Membrane Chromatography of Large Viral Particles". In: *Journal of Chromatography A* 1705 (2023), p. 464194. DOI: 10.1016/j.chroma.2023.464194.

[8] S. A. Sripada. "Advances and Opportunities in Process Analytical Technologies for Viral Vector Manufacturing". In: *Biotechnology Advances* 74 (2024), p. 108391. DOI: 10.1016/j.biotechadv.2024.108391.

[9] A. Schimek, J. K. M. Ng, and J. Hubbuch. "Navigating the Purification Process: Maintaining the Integrity of Replication-Competent Enveloped Viruses". In: *Vaccines* 13.5 (5 2025), p. 444. DOI: 10.3390/vaccines13050444.

[10] M. O. Mohsen and M. F. Bachmann. "Virus-like Particle Vaccinology, from Bench to Bedside". In: *Cellular & Molecular Immunology* 19.9 (Aug. 12, 2022), pp. 993–1011. DOI: 10.1038/s41423-022-00897-8.

[11] M. Saxena, S. H. Van Der Burg, C. J. M. Melief, and N. Bhardwaj. "Therapeutic Cancer Vaccines". In: *Nature Reviews Cancer* 21.6 (June 2021), pp. 360–378. DOI: 10.1038/s41568-021-00346-0.

[12] D. L. Bartlett, Z. Liu, M. Sathaiah, R. Ravindranathan, Z. Guo, Y. He, and Z. S. Guo. "Oncolytic Viruses as Therapeutic Cancer Vaccines". In: *Molecular Cancer* 12.1 (2013), p. 103. DOI: 10.1186/1476-4598-12-103.

[13] X. Li, Y. Le, Z. Zhang, X. Nian, B. Liu, and X. Yang. "Viral Vector-Based Gene Therapy". In: *International Journal of Molecular Sciences* 24.9 (Apr. 23, 2023), p. 7736. DOI: 10.3390/ijms24097736.

[14] M. Robert-Guroff. "Replicating and Non-Replicating Viral Vectors for Vaccine Development". In: *Current Opinion in Biotechnology* 18.6 (Dec. 2007), pp. 546–556. DOI: 10.1016/j.copbio.2007.10.010.

[15] M. bin Umair, F. N. Akusa, H. Kashif, Seerat-e-Fatima, F. Butt, M. Azhar, I. Munir, M. Ahmed, W. Khalil, H. Sharyar, S. Rafique, M. Shahid, and S. Afzal. "Viruses as Tools in Gene Therapy, Vaccine Development, and Cancer Treatment". In: *Archives of Virology* 167.6 (2022), pp. 1387–1404. DOI: 10.1007/s00705-022-05432-8.

[16] H. K. Ong, W. S. Tan, and K. L. Ho. "Virus like Particles as a Platform for Cancer Vaccine Development". In: *PeerJ* 5 (Nov. 15, 2017), e4053. DOI: 10.7717/peerj.4053.

[17] L. W. Seymour and K. D. Fisher. "Oncolytic Viruses: Finally Delivering". In: *British Journal of Cancer* 114.4 (Feb. 2016), pp. 357–361. DOI: 10.1038/bjc.2015.481.

[18] N. T. Martin and J. C. Bell. "Oncolytic Virus Combination Therapy: Killing One Bird with Two Stones". In: *Molecular Therapy* 26.6 (June 2018), pp. 1414–1422. DOI: 10.1016/j.ymthe.2018.04.001.

[19] D. K. Bhatt, L. Wekema, L. R. Carvalho Barros, R. Chammas, and T. Daemen. "A Systematic Analysis on the Clinical Safety and Efficacy of Onco-Virotherapy". In: *Molecular Therapy - Oncolytics* 23 (Dec. 2021), pp. 239–253. DOI: 10.1016/j.omto.2021.09.008.

[20] S. Brachelente, A. Galli, and T. Cervelli. "Yeast and Virus-like Particles: A Perfect or Imperfect Couple?" In: *Applied Microbiology* 3.3 (Sept. 2023), pp. 805–825. DOI: 10.3390/applmicrobiol3030056.

[21] R. Ma, Z. Li, E. A. Chiocca, M. A. Caligiuri, and J. Yu. "The Emerging Field of Oncolytic Virus-Based Cancer Immunotherapy". In: *Trends in Cancer* 9.2 (2023), pp. 122–139. DOI: 10.1016/j.trecan.2022.10.003.

[22] F. A. Murphy. *Vesicular Stomatitis Indiana Virus*. Virus Images. URL: https://www.utmb.edu/virusimages/VI/vesicular-stomatitis-indiana-virus (visited on 04/29/2025).

[23] T. Ogino and T. J. Green. "RNA Synthesis and Capping by Non-segmented Negative Strand RNA Viral Polymerases: Lessons From a Prototypic Virus". In: *Frontiers in Microbiology* 10 (July 10, 2019). DOI: 10.3389/fmicb.2019.01490.

[24] G. J. Letchworth, L. L. Rodriguez, and J. D. C. Barrera. "Vesicular Stomatitis". In: *The Veterinary Journal* 157.3 (1999), pp. 239–260. DOI: 10.1053/tvjl.1998.0303.

[25] I. S. Novella. "Contributions of Vesicular Stomatitis Virus to the Understanding of RNA Virus Evolution". In: *Current Opinion in Microbiology* 6.4 (Aug. 2003), pp. 399–405. DOI: 10.1016/S1369-5274(03)00084-5.

[26] D. R. Amor and J. Fort. "Virus Infection Speeds: Theory versus Experiment". In: *Physical Review E* 82.6 (Dec. 2010), p. 061905. DOI: 10.1103/PhysRevE.82.061905.

[27] P. Gadaleta, M. Vacotto, and F. Coulombié. "Vesicular Stomatitis Virus Induces Apoptosis at Early Stages in the Viral Cycle and Does Not Depend on Virus Replication". In: *Virus Research* 86.1–2 (June 2002), pp. 87–92. DOI: 10.1016/S0168-1702(02)00049-7.

[28] S. A. Kopecky, M. C. Willingham, and D. S. Lyles. "Matrix Protein and Another Viral Component Contribute to Induction of Apoptosis in Cells Infected with Vesicular Stomatitis Virus". In: *Journal of Virology* 75.24 (Dec. 15, 2001), pp. 12169–12181. DOI: 10.1128/jvi.75.24.12169-12181.2001.

[29] P. Ge, J. Tsao, S. Schein, T. J. Green, M. Luo, and Z. Hong Zhou. "Cryo-EM Model of the Bullet-Shaped Vesicular Stomatitis Virus". In: *Science* 327.5966 (2010), pp. 689–693. DOI: 10.1126/science.1181766.

[30] D. F. Stojdl, B. Lichty, S. Knowles, R. Marius, H. Atkins, N. Sonenberg, and J. C. Bell. "Exploiting Tumor-Specific Defects in the Interferon Pathway with a Previously Unknown Oncolytic Virus". In: *Nature Medicine* 6.7 (July 2000), pp. 821–825. DOI: 10.1038/77558.

[31] E. Hastie and V. Z. Grdzelishvili. "Vesicular Stomatitis Virus as a Flexible Platform for Oncolytic Virotherapy against Cancer". In: *Journal of General Virology* 93.12 (2012), pp. 2529–2545. DOI: 10.1099/vir.0.046672-0.

[32] C. Dold, C. Rodriguez Urbiola, G. Wollmann, L. Egerer, A. Muik, L. Bellmann, H. Fiegl, C. Marth, J. Kimpel, and D. von Laer. "Application of Interferon Modulators to Overcome Partial Resistance of Human Ovarian Cancers to VSV-GP Oncolytic Viral Therapy". In: *Molecular Therapy Oncolytics* 3 (2016), p. 16021. DOI: 10.1038/mto.2016.21.

[33] A. Muik, L. J. Stubbert, R. Z. Jahedi, Y. Geiß, J. Kimpel, C. Dold, R. Tober, A. Volk, S. Klein, U. Dietrich, B. Yadollahi, T. Falls, H. Miletic, D. Stojdl, J. C. Bell, and D. Von Laer. "Re-Engineering Vesicular Stomatitis Virus to Abrogate Neurotoxicity, Circumvent Humoral Immunity, and Enhance Oncolytic Potency". In: *Cancer Research* 74.13 (July 1, 2014), pp. 3567–3578. DOI: 10.1158/0008-5472.CAN-13-3306.

[34] R. Tober, Z. Banki, L. Egerer, A. Muik, S. Behmüller, F. Kreppel, U. Greczmiel, A. Oxenius, D. von Laer, and J. Kimpel. "VSV-GP: A Potent Viral Vaccine Vector That Boosts the Immune Response upon Repeated Applications". In: *Journal of Virology* 88.9 (May 2014), pp. 4897–4907. DOI: 10.1128/JVI.03276-13.

[35] A. Muik, I. Kneiske, M. Werbizki, D. Wilflingseder, T. Giroglou, O. Ebert, A. Kraft, U. Dietrich, G. Zimmer, S. Momma, and D. von Laer. "Pseudotyping Vesicular Stomatitis Virus with Lymphocytic Choriomeningitis Virus Glycoproteins Enhances Infectivity for Glioma Cells and Minimizes Neurotropism". In: *Journal of Virology* 85.11 (June 2011), pp. 5679–5684. DOI: 10.1128/JVI.02511-10.

[36] M. Wu, E. Zhou, R. Sheng, X. Fu, J. Li, C. Jiang, and W. Su. "Defective Interfering Particles of Influenza Virus and Their Characteristics, Impacts, and Use in Vaccines and Antiviral Strategies: A Systematic Review". In: *Viruses* 14.12 (Dec. 2022), p. 2773. DOI: 10.3390/v14122773.

[37] R. Habisch, P. Neubauer, J. Soza-Ried, and E. Puschmann. "Repeated Harvest Enables Efficient Production of VSV-GP". In: *Frontiers in Bioengineering and Biotechnology* 12 (2024), p. 1505338. DOI: 10.3389/fbioe.2024.1505338.

[38] D. Sviben, D. Forcic, J. Ivancic-Jelecki, B. Halassy, and M. Brgles. "Recovery of Infective Virus Particles in Ion-Exchange and Hydrophobic Interaction Monolith Chromatography Is Influenced by Particle Charge and Total-to-Infective Particle Ratio". In: *Journal of Chromatography B* 1054 (2017), pp. 10–19. DOI: 10.1016/j.jchromb.2017.04.015.

[39] D. Xin, L. Kurien, K. Briggs, A. Schimek, R. Dambra, D. Hochdorfer, T. A. Arnouk, M. Brgles, S. Gautam, D. Hotter, J. Solzin, T. Kriehuber, J. Ashour, A. Vigil, M. Hawley, and X. He. "Characterization of VSV-GP Morphology by CryoEM Imaging and SEC-MALS". In: *Molecular Therapy Methods & Clinical Development* 33.1 (2025), p. 101429. DOI: 10.1016/j.omtm.2025.101429.

[40] E. Heilmann, J. Kimpel, S. Geley, A. Naschberger, C. Urbiola, T. Nolden, D. Von Laer, and G. Wollmann. "The Methyltransferase Region of Vesicular Stomatitis Virus L Polymerase Is a Target Site for Functional Intramolecular Insertion". In: *Viruses* 11.11 (Oct. 26, 2019), p. 989. DOI: 10.3390/v11110989.

[41] T. K. Soh and S. P. J. Whelan. “Tracking the Fate of Genetically Distinct Vesicular Stomatitis Virus Matrix Proteins Highlights the Role for Late Domains in Assembly”. In: *Journal of Virology* 89.23 (Dec. 2015). Ed. by D. S. Lyles, pp. 11750–11760. DOI: 10.1128/JVI.01371-15.

[42] A. D. Tustian and H. Bak. “Assessment of Quality Attributes for Adeno-Associated Viral Vectors”. In: *Biotechnology and Bioengineering* 118.11 (2021), pp. 4186–4203. DOI: 10.1002/bit.27905.

[43] H. Malenovska. “Virus Quantitation by Transmission Electron Microscopy, TCID50, and the Role of Timing Virus Harvesting: A Case Study of Three Animal Viruses”. In: *Journal of Virological Methods* 191.2 (Aug. 2013), pp. 136–140. DOI: 10.1016/j.jviromet.2013.04.008.

[44] J. Vlasak, V. M. Hoang, S. Christanti, R. Peluso, F. Li, and T. D. Culp. “Use of Flow Cytometry for Characterization of Human Cytomegalovirus Vaccine Particles”. In: *Vaccine* 34.20 (Apr. 2016), pp. 2321–2328. DOI: 10.1016/j.vaccine.2016.03.067.

[45] Y. Panyukov, I. Yudin, V. Drachev, E. Dobrov, and B. Kurganov. “The Study of Amorphous Aggregation of Tobacco Mosaic Virus Coat Protein by Dynamic Light Scattering”. In: *Biophysical Chemistry* 127.1 (Apr. 1, 2007), pp. 9–18. DOI: 10.1016/j.bpc.2006.11.006.

[46] P. Kramberger, M. Ciringer, A. Štrancar, and M. Peterka. “Evaluation of Nanoparticle Tracking Analysis for Total Virus Particle Determination”. In: *Virology Journal* 9.1 (Nov. 12, 2012), p. 265. DOI: 10.1186/1743-422X-9-265.

[47] C. Fernandes, A. T. Persaud, D. Chaphekhar, J. Burnie, C. Belanger, V. A. Tang, and C. Guzzo. “Flow Virometry: Recent Advancements, Best Practices, and Future Frontiers”. In: *Journal of Virology* 99.2 (Jan. 2025), e01717–24. DOI: 10.1128/jvi.01717-24.

[48] A. D. Minh and A. A. Kamen. “Critical Assessment of Purification and Analytical Technologies for Enveloped Viral Vector and Vaccine Processing and Their Current Limitations in Resolving Co-Expressed Extracellular Vesicles”. In: *Vaccines* 9.8 (2021), p. 823. DOI: 10.3390/vaccines9080823.

[49] A. H. Ali. “High-Performance Liquid Chromatography (HPLC): A Review”. In: *Annals of Advances in Chemistry* 6.1 (June 2022), pp. 010–020. DOI: 10.29328/journal.aac.1001026.

[50] J. Kapteyn, M. Saidi, R. Dijkstra, C. Kars, J. Tjon, G. Weverling, M. Devocht, R. Kompier, B. Vanmontfort, and J. Guichoux. “Haemagglutinin Quantification and Identification of Influenza A&B Strains Propagated in PER.C6® Cells: A Novel RP-HPLC Method”. In: *Vaccine* 24.16 (Apr. 12, 2006), pp. 3137–3144. DOI: 10.1016/j.vaccine.2006.01.046.

[51] J. C. Kapteyn, A. M. Porre, E. J. P. de Rond, W. B. Hessels, M. A. Tijms, H. Kessen, A. M. E. Slotboom, M. A. Oerlemans, D. Smit, J. van der Linden, P. Schoen, and J. L. G. Thus. “HPLC-based Quantification of Haemagglutinin in the Production of Egg- and MDCK Cell-Derived Influenza Virus Seasonal and Pandemic Vaccines”. In: *Vaccine* 27.9 (Feb. 25, 2009), pp. 1468–1477. DOI: 10.1016/j.vaccine.2008.11.113.

[52] B. Lorbetskie, J. Wang, C. Gravel, C. Allen, M. Walsh, A. Rinfret, X. Li, and M. Girard. “Optimization and Qualification of a Quantitative Reversed-Phase HPLC Method for Hemagglutinin in Influenza Preparations and Its Comparative Evaluation with Biochemical Assays”. In: *Vaccine* 29.18 (Apr. 2011), pp. 3377–3389. DOI: 10.1016/j.vaccine.2011.02.090.

[53] A. Shytuhina, P. Pristatsky, J. He, D. R. Casimiro, R. M. Schwartz, V. M. Hoang, and S. Ha. "Development and Application of a Reversed-Phase High-Performance Liquid Chromatographic Method for Quantitation and Characterization of a Chikungunya Virus-like Particle Vaccine". In: *Journal of Chromatography A* 1364 (Oct. 17, 2014), pp. 192–197. DOI: 10.1016/j.chroma.2014.05.087.

[54] V. Klyushnichenko, A. Bernier, A. Kamen, and E. Harmsen. "Improved High-Performance Liquid Chromatographic Method in the Analysis of Adenovirus Particles". In: *Journal of Chromatography B: Biomedical Sciences and Applications* 755.1–2 (May 2001), pp. 27–36. DOI: 10.1016/S0378-4347(00)00597-1.

[55] J. Transfiguracion, H. Coelho, and A. Kamen. "High-Performance Liquid Chromatographic Total Particles Quantification of Retroviral Vectors Pseudotyped with Vesicular Stomatitis Virus-G Glycoprotein". In: *Journal of Chromatography B* 813.1–2 (Dec. 25, 2004), pp. 167–173. DOI: 10.1016/j.jchromb.2004.09.034.

[56] J. Transfiguracion, J. A. Mena, M. G. Aucoin, and A. A. Kamen. "Development and Validation of a HPLC Method for the Quantification of Baculovirus Particles". In: *Journal of Chromatography B* 879.1 (Jan. 1, 2011), pp. 61–68. DOI: 10.1016/j.jchromb.2010.11.011.

[57] J. Transfiguracion, A. P. Manceur, E. Petiot, C. M. Thompson, and A. A. Kamen. "Particle Quantification of Influenza Viruses by High Performance Liquid Chromatography". In: *Vaccine* 33.1 (Jan. 1, 2015), pp. 78–84. DOI: 10.1016/j.vaccine.2014.11.027.

[58] S. L. Khatwani, A. Pavlova, and Z. Pirot. "Anion-Exchange HPLC Assay for Separation and Quantification of Empty and Full Capsids in Multiple Adeno-Associated Virus Serotypes". In: *Molecular Therapy Methods & Clinical Development* 21 (June 11, 2021), pp. 548–558. DOI: 10.1016/j.omtm.2021.04.003.

[59] P. S. Chahal, J. Transfiguracion, A. Bernier, R. Voyer, M. Coffey, and A. Kamen. "Validation of a High-Performance Liquid Chromatographic Assay for the Quantification of Reovirus Particles Type 3". In: *Journal of Pharmaceutical and Biomedical Analysis* 45.3 (Nov. 2007), pp. 417–421. DOI: 10.1016/j.jpba.2007.06.025.

[60] J. Transfiguracion, M. Y. Tran, S. Lanthier, S. Tremblay, N. Coulombe, M. Acchione, and A. A. Kamen. "Rapid In-Process Monitoring of Lentiviral Vector Particles by High-Performance Liquid Chromatography". In: *Molecular Therapy Methods & Clinical Development* 18 (Sept. 11, 2020), pp. 803–810. DOI: 10.1016/j.omtm.2020.08.005.

[61] P. Steppert, D. Burgstaller, M. Klausberger, A. Tover, E. Berger, and A. Jungbauer. "Quantification and Characterization of Virus-like Particles by Size-Exclusion Chromatography and Nanoparticle Tracking Analysis". In: *Journal of Chromatography A* 1487 (Mar. 3, 2017), pp. 89–99. DOI: 10.1016/j.chroma.2016.12.085.

[62] M. A. Spitteler, A. Romo, N. Magi, M.-G. Seo, S.-J. Yun, F. Barroumeres, E. G. Régulier, and R. Bellinzoni. "Validation of a High Performance Liquid Chromatography Method for Quantitation of Foot-and-Mouth Disease Virus Antigen in Vaccines and Vaccine Manufacturing". In: *Vaccine* 37.36 (Aug. 23, 2019), pp. 5288–5296. DOI: 10.1016/j.vaccine.2019.07.051.

[63] J. Heckel, A. Martinez, C. Elger, M. Haindl, M. Leiss, R. Ruppert, C. Williams, J. Hubbuch, and T. Graf. "Fast HPLC-based Affinity Method to Determine Capsid Titer and Full/Empty Ratio of Adeno-Associated Viral Vectors". In: *Molecular Therapy - Methods & Clinical Development* 31 (Dec. 2023), p. 101148. DOI: 10.1016/j.omtm.2023.101148.

[64] E. Van Tricht, L. Geurink, H. Backus, M. Germano, G. W. Somsen, and C. E. Sänger–van De Griend. "One Single, Fast and Robust Capillary Electrophoresis Method for the Direct Quantification of Intact Adenovirus Particles in Upstream and Downstream Processing Samples". In: *Talanta* 166 (May 2017), pp. 8–14. DOI: 10.1016/j.talanta.2017.01.013.

[65] J. Heffron and B. K. Mayer. "Virus Isoelectric Point Estimation: Theories and Methods". In: *Applied and Environmental Microbiology* 87.3 (2020), e02319–20. DOI: 10.1128/aem.02319-20.

[66] D. Eckhardt, H. Dieken, D. Loewe, T. A. Grein, D. Salzig, and P. Czermak. "Purification of Oncolytic Measles Virus by Cation-Exchange Chromatography Using Resin-Based Stationary Phases". In: *Separation Science and Technology* 57.6 (2022), pp. 886–896. DOI: 10.1080/01496395.2021.1955267.

[67] FDA. *Analytical Procedures and Methods Validation for Drugs and Biologics*. 2015.

[68] K. Mojsiewicz-Pieńkowska. "Size Exclusion Chromatography a Useful Technique For Speciation Analysis of Polydimethylsiloxanes". In: *Green Chromatographic Techniques: Separation and Purification of Organic and Inorganic Analytes*. Ed. by Dr. Inamuddin and A. Mohammad. Dordrecht: Springer Netherlands, 2014, pp. 181–202. DOI: 10.1007/978-94-007-7735-4_9.

[69] K. Lothert, F. Eilts, and M. W. Wolff. "Quantification Methods for Viruses and Virus-like Particles Applied in Biopharmaceutical Production Processes". In: *Expert Review of Vaccines* 21.8 (Aug. 3, 2022), pp. 1029–1044. DOI: 10.1080/14760584.2022.2072302.

[70] J. Z. Porterfield and A. Zlotnick. "A Simple and General Method for Determining the Protein and Nucleic Acid Content of Viruses by UV Absorbance". In: *Virology* 407.2 (Nov. 25, 2010), pp. 281–288. DOI: 10.1016/j.virol.2010.08.015.

[71] A. J. Cox, A. J. DeWeerd, and J. Linden. "An Experiment to Measure Mie and Rayleigh Total Scattering Cross Sections". In: *American Journal of Physics* 70.6 (June 2002), pp. 620–625. DOI: 10.1119/1.1466815.

[72] A. Valentic, J. Müller, and J. Hubbuch. "Effects of Different Lengths of a Nucleic Acid Binding Region and Bound Nucleic Acids on the Phase Behavior and Purification Process of HBcAg Virus-Like Particles". In: *Frontiers in Bioengineering and Biotechnology* 10 (July 1, 2022). DOI: 10.3389/fbioe.2022.929243.

[73] "Protein Fluorescence". In: *Principles of Fluorescence Spectroscopy*. Ed. by J. R. Lakowicz. Boston, MA: Springer US, 2006, pp. 529–575. DOI: 10.1007/978-0-387-46312-4_16.

[74] "Solvent and Environmental Effects". In: *Principles of Fluorescence Spectroscopy*. Ed. by J. R. Lakowicz. Boston, MA: Springer US, 2006, pp. 205–235. DOI: 10.1007/978-0-387-46312-4_6.

[75] S. Chatterjee, R. Molenaar, L. Tromp, R. M. Wagterveld, H. D. W. Roesink, J. J. L. M. Cornelissen, M. M. A. E. Claessens, and C. Blum. "Optimizing Fluorophore Density for Single Virus Counting: A Photophysical Approach". In: *Methods and Applications in Fluorescence* 9.2 (Jan. 2021), p. 025001. DOI: 10.1088/2050-6120/abd8e4.

[76] P. J. Wyatt. "Multiangle Light Scattering: The Basic Tool for Macromolecular Characterization". In: *Instrumentation Science & Technology* 25.1 (Feb. 1997), pp. 1–18. DOI: 10.1080/10739149709351443.

[77] M. E. Shaheen, A. R. Ghazy, E.-R. Kenawy, and F. El-Mekawy. "Application of Laser Light Scattering to the Determination of Molecular Weight, Second Virial Coefficient, and Radius of Gyration of Chitosan". In: *Polymer* 158 (Dec. 5, 2018), pp. 18–24. DOI: 10.1016/j.polymer.2018.10.044.

[78] N. L. McIntosh, G. Y. Berguig, O. A. Karim, C. L. Cortesio, R. De Angelis, A. A. Khan, D. Gold, J. A. Maga, and V. S. Bhat. "Comprehensive Characterization and Quantification of Adeno Associated Vectors by Size Exclusion Chromatography and Multi Angle Light Scattering". In: *Scientific Reports* 11.1 (Feb. 4, 2021), p. 3012. DOI: 10.1038/s41598-021-82599-1.

[79] I. Makra, P. Terejánszky, and R. E. Gyurcsányi. "A Method Based on Light Scattering to Estimate the Concentration of Virus Particles without the Need for Virus Particle Standards". In: *MethodsX* 2 (Jan. 1, 2015), pp. 91–99. DOI: 10.1016/j.mex.2015.02.003.

[80] C. P. Gerba. "Applied and Theoretical Aspects of Virus Adsorption to Surfaces". In: *Advances in Applied Microbiology*. Ed. by A. I. Laskin. Vol. 30. Academic Press, Jan. 1984, pp. 133–168. DOI: 10.1016/S0065-2164(08)70054-6.

[81] A. Armanious, M. Aeppli, R. Jacak, D. Refardt, T. Sigstam, T. Kohn, and M. Sander. "Viruses at Solid–Water Interfaces: A Systematic Assessment of Interactions Driving Adsorption". In: *Environmental Science & Technology* 50.2 (Jan. 2016), pp. 732–743. DOI: 10.1021/acs.est.5b04644.

[82] I. H. Chennoufi, C. Zanane, T. Hakim, H. Zahir, F. Hamadi, A. El Ghmari, M. El Louali, and H. Latrache. "Estimation of the Negative Charge of Phi6 Virus and Its Variations with pH Using the Literature XPS Data". In: *Biophysica* 5.1 (1 Mar. 2025), p. 8. DOI: 10.3390/biophysica5010008.

[83] S. L. Penrod, T. M. Olson, and S. B. Grant. "Whole Particle Microelectrophoresis for Small Viruses". In: *Journal of Colloid and Interface Science* 173.2 (Aug. 1, 1995), pp. 521–523. DOI: 10.1006/jcis.1995.1354.

[84] B. Michen and T. Graule. "Isoelectric Points of Viruses". In: *Journal of Applied Microbiology* 109.2 (2010), pp. 388–397. DOI: 10.1111/j.1365-2672.2010.04663.x.

[85] G. A. Parks. "The Isoelectric Points of Solid Oxides, Solid Hydroxides, and Aqueous Hydroxo Complex Systems". In: *Chemical Reviews* 65.2 (Apr. 1, 1965), pp. 177–198. DOI: 10.1021/cr60234a002.

[86] N. M. Vlasova and O. V. Markitan. "Complexation on the Oxide Surfaces: Adsorption of Biomolecules from Aqueous Solutions: A Review". In: *Theoretical and Experimental Chemistry* 58.1 (Mar. 2022), pp. 1–14. DOI: 10.1007/s11237-022-09716-7.

[87] S. Fukuzaki, H. Urano, and K. Nagata. "Adsorption of Bovine Serum Albumin onto Metal Oxide Surfaces". In: *Journal of Fermentation and Bioengineering* 81.2 (Jan. 1996), pp. 163–167. DOI: 10.1016/0922-338X(96)87596-9.

[88] A. Takehara and S. Fukuzaki. "Effect of the Surface Charge of Stainless Steel on Adsorption Behavior of Pectin." In: *Biocontrol Science* 7.1 (2002), pp. 9–15. DOI: 10.4265/bio.7.9.

[89] J. Mathes and W. Friess. "Influence of pH and Ionic Strength on IgG Adsorption to Vials". In: *European Journal of Pharmaceutics and Biopharmaceutics*. Unmet Needs in Protein Formulation Science 78.2 (June 1, 2011), pp. 239–247. DOI: 10.1016/j.ejpb.2011.03.009.

[90] G. Sautrey. "An Update on Theoretical and Metrological Aspects of the Surface Hydrophobicity of Virus and Virus-Like Particles". In: *Advanced Biology* (2024), p. 2400221. DOI: 10.1002/adbi.202400221.

[91] C. Dika, M. H. Ly-Chatain, G. Francius, J. F. L. Duval, and C. Gantzer. “Non-DLVO Adhesion of F-specific RNA Bacteriophages to Abiotic Surfaces: Importance of Surface Roughness, Hydrophobic and Electrostatic Interactions”. In: *Colloids and Surfaces A: Physicochemical and Engineering Aspects*. Special Issue : IAP 2012 435 (Oct. 2013), pp. 178–187. DOI: 10.1016/j.colsurfa.2013.02.045.

[92] M. Duncan. “Influence of Surfactants upon Protein/Peptide Adsorption to Glass and Polypropylene”. In: *International Journal of Pharmaceutics* 120.2 (June 1995), pp. 179–188. DOI: 10.1016/0378-5173(94)00402-Q.

[93] P. Hambleton, W. John Lough, John Maltas, and Malcolm J. Mills. “Unusual Analyte Adsorption Effects on Inert Lc Components”. In: *Journal of Liquid Chromatography* 18.16 (Sept. 1, 1995), pp. 3205–3217. DOI: 10.1080/10826079508010445.

[94] D. R. Absolom, W. Zingg, and A. W. Neumann. “Protein Adsorption to Polymer Particles: Role of Surface Properties”. In: *Journal of Biomedical Materials Research* 21.2 (1987), pp. 161–171. DOI: 10.1002/jbm.820210202.

[95] J. D. Downey, A. M. Crean, and K. B. Ryan. “Impact of Protein Adsorption during Biopharmaceutical Manufacture & Storage”. In: *European Journal of Pharmaceutical Sciences* 209 (June 2025), p. 107071. DOI: 10.1016/j.ejps.2025.107071.

[96] F. A. Carneiro, M. L. Bianconi, G. Weissmüller, F. Stauffer, and A. T. Da Poian. “Membrane Recognition by Vesicular Stomatitis Virus Involves Enthalpy-Driven Protein-Lipid Interactions”. In: *Journal of Virology* 76.8 (Apr. 2002), pp. 3756–3764. DOI: 10.1128/jvi.76.8.3756-3764.2002.

[97] G. J. Guimaraes and M. G. Bartlett. “Managing Nonspecific Adsorption to Liquid Chromatography Hardware: A Review”. In: *Analytica Chimica Acta* 1250 (Apr. 2023), p. 340994. DOI: 10.1016/j.aca.2023.340994.

[98] R. Yumioka, H. Sato, H. Tomizawa, Y. Yamasaki, and D. Ejima. “Mobile Phase Containing Arginine Provides More Reliable SEC Condition for Aggregation Analysis”. In: *Journal of Pharmaceutical Sciences* 99.2 (Feb. 2010), pp. 618–620. DOI: 10.1002/jps.21857.

[99] S. I. Kovalchuk, N. A. Anikanov, O. M. Ivanova, R. H. Ziganshin, and V. M. Govorun. “Bovine Serum Albumin as a Universal Suppressor of Non-Specific Peptide Binding in Vials Prior to Nano-Chromatography Coupled Mass-Spectrometry Analysis”. In: *Analytica Chimica Acta* 893 (Sept. 17, 2015), pp. 57–64. DOI: 10.1016/j.aca.2015.08.027.

[100] E. K. Loveday, G. K. Zath, D. A. Bikos, Z. J. Jay, and C. B. Chang. “Screening of Additive Formulations Enables Off-Chip Drop Reverse Transcription Quantitative Polymerase Chain Reaction of Single Influenza A Virus Genomes”. In: *Analytical Chemistry* 93.10 (Mar. 16, 2021), pp. 4365–4373. DOI: 10.1021/acs.analchem.0c03455.

[101] T. Arakawa, K. Tsumoto, K. Nagase, and D. Ejima. “The Effects of Arginine on Protein Binding and Elution in Hydrophobic Interaction and Ion-Exchange Chromatography”. In: *Protein Expression and Purification* 54.1 (July 2007), pp. 110–116. DOI: 10.1016/j.pep.2007.02.010.

[102] L. Besnard, V. Fabre, M. Fettig, E. Gousseinov, Y. Kawakami, N. Laroudie, C. Scanlan, and P. Pattnaik. “Clarification of Vaccines: An Overview of Filter Based Technology Trends and Best Practices”. In: *Biotechnology Advances* 34.1 (2016), pp. 1–13. DOI: 10.1016/j.biotechadv.2015.11.005.

[103] M. M. Segura, A. A. Kamen, and A. Garnier. "Overview of Current Scalable Methods for Purification of Viral Vectors". In: *Viral Vectors for Gene Therapy*. Ed. by O.-W. Merten and M. Al-Rubeai. Vol. 737. Totowa, NJ: Humana Press, 2011, pp. 89–116. DOI: 10.1007/978-1-61779-095-9_4.

[104] K. L. Roberts and G. L. Smith. "Vaccinia Virus Morphogenesis and Dissemination". In: *Trends in Microbiology* 16.10 (2008), pp. 472–479. DOI: 10.1016/j.tim.2008.07.009.

[105] F. Eilts, J. J. Labisch, S. Orbay, Y. M. Harsy, M. Steger, F. Pagallies, R. Amann, K. Pflanz, and M. W. Wolff. "Stability Studies for the Identification of Critical Process Parameters for a Pharmaceutical Production of the Orf Virus". In: *Vaccine* 41.32 (2023), pp. 4731–4742. DOI: 10.1016/j.vaccine.2023.06.047.

[106] R. O'Keeffe, M. D. Johnston, and N. K. H. Slater. "The Primary Production of an Infectious Recombinant Herpes Simplex Virus Vaccine". In: *Biotechnology and Bioengineering* 57.3 (1998), pp. 262–271. DOI: 10.1002/(sici)1097-0290(19980205)57:3<262::aid-bit2>3.0.co;2-f.

[107] A. Bakhshizadeh Gashti, P. S. Chahal, B. Gaillet, and A. Garnier. "Purification of Recombinant Vesicular Stomatitis Virus-Based HIV Vaccine Candidate". In: *Vaccine* 41.13 (Mar. 2023), pp. 2198–2207. DOI: 10.1016/j.vaccine.2023.02.058.

[108] A. Negrete, A. Pai, and J. Shiloach. "Use of Hollow Fiber Tangential Flow Filtration for the Recovery and Concentration of HIV Virus-like Particles Produced in Insect Cells". In: *Journal of Virological Methods* 195 (2014), pp. 240–246. DOI: 10.1016/j.jviromet.2013.10.017.

[109] R. Kilgore, A. Minzoni, S. Shastry, W. Smith, E. Barbieri, Y. Wu, J. P. LeBarre, W. Chu, J. O'Brien, and S. Menegatti. "The Downstream Bioprocess Toolbox for Therapeutic Viral Vectors". In: *Journal of Chromatography A* 1709 (Oct. 2023), p. 464337. DOI: 10.1016/j.chroma.2023.464337.

[110] Weiss. "Influence of Process Conditions on Measles Virus Stability". In: *American Journal of Biochemistry and Biotechnology* 9.3 (2013), pp. 243–254. DOI: 10.3844/ajbbsp.2013.243.254.

[111] F. Higashikawa and L.-J. Chang. "Kinetic Analyses of Stability of Simple and Complex Retroviral Vectors". In: *Virology* 280.1 (2001), pp. 124–131. DOI: 10.1006/viro.2000.0743.

[112] I. Mihelič, D. Nemec, A. Podgornik, and T. Koloini. "Pressure Drop in CIM Disk Monolithic Columns". In: *Journal of Chromatography A* 1065.1 (Feb. 2005), pp. 59–67. DOI: 10.1016/j.chroma.2004.10.054.

[113] J. Mrowiec-Białoń, J. M. Malinowski, A. Ciemięga, and K. Maresz. "Comparative Study of Continuous-Flow Microreactors Based on Silica Monolith Smodified with Lewis Acid Centres". In: *Chemical and Process Engineering* 39.1 (2018). DOI: 10.24425/119097.

[114] M. González-González, J. González-Valdez, K. Mayolo-Deloisa, and M. Rito-Palomares. "Monolithic Chromatography: Insights and Practical Perspectives". In: *Journal of Chemical Technology & Biotechnology* 92.1 (Jan. 2017), pp. 9–13. DOI: 10.1002/jctb.5040.

[115] V. Rajamanickam, C. Herwig, and O. Spadiut. "Monoliths in Bioprocess Technology". In: *Chromatography* 2.2 (Apr. 17, 2015), pp. 195–212. DOI: 10.3390/chromatography2020195.

[116] G. Guiochon. "Monolithic Columns in High-Performance Liquid Chromatography". In: *Journal of Chromatography A* 1168.1–2 (Oct. 2007), pp. 101–168. DOI: 10.1016/j.chroma.2007.05.090.

[117] A. Podgornik, J. Jančar, I. Mihelič, M. Barut, and A. Strancar. "Large Volume Monolithic Stationary Phases: Preparation, Properties, and Applications." In: *Acta chimica Slovenica* 57.1 (2010), pp. 1–8.

[118] M. Merhar, A. Podgornik, M. Barut, M. Žigon, and A. Štrancar. "Methacrylate Monoliths Prepared from Various Hydrophobic and Hydrophilic Monomers – Structural and Chromatographic Characteristics". In: *Journal of Separation Science* 26.3–4 (Mar. 2003), pp. 322–330. DOI: 10.1002/jssc.200390038.

[119] I. Nischang. "Porous Polymer Monoliths: Morphology, Porous Properties, Polymer Nanoscale Gel Structure and Their Impact on Chromatographic Performance". In: *Journal of Chromatography A* 1287 (Apr. 2013), pp. 39–58. DOI: 10.1016/j.chroma.2012.11.016.

[120] A. Podgornik, A. Savnik, J. Jančar, and N. L. Krajnc. "Design of Monoliths through Their Mechanical Properties". In: *Journal of Chromatography A* 1333 (Mar. 2014), pp. 9–17. DOI: 10.1016/j.chroma.2014.01.038.

[121] A. Podgornik, M. Barut, A. Štrancar, D. Josić, and T. Koloini. "Construction of Large-Volume Monolithic Columns". In: *Analytical Chemistry* 72.22 (Nov. 1, 2000), pp. 5693–5699. DOI: 10.1021/ac000680o.

[122] R. Hahn, A. Tscheliessnig, P. Bauerhansl, and A. Jungbauer. "Dispersion Effects in Preparative Polymethacrylate Monoliths Operated in Radial-Flow Columns". In: *Journal of Biochemical and Biophysical Methods* 70.1 (2007), pp. 87–94. DOI: 10.1016/j.jbbm.2006.09.005.

[123] M. Š. Kodermac, S. Rotar, D. Dolenc, K. Božič, A. Štrancar, and U. Černigoj. "Grafting Chromatographic Monoliths with Charged Linear Polymers for Highly Productive and Selective Protein or Plasmid DNA Purification". In: *Separation and Purification Technology* 353 (Jan. 19, 2025), p. 128253. DOI: 10.1016/j.seppur.2024.128253.

[124] J. Vidič, A. Podgornik, J. Jančar, V. Frankovič, B. Košir, N. Lendero, K. Čuček, M. Krajnc, and A. Štrancar. "Chemical and Chromatographic Stability of Methacrylate-Based Monolithic Columns". In: *Journal of Chromatography A*. 2nd Summer School on Monolith Technology for Biochromatography, Bioconversion and Solid-Phase Synthesis 1144.1 (Mar. 2007), pp. 63–71. DOI: 10.1016/j.chroma.2006.11.030.

[125] E. I. Trilisky and A. M. Lenhoff. "Flow-dependent Entrapment of Large Bioparticles in Porous Process Media". In: *Biotechnology and Bioengineering* 104.1 (2009), pp. 127–133. DOI: 10.1002/bit.22370.

[126] N. Pavlin, U. Černigoj, M. Bavčar, T. Plesničar, J. Mavri, M. Zidar, M. Bone, U. K. Savič, T. Sever, and A. Štrancar. "Analytical Separation of Plasmid DNA Isoforms Using Anion Exchanging Chromatographic Monoliths with 6 µm Channels". In: *ELECTROPHORESIS* 44.24 (2023), pp. 1967–1977. DOI: 10.1002/elps.202300031.

[127] Š. Kralj, Š. M. Kodermac, I. Bergoč, T. Kostelec, A. Podgornik, A. Štrancar, and U. Černigoj. "Effect of Plasmid DNA Isoforms on Preparative Anion Exchange Chromatography". In: *ELECTROPHORESIS* 44.24 (2023), pp. 1953–1966. DOI: 10.1002/elps.202300035.

[128] C. Ladd Effio, T. Hahn, J. Seiler, S. A. Oelmeier, I. Asen, C. Silberer, L. Villain, and J. Hubbuch. "Modeling and Simulation of Anion-Exchange Membrane Chromatography for Purification of Sf9 Insect Cell-Derived Virus-like Particles". In: *Journal of Chromatography A* 1429 (Jan. 2016), pp. 142–154. DOI: 10.1016/j.chroma.2015.12.006.

[129] N. Jakobsson, M. Degerman, E. Stenborg, and B. Nilsson. "Model Based Robustness Analysis of an Ion-Exchange Chromatography Step". In: *Journal of Chromatography A* 1138.1 (Jan. 5, 2007), pp. 109–119. DOI: 10.1016/j.chroma.2006.10.057.

[130] G. Wang, T. Briskot, T. Hahn, P. Baumann, and J. Hubbuch. "Root Cause Investigation of Deviations in Protein Chromatography Based on Mechanistic Models and Artificial Neural Networks". In: *Journal of Chromatography A* 1515 (Sept. 2017), pp. 146–153. DOI: 10.1016/j.chroma.2017.07.089.

[131] E. Velali, B. Stute, M. Leuthold, and E. von Lieres. "Model-Based Performance Analysis and Scale-up of Membrane Adsorbers with a Cassettes Format Designed for Parallel Operation". In: *Chemical Engineering Science* 192 (Dec. 31, 2018), pp. 103–113. DOI: 10.1016/j.ces.2018.07.020.

[132] L. K. Shekhawat and A. S. and Rathore. "An Overview of Mechanistic Modeling of Liquid Chromatography". In: *Preparative Biochemistry & Biotechnology* 49.6 (July 3, 2019), pp. 623–638. DOI: 10.1080/10826068.2019.1615504.

[133] A. Jungbauer and R. Hahn. "Polymethacrylate Monoliths for Preparative and Industrial Separation of Biomolecular Assemblies". In: *Journal of Chromatography A* 1184.1–2 (Mar. 2008), pp. 62–79. DOI: 10.1016/j.chroma.2007.12.087.

[134] F. C. Leinweber and U. Tallarek. "Chromatographic Performance of Monolithic and Particulate Stationary Phases Hydrodynamics and Adsorption Capacity". In: *Journal of Chromatography A* 1006.1–2 (2003), pp. 207–228. DOI: 10.1016/s0021-9673(03)00391-1.

[135] R. Hahn, M. Panzer, E. Hansen, J. Mollerup, and A. Jungbauer. "Mass Transfer Properties of Monoliths". In: *Separation Science and Technology* 37.7 (May 28, 2002), pp. 1545–1565. DOI: 10.1081/SS-120002736.

[136] S. Golshan-Shirazi and G. Guiochon. "The Equilibrium-Dispersive Model of Chromatography". In: *Theoretical Advancement in Chromatography and Related Separation Techniques*. Ed. by F. Dondi and G. Guiochon. Dordrecht: Springer Netherlands, 1992, pp. 35–59. DOI: 10.1007/978-94-011-2686-1_2.

[137] I. Langmuir. "The Constitution and Fundamental Properties of Solids and Liquids. Part I. Solids." In: *Journal of the American Chemical Society* 38.11 (Nov. 1, 1916), pp. 2221–2295. DOI: 10.1021/ja02268a002.

[138] G. Guiochon. *Fundamentals of Preparative and Nonlinear Chromatography*. 2nd ed. Chantilly: Elsevier Science & Technology, 2006.

[139] F. Charton and R.-M. Nicoud. "Complete Design of a Simulated Moving Bed". In: *Journal of Chromatography A*. 1994 International Symposium on Preparative Chromatography 702.1 (May 1995), pp. 97–112. DOI: 10.1016/0021-9673(94)01026-B.

[140] Y. Liu and L. Shen. "From Langmuir Kinetics to First- and Second-Order Rate Equations for Adsorption". In: *Langmuir* 24.20 (Oct. 21, 2008), pp. 11625–11630. DOI: 10.1021/la801839b.

[141] V. Kumar, S. Leweke, E. von Lieres, and A. S. Rathore. "Mechanistic Modeling of Ion-Exchange Process Chromatography of Charge Variants of Monoclonal Antibody Products". In: *Journal of Chromatography A* 1426 (Dec. 24, 2015), pp. 140–153. DOI: 10.1016/j.chroma.2015.11.062.

[142] C. A. Brooks and S. M. Cramer. "Steric Mass-action Ion Exchange: Displacement Profiles and Induced Salt Gradients". In: *AIChE Journal* 38.12 (Dec. 1992), pp. 1969–1978. DOI: 10.1002/aic.690381212.

[143] J. M. Mollerup, T. B. Hansen, S. S. Frederiksen, and A. Staby. "Thermodynamic Modeling of Chromatographic Separation". In: *Advances in chromatography* 48 (2009), p. 57.

2 Thesis Outline

2.1 Research Proposal

It is projected that cancer will become the leading cause of premature deaths worldwide within the next decades [1]. Conventional anti-cancer treatments, such as surgery, chemotherapy, radiation therapy, and hormonal therapy have been applied for decades or even centuries. Despite ever-progressing refinements of these technologies and recent advancements, these conventional methods have a limited success rate or are accompanied by severe side effects [2]. Current approaches in cancer therapy are increasingly focused on redirecting the immune system to target tumor cells while simultaneously altering the tumor microenvironment to enhance treatment efficacy. Oncolytic viruses (OVs) are engineered to selectively infect and replicate within cancer cells. Through their replication cycle, they can induce lysis of the host tumor cells, releasing viral progeny and tumor antigens into the surrounding tissue. Immunologically 'cold' tumors are transformed into 'hot' ones while the tumor burden is reduced. Additional therapeutic cargos in OVs can further modulate the immune response. Another approach involving virus particles (VPs) are cancer vaccines which deliver gene cassettes encoding tumor-associated antigens. The expression and presentation of these antigens primes the immune system. Vesicular stomatitis virus (VSV) is a well researched enveloped virus which shows inherent oncolytic activity as wild type variant and is thus suitable as OV platform [3]. A pseudotyped variant, VSV-GP, was utilized in this study, which has a lower immunogenicity and enhanced oncolytic properties compared to the wild type [4]. The variant is currently being tested in a phase 1 clinical study [5] and thus bioprocessing optimizations to ensure efficient and robust manufacturing of high quality VPs become relevant.

The fragile lipid membrane of enveloped VPs requires mild and optimized bioprocesses to maintain particle integrity and preserve infectivity during manufacturing. High concentrations of infectious and replication-competent particles are essential to achieve the desired therapeutic effect on tumor cells. Despite the development of new analytical and preparative methods tailored for viral particle applications, challenges and gaps remain. It is difficult to transfer process knowledge between different virus strains due to their different properties. Process experience is therefore limited to specific virus strains. E.g, the impact of bioprocessing steps on the integrity of various virus strains is complex and not fully understood. Additionally, process development is limited by the lack of rapid and reliable analytical methods for efficient evaluation of process steps. This limitation impedes technological advancements such as mechanistic modeling, which demands reliable, in-depth characterization of process steps.

Enveloped VPs offer large capacities for transgenes due to their size and non-rigid envelope structure, however, the size and labile envelope structure also renders these particles susceptible to inactivation and degradation. Particularly OVs must maintain their integrity to remain infectious and replication-competent and thus effectively exert their therapeutic impact. Bioprocesses need to address these challenges while providing high titers for which conventional bioprocessing methods are typically

unsuitable. Although new and often VP-tailored methods have been developed, the experience for those are limited. In chapter 3 this thesis provides a comprehensive assessment of bioprocessing steps for replication-competent enveloped VPs emphasizing on the process impact towards viral integrity. Advanced analytical methods are required to evaluate particle quality during process development and are thus included in the assessment. Current knowledge gaps and analytical challenges impeding efficient process development are identified. The review offers an overview to support the development of efficient and robust bioprocesses for safe and effective therapeutics based on enveloped VPs.

Analytical tools are essential for process characterization, especially when online detectors are not informative or compromised by co-eluting impurities as e.g., in the capture step. Conventional methods for enveloped VP quantification are often imprecise and time-consuming, or dependent on specialized equipment and skilled operators. The iterative process development requires methods capable of handling large sample quantities while delivering robust and precise results suitable for yield calculations through mass balances. The quantification of an analyte requires either a highly specific measurement principle or the separation of the analyte from interfering impurities prior to measurement. In chapter 4, the analytical quantification gap for VSV-GP samples is addressed utilizing analytical SEC and UV for quantification without the need for specialized equipment. A thorough validation should ensure requirements for process development samples are met, and particle recoveries are sufficient and reliable for automated measurements to increase throughput. This method will enable in-depth process characterizations necessary for knowledge-based process development and technological advancements such as mechanistic models.

The capture step critically influences purification process robustness and performance, offering high optimization potential particularly for enveloped VPs, for which no specified capture method exists. IEX being highly flexible is routinely used as capture step and in combination with convective monoliths columns suitable to concentrate VPs from high-volume, low-concentration harvests containing high amounts of impurities. However, process knowledge is limited for monoliths which manifested itself in the occurrence of an unexpected fluid dynamic effect leading to peak tailing and subpopulation separation. In chapter 5, this effect is identified and characterized, which resulted in convective entrapment (CE) [6, 7] as most plausible cause. Gained knowledge was used to develop an *in silico* representation of CE to be used in mechanistic models. The established monolith model incorporating electrostatic interactions and the CE effect will enable the impact evaluation of CE and provide insights for the applicability of monoliths. The obtained process knowledge aids future process optimizations and the robust manufacturing of enveloped VPs using monoliths.

2.2 Manuscript Overview

This section provides an overview of the publications that constitute this thesis. The first publication reviews the *status quo* of purification process technologies for replication-competent enveloped VPs with focus on viral integrity. The second publication describes a rapid and precise quantification method for enveloped VPs. The third publication describes the mechanistic elution behavior of an enveloped VP, supported by *in silico* modeling. Both the electrostatic interactions and the elution delays due to convective entrapment were represented in the model. The manuscripts have been published internationally in established peer-reviewed journals and have not been used elsewhere as qualification to obtain an academic degree.

Chapter 3: Navigating the purification process: Maintaining the integrity of replication-competent enveloped viruses

Adrian Schimek, Judy King Man Ng, Jürgen Hubbuch

Vaccines, **2025**, Vol. 13(5), p. 444

This literature review comprehensively reviews the challenges and advancements in purification technologies for replication-competent enveloped VPs, which have therapeutic potential as oncolytic viruses or as cancer vaccines. The importance of maintaining viral integrity, both structural and functional, is highlighted and examined throughout the purification process, from cell culture harvest to final sterile filtration. Bioprocessing methods assessed include centrifugation, filtration, and chromatographic techniques. The focus is set on the sensitivity of enveloped VPs to environmental factors, shear forces, and non-specific adsorption, which can compromise their quality and production efficiency. The chapter is extended by an introduction of relevant analytical methods which are required to assess the VP quality and integrity. The methods include infectious titer assays, total VP quantification methods, and structural and compositional analysis. To cover the entire purification scheme, the impact of upstream considerations and formulation and storage strategies are assessed as well. This review guides researchers in developing robust and safe processes for complex and sensitive enveloped VPs. [8]

Chapter 4: An HPLC-SEC-based rapid quantification method for vesicular stomatitis VPs to facilitate process development

Adrian Schimek, Judy K.M. Ng, Ioannes Basbas, Fabian Martin, Dongyue Xin, David Saleh, Jürgen Hubbuch

Molecular Therapy Methods and Clinical Development, **2024**, Vol. 32 (2), p. 101252

This research article introduces a label-free, and high-precision analytical method for the quantification of a modified VSV, a replication-competent enveloped virus. The method employs an HPLC device equipped with an SEC chromatography column for separation of VPs and smaller impurities. UV detection is utilized for particle quantification and additionally MALS for particle characterization. The method enables same-day results with minimal hands-on time and validated precision for process development samples. The method development is elaborated which included buffer optimization and sample stability optimization, both needed to prevent non-specific interactions and establish high recoveries from the SEC column, as well as the sample vial. The developed method demonstrates high accuracy, repeatability, and intermediate precision, with a linear quantification range spanning more than two orders of magnitude. Its robustness was validated across various in-process sample matrices typically encountered during purification. The applicability was shown in the mass balancing of a chromatography step. This HPLC-SEC method provides a rapid total particle quantification that supports the advancement and commercialization of virus-based therapies through faster and informed process development decisions. [9]

Chapter 5: Mechanistic modeling of the elution behavior and convective entrapment of vesicular stomatitis virus on an ion exchange chromatography monolith

Adrian Schimek, Judy Ng, Federico Will, Jürgen Hubbuch

Journal of Chromatography A, **2025**, Vol. 1748, p. 465832

The IEX monolith chromatography step, which is used as capture step for VSV-GP, showed an unexpected peak tailing and subpopulation separation. This phenomenon could not be explained by anticipated fluid dynamics in chromatographic monoliths and particle-resin interactions. The most plausible cause was identified as convective entrapment effect, where large biomolecules are pushed into and temporarily retained in narrow constriction sites of the resin by advection, and only released by diffusion. Other factors were discussed and ruled out after extensive experimental characterization of the effect. The conventional SMA formalism was extended by incorporating a Langmuir approximation to describe the convective entrapment. The extended mechanistic model successfully reproduced the observed tailing and retention due to the CE. Model simulations showed the cause of partial separation of subpopulations due to different entrapment behaviors. It is concluded that this phenomenon has implications for both preparative scale-up and analytical method development for large biomolecules on convective media, highlighting the need to understand recovery losses and adjust CIP steps. Further studies could extend the model frame including flow rate to optimize processes for low CE. [10]

References

[1] B. Cao, F. Bray, A. Ilbawi, and I. Soerjomataram. "Effect on Longevity of One-Third Reduction in Premature Mortality from Non-Communicable Diseases by 2030: A Global Analysis of the Sustainable Development Goal Health Target". In: *The Lancet Global Health* 6.12 (Dec. 2018), e1288–e1296. DOI: 10.1016/S2214-109X(18)30411-X.

[2] A. Zafar, S. Khatoon, M. J. Khan, J. Abu, and A. Naeem. "Advancements and Limitations in Traditional Anti-Cancer Therapies: A Comprehensive Review of Surgery, Chemotherapy, Radiation Therapy, and Hormonal Therapy". In: *Discover Oncology* 16.1 (Apr. 2025), p. 607. DOI: 10.1007/s12672-025-02198-8.

[3] E. Hastie and V. Z. Grdzelishvili. "Vesicular Stomatitis Virus as a Flexible Platform for Oncolytic Virotherapy against Cancer". In: *Journal of General Virology* 93.12 (2012), pp. 2529–2545. DOI: 10.1099/vir.0.046672-0.

[4] A. Muik, L. J. Stubbert, R. Z. Jahedi, Y. Geiß, J. Kimpel, C. Dold, R. Tober, A. Volk, S. Klein, U. Dietrich, B. Yadollahi, T. Falls, H. Miletic, D. Stojdl, J. C. Bell, and D. Von Laer. "Re-Engineering Vesicular Stomatitis Virus to Abrogate Neurotoxicity, Circumvent Humoral Immunity, and Enhance Oncolytic Potency". In: *Cancer Research* 74.13 (July 1, 2014), pp. 3567–3578. DOI: 10.1158/0008-5472.CAN-13-3306.

[5] M. Porosnicu, A.-M. Quinson, K. Crossley, S. Luecke, and U. M. Lauer. "Phase I Study of VSV-GP (BI 1831169) as Monotherapy or Combined with Ezabenlimab in Advanced and Refractory Solid Tumors". In: *Future Oncology (London, England)* 18.24 (Aug. 2022), pp. 2627–2638. DOI: 10.2217/fon-2022-0439.

[6] E. I. Trilisky and A. M. Lenhoff. “Flow-dependent Entrapment of Large Bioparticles in Porous Process Media”. In: *Biotechnology and Bioengineering* 104.1 (2009), pp. 127–133. DOI: 10.1002/bit.22370.

[7] H. Koku, R. S. Maier, M. R. Schure, and A. M. Lenhoff. “Modeling of Dispersion in a Polymeric Chromatographic Monolith”. In: *Journal of Chromatography A* 1237 (May 2012), pp. 55–63. DOI: 10.1016/j.chroma.2012.03.005.

[8] A. Schimek, J. K. M. Ng, and J. Hubbuch. “Navigating the Purification Process: Maintaining the Integrity of Replication-Competent Enveloped Viruses”. In: *Vaccines* 13.5 (5 2025), p. 444. DOI: 10.3390/vaccines13050444.

[9] A. Schimek, J. K. M. Ng, I. Basbas, F. Martin, D. Xin, D. Saleh, and J. Hubbuch. “An HPLC-SEC-based Rapid Quantification Method for Vesicular Stomatitis Virus Particles to Facilitate Process Development”. In: *Molecular Therapy - Methods & Clinical Development* 32.2 (2024), p. 101252. DOI: 10.1016/j.omtm.2024.101252.

[10] A. Schimek, J. Ng, F. Will, and J. Hubbuch. “Mechanistic Modeling of the Elution Behavior and Convective Entrapment of Vesicular Stomatitis Virus on an Ion Exchange Chromatography Monolith”. In: *Journal of Chromatography A* 1748 (2025), p. 465832. DOI: 10.1016/j.chroma.2025.465832.

3 Navigating the Purification Process: Maintaining the Integrity of Replication-Competent Enveloped Viruses

Adrian Schimek[a], Judy King Man Ng[a], Jürgen Hubbuch[b]

[a] ViraTherapeutics GmbH, Bundesstraße 27, 6063 Rum, Austria

[b] Karlsruhe Institute of Technology, Institute of Process Engineering in Life Sciences, Section IV Biomolecular Separation Engineering, Fritz-Haber-Weg 2, 76131 Karlsruhe, Germany

Corresponding authors:

(J.N.) judy.ng@boehringer-ingelheim.com

(J.H.) juergen.hubbuch@kit.edu

First author contribution (A.S.):
Conceptualization, Writing - original draft, Writing - review and editing

Reproduced from:
A. Schimek, J. K. M. Ng, and J. Hubbuch. "Navigating the Purification Process: Maintaining the Integrity of Replication-Competent Enveloped Viruses". In: *Vaccines* 13.5 (5 2025), p. 444. DOI: 10.3390/vaccines13050444.

vaccines

MDPI

Review

Navigating the Purification Process: Maintaining the Integrity of Replication-Competent Enveloped Viruses

Adrian Schimek [1], Judy King Man Ng [1,*] and Jürgen Hubbuch [2,*]

[1] ViraTherapeutics GmbH, Bundesstraße 27, 6063 Rum, Austria
[2] Karlsruhe Institute of Technology, Institute of Process Engineering in Life Sciences, Section IV Biomolecular Separation Engineering, Fritz-Haber-Weg 2, 76131 Karlsruhe, Germany
* Correspondence: judy.ng@boehringer-ingelheim.com (J.K.M.N.); juergen.hubbuch@kit.edu (J.H.)

Abstract: Replication-competent virus particles hold significant therapeutic potential in application as oncolytic viruses or cancer vaccines. Ensuring the viral integrity of these particles is crucial for their infectivity, safety, and efficacy. Enveloped virus particles, in particular, offer large gene insert capacities and customizable target specificity. However, their sensitivity to environmental factors presents challenges in bioprocessing, potentially compromising high quality standards and cost-effective production. This review provides an in-depth analysis of the purification process steps for replication-competent enveloped virus particles, emphasizing the importance of maintaining viral integrity. It evaluates bioprocessing methods from cell culture harvest to final sterile filtration, including centrifugation, chromatographic, and filtration purification techniques. Furthermore, the manuscript delves into formulation and storage strategies necessary to preserve the functional and structural integrity of virus particles, ensuring their long-term stability and therapeutic efficacy. To assess the impact of process steps on particles and determine their quality and integrity, advanced analytical methods are required. This review evaluates commonly used methods for assessing viral integrity, such as infectious titer assays, total virus particle quantification, and structural analysis. By providing a comprehensive overview of the current state of bioprocessing for replication-competent enveloped virus particles, this review aims to guide researchers and industry professionals in developing robust and efficient purification processes. The insights gained from this analysis will contribute to the advancement of virus-based therapeutics, ultimately supporting the development of safe, effective, and economically viable treatments for various diseases.

Keywords: enveloped virus particles; replication-competent virus particles; virus purification; oncolytic viruses; cancer vaccines

Academic Editor: Ralph A. Tripp

Received: 10 March 2025
Revised: 14 April 2025
Accepted: 18 April 2025
Published: 23 April 2025

Citation: Schimek, A.; Ng, J.K.M.; Hubbuch, J. Navigating the Purification Process: Maintaining the Integrity of Replication-Competent Enveloped Viruses. *Vaccines* **2025**, *13*, 444. https://doi.org/10.3390/vaccines13050444

1. Introduction

Virus-based therapeutics is a rapidly evolving field, leveraging the unique properties of viruses to treat a variety of diseases. These therapeutics include vaccines against infectious diseases and cancer, gene therapies, and oncolytic therapies, each with its unique mechanism of action and therapeutic potential [1].

Vaccines, the most well-known type of virus-based therapeutics, use viruses or parts of the virus particle to stimulate the body's immune response. This concept of immunization to prevent disease dates back to the late 18th century when Edward Jenner developed the smallpox vaccine. Nowadays, conventional vaccines use live-attenuated or inactivated pathogenic viral particles or viral subunits. More recently developed vaccines, primarily due to the pandemic outbreak of coronavirus, utilize viral vectors or vehicles to deliver

the genetic information to cells for expression of viral subunits. Vaccination strategies that prevent oncovirus infections and, thereby, prevent infection-related cancers are considered cancer vaccinations as they mitigate the cause of tumor formation [2].

Gene therapies use virus particles (VPs) as vectors to deliver therapeutic genes into patients' cells, offering potential treatments for genetic disorders. The first approved gene therapy was alipogene tiparvovec, marketed as Glybera, approved in Europe in 2012 for the treatment of lipoprotein lipase deficiency [3]. Due to increased malignancy risks correlated to the replication-competency of viruses, VPs for gene therapies are engineered to transduce genes but not to replicate or regain replication-competency [4].

Oncolytic virus (OV) therapies, on the other hand, employ replication-competent viruses that preferentially affect cancer cells over normal cells, leading to the lysis of tumor cells and the stabilization and reduction of tumor progression [5]. Surface-presented proteins on VPs confer their tropism for specific cells in the host, and they can be redirected to other cells of interest by manipulation through genetic engineering of the virus. In addition to direct tumor cell lysis, OVs can stimulate the immune system to mount an anti-tumor response. This is achieved by modifying the tumor microenvironment from an immune-tolerant state to an inflamed state, enabling the immune system to effectively target and kill abnormal cells [6]. This mode of action is known as cancer vaccine treatment and can be enhanced by inserting transgenes into OVs to modify viral competencies or to specifically modulate the host response [7].

OVs should be capable of replicating within the host's cells while being attenuated to prevent pathological infection. The advantage of using replication-competent viruses is that they can amplify their numbers within the tumor, leading to the spread of virus infection and increased expression of transgenes. Replication-competency is a key factor for OVs to facilitate an enhanced therapeutic effect. The first FDA-approved OV therapy was Talimogene laherparepvec (T-VEC) in 2015 for the treatment of melanoma. T-VEC is an example of a replication-competent OV, which is a modified herpes simplex virus (HSV). In this example, neurovirulence genes were deleted to improve safety and efficacy, while added immunomodulating genes enhanced the host immune response [8].

Of the 103 active clinical studies involving OVs at the beginning of 2025, 65% were utilizing enveloped VPs (env. VPs) [9]. The outermost layer of env. VPs is a lipid bilayer derived from the host cell. This envelope embeds viral proteins, predominantly glycoproteins, equipping the VPs with special properties useful for therapeutic applications. Envelope proteins responsible for cell recognition and attachment can be replaced, modified, or added, generating pseudotyped viruses. This pseudotyping of replication-competent env. OVs are typically performed by genetic engineering. For non-enveloped VPs, the highly structured capsid layer constrains the incorporation or modification of surface structures. Capsid engineering requires more sophisticated techniques for tropism modifications without compromising the capsid integrity [10]. Another reason for the widespread use of env. VP for therapeutic applications is the large capacity for gene inserts [11]. However, envelope VPs have inherent drawbacks mostly related to their labile lipid envelope structure and its variability, presenting challenges for bioprocessing, which will be elaborated in Section 1.1.

Manufacturing requirements for advanced therapy medicinal products (ATMPs), which include virus-based therapies, are formulated by regulatory agencies in several guidelines [12,13]. Drug product quality attributes such as identity, purity, potency, and safety might be impacted by the bioprocess and need to be assessed to ensure a safe and effective application of viral therapeutics [14]. Therapeutic products based on replication-competent env. VPs constitute an especially labile drug substance. Live attenuated vaccines and oncolytic VPs both fall into this category, but oncolytic VPs are subject to stricter

specifications. This combination of sensitive drug substances and high requirements poses challenges to biomanufacturing and the purification process in particular.

This review focuses on the purification of replication-competent env. VPs with therapeutic applications. A selection of viruses within this scope that are currently in development is shown in Table 1. The status quo regarding current challenges, best practices, and the impact of process steps on the integrity of viral particles are evaluated using published references. However, reviews, case studies, and protocols are not always available for this set frame. The bioprocessing literature landscape for replication-deficient VPs and virus-like particles (VLPs), enveloped or non-env. VPs lacking therapeutic applications is substantially broader. For these products, analytical methods and purification processes are often simpler and more widely implemented due to their less complex particle structures and lower processing demands. However, where transferability between virus modalities could reasonably be inferred, references from other viral modalities were included and discussed.

Table 1. Selected DNA and RNA enveloped virus species currently in development as oncolytic virus or cancer vaccine.

	Virus Family	Particle Geometry	Genome Size	References
DNA viruses				
Herpes simplex virus (e.g., HSV-1)	Herpesviridae	155–240 nm, icosahedral	152 kb	[14]
Orf	Poxviridae	220–300 × 140–200 nm, ovoid shaped	140 kb	[15]
Vaccinia	Poxviridae	360 × 270 × 250 nm, brick shaped	190 kb	[14]
Myxoma	Poxviridae	320 × 235 nm, brick shaped	162 kb	[16,17]
RNA viruses				
Measle	Paramyxoviridae	100–300 nm, helical	15.8 kb	[14]
VSV (vesicular stomatitis virus)	Rhabdoviridae	70 × 200 nm, bullet shaped	11 kb	[14,18]
NDV (Newcastle disease virus)	Paramyxoviridae	100–500 nm, spherical	15 kb	[14,19]
LCMV (lymphocytic choriomeningitis virus)	Arenaviridae	78–90 nm, spherical	10.6 kb (segmented)	[20–22]
Influenza	Orthomyxoviridae	50–120 nm, spherical + longer filamentous forms	13.6 kb	[23,24]

1.1. Challenges in the Purification of Enveloped VPs

The complexity and non-rigid structure of the lipid membrane makes env. VPs vulnerable to perturbations of optimal environmental conditions, such as elevated temperatures [25–28], pH [26–29], osmolarity, and ionic strength [30]. Solvents, detergents [31,32], and excipients, such as arginine, might impede viral activity [33]. Previously exploited for viral inactivation [31], these conditions must be avoided in purification approaches. Furthermore, freeze/thaw-cycles (FT-cycles) [34,35] and shear forces [27,28,36] can cause VP degradation, leading to a decrease in infectious titers while increasing impurity content. Furthermore, sample handling and conditions during analytical methods can skew analytical results [28,37]. Forced degradation studies may help to find conditions that maintain viral integrity [27,38]. In general, the processing time and number of steps should be minimized. Purification processes might also be conducted in a cooled environment, but scalability issues are apparent [39].

The lipid membrane is variable in the composition of lipids and viral and host cell proteins (hcPs) [40]. Differences between virus species, strains, serotypes, and engineered virus variants are evident. Structural differences between virus types exist in size, morphology, and number of envelopes. The heterogeneity and complexity impede the development of efficient platform processes. Hence, process development efforts often start anew if process knowledge is not available or methods cannot be transferred. Genomic variants, established via evolution or genetic modifications might also require adaptations of process parameters [41]. Heterogeneity of VPs also prevails between production batches due to direct dependency on the cell culture, which is subject to variability and, furthermore, leads to heterogeneity of particles within the same batch [42–45].

In biopharmaceutical processes, impurities from cell culture, such as whole cells, hcPs, and host cell DNA (hcDNA), need to be depleted. However, during the budding of env. VPs, viral proteins as well as host cell-derived proteins are incorporated either in the tegument or the envelope [46–48]. Some incorporated cellular proteins may contribute to viral replication, which complicates the definition of the target product profile [46,49,50].

Impurities of the same size range as the VPs, such as extracellular vesicles (EVs), are more complex to separate [51]. EVs are membrane particles secreted naturally by cells in various sizes and with diverse enclosed content and membrane proteins. Viruses and EVs use overlapping cellular pathways which results in a high similarity between them regarding structure and protein/DNA content [52]. EVs' biological function and their role in viral infectious is a topic of ongoing research. Some EVs are shown to facilitate viral infection, while other EVs carry anti-viral features [53]. Increased EV production upon cell infection was observed for multiple virus strains [54]. This class of impurities is difficult to assess and it is unclear if it should be regarded as impurities [51].

By comparing the count of non-infectious VPs (non-inf. VP) to infectious (inf. VP), the particles-to-infectious unit ratio (P:IU) can be derived. Corresponding analytical methods are discussed in Section 2.1. A longstanding challenge in virus bioprocessing is the population of non-inf. VPs that usually predominate the material generated [55,56]. Non-inf. VPs lost, or never gained, their functional integrity due to malformations or errors in composition. The initial amount of non-inf. VPs is dependent on host cell type and upstream conditions [45,57,58]. In non-clinical efficacy and safety-studies, usually only infectious titers are reported. Correlations of side effects with non-inf. VPs can, therefore, not be made. At the same time, viral therapies have been applied and clinically tested for decades and are generally considered safe [59]. The practical approach to purifying VPs aims to minimize the presence of non-inf. VPs. From a processing perspective, EVs and all non-inf. VPs reduce the efficiency of purifying the desired infectious VPs [60].

Dosages of live attenuated vaccines are in the range of 10^4 to 10^8 infectious units (IUs) per dose [61], whereas the dosages for enveloped OVs reach up to 10^{11} IU per dose for intravenous applications [62,63]. High dosage requirements for OVs at the drug product level necessitate the processing of high volumes and efficient concentration due to usually lower titers at harvest level. During the whole bioprocess, the functional integrity which is key for the replication-competency and, thus, therapeutic effect, must remain intact. Ideally, non-infectious particles are reduced together with the depletion of immunogenic impurities such as hcP and hcDNA.

The size of env. VPs enables the insertion of transgenes for therapeutic applications but also increases their complexity and sensitivity to environmental stress and poses a challenge for the bioprocess. Conventional methods for processing biopharmaceuticals are primarily designed for protein molecules, like antibodies, which are significantly smaller in size. Other novel chromatographic and filtration approaches are used to overcome these size limitations. Experience and knowledge applying these methods are currently generated.

Unexpected effects arise, such as convective particle entrapment (see Section 7.2.3), multi-point binding of VPs (see Section 7.1.5) and irreversible time-dependent binding (see Section 7.1.5), for which mechanistic insights and solutions are needed.

In addition to the aforementioned challenges directly involved with the bioprocessing of env. VPs or VPs in general, analytical methods to evaluate VP preparation are limited. As further discussed in Section 2, the available analytical panel lacks accuracy, high throughput, and quick turnover time.

1.2. General Purification Scheme for Therapeutic Enveloped VPs

Replication-competent VPs are propagated by infection of permissive production cell lines. Sophisticated bioreactors, simple shake flasks, or supports for adherent cell lines are used for cell culture in which the cells are provided with the necessary nutrients and conditions to grow and produce. Once the cells have reached a target density, they are infected with a replication-competent virus at a specified multiplicity of infection (MOI) ratio. The virus uses the cells' machinery to replicate itself, producing virus progeny.

A general purification scheme for VPs intended for clinical grade material production, as shown in Figure 1, is the following: clarification, capture, polishing, and sterile filtration. Further unit operations may be included as required, dependent on the virus life cycle, harvest strategy for the VPs, and target purification requirements.

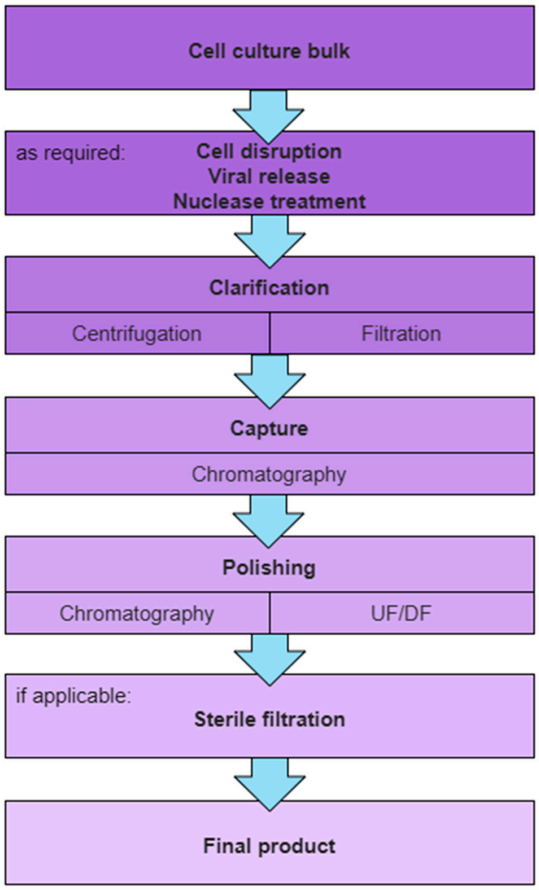

Figure 1. Generalized purification scheme for replication-competent enveloped VPs.

Prior to a clarification step, cell disruption, viral release, or a nuclease treatment may be performed to improve initial VP titers and VP recovery. Cell disruption aims to break up cells to release intracellular VPs to render them accessible for purification. VPs might be non-covalently attached to cells or cell debris and thus cell-associated. A viral release step involving the addition of additives (e.g., salt) can facilitate the release of VPs into the supernatant. The addition of nucleases degrades free DNA and RNA chains and also reduces viscosity, which improves the processability of the harvested material.

Initial clarification of harvest material is essential to remove solids in the feed stream, such as cells, cell debris, and aggregates, all while ensuring the maximal recovery of intact VPs. Techniques such as centrifugation and filtration are commonly employed. At lab scale, the clarification is often divided into primary and secondary clarification, providing a robust setup for the removal of, first, large particulate matter, such as intact and non-viable cells, and, subsequently, colloidal matter, such as large aggregates, without exceeding device limitations.

The capture step aims to selectively concentrate VPs from clarified harvest, effectively separating them from the bulk of process-related impurities and reducing the process feed volume. Chromatographic modalities such as ion exchange chromatography (IEX), hydrophobic interaction chromatography (HIC), and affinity ligands confer specific binding to VPs while most impurities are in the flowthrough. To maintain reasonable processing times with high volumetric feeds, high flow rates are necessary, making convective chromatographic media like membrane and monolithic stationary supports preferable.

The polishing step is designed to further reduce remaining impurities to achieve the low levels demanded by regulatory bodies for clinical application. A buffer exchange into the formulation buffer is typically applied at this stage as well; thus, flowthrough (FT) chromatography, size exclusion chromatography (SEC), or ultrafiltration and diafiltration (UF/DF) are applied. Subsequently, stabilizers or other additives might be added to ensure the VPs remain stable and effective.

The final step is to sterilize the VP preparation to remove any remaining contaminants. In case conventional microfiltration is not applicable due to the size of VPs, the entire bioprocess must be conducted under aseptic conditions.

2. VP Integrity and Analytical Methods for Its Assessment

VPs comprise a genome (DNA or RNA) bound by capsid proteins and additional viral-encoded proteins. Env. VPs are additionally surrounded by a lipid bilayer derived from the host cell membrane that incorporates virus- or host-cell-derived and potentially glycosylated proteins [64]. This envelope is not merely a protective layer; it is integral to the virus's morphology and stability.

The envelope and the correct assembly of all viral components, such as the capsid and the viral genome, provide the framework for a functioning replication-competent VP. The physical intactness of all VP components and structure is termed structural integrity. Any damage or alteration to the structural integrity can affect the virus' ability to infect host cells and replicate and, thus, influence the responses they provoke in both in vitro and, notably, in vivo experiments. The components also account for the stability of the structural integrity and are, therefore, virus-specific, whereas env. VPs are particularly labile due to their envelope, as discussed in the introduction.

Functional integrity, on the other hand, refers to the virus' ability to perform its intended functions. This includes the ability to bind to host cells, enter these cells, replicate its genome, express viral proteins, assemble new VPs, and exit the host cell. As part of the infectious cycle, proteins encoded on the genome are expressed, including introduced

transgenes with therapeutic effects. Any disruption of listed functions can significantly impact the virus' infectivity and, thus, its efficacy as a therapeutic agent.

For bioprocessing, maintaining the structural and functional integrity of env. VPs is critical to ensure high infectious titers. Understanding and monitoring viral integrity is an important aspect during the development of purification strategies for VPs. This knowledge can help improve the production process, ensure the quality of the viral products, and, ultimately, contribute to the development of safe and effective viral therapies and vaccines.

2.1. Quantification Methods

For virus process development, in-process control samples are taken to assess virus yield, depletion of host cell impurities, and presence of contaminants (not part of this review). Yield of env. VP processes are typically assessed by measuring both inf. VP titer and total VPs (inf. VPs + non-inf. VPs), which together are informative regarding the influence of the unit operation on the recovery performance and its influence on VPs functional integrity. The derived P:IU ratio depends on the specific analytical methods used to determine the individual values. For total VP count, several methods exist; each method targets a specific property or particle characteristic, e.g., genomic content, light scattering events, or antigen content. Hence, results can differ, and population overlaps between different analytical methods are difficult to derive. The specific methods and their limitations should be considered in the evaluation of the P:IU ratio. Most quantification methods can also be applied for non-enveloped VPs, and additional methods exist to determine the full/empty state of particles. Lothert et al. recently reviewed and evaluated available quantification methods for VPs to which the reader is referred for more information regarding the individual analytical methods [65].

2.1.1. Infectious Titer Assays

Infectious titer is conventionally measured by end-point cell-based assays: 50% tissue culture infective dose assay ($TCID_{50}$) or plaque assay-determined plaque forming units (pfu). These assays are straightforward to perform and do not require sophisticated equipment. Although they are applicable to different viruses, the actual setup must be adapted for each virus to be measured (especially permissive cell line and incubation time). However, they rely on multiple rounds of viral replication, which may take up to a week for evaluation and are sensitive to operator handling [65]. Generally, a $TCID_{50}$ variability of 0.5 log steps is reported [66,67]. Contemporary applications of the $TCID_{50}$ method reduce hands-on time by using pipetting robots and digital image analysis for the evaluation of infected cells. The approach reduces variability to approx. 20% [68].

Other faster and more sensitive infectivity measurement methods have been developed. These require only one round of replication and quantifying the inf. VP titer against a calibration curve. Cytopathic effects in the cell culture may be quantified based on changes in cell morphology by imaging, and reach variabilities of below 20% [69]. Alternatively, fluorescent markers, either expressed in infected cells or by antibody stain labeling, can be measured with flow cytometry or imaging [70]. However, these enhanced infectivity methods are more technically challenging and require specialized equipment.

2.1.2. Total Virus Particles

Total VPs can be measured by quantifying viral antigens and viral genome, and by particle analysis. Structural viral antigens may be measured using immune techniques such as enzyme-linked immunosorbent assay (ELISA) or indirectly using hemagglutination (HA) and radial immunodiffusion (RID) assays [65]. These assays provide same-day results, but they require specialized substrates and a standard curve for quantification. For enveloped viruses, these methods may overestimate actual virus titers due to potential variation

in the amount of incorporated viral proteins on the outer lipid membrane dependent on upstream conditions as well as the method of clarification. Viral genomic copies can be measured by polymerase chain reaction (PCR). Upon extraction of the viral DNA or RNA, the method of choice is quantitative PCR (qPCR) using a suitable pair of primers and detecting the amount of amplification by measuring fluorescent intensity after each cycle. Genomic copies are quantified based on a calibration curve using a known standard. Further advanced PCR methods, such as digital PCR and digital droplet PCR (dPCR and ddPCR), can directly quantify the viral genome without reliance on a calibration curve and may be performed with less sample handling. Digital PCR methods are characterized by improved precision, with a report showing a 5-fold improvement in precision and a 20-fold improvement in accuracy for human immunodeficiency viruses (HIV) genomic copies analyzed by ddPCR compared to conventional qPCR [65,71]. PCR methods can reliably quantify viral genome copies, but for env. VPs, they potentially overestimate total VPs as not all viral genomes detected are incorporated into VPs with full functional integrity. Furthermore, dependent on the amplicon chosen for the assay, it does not distinguish between complete and truncated genomes. A multiplex ddPCR result for (non-enveloped) adeno-associated viral vectors (AAVs) showed a discrepancy of 40% between amplicons used due to AAVs containing incomplete genomic copies [72].

2.1.3. Total Particles by Light Scattering (LS)

Total particles can be rapidly quantified by LS techniques using both dynamic and static LS (SLS). Such techniques require a laser beam directed at the sample, and fluctuation of scattered light based on the Brownian motion of particles, as well as the intensity of the scattered light, are detected [65]. Dynamic LS (DLS) and nanoparticle tracking analysis (NTA) are both methods that rely on the detection of the Brownian motion of particles in solution to ascertain the size distribution of a particle population. While NTA tracks individual particles using microscopy lenses, the DLS indirectly calculates the particle count based on the intensity of the scattered light. Both methods are vulnerable to drift motions in the measurement chamber and the influence of solvent composition, and their particle concentration range for measurement is limited [73,74]. Furthermore, for polydisperse samples, especially those containing impurities of large sizes and aggregates, the result can be skewed. The increased scattering intensity of larger particles can lead to an underestimation of smaller particle populations, and results depend highly on chosen device settings [75,76]. Thus, measurement parameters must be tightly controlled for the precision of the result. Multi-angle LS (MALS) is an advanced method using SLS at different angles to obtain information on particle size, shape, and molecular weight, as well as particle count. It is primarily used in conjunction with a separation technique such as chromatography or field-flow fractionation (FFF) [77]. However, the full potential of a MALS analysis is often not reached for enveloped viruses due to the heterogeneity of VPs and sample composition, as well as unknown particle properties such as the refractive index (RI) increment.

LS measurements are non-invasive and can provide rapid results, making them suitable for real-time measurements during a process [77] and as a quality control method. A reported quantification method using FFF-MALS showed good accuracy and precision (<5% and <2%) [78]. However, LS methods indiscriminately consider all particle types present in the solution, env. VPs and also EVs, and the extent of such overestimation of total env. VPs depends on upstream conditions as well as the purification stage of the sample. The separation capability of current analytical assays is insufficient to separate EVs from VPs [51].

2.2. Structure and Composition

The structural integrity of VPs is defined by their intact structure and correct composition of components. The composition of env. VPs is determined not only by the viral genome but also by the production cell line and the specific upstream conditions [61]. The virus structure can be evaluated by a combination of advanced imaging techniques, assessment of viral envelope, as well as X-ray crystallography (used for viral research). Mass spectrometry (MS), capillary gel electrophoresis (cGE), and Western blotting are common methods to look at particle composition. Recent developments adapting flow cytometers for the detection of viruses gave rise to the method referred to as flow virometry. It is a rapid method that allows for the detection and analysis of single VPs in a bulk sample based on its known characteristics like size, surface structure, and composition [79].

2.2.1. Structure

To understand the effect of a unit operation on VPs, high-resolution images that can facilitate a close examination of VP structure and substructure on a single particle level are essential. Of particular interest is to look at samples taken before and after a process step for the proportion of intact particles versus degraded particles, empty vesicles and EVs, and VP aggregates. Electron microscopy (EM) can facilitate the capture of such images, either by cryogenic EM (cryo-EM) looking at snap-frozen VPs in a hydrated state or by negative staining EM (nsEM) in a dehydrated state [64]. Cryo-EM can be performed on VPs in their native state in various conditions, requires a small amount of virus, and is suitable for viruses that take up a symmetric shape and also irregular shape, albeit at a lower resolution [80]. Studies of dengue virus (DENV) by cryo-EM revealed the influence of temperature on the conformation of the envelope [81]. NsEM can reveal in detail VP substructures and also surface protrusions from enveloped incorporated glycoproteins [82].

Structural variability of env. VPs is first introduced upstream during virus budding, reflecting the host cell line, the state of the cells after infection, and the specific virus budding mechanism [80]. During a unit operation, VPs can be (partially) degraded (degradation of surface glycoproteins, leakage of nucleocapsid, irregular shapes) and form small aggregates. While some degraded particles and VP aggregates retain infectivity, as seen in infectious titer measurements, they elicit unwanted effects during in vivo experiments [61]. Detection of undesired particle degradation through high-resolution imaging is crucial for the evaluation of the quality of the target VPs during production.

While EM imaging can provide detailed structural information on single VPs, as well as detect the presence of non-VPs, the technique is accessible only in specialized labs and can be performed only on a limited number of samples. LS techniques analyze whole VP samples to obtain size distribution information, which can be useful for detecting significant particle degradation as well as aggregation. Correlations between the resulting size distribution and EM imaging results may provide quick insight into the potential detrimental effects of a unit operation on VPs [83].

2.2.2. Composition

For therapeutic applications, viruses are often engineered with exogenous sequences inserted into the genome, while viral genes that confer undesired pathogenicity are deleted [84,85]. The genomic stability of the target virus should be examined, especially during upstream parameter optimization (e.g., multiplicity of infection (MOI), timepoint of infection (TOI), and timepoints of harvest (TOH)). While PCR-based methods and Sanger sequencing are readily accessible techniques to examine specific genomic stretches, next-generation sequencing (NGS) and deep sequencing methods provide a more comprehensive view of the entire genome.

The composition of viral and acquired cellular proteins reflects cell culture conditions and is indicative of its function in terms of infectivity and potential subsequent immunogenicity. Characterization and absolute quantification of protein content, including post-translational modifications, was performed for a vesicular stomatitis virus (VSV) pseudovirus by multiple reaction monitoring MS [86]. A number of host-derived proteins have been characterized for their function in the virus replication cycle, such as chaperones for protein folding, complement control proteins, vesicular transport proteins, and adhesion molecules [46]. Relative quantification techniques by MS would be instrumental in not only the identification of such incorporated host cellular proteins but also their differential proportions relative to viral proteins for samples taken during upstream optimization [87,88]. Further, the lipid and glycoprotein content of env. VPs should be examined, especially when choosing a production cell line. The envelope's fluidity and, thus, its stability and integrity were shown to depend on the host cell line [89]. Envelope-incorporated glycoproteins impact the stability, shown in increased resistance against shear forces in process unit operations [90,91]. Kim et al. observed a higher functional stability for retroviruses pseudotyped using the VSV-G glycoprotein compared to pseudotyping with an influenza envelope protein [91]. Specific to the virus life cycle, the lipid membrane may be derived from intracellular structures, the plasma membrane, and sometimes it is derived from a distinct membrane region such as lipid rafts. Additionally, the glycosylation pattern of lipids and incorporated glycoproteins may differ between different cell lines, as identified using matrix-assisted laser desorption/ionization MS (MALDI-MS) upon lipid isolation [92]. These attributes have direct consequences on VP stability in solution and its reception in vivo. As MS techniques are not ubiquitously accessible, Western blotting and cGE can be used for virus identification and estimation of the number of individual proteins for in-process control samples taken during process development [93,94].

2.2.3. Flow Virometry

Flow virometry is a recently developed technique that facilitates the examination of viral particles (VPs) at a singular particle level, providing insights into their size, structural integrity, and biochemical composition. This method hinges on the specific labeling of VP components in a solution, followed by the passage of these particles through a detector [95]. Simultaneous labeling of VPs facilitates a multiplexing approach [96]. The technique is potentially of high throughput while generating rapid results, and it can be set up in process development labs as an at-line assay. Not only can it provide insight into particle concentration and purity (quantification of non-viruses), but it can also detect VPs that are degraded during a production process [97,98]. With such real-time insights, this technique facilitates the improvement of production quality and yield overall. Moreover, flow virometry can also be used to evaluate host antibody-mediated immunogenicity against the VP preparation [99].

2.2.4. Mass Balance for Virus Process Development

For virus process development, mass balance is essential though challenging to achieve. This is due to the complexity of measuring specific components in a complex biological system, as well as the dependency on biological assays to measure functional integrity. Measuring all components in an in-process control sample accurately and simultaneously requires advanced analytical techniques. Recent developments in analytical separation techniques such as SEC and FFF coupled with multiple online detectors (including UV, RI, DLS, and MALS) facilitate mass balance measurements. VPs can be quantified in a bulk sample with good accuracy and precision. These methods are especially useful for enveloped virus (or virus-like) particles that are not replication-competent for accurate

particle quantification [65]. Further, this approach can be used to quantify protein and nucleic acid components in complex samples due to the separation from smaller process impurities. It may be used as a quality control method, and also as an at-line measurement during a production process or process development.

For non-enveloped coxsackievirus, a method for VP characterization including quantification of drug substance and process intermediates has been developed based on SEC separation [100]. In another study, an FFF-MALS characterization method was established for the influenza virus as a vaccine candidate [78]. The reported precision for both methods was <2% and, therefore, is very useful for mass balance applications, though such use cases were not applied. In a similar quantification method for a VSV pseudovirus, the mass balance of a chromatographic unit operation was performed, and the virus content in the samples was quantified using an HPLC-SEC setup. The reported method precision was <3%, which resulted in an overall mass balance discrepancy of about 15% [37].

2.3. Further Commentary

Process development, being upstream optimizations or downstream endeavors, can only be pursued if the outcome of process changes can be evaluated. Analytical methods are required to characterize process steps in regard to the structural and functional integrity of VPs as well as the preparations' purity. Ideally, analytical methods are high-throughput, accurate, precise, and deliver same-day results. Currently used and well-established methods do not fulfill these requirements. Many different methods exist, each with its own drawbacks, e.g., low VP specificity for NTA and DLS measurements, tedious and low precision for infectivity assays such as $TCID_{50}$ and plaque assays, or skewed PCR results due to the counting of free or EV-associated DNA or RNA [65]. To gain a complete picture despite the mentioned drawbacks of current analytical methods, an analytical panel of various methods is typically used at the moment. However, performing such a panel is time-intensive and is not conducive to making fast decisions during process development.

Furthermore, analytical methods cannot be easily transferred between different viral particles. Methods need to be developed, validated, and established before usage. Here, analytical development and process development are co-dependent and represent a 'chicken-or-the-egg' dilemma, with process development requiring established analytical methods and analytical development requiring purified and well-characterized material. Thus, both developments should be conducted in parallel.

Ideally, the results of multiple assays can be allocated to particle populations and, thus, subpopulations distinguished by various properties quantified. This would enable a comprehensive evaluation of particle integrity and its correlation with functional integrity. Distinct properties such as glycoprotein content, genomic content, morphology, and infectivity would need to be allocated. This requires either multidimensional assays or assays capable of multiplexing on a singular particle level. Multiplex approaches utilizing microfluidic devices and immunostainings (ELISA or flow virometry [96,101]) and multiplex qPCR assays [72] exist. However, simultaneous detectable properties are limited and insufficient for the afore-drawn ideal case. Furthermore, these analytical methods are complex and not ubiquitous. Hence, only individual properties within the whole population can be evaluated and their change within the process monitored.

3. Cell Culture and Infection

Replication-competent VPs are produced by propagation in a susceptible production host cell under optimized culture conditions [102]. The lipid bilayer of env. VPs is derived from the host cell, and thus, its structure and composition depend on the cell line. While

this does not necessarily impact infectivity [89], virion structural integrity relies on the envelope composition.

Current viral vector production processes rely on both adherent and suspension cell cultures in chemically defined media. While technologies exist to upscale both culture platforms, suspension culture is advantageous for the operator due to easier handling and scalability. However, bioreactors induce shear forces through agitation and aeration, for example, stirred tank reactors (STRs) that utilize impellers and gas spargers [103]. VPs that are released extracellularly in the culture are exposed to the resulting shear stress and may be negatively impacted. Grein et al. observed a high impact of aeration and agitation on measles virus productivity in a STR for Vero cells using microcarriers [104]. The increase in aeration in response to elevated oxygen consumption of infected cells resulted in a 4-log reduction in viral titers. The authors suggested the utilization of bubble-free aeration methods, which were shown to work for high oxygen-demanding cell cultures [104]. Another type of microcarrier was introduced by Yekrang Safakar et al. which locally shields cells from shear stress by a hollow structure. While the structure's benefits were shown for sensitive stem cell cultivation [105], the impact on viral productivity has yet to be shown. New impeller concepts utilizing a flexible, multiple impeller setup aim to reduce introduced shear stress while keeping sufficient agitation and simple scalability [106].

Infecting the cell culture at the late exponential (G2M) phase of the cell cycle typically yields the highest infectious titers for enveloped viruses [107,108]. The ratio of applied inf. VPs-to-viable cells is described by the MOI. Upstream parameters, including TOI, MOI, cell density, and time of harvest (TOH), are interlinked, and remain to be optimized to produce each virus according to its specific virus life cycle [109]. While a low MOI reduces the required amount of the master seed virus, a high MOI usually results in an earlier harvesting time point [110]. Especially for enveloped RNA viruses, VPs with truncated genomes of variable sizes, namely defective interfering particles (DIPs), naturally occur and can spontaneously arise in culture [111]. The DIPs are by-products of virus production that share structural similarities with replication-competent VPs but contain a significantly truncated genome. They cannot replicate on their own but compete with standard VPs for replication in co-infected cells, thereby reducing the infectious titer, and should be monitored in virus production. By using low MOIs, the likelihood of co-infections is reduced, and reports show a lower DIP count [112].

Developments toward process intensification demonstrate a positive correlation between virus titer and cell density at TOI [113–115], using both simple fed-batch or sophisticated perfusion systems using cell retention devices. Gutiérrez–Granados et al. provide a good overview of perfusion culture systems in their review of process intensification methods for viral vaccine and viral vector production [116]. However, the impact on viral integrity was not evaluated.

4. Harvest of Viral Particles

At time of harvest (TOH), VPs are collected from the host cell culture and fed into the subsequent purification process. Harvesting conditions, such as TOH and cell disruption methods, impact viral integrity and impurity content and, thus, have an influence on the overall process performance.

Virus-infected cells produce viral progeny until cells eventually die due to the overuse of metabolic pathways for viral replication or induced viral cytopathic effects, e.g., apoptosis by VSV infection [117]. For bioprocessing, harvesting of extracellular VPs should be performed prior to the exponential cell viability drop to reduce the impurity burden on purification steps while maximizing yield. However, from a biological point of view, the optimal TOH needs to be evaluated in terms of viral integrity. The condition of an infected

cell's culture at early and late stages influences viral integrity and composition, as seen by their release of different amounts of infectious and non-inf. VPs as well as EVs [45,118]. Furthermore, morphological and functional differences are observed for early (24 hpi (hours post-infection)) and late (≥48 hpi) harvested paramyxovirus particles cultivated in eggs [119]. The mechanistic understanding of the cellular state after infection and the viral integrity of VPs remains a knowledge gap. Hence, VP quality and concentration, as well as impurity levels due to dying host cells, need to be considered and evaluated to find the cell culture and virus-specific optimal TOH. Dielectric spectroscopy has been applied as an online detector for frequency-dependent capacitance measurements, and thus, cell culture state and level of infection could be derived in real time [120]. It proved to be useful to support TOH optimization efforts and real-time control of the optimal TOH.

4.1. Continuous Harvest

Infectivity loss of VPs over time in a production culture has been shown in a bioreactor. The elevated cell culture temperatures and exposition of VPs to proteases and shear stress in the cell culture are presumed to reduce the infectivity of influenza and measles VPs [121–123]. Perfusion systems, initially developed for process intensification, have been explored for continuous extraction of VPs. The continuous harvesting approach improved cell-specific productivity for influenza VPs by a factor of four compared to a batch process [121]. At the same time, inhibitors of the viral replication are removed, and depleted nutrients are replaced, which was shown to keep viral productions high (e.g., for VSV in HEK293F cells [124] and HSV-1 in Vero cells [125]).

Membrane-based cell retention systems have been successfully utilized in different modalities for the continuous harvest of env. VPs, including tangential flow filtration (TFF) [126], alternating TFF (ATF) [127], and tangential flow depth filtration (TFDF) [115]. A recurring issue of the membrane technology is membrane fouling and, thus, loss of perfusion functionality. High optimization efforts are required to establish a suitable system for cell retention and continuous viral harvest without early membrane fouling. Non-membrane devices such as acoustic settlers do not suffer from fouling issues. An influenza perfusion cell culture utilizing an acoustic settler showed a 1.5 to 3 times increased volumetric productivity compared to an ATF perfusion device [122]. The comparison of the acoustic settler perfusion process to a batch process for a purification-challenging fusogenic VSV pseudovirus showed an increase of factor 15 to 30 in volumetric productivity [128].

The prerequisite for a continuous harvesting approach is a prolonged harvesting window before the viral cytotoxic effects dominate, leading to a high impurity content at low additional productivity. Non-destructive virus budding exists also for some enveloped viruses, allowing an extended virus production phase in the host cell. Both possibilities enable a continuous viral production (e.g., vaccinia on AGE1.CR.pIX [129]) or several rounds of harvesting [45], which can be exploited in perfusion reactors (HSV-1 on Vero cells [125] and VSV on BHK-21 [115]).

Continuous or repeated harvest during a perfusion culture may not necessarily improve yields significantly to justify the increased development and processing effort, as shown for a VSV perfusion culture [124] and temperature-stable modified vaccinia Ankara (MVA) VPs [130]. Additionally, as discussed in the introduction to this section, the VP quality depends on the TOH and needs to be evaluated (P:IU changes for mumps and measles VPs [45]).

Online monitoring of processing parameters, e.g., by real-time process analytical technologies (PAT), is especially useful for continuous processes to control the process and derive real-time process and quality attributes. In VP processes, it is difficult to derive real-time information from online detectors due to the complex VP structures, VP

heterogeneity, and similarities to impurities [131]. Referenced studies in this section, thus, relied mostly on the application of at-line or offline analytical methods to evaluate cell culture conditions and product quality. However, it was shown that the application of an online dielectric spectroscopy detector could provide not only the state of the cell culture in real-time but also valuable information about the state of infection in cell cultures infected by env. VPs [101,120]. Different dielectric frequencies were used to distinguish between capacitance measurements for cells and VPs, enabling the estimation of VP count. An application to continuous harvesting approaches could increase process robustness through process control and provide real-time estimation of VP count. Gränicher et al. used capacitance measurements to monitor cell culture parameters, control perfusion conditions, and optimize TOH for vaccinia release [129]. However, the precision of the release timepoint was low (±4 h), and no VP count estimation was derived from capacitance measurements. More studies evaluating the use of online dielectric spectroscopy are required to determine the usefulness for env. VP processes.

4.2. Cell Disruption

During the viral replication cycle, env. VPs acquire a host-derived lipid membrane through a budding process from host cell membranes. Intracellular and extracellular budding exist, whereas the latter budding results in a cellular egress [132]. Viruses being developed for therapeutic application that first undergo intracellular budding include poxviruses [133] and HSV [134]. Intracellular budding viruses go through several intermediates within the host cell, distinguished by shape and the number of acquired lipid membranes. Mature particles can egress by exocytosis or after cell lysis, while the intermediate stages can already be infectious and accumulate in large numbers, as shown, e.g., for vaccinia [135]. Thus, at the time point of harvest, cell-disruption methods can be applied to increase VP titers. It is worth noting that the viral intermediates differ in surface protein composition, which impacts viral attachment and entry, as observed for multiple poxviruses [136,137]. To our knowledge, there is no published study evaluating the functional integrity of derived subpopulations and their effects on therapeutic applications.

Cell-disruption methods include manifold mechanical methods, as well as chemical lysis used to release viral particles from cells. At the lab scale, a combination of FT-cycles and sonication is commonly used to increase harvest recoveries for VPs (e.g., HSV-1 [138], Orf [139], and Newcastle disease virus (NDV) [140]). The formation of ice crystals impairs the stability of the cellular lipid bilayer. At the same time, FT-cycles also impact the viral integrity of env. VPs (herpesvirus [141], retrovirus [35], VSV [34]). Furthermore, FT-cycles are impractical for large-scale production volumes.

Sonication as an alternate method of mechanical lysis is scalable with flow-through probe devices [142]. However, sonication induces shear forces due to cavitation, which results in cell disruption, a phenomenon that may also negatively affect env. VPs. This is observed in surrogate VPs over extended time frames [143]. The power densities and exposure time required for cell disruption are notably lower than those applied to the surrogate VPs. In a stability study for orf particles, a decrease in infectious titers was observed within minutes of sonication, though the loss may be attributed to the uncooled environment [38]. It is imperative to maintain temperature control of the material and to minimize the induced energy to mitigate potential detrimental effects on viral integrity.

Homogenizers are another cell disruption category with a multitude of devices and scale-up possibilities available [142]. Mundle et al. compared sonication and microfluidization methods for Vero cell disruption and harvest of respiratory syncytial virus (RSV) particles [144]. A similar increase in infectious titer could be achieved for sonication and low-pressure microfluidization of harvest, whereas repeated or higher pressure microflu-

idization showed a lower or decreased infectious titer. With both methods, an expected increase in soluble host cell impurities was observed [144]. The question of the structural impact of the cell disruption methods was not evaluated, although mechanical stress has been shown to generally impair the envelope of viral particles [119].

Cell disruption by osmotic pressure (hypotonic conditions) is a mild method to release intracellular components. Laposova et al. showcased the beneficial use of deionized water on BHK-21 cells for disruption and release of lymphocytic choriomeningitis (LCMV) particles [145].

Using solely deionized water for disruption showed higher infectivity yield compared to a combined approach with sonication and FT-cycles, which presumably impaired viral integrity. On the other hand, the use of a low ionic buffer to establish hypotonic conditions was insufficient to release VPs. Moreover, the additional use of sonication and FT-cycles did not enhance infectivity and may have further reduced it. Kong et al. observed diverging results using double distilled water to lyse two different cell types under hypotonic conditions. The recovery of infectious avian metapneumovirus (aMPV) by water lysis compared to FT-cycles was only beneficial for an avian cell line (TT-1) and not for Vero cells [146]. Env. VPs seem to mechanically withstand the osmotic pressure in hypotonic environments, as shown for influenza particles, which only react by swelling but without loss of activity [147]. Despite these advantages, hypotonic cell disruption is rarely used, possibly due to the buffer exchange required and, thus, the lack of scalability. Moreover, hypotonic environments failed to efficiently release VPs from cells and cell debris attachment, supposedly due to high prevailing electrostatic interaction in low ionic environments [148].

Chemical lysis is the method of choice for non-env. VP production due to ease of use and scalability. In the case of env. VPs, most detergents impair the VP due to the exposed membrane proteins [149]. Furthermore, lysis chemicals might pose a safety risk in vivo, and their removal must be considered during purification [150].

Overall, cell disruption methods can increase infectious VP titers accessible for further purification but also release cell-derived impurities. It increases the burden for the purification process, e.g., impurities can bind to chromatographic resins, thus decreasing binding capacity and the probability of filter fouling as filtration steps increase. The application of cell disruption and increased purification burden needs to be justified by increased VP yields at sufficient purity.

4.3. Viral Release

Even after cellular egress of VPs, viral particles can still be attached to the cell surface. For vaccinia, these cell-associated VPs are believed to drive cell-to-cell infections in combination with an actin tail propulsion [136]. Cell-associated VPs can be released by the addition of release agents. The use of heparin and dextran sulfate was shown to dissociate VPs from cells and cell debris through electrostatic interaction with viral envelope proteins [148]. Increased titers were also observed for VSV after the addition of salt or dextran sulfate [124,151]. An electrostatic interaction hindering the release of VPs into the culture supernatant was presumed.

4.4. Nuclease

Nucleases are used to degrade hcDNA and reduce its associated viscosity in the harvest. The high cost of these enzymes and their narrow optimal working window require targeted placement within the process. Process conditions, such as pH, temperature, incubation time, ionic strength, nuclease type, and nuclease concentration, have a high influence on nuclease efficacy and can easily be optimized by a DoE approach [152]. Cell disruption typically releases high amounts of hcDNA, and thus, a subsequent nuclease

step is commonly implemented, though the large working volume at the harvest stage necessitates a high amount of enzyme, increasing the costs for this digest step.

In a VSV production process, the placement of a nuclease step at various purification stages was tested, and the nuclease step immediately after the harvest stage facilitated the best overall VP recovery [153]. In addition to measuring the reduction in hcDNA, infectious titers need to be monitored, as elevated temperatures and incubation times can reduce infectivity [154]. In some cases, the nuclease step had an additional positive influence on the clarification recovery, as observed for an orf virus production [152]. Filterability was not only improved due to viscosity reduction but also due to a hypothesized dispersion of large aggregates of VPs bound together by DNA chains. In a study by Mayer et al., the nuclease step improved the recovery of a subsequent affinity chromatography step without reported negative impact [155].

Destabilization of chromatin structures by salt addition has been reported [156]. The tight packing of DNA with histones in chromatin shields DNA chains from nuclease digestion and the application of salt-tolerant nucleases in increased salt conditions was shown to improve DNA removal [157]. In another report, Vincent et al. assumed negative impacts of chromatin/VP complexes on a chromatographic purification step [158]. The positively charged chromatin reduced the binding capacity of a cation-exchange chromatography (CEX) column through binding competition. Furthermore, the binding strength of VPs was increased due to chromatin/VP complexation, presumed due to the co-elution of both at high salt conditions [158].

5. Centrifugation Methods

5.1. Low-Speed Centrifugation: Clarification

The clarification step aims to remove cells and other insoluble large impurities, such as cell debris, from the cell culture harvest. Differential centrifugation applied at low speeds (<10,000× *g*) is used to pellet large, insoluble components of the cell culture harvest at mild process conditions. Excellent recoveries have been reported for the centrifugation clarification step [159], and in the case of env. VPs, clarification by low-speed centrifugation alone or in combination with a subsequent filtration is commonly used at lab scale [153,160–164]. Centrifugation increases filtration capacity by reducing membrane fouling when performed prior to a filtration step. Sviben et al. compared low-speed centrifugation at 3000× *g* and a 0.45 µm polyvinylidene fluoride (PVDF) filtration for the clarification of mumps and measles VPs. The authors showed higher infectious step recoveries for both VPs for clarification by filtration and observed a reduction in particle size after centrifugation. Shearing in the centrifuge was assumed to reduce the recovery, which is coherent with VPs being sensitive to vortexing observed in the same study [28]. Systematic evaluations of centrifugation properties and its impact on infectious titers are rarely reported. One reason is the difficulty of scaling centrifugation steps due to the lack of transferability across scales in combination with high initial and maintenance costs [159]. Hence, filtration steps are preferred if process scale-up is intended.

5.2. Differential Centrifugation: Concentration and Partial Purification

Differential centrifugation is used for the concentration of VPs, which leads to the pelleting of particles under ultracentrifugation force, usually greater than 20,000× *g*. VPs, but also impurities, end up at high concentrations in the pellet, which is afterward resuspended. The force impact on VPs and overcompaction within the pellet was shown to reduce viral infectivity of env. VPs in inverse proportion to centrifugal time and force [165–167]. The co-precipitation of impurities (e.g., cell debris, proteins) can lead to neuro-inflammatory responses in vivo, and thus, further purification is required [168]. A high-density cushion,

such as a sucrose cushion (SC), can be used to retain smaller impurities while pelleting the VPs to reach partial purification [169,170]. However, chromatographic steps, in comparison, show higher recoveries of infectious particles (for an orf process [15]) and lower amounts of contaminants (for a VSV process [162]).

5.3. Density Gradient Centrifugation: Concentration and Purification

Density gradients leverage differences in sedimentation velocities (rate-zonal centrifugation) or in buoyancy (isopycnic centrifugation) to separate particles. The differences are established by high-density media, e.g., sucrose, CsCl, iodixanol, or others. In-depth information can be found in the book Nanoseparation Using Density Gradient Ultracentrifugation, chapter 2 [171]. Depending on the centrifugation conditions and processing step, density gradients are used for VP concentration and/or separation from cells, large cell debris, as well as impurities that are smaller in size. Separation of VPs from EVs and microvesicles has been reported for herpesviruses [49] and HIV [52]. Still, due to the heterogeneity of EVs and their similarities in density and size with env. VPs, a complete separation is not feasible [51].

A high resolution is established in density gradients via long centrifugation time and high centrifugation forces. Both increase the induced mechanical stress on VPs, potentially resulting in the loss of surface structures and, thus, infectivity loss, reported to be up to 99% [172,173]. A high sucrose concentration increases the osmotic pressure [174] in solution, which impairs cell cultures and living organisms when administered intravenously. A 20% sucrose solution resulted in an intense diuresis in rabbits [175]. Lengthy wash steps, such as dilution and pelleting through centrifugation, are applied to reduce sucrose before in vitro or in vivo applications [176].

CsCl, compared to sucrose as a medium, has advantages due to a lower viscosity and faster centrifugation, but both are hyper-osmotic in the concentration range applied. The sudden change in osmotic pressure can impact cell cultures, as well as the viral envelope's integrity, thus reducing safety and infectivity [147]. Still, protocols of the last decade for the purification of preclinical orf and NDV material include sucrose and iodixanol density gradients [139,177]. In addition to preparative applications, analytical methods exploit the high separation resolution in isopycnic applications to analyze density populations [178] or conduct subsequent proteomics [179].

5.4. Centrifugation Summary

Centrifugation methods for concentration and partial purification can induce mechanical stress that leads to lower recovery of inf. VP titers. Scale-up techniques are limited, and thus, industrial preparative processes rely on other methods, as detailed in the following sections [180]. However, density gradient centrifugation techniques are still used ubiquitously in original lab-scale processes and present advantages due to their fast process development and simple application with the possibility for buffer exchange. Especially in virology research labs, these methods are commonly used, even though their purification capabilities and scalability are limited, and their negative effects on viral integrity is known.

6. Filtration Methods

Filtration methods are ubiquitously performed in VP bioprocessing. There are filtration membranes of various materials with a range of pore sizes employed in different designs and flow patterns suitable for each specific application. Clarification by filtration uses the steric retention of cells and large particulates from the harvest material, thereby reducing turbidity and enhancing subsequent processability. UF/DF utilizes membranes to retain VPs based on size, effectively concentrating VPs and removing smaller, undesirable

impurities and soluble buffer components. Sterile filtration at the end of bioprocesses employs a microfilter to ensure sterility of the final product, but challenges exist for VPs larger than the typical filter cutoff of 0.2 µm.

Env. VPs are prone to adsorption on the filter membrane due to their lipid membrane facilitating unspecific binding primarily by electrostatic or hydrophobic interactions. Unspecific binding was shown to significantly decrease overall yield [181,182] and might result in early membrane fouling, possibly stopping membrane flux. Screening of different filter membrane materials must be performed early on to identify a suitable material for the particular VP of interest.

Charged membranes and filter aids are designed to reduce impurity content, typically applied as depth filters in clarification. They have been shown to be unsuitable for VPs because the strong electrostatic binding reduces VP yield [152,154]. For lentivirus (LV) purification, however, the use of diatomaceous earth (DE) as a filter aid simplified the clarification [183]. DE increased the filtration capacity and purity by prolonging the processing time until clogging and cake formation. Even though this one-step filtration reduced inf. VP yield by 35% compared to the alternative two-step clarification, it was regarded beneficial by the authors due to faster processing, safer VP handling, and improved robustness [183].

Filter membranes of different materials are available, such as PVDF, polyethersulfone (PES), polypropylene (PP), glass fibers (GF), nylon (NYL), and cellulose-based membranes like cellulose acetate (CA), cellulose esters (CE), nitrocellulose (NC), and regenerated cellulose (RC). Suitability tests for env. VPs are scarcely reported, and a thorough screening including the influence of pore sizes and feed parameters is lacking. The application of filter devices incorporating multiple filters with different materials as coarse prefilters hinders a distinct material evaluation [184].

A recent study by Labisch et al. for the purification of LVs screened different materials and pore sizes of filters in three different devices: centrifugation filters, stirred cells, and crossflow cassettes [185]. Interestingly, the authors found the overall best-performing filters in terms of inf. VP recovery and impurity removal to have different pore size specifications: reinforced 100 kDa PES, 300 kDa cellulose-based filter. The reinforced PES membrane outperformed other membranes across all devices, also in comparison to non-reinforced PES membranes. This was contributed to tighter pores due to polymer fleece reinforcements within the PES membrane, resulting in optimal retention of LV particles while effectively passing small impurities. Large differences in inf. VP recovery were found between the individual filter devices, even with the same membranes. This emphasizes the impact of device design and flow patterns on concentration polarization, filter fouling, and separation performance [185].

For a primary clarification of influenza VLPs, Carvalho et al. observed complete recovery of HA activity when applying different filter materials with pores sizes between 0.55 µm and 10 µm (PP, PVDF, and depth filters with material combinations of cellulose, PP, glass fiber, and DE filter aid) (Carvalho et al., 2019 [186]). In a second clarification step utilizing pore sizes of 0.2 to 1.2 µm, most materials (CE, PES, and mixed material depth filters) showed complete recoveries, whereas PVDF and PP showed reduced functional recoveries. Only the PES filter additionally reduced residual, and in this case contaminating, baculovirus (BV) particles, most likely due to steric hindrance.

Especially for later purification stages with reduced protein impurities or no excipients, which prevent unspecific interaction, the material choice has a substantial impact [181,187]. Pre-coating of membranes using proteins can improve recoveries [182,188] but also introduces impurities to the process. On the other hand, residual hcPs at levels of about 25 µg/mL have been shown to negatively impact the sterile filtration step for VSV on PVDF and PES membranes through accelerated filter fouling [189].

It is worth noting that PVDF belongs to the category of per- and polyfluoroalkyl substances (PFAS) for which the European Union plans a ban due to health and environmental hazards [190].

6.1. Normal Flow Filtration (NFF)

In NFF, also known as dead-end or direct flow filtration, the fluid is passed perpendicularly through the filter membrane, trapping the larger particulates on the filter surface. Common applications for envelope VPs involve clarification and sterile filtration. At the lab scale, centrifugal NFF devices are also applied in sample preparation for volume reduction [15,28,185].

6.1.1. NFF for Clarification

Clarification by filtration aims to separate large contaminants in the retentate while VPs are collected in the filtrate. A large variety of filter materials and modalities exist, and the optimal devices need to be chosen based on the VP and feed properties, as well as purification requirements. Due to the broad size range of particulates to be depleted in clarification, multiple subsequent filters with degressive pore sizes (filter train) or a combination with other clarification methods are used [129,154,160,162]. A filter train increases the capacity of the latter filters by pre-filtration steps for large particles. At lab scale, membrane areas can easily be enlarged; however, at large scale, this might lead to practical and economic difficulties [152]; thus, filtration trains are preferred [191]. In the case of prior cell lysis, the burden on the clarification step is increased, usually necessitating a pre-filtration. In a protocol for a lab-scale orf virus production, the exchange of the pre-filter after cell lysis is recommended due to fast filter fouling, highlighting the high burden on the subsequent clarification step [139].

As each VP and purification process has its own requirements and specific feed properties, finding the optimal inert filter material and filter pore size requires extensive screening. Small screenings of filter materials might not result in a satisfactory balance of VP recovery and impurity clearance. This was observed for replication-defective HSV particles, leaving room for optimization after four materials (NC, NYL, CA, PES) were tested [167]. Modern high-throughput (HT) screening devices such as the Ambr crossflow (Sartorius, Göttingen, Germany) facilitate this effort, as shown by Pagallies for an orf virus clarification [152]. Filter properties, as well as nuclease treatment and TOH, are significant factors influencing the recovery of the clarification step. After HT screening and optimization, a recovery of up to 80% was reached for a combination of two PP filters, while turbidity was reduced to a third of the initial level. Additionally, a prior nuclease step improved recovery, presumably due to the breakdown of DNA-VP complexes, as discussed in Section 4.4. Other reports showed a similar breakdown effect by the addition of salt [129] or the introduction of a homogenization step [192], whereas the latter led to increased impurity content in the filtrate.

6.1.2. NFF for Sterile Filtration

Conventional final filtration in biopharmaceutical processes consists of a sterile filtration step to fulfill regulatory requirements to deplete potential bacterial contaminations. The same microfiltration step of 0.22 µm has been applied for various env. VPs, though, in general, high product losses were reported for PES and PVDF membranes [189]. Transfiguracion et al. screened filter membranes and the influence of buffer matrix for the final filtration of BV particles [193]. Unspecific binding was presumed to reduce recovery to approx. 20% for a PES membrane. The addition of salt did not increase recoveries, in contrast to the well working improvement by salt addition for the prior SEC step. The tested polysulfone (PS) membrane yielded a maximum inf. VP recovery of 79%. Again,

salt addition did not improve recovery but led to VP inactivation [193]. In another screening by Shoaebargh et al., the influence of filter material morphologies was tested for the filtration of VSV particles [184]. Total particle recoveries were generally low (<25%), and no correlation to membrane morphologies or the incorporation of pre-filters could be taken. However, utilization of two-layered filters delayed transmembrane pressure (TMP) increase and aided the filterability. This was attributed to filter blockage by VP aggregates [184], in line with the findings of a recent study for a vaccine VP [194]. On the contrary, Fernandes et al. had no issue with the final filtration of VSV particles [154]. The sterile filtration utilizing a PES membrane achieved full reported recovery of inf. VPs. It is unclear whether the differences arose from different VP formulations or the higher purification state in the study by Fernandes [154]. Considering protein impurities, Wright et al. observed the impact of residual hcPs in accelerating membrane fouling. An effect of hcP resulting in filter blockage or the mediation of VP attachment to the membrane was presumed [189]. However, as the last step in the purification step, hcP levels should be sufficiently low to prevent these effects.

Larger env. VPs such as poxvirus and vaccinia viruses exceed the exclusion limit of 0.22 µm sterile filters. Larger filter pore sizes such as 0.45 µm or 0.65 µm have lower bacterial retention capacity, and their application, if utilized, must be justified. As stated in regulatory guidelines [195], an aseptic process may become necessary, but this requires much higher technical efforts.

Sterile filtration of VPs is a crucial step that can limit overall process recoveries tremendously. The step performance is impacted by variabilities in the purification process. Screening for the optimal membrane material for filtration of VPs in its formulation must be performed, and the amount of VP aggregation before and after filtration, as well as the influence of residual proteins, should be controlled.

6.2. Tangential Flow Filtration (TFF)

TFF is an essential technique in the bioprocessing of env. VPs. It operates by allowing a feed solution to flow tangentially across a selective membrane, reducing the build-up of solids on the filter and prolonging the operational life of the filter medium. For harvest clarification, VPs are filtered out in the permeate while the cell culture and large debris remain in the retentate. This can be implemented in a perfusion culture setup as well as a batch setup. The main application of TFF is the retention of VPs enabling concentration and buffer exchange. It is readily scalable, rendering it very interesting for industrial applications [196].

TFF applications have been shown to successfully concentrate shear-sensitive measles VPs using the lowest possible TMP [187]. Depending on the application and feed properties, higher flow rates in the retentate loop may be required to reduce membrane fouling and speed up processing times. Peristaltic pumps, commonly used for TFF systems, have been correlated with reduced recoveries of VPs [38,196] and attributed with increased shear rates [197]. ATF utilizing diaphragm pumps as well as centrifugal pumps designed for low shear rates have been shown to prevent membrane fouling as well as improving recovery for shear-sensitive particles [197]. It is worth noting that specific glycoproteins on the envelope of VPs can increase viral stability, as shown for HIV VLPs [90]. As discussed in Section 2.2.2, env. VPs can be engineered for stability by design to sustain mechanical forces during the purification process.

Hollow fibers and flat sheet cassettes are commonly used for env. VPs or VLPs [187,198,199], although no comparative study between these devices was identified at this time. Differences in surface area per volume, flow distribution, scalability, and ease of use are apparent and need to be evaluated for the specific use case. Nonetheless, hollow fibers are

presumed to induce less shearing due to larger internal channels [200]. Performance and recovery of inf. VPs seem to be largely dependent on filter material and pore sizes and less dependent on the specific device used.

6.2.1. TFF for Clarification

TFF microfiltration can be used to prevent early membrane fouling in clarification without increasing membrane area or filtration steps. For example, in the production of HIV VLPs, a TFF microfiltration step using a 0.45 µm filter was used for clarification prior to a second TFF UF step with a 500 kDa cutoff membrane [199]. An overview of the advantages and disadvantages of filtration methods is provided by Besnard et al. [159]. Generally, TFF is more laborious compared to NFF and is only beneficial for high volumetric feeds. Thus, it is mainly used for lab-scale harvest if a continuous or repeated harvest is developed, see Section 4.1. At large scale, TFF applications have not been reported for clarification purposes, although filtration modules for scale-up are commercially available for pore sizes 0.1 µm and larger. The effect of shear stress in TFF systems for VPs during the processing of large volumes must be considered, although this may be controlled with an optimized flow rate.

6.2.2. TFF for Buffer Exchange and Concentration

TFF is primarily applied as UF/DF. It is a useful method for processing feed concentration and buffer exchange, for example, at the end of a production process for formulation and adjusting the VP concentration to reach specified titer ranges. For env. VPs or VLPs particle recovery rates of up to 100% have been reported [198]. However, the impact on replication-competent VPs has not been evaluated in many studies. Fernandes et al. used a hollow fiber setup for UF/DF of VSV particles. After 6 times DF and 4 times concentration, the authors reached an inf. VP recovery of about 50%. No impact of shearing was observed as an increase in flow rate achieved similar inf. VP recoveries but rounded, non-native particles have been observed in transmission electron microscopy (TEM) analysis [154]. Another study reported the regular occurrence of such rounded particles in VSV bioprocessing [83]. Loewe et al. screened different TFF membranes for their UF/DF application for measles VPs [187]. They reported no impact of filter material on retention of VPs and that a 15-times concentration could be achieved for three different membranes; however, no inf. VP recovery values were reported.

6.3. Filtration Summary

Filtration is essential in VP bioprocessing for clarification, concentration, buffer exchange, and, in the case of small VPs, sterile filtration. However, infectivity loss and also membrane fouling are challenges to be addressed with enveloped VPs. Optimization of a filtration step is crucial but may require extensive screening of filter materials (e.g., PVDF, PES, PP). Charged membranes and filter aids are generally unsuitable despite some success with DE for lentivirus clarification.

Filter design and flow patterns significantly impact VP recovery, while material selection becomes especially important in later, more purified stages to minimize unspecific adsorption. NFF is favored for clarification, and filter trains starting with coarse filters are especially useful when the feed is crude harvest. TFF is suitable for concentration and buffer exchange, though some pumps (e.g., peristaltic) and a non-optimized setup can damage shear-sensitive VPs. Sterile filtration is not always possible for the bioprocessing of larger VPs, necessitating aseptic conditions for the entire process.

Optimizing filtration of enveloped VPs demands extensive screening of materials, devices, and parameters to address binding, fouling, and product loss. Tailored strate-

gies are essential for effective clarification, robust and high VP recovery, and a sterile drug substance.

7. Chromatography Methods

Chromatography is a conventional purification method widely used for VPs. SEC, as well as ligand-based modalities such as IEX and HIC, are commonly used. Moreover, specific affinity ligands were recently developed for VP application. Stationary supports that facilitate high mass transfer and high flow rate are especially beneficial for VP purification. The impact and suitability of relevant modalities and stationary phases are discussed in the next subsections, together with the evaluation of relevant published studies. Chromatography in bind-and-elute (B&E) mode is favored as an initial capture step to process large volumes with typically low VP concentrations at the harvest stage. Chromatography in FT mode is designed to retain impurities and is thus typically used as a polishing step to deplete residual impurities.

7.1. Chromatographic Modalities

7.1.1. Ion Exchange Chromatography (IEX)

IEX might be used as capture for VP purification in B&E-mode after a clarification step as well as a polishing step to further deplete impurities. It operates based on charge, which is dependent on the isoelectric point (IEP) and surrounding pH. The IEP of env. VPs is not easily predictable due to the high variability of envelope lipid and glycoprotein composition. Published experimentally determined IEPs for env. VPs are rare, and multiple literature values might not match due to a high dependency on the upstream [201].

Env. VPs carry an overall negative charge at neutral pH, which points to the use of anion-exchange chromatography (AEX). Several publications show the successful application of AEX chromatography with infectious step recoveries of up to 86%, including NDV and influenza on AEX monoliths [19,202] and VSV pseudovirus on an AEX membrane [154]. However, the net charge itself is not sufficient to determine suitable process conditions for the IEX step. Measles VPs have been shown to form such a strong electrostatic binding to AEX resins that it is not possible to recover infectious VPs [45,203]. Instead, a CEX column was utilized by Eckhardt et al., indicating sufficient positive patches for binding on the VPs. Additionally, Gautam et al. used a CEX membrane adsorber for the purification of VSV particles [162].

Impurity content and properties, as well as VP properties, are cell culture-dependent and variable [158,163], and thus challenge the robustness of an IEX step and its suitability as a platform process step. Impurities carrying similar charge properties are co-purified and reduce the binding capacity for VPs. Multi-point binding of VPs, further discussed in Section 7.1.5, is established through ligands conjugated on linker polymers, as in tentacle resins. This increases binding strength to the resin and sets it further apart from weakly bound smaller impurities. By modulating the salt concentration during loading, 'interference chromatography' [204] aims to exploit the 'sweet spot' in which VPs bind, but smaller impurities with fewer surface charges do not. This method is presumed to be especially successful for high ligand-density IEX adsorbers and increases binding capacity as well as separation performance. Fernandes et al. showcased the beneficial utilization of citrate for the purification of VSV particles on an AEX column, increasing the dynamic binding capacity (DBC) and purification performance [154].

IEX chromatography performance depends on loading parameters such as pH and salt concentration. The capture of VPs directly from clarified harvest without adjustments requires a robust unit operation that can withstand expected feed variabilities. Rogerson et al. used a HeLa cell culture to produce NDV VPs and evaluated the influence of pH and

conductivity for the AEX capture step [19]. In the range of pH 7 to 7.6 and loading conductivity of 8 to 17 mS/cm, their robustness study showed a constant recovery of infectious particles of 25% to 33% and an impurity reduction of above 53% for hcDNA and 89% for hcP was reached. However, in an upscaled application, an inf. VP recovery of 37% with a StD of 14% (incl. assay variability, n = 5) was realized. Harvest composition variabilities due to the upstream were assumed to be responsible for the increased variability.

IEX for the polishing step in FT mode can be performed after a concentration step. The stationary phase is functionalized ideally with ligands only accessible to small impurities. Restricted access media (RAM) is specifically designed for this application and discussed in Section 7.2.7, including polishing chromatography.

7.1.2. Affinity Chromatography

Affinity chromatography is the preferred capture method in biopharmaceutical processes due to its high specificity and, therefore, high purification capability. As a prerequisite, a suitable ligand/target combination must be identified while considering purification capabilities and economic factors. Currently, applications of affinity chromatography methods are found mainly for vaccines and VLPs, for which Lothert et al. give an extensive overview [205]. Transferable knowledge for this technique to replication-competent env. VPs is summarized here, together with the evaluation of relevant published studies.

Heparan sulfate on cell surfaces assists in the attachment of VPs. The specific affinity of VPs to heparan sulfate and its analog heparin have been exploited in affinity columns for the capture of VPs. Nasimuzzaman et al. showed a strong binding of BV particles to a heparin column, which requires high salt concentrations for virus elution [206]. Due to an immediate stabilization by dilution of eluted particles, inf. VP recoveries of up to 85% were reached [206]. Due to the animal origin of heparan sulfate and heparin and the high costs for recombinant alternatives, heparin-mimicking sulfated polysaccharides have been developed. Sulfated cellulose and dextran have been successfully utilized for enveloped virus vaccines such as MVA [207] and influenza [208] but showed only very low inf. VP recovery for measles VPs in comparison to a heparin purification [155].

The development of new ligand/target combinations for env. VPs is an ongoing process. Engineering VPs to include targets on the surface, such as biotin-mimicking tags to bind to streptavidin [209] or histidine tags for metal affinity [210], were successfully implemented for enveloped VLPs and vaccines but come with limitations for applicability for replication-competent viruses. The impact of such tags on replication cycles and in vivo effects is unknown, and leachable metal ions lead to virus inactivation [211].

More recent studies applied in silico modeling and experimental screening setups to identify ligands with high specificity. For instance, LVs with VSV-G glycoprotein were successfully targeted [160]. Promising results were reported in other studies that used phage display for LV particles [212] and coronavirus purification [213]. However, the transferability of customized ligands to capture replication-competent VPs remains outstanding. The advantages of high specificity must be balanced with the high development efforts required, and this strategy may only be beneficial for widely used virus platforms with conserved glycoproteins. The question of cost/benefit, column production cost, reliability in supply and quality, and column reusability for potentially expensive ligands remains.

7.1.3. Hydrophobic Interaction Chromatography (HIC)

HIC has been successfully used as a capture step in the purification of env. VPs. Sviben et al. showed infectious recoveries for mumps and measles VPs of over 60% [45]. High titers could be achieved while hcDNA was depleted. For vaccinia particles, an inf. VP recovery of above 50% was reached, while hcDNA was reduced by 99% [158]. In both studies, hcDNA

was depleted without prior nuclease treatment. However, when HIC was applied as a polishing step for MVA, it was not sufficient to deplete the residual hcDNA after an affinity capture step [214]. It is noteworthy that only double-stranded nucleic acids flow through the resin due to their hydrophobic patches being shielded by the double structure, unlike single-stranded nucleic acids, in which hydrophobic patches are exposed [215].

There are some notable disadvantages to HIC. A high salt concentration is required for the binding of particles. Ammonium sulfate is typically used for the binding of VPs, but at high concentrations, it has been found to precipitate and inactivate VPs [45,158,216]. Vicente et al. substituted ammonium sulfate with NaCl to prevent aggregation and resolve filterability issues of vaccinia VPs. The impact of salt concentration on the flowthrough of hcDNA was found to be minimal [158,214]. In all applications, a balance between the salt concentration required for VP binding and the detrimental effect on the viral integrity must be determined. HIC is, thus, best-suitable for VPs with a high salt tolerance.

7.1.4. Steric Exclusion Chromatography (SXC)

SXC has emerged as a promising technique for the purification of VPs, leveraging specific properties of polyethylene glycol (PEG). The method is based on steric exclusion effects, where PEG molecules induce a crowding effect that facilitates the capture of large targets on a hydrophilic stationary phase without direct binding [217]. SXC is particularly advantageous for the purification of large, labile biomolecules due to its gentle nature and the absence of direct chemical interactions, which helps maintain the structural integrity of sensitive viral components [218]. Furthermore, the addition of PEG to the load material is presumed to shield VPs from shear stress [219]. The application of SXC for env. VP purification has been shown in various studies, the majority being vaccine or VLP applications, including BV [220], influenza [221], Hepatitis C [222], and LV [219].

Two studies are available that capture replication-competent orf VPs using SXC, achieving inf. VP recoveries of 85% [15] and over 90% [70]. Protein depletion is efficient, with over 98% protein reduction in both studies. For hcDNA reduction, a prior nuclease step was used to increase its size difference to VP, and thereby reductions of about 80% were achieved. Even though the inf. VP recovery was much higher for SXC compared to SC purification, the eluted concentration of orf was in the range of 10^6 IU/mL, and thus three log-steps lower compared to SC [15]. Eilts et al. analyzed the VP quality after SXC and observed a monodisperse size distribution of VPs and minimal morphological changes in TEM, indicating a good VP quality [15]. Lothert et al. further evaluated the method for two different virus genotypes. Pressure issues arose for one genotype during loading, presumably due to the genotype's surface properties and resulting aggregation of VPs. In a low-loading setup (<$DBC_{10\%}$) of SXC, similar performances for both genotypes were observed, showing the method's robustness for virus strain variations. No relevant aggregation levels were observed after SXC purification [70]. However, both studies presumed residual PEG molecules after the process despite a second purification step. PEG removal and monitoring after the SXC step is not yet sufficiently reported and poses a safety concern due to the rare prevalence of PEG allergies [218].

SXC purification performance and DBC, as well as the extent of VP aggregation and resulting pressure increases, are dependent on process parameters. PEG concentration and molecule size and the feed matrix in terms of buffer composition can be optimized. High recoveries were shown to be achievable for different viral strains, whereas the infectious recoveries for labile VPs such as influenza and measles are still to be evaluated. Additionally, PEG is introduced at high levels, which must be treated as a process impurity at subsequent purification stages. Additionally, as the collection of VPs on the initial membrane surface leads to pressure issues and potentially reduced binding capacities, there remain challenges

in membrane design that must be addressed to facilitate the scaling-up of this method to production scale [223].

7.1.5. Surface Functionalization

The manner in which ligands are presented influences both their ability to bind (binding capacity) and the strength of their interactions (binding strength). Polymers can be grafted on a stationary support to act as ligand linkers, extending the reach of ligands and increasing the overall ligand density. These flexible linker polymers are termed tentacles. A multi-point binding principle is assumed to be facilitated through the flexibility of linker polymers and increased ligand density. The multiple binding points increase the overall binding strength and make the interaction robust in the case of IEX against changes in salt concentrations. Increased salt concentrations in the feed prevent the binding of impurities to the column, increasing the separation efficiency and capacity for VPs [204,224]. Eckhardt et al. showcased the higher performance of Eshmuno CPX (Merck, Darmstadt, Germany), a bead-based resin using linker polymers, in a screening of IEX bead-based resins for the purification of measles VPs [203]. Aguilar et al. showed the sufficient binding of enveloped VLPs on the exterior surface of linker polymer bead resin [225]. Moreover, the use of linker polymer resins is also highlighted in the literature for their efficacy in viral clearance [226].

On the contrary, reports also show that ligands at high density can result in a binding strength that negatively impacts the recovery and infectivity of VPs. Turnbull et al. showed a time- and ligand-density-dependent yield reduction of non-env. VPs for ligands directly grafted on an AEX fiber resin [227]. A high ligand density in combination with an increased polymer layer thickness was also shown to reduce the infectivity of eluted env. VPs and lead to co-purification of impurities [224,228]. Pamenter et al. observed time-dependent two-step adsorption of LV particles on a strong AEX membrane adsorber [229]. The authors hypothesized a conformational change as the second binding step, resulting in a strong multi-point binding. Strongly bound VPs could only be eluted during the cleaning-in-place (CIP) step. A kinetic approximation resulted in a halving time for the second step of approximately 15 min. A more rigid VP is presumed to withstand the induced conformational change [229].

In ligand density screenings for enveloped and non-env. VPs, the lowest tested density yielded the highest recovered infectious titers [224,228]. Low ligand densities and a shallow polymer layer also reduce ligands that are accessible only to smaller impurities and, thus, decrease the co-purification of such, as observed by Vicente et al. [228].

Parameters such as polymer layer thickness, polymer density, and ligand density remain to be optimized specific to each VP application. This is not feasible within a virus process development. Moreover, customized stationary phases carry a high cost for later upscaling. It is also worth noting that grafted polymer layers reduce the pore or channel diameters, which might result in increased backpressure during loading, prolonging the processing time.

7.1.6. Size Exclusion Chromatography (SEC)

Preparative SEC can be used to separate VPs from smaller, soluble impurities. SEC resins exclude VPs from the resin pores while impurities can enter, resulting in VPs eluting in the void volume and impurities at later fractions. However, it cannot effectively separate impurities near the size of VPs. A buffer exchange can be implemented, which makes this step suitable for polishing. As low flow rates and low feed volumes are required for SEC, a prior concentration step might be needed. SEC steps are characterized by low productivity, lack of scalability, and inevitable dilution [230].

The exclusion of the large VPs, and thus, good separation from impurities, facilitated an overloading of BV particles on a Sepharose SEC column (Cytiva, Marlborough, MT, USA) with still good purification performance [193]. With this approach, the low productivity of SEC was improved by Transfiguracion et al. The SEC nonetheless took 85 min using a 69 mL column and achieved a step recovery of 73% total particles and 64% inf. VPs [193]. Kröber et al. addressed the low productivity of SEC columns by utilizing a simulated moving bed (SMB) approach and coupling multiple columns in a continuous process for the purification of influenza particles [231]. The authors achieved a maximum productivity increase of factor 3.8; however, a scale-up would require longer processing times, thus reducing productivity [231]. An early publication for the purification of coronavirus particles reported superior capabilities of SEC purification compared to overnight SC purification [216]. However, no time benefit was achieved by the utilization of the 466 mL column requiring over 7.5 h for one column exchange.

One advantage of SEC is its ability to facilitate buffer exchange and desalting. This feature allows the use of a favorable buffer environment, which ensures virus integrity during the process. However, it is important to carefully select buffer conditions to prevent any unspecific interactions of VPs which could negatively impact the purification as well as the viral particle integrity. Transfiguracion et al. highlighted the importance of buffer screening and optimization due to the fact that three out of four screened buffers had an initial infectious recovery of below 10% for BV particles [193]. After buffer and salt concentration optimization, a maximum of 97% infectious yield could be reached.

SEC has been observed to exert shear stress on large molecules, a phenomenon that has been particularly noted in polymers and HPLC applications [232]. A study for preparative SEC purification reported significant activity reduction for a non-enveloped and inactivated VP in the foot-and-mouth disease virus (FMDV) [233]. Shearing of VPs within pores has been found to cause alterations in the secondary and tertiary peptide structures on the surface of viruses. However, the negative impacts on VP stability and immunogenicity could be overcome by stabilizing buffer components [233]. In the case of env. VPs, the usually larger particle sizes exclude VPs from entering pores, thus reducing the observed impact. The hydraulic diameter, a value characterizing the flow pattern in the column, has been found to be inversely proportional to the shear rate. Larger resin beads and lower flow rates thus reduce shearing [234].

7.2. Chromatographic Stationary Phases

Various conventional, as well as novel stationary phases have been applied for the purification of virus particles. Illustrated schematics of subsequently discussed stationary phases are shown in Figure 2.

7.2.1. Bead-Based Resins

Conventional chromatography resins typically used for antibody purification are based on porous and functionalized beads. These beads have a highly porous internal volume to increase the functionalized surface area. The internal bead volume is not accessible to enveloped viruses due to steric hindrance based on their large size. Additionally, the low diffusional movement of VPs leads to a high mass transfer resistance. Consequently, the binding capacity of bead-based resins for large VPs is primarily dependent on the outer surface area of the beads, which in turn is influenced by the size of the beads [235]. The size of the beads also has a direct impact on backpressure and shear rates and, thus, the applicable flow rate. Specifically, smaller beads result in an increased binding capacity, but also increased backpressure. This necessitates a reduction in flow rate, rendering this setup unsuitable for a capture step in B&E-mode in which high volumetric feeds need to be

processed. In contrast, larger beads induce low shear rates and have a reduced binding capacity of VPs while sustaining a high binding capacity for impurities. This makes bead-based columns generally more suitable for polishing applications in FT mode instead of B&E capture applications. Specifically optimized resins for VP polishing applications are RAMs, which are discussed in Section 7.2.7.

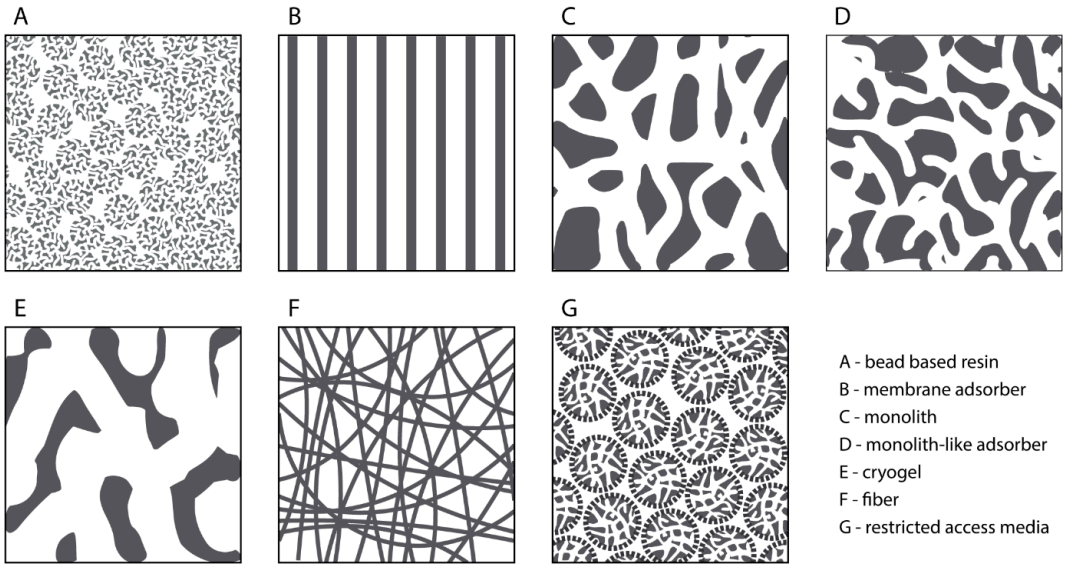

Figure 2. Illustrated schemes of chromatography stationary phases applied for the purification of virus particles. Illustrations not to scale.

The application of VP binding on bead-based resins is explored in several publications. In one study, Rogerson et al. conducted a screening of AEX resins, evaluating the DBC specifically for NDV VPs of size 100 to 500 nm [19]. Their findings revealed a 10-fold higher DBC when using a Poros AEX resin (Thermo Fisher Scientific, Waltham, MA, USA) in comparison to other resin beads. The authors attributed the difference to the larger pore structure of Poros resin. Poros resins are perfusion resins featuring a bimodal pore size distribution of convective macropores and diffusional micropores. Macropores were examined to be in the size range of 100 to 500 nm by Wu et al. [236]. Contractionary to Rogerson et al., Wu et al. observed that human papillomavirus (HPV) VLPs of 50 and 100 nm in size blocked the macropore structures at the surface of the Poros beads and, thus, the internal bead structures were not accessible [236,237]. It is unknown if the observed differences are attributed to different ligand chemistries or the differences in VP types. Regardless of the contradiction, Rogerson et al. demonstrated an NDV concentration ranging from 25- to 60-fold, alongside a 90% reduction in impurity proteins. Despite the promising results with Poros resins, Rogerson's research suggests that convective chromatographic media, such as monoliths, may still offer superior performance. The study reported DBCs up to 7 times higher using a monolith [19].

The use of chromatographic beads featuring tentacle resins, such as Eshmuno (Merck, Darmstadt, Germany), has been highlighted in the literature for their efficacy in viral clearance. This was demonstrated in a study by Aguilar et al. in which an enhancement in specificity and binding capacity was observed [225]. This improvement is believed to be due to an increased virus-accessible functionalized surface area on the bead's exterior and increased binding strength, as discussed in Section 7.1.5. This aligns with a screening of CEX resins conducted by Eckhardt et al. [203] for the purification of oncolytic measles

VPs. Despite the size of measles particles (100 to 300 nm) exceeding the pore size of the beads (80 nm [238]), the Eshmuno CPX column still exhibited the best performance in terms of recovery. A notable disparity between the DBC and the static binding capacity (SBC) was observed by Eckhardt et al.; only 2.3% of the SBC could be realized in DBC in regard to inf. VPs. The potential impact of shearing was considered, as higher flow rates were observed to result in lower infectious particle recovery. In spite of that, the total particle count, including inactivated VPs, was not determined, and thus, slow mass transfer rates can be causative as well. However, the lab-scale experiments yielded an infectious recovery of 81%, albeit with a 17% reduction in the infectious particle ratio. Significant decreases in total protein and hcDNA were observed, with removal rates of 98% and 81%, respectively [203].

Flow rate-related inactivation of env. VPs was observed by Ta et al. on a different AEX tentacle resin, the Nuvia HP-Q (Bio-Rad, Hercules, CA, USA) [239]. In this case, shearing was determined to result in the fragmentation of VPs and, thus, inactivation of influenza VPs. A flow rate reduction improved inf. VP recovery to some extent; however, another reduction did not recover further inf. VPs. A structural change due to strong binding was assumed to be partially responsible for the virus inactivation [239]. Pamenter et al. provide a mechanistic explanation for structural changes of env. VPs due to binding to strong AEX on tentacles [229], which is discussed in Section 7.1.5.

7.2.2. Membrane Adsorber

Membrane chromatography features convective channels through the membrane stationary support with the benefit of low backpressure and high flow rates during loading. These attributes are ideal for early high-volumetric purification stages. The fast mass transfer in convective channels without diffusional limitations ensures constant DBCs over a wide range of flow rates. Membranes with additional diffusional pores are available, but due to the size and diffusional limitations of VPs, these membranes are more suited for polishing VPs in FT mode.

The adsorber membrane is manufactured as a flat sheet and is then packed in a suitable housing to provide an inlet and outlet stream, as well as an ideally even flow distribution over the membrane area. The low ratio of bed height-to-frontal area, typical for membranes, challenges device design to keep an even flow distribution over the membrane. This is achieved through void volumes in the housing, which also facilitates unfavored dispersion and local concentration of particles, thus resulting in early breakthrough and low resolution [240]. Device designs used for lab-scale applications, stacked-disc devices, as well as upscaled radial flow devices, were shown to have low resolution [241]. Lateral flow devices, engineered specifically for large-scale applications, address these issues and, thus, yield an overall better performance [241]. Still, flow velocity heterogeneities that prevail may induce shear stress on particles at high flow rates [242]. The membrane adsorber resin itself has good linear scalability, but the different scale performances need to be considered. With the development of mechanistic models, the effects of hydrodynamic dispersion can be decoupled from particle/membrane interaction and can, thus, support scale-up, even across different device designs [243].

A grafted polymer layer on adsorbers can increase the binding capacity for VPs and impurities as well as inactivate VPs, as discussed in Section 7.1.5. Gautam et al. used a CEX membrane adsorber including a grafted polymer for VSV purification [162]. Sufficient impurity reduction for in vivo studies was reached by the membrane adsorber with an hcP dose level of approx. 40 ng/10^9 $TCID_{50}$. No deformation of particles was observed in TEM analysis, and in vivo studies showed no difference in comparison to a clinical grade process. The question remains if an optimized grafted polymer layer can further reduce the

level of co-purified hcPs. Gautam et al. reached a high concentration factor for VPs using the membrane adsorber; however, presumably due to stringent cutting criteria and low peak resolution, the recovery of infectious particles in the elution fraction was only 30%. Furthermore, a six-times dilution had to be introduced to reduce the salt concentration that was required for the CEX elution [162]. Fernandes et al. evaluated two membrane adsorbers with grafted polymer layers (Sartobind Q, Sartorius, Goettingen, Germany and Mustang Q, Cytiva, Marlborough, MT, USA) in an IEX capture chromatography screening for a VSV pseudovirus purification [154]. Initial screening showed higher performance of these membrane adsorbers compared to the bead-based column in terms of inf. VP recovery and impurity reduction. The use of citrate in the feed improved impurity removal and increased binding capacity for VPs on the membrane. In the final process, an inf. VP step recovery of 80% could be reached and inf. VPs were enriched compared to non-inf. VPs. No significant impact on the oncolytic potency was observed [154]. A TEM analysis showed native bullet-shaped particles as well as round-shaped particles, which has also been reported elsewhere as a processing outcome for VSV particles [83].

The continuous application of membrane adsorbers in a periodic countercurrent chromatography (PCC) setup efficiently uses high flow rates due to low column backpressure while overcoming the limitations of low binding capacity. Due to convective channels, the mass transfer is high, and binding kinetics are relatively independent of flow rates [244]. In a PCC setup, the FT and/or the wash of one column is fed into the next column, achieving a higher loading density on the first column, while unbound VPs bind on the next column. Periodic change of columns achieves a continuous, near-maximal loading and elution of highly concentrated VPs while reducing the required membrane area. The outcome is an increased productivity per membrane area as well as a robustness increase. Matos et al. showcased the application of PCC for the purification of a defective herpesvirus using four membrane units [245]. The challenge in this purification step, namely the low binding strength of VPs and, thus, virus loss during washing was overcome by the post-wash load of the PCC application. A constant yield of over 80% was achieved compared to the variable recovery of 65 to 80% in the batch process [245]. Fortuna et al. applied a pseudo-affinity PCC consisting of 3 membrane units for the purification of inactivated influenza particles and reached a 2.3-fold increase in productivity compared to batch due to efficient utilization of binding capacity [246]. Both examples dealt with the purification of replication-incompetent env. VPs. Applications for replication-competent have only been reported for non-membrane chromatographic systems and non-env. VP [247,248]. It remains to be shown if the continuous PCC approach is also beneficial for replication-competent env. VPs that are more labile and sensitive to environmental stress. PCC systems incorporate a complex fluid stream with more pumps, valves, and flow rate changes, inducing an increased amount of shear stress on particles. Furthermore, PAT sensors in the ATMP field are lacking but are required for dynamic control of PCC and, thus, robust application [245]. While current development is still early, continuous membrane-based PCC systems have the potential to reduce manufacturing costs at a large scale [245].

7.2.3. Monolith Resins

Monoliths share similar properties and advantages over bead-based resins as the membranes discussed earlier. Monoliths are also comprised of convective channels, eliminating diffusional limitations and ensuring a high mass transfer and low backpressure. The difference lies in the polymerization of the resin, which, in the case of the monolith, occurs directly in its final shape—most commonly a hollow cylinder. Thus, no packing or stacking irregularities are observed in monoliths [240,249]. The scalability of monoliths is made possible through the availability of distinct column sizes over a large range of

volumes. It is worth noting that monoliths of different base materials exist. In the case of env. VP purification, usually polymeric-based monoliths comprised of channel sizes in the micrometer range are utilized. Silica-based monoliths are available as well; however, they are comprised of additional diffusional pores, which are inaccessible for VPs and are, thus, not suitable [250].

Due to the convective channels, high mass transfer, and low backpressures, monoliths can be loaded with high flow rates without compromising on DBC, as shown for NDV [19] and influenza VPs [202]. However, the binding kinetic itself might be flow rate limiting, as Gerster et al. reported for the purification of BV particles [163]. This limitation is independent of resin type and has also been reported for membrane adsorbers [207,251]. For column screenings at a small scale and analytics, axial flow disks are utilized, which can be stacked in an appropriate housing to achieve a flexible column volume. Dispersion effects have been observed due to a certain heterogeneity of pore sizes, leading to flow variances within the resin, thus reducing resolution [252]. A radial flow design is used for larger scales. To control the polymerization temperature and, thus, channel sizes of monoliths, the resin geometry is limited in its thickness. Thus, a tubular design with radial flow is used for lab-scale as well as production-scale applications [253]. Due to the required flow distribution for radial flow, the void volume in the device is increased, leading to an additional dispersion factor [254].

Monolith resins are available with different channel sizes, which influences the separation performance and flow properties. Larger channels reduce backpressure, and thus, a higher flow rate can be used, which is beneficial for high-volumetric feeds. However, larger channels also reduce the binding capacity due to a less available surface area. Small channels might not be suitable for the purification of large env. VPs, even though the particle size is smaller than the channel diameter. This was observed for mumps VPs using an immunoaffinity monolith [255], mumps and measles VPs using a HIC monolith [45], and NDV on an AEX monolith [19]. In all cases, no flowthrough and low elution of particles were observed for the lower channel size (1.3 µm), whereas larger channel sizes (2 µm or 6 µm) achieved sufficient recovery of inf. VPs. Sviben et al. assumed convective entrapment or increased shear stress for smaller channels to be the cause [45].

Convective entrapment has been shown to reduce recoveries of various VPs as well plasmids in monoliths for small as well as for larger channels [256–259]. The flow-rate-dependent entrapment in narrowing funnels might be facilitated due to the alternation of narrow and large channel sizes, a structure leading to velocity heterogeneity within the monolith [260]. High flow rates [256,259] and small channel sizes [257] promote entrapment. Low flow rates are impractical in the capture step for VPs where usually a high volumetric feed must be processed. Thus, some extent of entrapment cannot be prevented but should be considered in designing CIP steps to prevent carryover and fouling if monoliths are reused.

Fouling of channels and, ultimately, channel blocking, can also occur for feed material containing high amounts of lipids, as shown for an OH monolith by Burden et al. using a feed derived from a yeast culture [261]. Lipid molecules also compete for binding sites and thus reduce binding capacity if not depleted beforehand. Gerster et al. describe a presumed lipid fouling of an AEX monolith resin leading to reduced recoveries of BV particles [163]. Negatively charged phospholipid fragments become tightly bound to the ligands and capture VPs through membrane fusion. The strong interaction leads to an irreversible capture and reduces recoveries as well as binding capacity. The utilization of an epoxy pre-column column to deplete phospholipid fragments improved the performance of the subsequent AEX monolith (97% VP recovery in all elution fractions compared to 77.6% without a pre-column). An AEX-based purification method for NDV particles was

developed by Rogerson et al. [19], showing a factor of 5 to 65 higher DBC compared to bead-based resins. Interestingly, the breakthrough signal surpassed the feed signal in the chromatogram, presumably due to the displacement of retained particles when the monolith is overloaded.

7.2.4. Monolith-like Particles (MLP)

A novel class of bead-based resins are cellulose-based monolith-like particles that comprise large internal pore structures accessible to large biomolecules. Kadoi et al. polymerized spherical beads of approx. 90 µm in an oil/water emulsion having internal pores of 3 µm mode size [262]. The authors modified the beads for mechanical stability and functionalized them using dextran sulfate as a pseudo-affinity ligand. For inactivated influenza particles, these MLPs showed an HA activity recovery rate of 69% compared to commercially available bead-based pseudo-affinity resins with 35% and lower. Impurity reduction levels were comparable across all resins, while determined DBC was highest for the MLP resin. The handling and scalability of MLPs are comparable to conventional bead-based columns, while the functional properties are more like monoliths. Kadoi et al. showed low backpressure while using high flow rates; however, the question of flow-rate-dependent DBC was not addressed. Large particles are slow in diffusion, thus long diffusional paths into beads require long residence times of particles in the column. Furthermore, the suitability of the MLP approach was shown only for inactivated particles up to 100 nm [262].

7.2.5. Cryogels

Cryogels, structurally akin to monoliths, are characterized by a flexible and sponge-like structure. Their manufacturing process, known as cryopolymerization, leverages a frozen phase to instill porosity within the resin [263]. Compared to monoliths, cryogels consist of significantly wider convective channels, ensuring even lower backpressures but also reduced capacities. Additionally, their elasticity can lead to compression of the structure at higher flow rates and, thus, a sudden increase in backpressure [264]. Despite this, cryogels might allow the direct purification of cell cultures without the need for clarification [264]. In addition, the use of acrylamide monomers for polymerization enables inherent hydrophilicity of the resin surface and thus prevents unspecific adsorption of proteins.

The use of cryogels for affinity chromatography of LV particles was previously described; however, difficulties were reported [264–266]. A limitation of cryogels is their low binding capacity due to the wide channels. Compared to a monolith, cryogels were shown to exhibit an overall lower performance [265]. Streptavidin-coated cryogels were successfully used to bind biotinylated LVs; however, the particles cannot be eluted [266]. Grafted polymer layers have been added to improve the binding capacities of cryogels, and beneficial use could be shown for protein purification [267]; however, published applications for VPs could not be found.

The application of cryogels might be beneficial if non-clarified harvest can be directly purified; however, properties such as capacity, specificity, and mechanical stability to ensure fast processing of high volumetric feeds are a prerequisite.

7.2.6. Fibers

Functionalized fibers assembled as a non-woven fabric membrane have been developed to achieve scalable, convective-driven chromatography devices with fast mass transfers [268]. For instance, cellulose-based nanofiber adsorbers with channels of around 2–3 µm enable the application for large biomolecules such as VPs. Ruscic et al. used AEX-functionalized RC fibers for the purification of LVs and achieved up to 90% recovery

of transduction-active particles [269]. No impact of the nanofiber chromatography step on functional as well as structural viral integrity was observed as evaluated by FT runs and extensive analytical assays such as TEM. The high concentration factor and the possibility to use high flow rates (100 CV/min) rendered it an ideal method for the initial high volumetric reduction step. A 2-log hcP reduction was reached, while hcDNA could not be reduced without nuclease treatment [269]. Using cellulose-based fibers as well, Turnbull et al. evaluated the influence of AEX ligand density and residence time on the infectious recovery of adenoviruses [227]. As discussed in Section 7.1.5, a negative impact of high ligand densities and, thus, reduced recoveries was observed.

7.2.7. Restricted-Access-Media (RAM)

RAM are bead-based resins that feature a functionalized core shielded by a porous layer, thus restricting access to large particles. It is used as a polishing step in FT mode for the removal of small impurities that diffuse through the pores and bind to the core while VPs flow through the resin [270]. RAM can be used irrespective of differences introduced in the genotype of viruses as long as unspecific binding is not introduced, as shown for two orf virus subtypes [70].

Various materials, shell pore sizes, and ligand functionalities are available, 12 of which were challenged by Lothert et al. with clarified harvest containing high impurity levels for an orf purification screening [161]. The authors showed generally similar behavior for the columns, with infectious recoveries in the range of 42% to 87%. Some columns showed a higher capacity for impurity removal; however, these were columns at the lower end of inf. VP recoveries. The choice of RAM depends largely on the feed composition. Shear stress, on-column inactivation, or accessibility of HIC ligands were discussed but not further investigated. Overall, all columns showed low reusability, as impurity reduction worsened after each subsequent cycle, even though thorough CIP steps were applied. In two other studies, Lothert et al. used the CaptoCore700 (CC700, Cytiva, Marlborough, MT, USA) for polishing of orf virus and achieved inf. VP step recoveries of 90% and over 95% [70,271]. The CC700 outperformed other resin and ligand types in terms of recovery and hcDNA depletion [271], while viral integrity remained unimpaired [70].

The application of CC700 as the first chromatographic step before concentration, contrary to its intended use, is reported by Steppert et al. for the purification of measles VPs [67]. The authors loaded clarified harvest directly on the CC700 and yielded an inf. VP recovery of 61%, which was higher than compared to B&E-mode resins. High impurity binding capacities of the CC700 were observed. A scale-up for 8.9 L clarified and nuclease-treated harvest material was processed on a 190 mL column with 4 min column residence time and resulted in near complete inf. VP recovery. However, RAM columns dilute the load instead of concentrating, so a subsequent UF/DF-step for concentration was applied [67].

7.3. Chromatography Summary

Conventional chromatography concepts, such as IEX and SEC, have been successfully applied for env. VPs, and new methods such as SXC are being developed and tested for further process improvements. Especially with affinity chromatography, more development can be expected as the field of viral therapeutics continuous to grow and establishes itself amongst biopharmaceuticals. Intelligent ligand design and novel surface functionalization will improve and better modulate binding strength, and more research will be required to fully understand such binding mechanics.

Additional to the conventional chromatographic stationary phases, novel stationary phases are being developed. These are tailored to accommodate large VPs and high

volumetric process streams. Overall, convective-driven stationary phases have prevailing advantages due to the higher flow rate limits and increased mass transfer rates.

As different viruses most likely differ in key properties influencing binding behavior and process knowledge is unfortunately limited, screening experiments are essential to ascertain the optimal chromatography modalities for each process step.

8. Further VP Purification Techniques

8.1. Flocculation

Alternative purification methods have been explored or transferred from other fields for the purification of env. VPs in occasional studies. For instance, flocculation is conventionally used for viral clearance, but promising results for purification applications have been shown as well [272]. By the addition of high salt or osmolyte concentrations, VPs are specifically flocculated, meaning aggregated. This leads to an even bigger size difference of VPs compared to non-flocculated impurities, and the flocculated VPs are retained in a subsequent filtration step. Diluting the filter retentate afterward reduces the flocculation agent concentration and reverses the flocculation, thereby recovering inf. VPs. This concept was used for enveloped Sindbis VPs, and realized as a three-step filtration process with the initial purification step achieving recoveries of up to 96% [273]. Removal of large amounts of protein was reported, but hcDNA co-aggregated with VPs and, thus, was co-purified. The authors utilized mannitol as a flocculation agent which was shown to work also for a non-enveloped virus, although with a lower recovery rate [273]. Hasan et al. reviewed the utilization of osmolytes as excipients and flocculation agents for vaccine VPs [274]. The authors highlighted the stabilizing effects of osmolytes, contrary to high salt concentrations, and their use as adjuvants and concluded there might not be any need for removing these agents after flocculation.

8.2. Aqueous Two-Phase (ATP) System

Aqueous two-phase (ATP) systems utilize two immiscible aqueous phases, each characterized by distinct partition coefficients for VPs, hcDNA, and hcPs. This differential partitioning facilitates the effective separation of target molecules from impurities. One of the key features of ATP systems is the use of polymers, which can also aid in stabilizing env. VPs. The gentle processing method avoids harsh conditions and minimizes unwanted interactions with the VPs [275]. Various applications for enveloped VLPs or inactivated env. VPs show general good recoveries and purification performances. The flexibility of this system was shown in a continuous setup with the use of an in-line helical mixer and separator, reaching nearly 100% recovery [276]. Optimization possibilities were shown with different polymer chain lengths, e.g., PEG size [277] and osmolyte addition [278]. The only reported application for the purification of infectious VPs was published by Kim et al. for Hepatitis C VPs [279]. A PEG/Dextran system and subsequent low-speed centrifugation for VP recovery was applied, yielding in an inf. VP recovery of 40%.

9. Formulation and Storage

For a safe and effective drug product, it is necessary to maintain high inf. VP titers throughout long-term storage. Storage of VPs is typically in a dried state or at ultra-low temperature. Functional integrity must be preserved through a stable structural integrity, and causes of particle degradation must be eliminated. Physical and chemical factors resulting in the degradation and loss of particles include freeze/thaw damage, pH changes, surface adsorption, shear stress, oxidative denaturation, and thermal stress. Pan et al. provide an extensive evaluation of these factors and describe formulation strategies for VPs for preventing or at least minimizing their negative impacts [280]. Membrane

proteins, exposed on the outside of env. VPs, are especially prone to degradation. Surface glycoproteins such as spike proteins enable attachment to host cells and thus initiate the viral replication cycle. Their functionality must be preserved, and the task of VP formulation is thus similar to protein formulation.

At the end of a production process, env. VPs, and also other VPs, undergo buffer exchange into the final formulation buffer. Direct addition of excipients may also be required prior to a sterile filtration step. The formulation buffer composition depends on the biophysical properties of the VPs, along with the desired storage conditions. In addition, safe patient administration must be achieved. Although the mechanisms of storage degradation processes and their prevention by excipients are understood to some extent [280], a thorough screening of stabilizing agents is usually needed [281,282]. For each VP in development, forced degradation studies are performed to define the space for later formulation, including FT-cycle stability, pH and salt tolerability, temperature and mechanical stability, and propensity for aggregation with test excipients [281,282]. Beyond that, formulation screenings involve stability studies at storage conditions and accelerated storage conditions [281,282]. For instance, Homan et al. reviewed stability studies of env. and non-env. VPs in liquid formulations which were stored at different temperatures [283]. They found that lower temperatures correlated with longer functional stability. It is noteworthy that the authors pointed out the importance of storing VPs below the solution's glass transition temperature (Tg), at which molecules' and atoms' severely limited motion prevent degradation processes. Tg is estimated for VP solutions to be between −35 °C and −60 °C. At temperatures of at least 50 °C below Tg, reached only in liquid nitrogen tanks, almost infinite stability is reached. Homan et al. had access to stability studies of seven different virus strains and developed a generalized stability model, predicting long-term recovery losses. In these long-term stability studies, degradation due to the freezing and thawing process is excluded from the results and evaluated in specialized studies. An extrapolation over 10, 20, and 30 years of VP solution stored at −70 °C predicted infectivity losses to be lower than 0.3, 0.5, and 0.7 $\log_{10}$, respectively [283].

9.1. Liquid Formulation

VPs stored in a liquid formulation for drug products require aliquoting into small-volume containers and the subsequent freezing and storage at temperatures below −70 °C [283]. The formulation is designed to maintain VP stability during the FT-cycle, and also while in frozen storage. Various buffer components and excipients can be used to maintain particle infectivity during this process.

Buffering agents are essential in maintaining the pH of the formulation, which is critical for the stability and activity of the VPs. Common buffering agents include phosphate buffers, histidine, and citrate. These agents stabilize the pH at a virus-specific optimal setpoint, thus preventing pH-induced degradation. During freezing, the pH of the buffer solution can change drastically due to the successive crystallization of buffer substances. The intensity of this change depends on the type and concentration of the buffer components. Salts can be added to mitigate pH shift, and amorphous excipients like sucrose or alginate can inhibit buffer crystallization [280].

The concentration changes upon freezing can also result in osmotic pressure impacting the viral integrity as well as the VP's surrounding hydration layer, which influences membrane protein functionality. Virus inactivation, degradation, and aggregation follow. Cryoprotectants serve as stabilizing agents, reducing ice crystal formation, balancing the osmotic pressure, and replacing water molecules bound to proteins. Cryoprotectants used in viral formulations include saccharides (e.g., sucrose, trehalose), polyols (e.g., sorbitol, PEG), and albumin, as well as cations such as calcium and magnesium [280,282].

Surface adsorption of VPs results in particle aggregation and is accelerated through mechanical forces like stirring and shaking. Surfactants such as polysorbate and poloxamer are used to prevent adsorption through the shielding of interfaces [284]. However, polysorbate degradation by residual enzymatic hcPs is a known challenge in industry [285] and degradation products of polysorbate were shown to inactivate env. VPs [286]. Oxidation processes can alter membrane protein and lipids of env. VPs resulting in inactivation [178,280]. Cellular proteins such as albumin, as well as amino acids such as methionine and histidine, were shown to protect VPs from oxidation.

9.2. Lyophilized Formulation

The subsequent sublimation process, the removal of water from virus formulations, further stabilizes virus preparations. After lyophilization, the dried preparations can be stored at higher temperatures, for live vaccines usually at −20 °C or, as reported by Hansen et al., between 2 and 8 °C [287]. This reduces the requirements on storage and logistics but, at the same time, introduces another process step, potentially reducing the infectivity of VP. Lyophilized formulations require the addition of a bulking agent to guarantee the formation of a solid cake when lyophilized. Commonly used bulking agents include mannitol and amino acids such as glycine [280]. Env. VPs, as highly sensitive particles, require a high amount of stabilizers and complex formulations to facilitate sufficient inf. VP recovery [288,289]. These formulations necessitate a high development effort. An alternative to lyophilization is spray drying, which embeds the VPs in a glassy matrix of, e.g., starch, thus preserving its function [289]. The potential detrimental freezing process is prevented, and the water is evaporated. Coleman et al. compared both processes for the storage of BV. No loss of infectivity was observed for spray drying or lyophilization. Spray-dried VPs showed enhanced stability against high temperatures of, e.g., 85 °C for 1 h or 30 °C for one week, which significantly reduces storage requirements [289].

10. Summary and Conclusions

Process development for replication-competent env. VPs for therapeutic purposes is particularly challenging due to their high sensitivity to environmental stress. The functional integrity of these particles is crucial for a safe and effective treatment, but the manufacturing process imposes a negative impact and challenges this integrity. Thus, thorough evaluation and then optimization of potential impacting parameters are indispensable.

Advanced analytical methods are essential to assess the impact of process steps on particles and determine their quality and integrity. A combination of such methods is required to evaluate VP preparations completely, and methods include infectious titer assays, total virus particle quantification, and structural analysis.

A comprehensive overview of the current state of bioprocessing for replication-competent env. VPs is provided in this review. Bench-scale centrifugation methods for concentration and purification are less effective compared to contemporary chromatographic techniques, which offer higher recovery and purity. Both conventional and modern chromatographic techniques are evaluated, with variable reported recoveries across different publications, mainly dependent on the viruses studied. Table 2 presents an exemplary selection of contemporary and scalable purification processes for several env. VPs. Differences in purification strategies due to specific VP properties and virus life cycles are apparent. For intracellular VPs, cell disruption is necessary, but it introduces additional impurities that burden downstream processes. The orf process described by Lothert et al. utilizes an FT-cycle for cell disruption and requires a subsequent filtration train for clarification, with a coarse primary filtration step [70]. In the measles process by Steppert et al., a single and coarse clarification filter is sufficient due to the subsequent RAM chro-

matography step in FT mode [67]. This enables a gentle initial processing for the sensitive measles VPs, however requires a subsequent UF/DF step for concentration. Upstream conditions significantly influence VP quality and heterogeneity, with continuous harvest concepts aiming to mitigate the adverse effects of the cell culture environment. However, Gränicher et al. compared the batch and continuous harvest bioprocessing of vaccinia VPs, showing similar results in overall yield and impurities [129]. However, the final VP titers are not explicitly stated. Nuclease treatment is often necessary to degrade hcDNA and improve the processability of the virus feed. This is also observed in Table 2, in which the sole use of fine filters ($\leq$1 µm) for clarification is only applied if the nuclease step is applied prior to clarification. Filtration methods are ubiquitously used in the purification process of env. VPs, but careful selection of filter materials and optimization of pore sizes are necessary to maintain viral integrity and achieve high yield. Various UF/DF modalities and filter materials are applied in the referenced processes in Table 2, each optimized to the specific VP properties. Convective-driven stationary phases are beneficial for processing high volumes without mass transfer resistances, especially immediately after the harvest stage. This is also reflected in Table 2 with the use of solely membrane stationary phases for B&E chromatography steps.

Emerging trends and technologies in the field of VP purification include the development of more specific and high-throughput analytical methods, continuous processing techniques, and advanced chromatographic methods. These advancements have the potential to significantly impact the field by improving the efficiency and robustness of VP purification processes. However, every virus is different, and purification approaches need to be tested for every virus, especially if the separation principle relies on virus-specific characteristics such as size, structure, stability, and surface proteins. Many approaches have proven beneficial for vaccine or virus-like particle (VLP) applications, but method transfer and optimization for more sensitive replication-competent env. VPs are often still outstanding.

This review highlights the demand for optimized purification strategies to ensure the safety and efficacy of virus-based therapeutics. By addressing the complexities and providing insights into best practices, valuable knowledge is contributed to the field of viral bioprocessing, ultimately supporting the development of effective and stable viral therapies and vaccines.

Table 2. Selected examples include technical details of scalable VP purification processes of VPs within the scope of the review (replication-competent, enveloped VPs with therapeutic application potential). No complete process descriptions including infectivity analysis could be found for myxoma virus, NDV, LCMV, and influenza. Abbreviations: adh.—adherent; susp.—suspension; conc.—concentration; n.a.—not applicable. Manufacturer information: c-LEcta (Leipzig, Germany), Cytiva (Marlborough, MT, USA), Merck (Darmstadt, Germany), Sartorius Stedim (Goettingen, Germany), Spectrum Laboratories (Rancho Dominguez, CA, USA).

Virus	Upstream			Downstream				Final Product	Process Performance
	Cell Culture	Virus Harvest and Release	Nucleic Acid Digestion	Clarification (Primary and Secondary)	1st Purification (Capture)	2nd Purification (Polish)	Sterile Filtration	Infectivity, Dosage, and Impurities	IU Overall Process Yield
HSV-2 [290], (repl.-def. vaccine production)	Adh. Vero cells, MOI 0.01, TOH 24–72 hpi	Dextran sulfate, 100 µg/mL, up to 24 h, further processing of supernatant	e.g., Benzonase (Merck): 90 U/mL + 5 mM $MgCl^2$, at 25 °C for 4–6 h	Filtration (e.g., Sartopure PP2, 0.65 µm (Sartorius Stedim))	AEX (e.g., Mustang Q membrane (Cytiva)): high-salt elution (2 M NaCl)	UF/DF (e.g., hollow fiber PS, 100 kDa, Spectrum Laboratories): TFF conc. (5–10×), DF (3–5×)	n.a. due to VP size, aseptic process suggested	>1 × 10^7 pfu/mL hcDNA < 10 ng/dose hcP: 30 µg/mL 10^7 pfu/dose	10% to 20%
Orf [70]	Adh. Vero cells, MOI 0.05, TOH 120 hpi	Intracellular VP release by a FT-cycle, further processing of complete broth	Benzonase (Merck): 250 U/mL, 1 h at RT, after clarification	Filtration 5 µm and 0.65 µm, Sartopure PP3 (Sartorius) or Millistak cellulose with DE (Merck)	SXC binding at 8% PEG8000 on RC membrane stack (pore size 1 µm)	RAM: CC700 (Cytiva)	not discussed	1.1–4.2 × 10^6 IU/mL total DNA: ~1 ng/dose total protein < LOD 10^6 IU/dose	64%
Vaccinia [129], (MVA, batch process)	Avian susp. cells, MOI: 0.05, TOH at cell viability ~70%	Cell culture broth was further processed	Denerase (c-LEcta): 35 U/mL + 3 mM $MgCl^2$, 4 h 37 °C, after clarification	Primary: Acoustic settler (3 W, 2.1 MHz, 252 mL/h) Secondary: Filtration 0.45 µm, Sartopure PP3 (Sartorius Stedim)	Pre-filtration (0.45 µm, CA SXC: binding at 7.2% PEG6000 on RC membrane stack (pore size 1 µm)	n.a.	not discussed	>5 × 10^7 $TCID_{50}$/mL hcDNA < 10 ng/dose total protein: 11–37 µg/dose 1.4 × 10^8 $TCID_{50}$/dose	55%
Vaccinia [129], (MVA, continuous perfusion process)	Avian susp. cells, MOI 0.05, TOH start 40 hpi	Continuous harvest of cell culture broth	Denerase (c-LEcta): 37 U/mL + 4 mM $MgCl^2$, 4 h 37 °C, after clarification	As batch process	As batch process	n.a.	not discussed	Titers as batch process hcDNA < 10 ng/dose total protein: ~10 µg/dose 1.4 × 10^8 $TCID_{50}$/dose	51%
Measles [67]	Adh. Vero cells, MOI: 0.001 to 0.01	Supernatant was further processed	Benzonase (Merck): 50 U/mL + 2 mM $MgCl_2$ for 1 h 37 °C after clarification	Filtration, 3 µm: Sartopure PP3 (Sartorius Stedim)	RAM: CC700 (Cytiva)	UF/DF (cellulose flat sheet membrane, 100 kDa, Merck): TFF conc. (~9×), DF (5×)	n.a. due to VP size, aseptic process suggested	7.9 × 10^6 $TCID_{50}$/mL dsDNA: 354 ng/mL → 18 ng/dose hcP: 18 µg/mL → 1 µg/dose 10^5 IU/dose	only step yields are disclosed, see reference
VSV [154], (rVSV-NDV, fusogenic virus)	Avian susp. cells, MOI 0.0001, TOH at cell viability ~90% (between 48 and 67 hpi)	Cell culture broth was further processed	Denerase (c-LEcta): 20 U/mL + 2 mM $MgCl_2$, 1 h at RT	Primary: Filtration 1–0.4 µm Millistak CE (Cytiva) Secondary: Filtration 0.45 µm Sartopure PP3 (Sartorius Stedim)	AEX membrane Sartobind Q (Sartorius): Elution at 1.2 M NaCl	Pre-dilution (4×), UF/DF (PES hollow fiber, 750 kDa, Cytiva): TFF conc. (4×), DF (6×)	Supor EKV Mini Kleenpak filter 0.2 µm (Cytiva)	4 × 10^9 $TCID_{50}$/mL total DNA: 1.4 ng/mL total protein: 0.3 µg/mL 5 × 10^7 to 5 × 10^{10} IU/dose	65%

Author Contributions: Conceptualization, A.S., J.K.M.N. and J.H.; writing—original draft preparation, A.S.; writing—review and editing, A.S., J.K.M.N. and J.H. All authors have read and agreed to the published version of the manuscript.

Funding: This research received no external funding.

Data Availability Statement: No new data were created or analyzed in this study. Data sharing is not applicable to this article.

Conflicts of Interest: Adrian Schimek and Judy Ng report a relationship with ViraTherapeutics GmbH that includes employment. Judy Ng has patent #US20220010286A1 pending to BoehringerIngelheim International GmbH. If there are other authors, they declare that they have no known competing financial interests or personal relationships that could have appeared to influence the work reported in this paper.

Abbreviations

The following abbreviations are used in this manuscript:

AAV	adeno-associated viral vectors
AEX	anion-exchange chromatography
ATF	alternating TFF
ATMP	advanced therapy medicinal product
ATP	aqueous two-phase
B&E	bind-and-elute
BV	baculovirus
CA	cellulose acetate
CC700	CaptoCore700
CEX	cation-exchange chromatography
CIP	cleaning-in-place
DBC	dynamic binding capacity
DE	diatomaceous earth
DENV	dengue virus
DF	diafiltration
DIP	defective interfering particle
DLS	dynamic light scattering
DNA	deoxyribonucleic acid
ELISA	enzyme-linked immunosorbent assay
EM	electron microscopy
EU	European Union
EV	extracellular vesicle
FDA	food and drug administration
FFF	field flow fractionation
FMDV	foot-and-mouth-disease virus
FT	flowthrough
FT-cycle	freeze/thaw cycle
GF	glass fibers
HA	hemagglutination assay
HIC	hydrophobic interaction chromatography
HIV	human immunodeficiency viruses
HPLC	high-performance liquid chromatography
HPV	human papillomavirus
HSV	herpes simplex virus
IEP	isoelectric point
IEX	ion exchange chromatography

IU	infectious unit
LCMV	lymphocytic choriomeningitis
LS	light scattering
LV	lentivirus
MALDI-MS	matrix-assisted laser desorption/ionization MS
MALS	multi-angle LS
MLP	monolith-like particles
MOI	multiplicity of infection
MS	mass spectrometry
MVA	modified vaccinia ankara
NC	nitrocellulose
NDV	Newcastle disease virus
NFF	normal flow filtration
NGS	next-generation sequencing
NTA	nanoparticle tracking analysis
NYL	nylon
OV	oncolytic virus
P:IU	particles-to-infectious unit ratio
PAT	process analytical technology
PCC	periodic countercurrent chromatography
PCR	polymerase chain reaction
PEG	polyethylene glycol
PES	polyethersulfone
PFAS	polyfluoroalkyl substance
PP	polypropylene
PS	polysulfone
PVDF	polyvinylidene fluoride
RAM	restricted access media
RC	regenerated cellulose
RI	refractive index
RID	radial immunodiffusion
RNA	ribonucleic acid
RSV	respiratory syncytial virus
SBC	static binding capacity
SC	sucrose cushion
SEC	size exclusion chromatography
SLS	static LS
SMB	simulated moving bed
STR	stirred tank reactor
SXC	steric exclusion chromatography
T-VEC	Talimogene laherparepvec
TCID50	50% tissue culture infective dose assay
TEM	transmission electron microscopy
TFDF	tangential flow depth filtration
TFF	tangential flow filtration
TMP	transmembrane pressure
TOH	timepoints of harvest
TOI	timepoint of infection
UF	ultrafiltration
UV	ultraviolet
VLP	virus-like particle
VP	virus particle
VSV	vesicular stomatitis virus
aMPV	avian metapneumovirus

cGE	capillary gel electrophoresis
cyro-EM	cryogenic EM
dPCR	digital PCR
ddPCR	digital droplet PCR
env. VP	enveloped VP
hcDNA	host cell DNA
hcP	host cell protein
hpi	hours post-infection
inf. VP	infectious VP
non-env. VP	non-enveloped VP
non-inf. VP	non-infectious VP
nsEM	negative staining EM
pfu	plaque-forming units
qPCR	quantitative PCR

References

1. bin Umair, M.; Akusa, F.N.; Kashif, H.; Seerat-e-Fatima; Butt, F.; Azhar, M.; Munir, I.; Ahmed, M.; Khalil, W.; Sharyar, H.; et al. Viruses as Tools in Gene Therapy, Vaccine Development, and Cancer Treatment. *Arch. Virol.* **2022**, *167*, 1387–1404. [CrossRef]
2. Montero, D.A.; Vidal, R.M.; Velasco, J.; Carreño, L.J.; Torres, J.P.; Benachi O., M.A.; Tovar-Rosero, Y.-Y.; Oñate, A.A.; O'Ryan, M. Two Centuries of Vaccination: Historical and Conceptual Approach and Future Perspectives. *Front. Public. Health* **2024**, *11*, 1326154. [CrossRef]
3. Salmon, F.; Grosios, K.; Petry, H. Safety Profile of Recombinant Adeno-Associated Viral Vectors: Focus on Alipogene Tiparvovec (Glybera®). *Expert Rev. Clin. Pharmacol.* **2014**, *7*, 53–65. [CrossRef] [PubMed]
4. White, M.; Whittaker, R.; Gándara, C.; Stoll, E.A. A Guide to Approaching Regulatory Considerations for Lentiviral-Mediated Gene Therapies. *Hum. Gene Ther. Methods* **2017**, *28*, 163–176. [CrossRef]
5. Alwithenani, A.; Hengswat, P.; Chiocca, E.A. Oncolytic Viruses as Cancer Therapeutics: From Mechanistic Insights to Clinical Translation. *Mol. Ther.* **2025**. [CrossRef] [PubMed]
6. Schoeps, B.; Lauer, U.M.; Elbers, K. Deciphering Permissivity of Human Tumor Ecosystems to Oncolytic Viruses. *Oncogene* **2025**, *44*, 1069–1077. [CrossRef] [PubMed]
7. Bartlett, D.L.; Liu, Z.; Sathaiah, M.; Ravindranathan, R.; Guo, Z.; He, Y.; Guo, Z.S. Oncolytic Viruses as Therapeutic Cancer Vaccines. *Mol. Cancer* **2013**, *12*, 103. [CrossRef]
8. Kohlhapp, F.J.; Kaufman, H.L. Molecular Pathways: Mechanism of Action for Talimogene Laherparepvec, a New Oncolytic Virus Immunotherapy. *Clin. Cancer Res.* **2016**, *22*, 1048–1054. [CrossRef]
9. U.S. National Library of Medicine. On Clinicaltrials.gov, the Search Term "Oncolytic Virus" was Used as a Keyword in the Field Other Terms. The Recruitment Status Was Filtered for not yet Recruiting; Recruiting; Enrolling by Invitation; Active, Not Recruiting. The search was Conducted on 21 February 2025 with 103 Results (67 using Enveloped, 33 non-Enveloped VPs). Available online: https://clinicaltrials.gov/search?term=oncolytic%20virus (accessed on 21 February 2025).
10. He, B.; Wilson, B.; Chen, S.-H.; Sharma, K.; Scappini, E.; Cook, M.; Petrovich, R.; Martin, N.P. Molecular Engineering of Virus Tropism. *Int. J. Mol. Sci.* **2024**, *25*, 11094. [CrossRef]
11. Lundstrom, K. Viral Vectors in Gene Therapy: Where Do We Stand in 2023? *Viruses* **2023**, *15*, 698. [CrossRef]
12. EMA (European Medicines Agency), Guideline on Quality, Non-Clinical and Clinical Requirements for Investigational Advanced Therapy Medicinal Products in Clinical Trials; Ref. No. EMA/CAT/22473/2025, 2025.
13. EMA (European Medicines Agency), Guideline on the Quality, Non-Clinical and Clinical Aspects of Gene Therapy Medicinal Products; Ref. No. EMA/CAT/80183/2014, 2018.
14. Ungerechts, G.; Bossow, S.; Leuchs, B.; Holm, P.S.; Rommelaere, J.; Coffey, M.; Coffin, R.; Bell, J.; Nettelbeck, D.M. Moving Oncolytic Viruses into the Clinic: Clinical-Grade Production, Purification, and Characterization of Diverse Oncolytic Viruses. *Mol. Ther. Methods Clin. Dev.* **2016**, *3*, 16018. [CrossRef] [PubMed]
15. Eilts, F.; Steger, M.; Pagallies, F.; Rziha, H.-J.; Hardt, M.; Amann, R.; Wolff, M.W. Comparison of Sample Preparation Techniques for the Physicochemical Characterization of Orf Virus Particles. *J. Virol. Methods* **2022**, *310*, 114614. [CrossRef] [PubMed]
16. Ma, R.; Li, Z.; Chiocca, E.A.; Caligiuri, M.A.; Yu, J. The Emerging Field of Oncolytic Virus-Based Cancer Immunotherapy. *Trends Cancer* **2023**, *9*, 122–139. [CrossRef]
17. Rossini, E.; Bazzucchi, M.; Trocchi, V.; Merzoni, F.; Bertasio, C.; Knauf, S.; Lavazza, A.; Cavadini, P. Identification and Characterisation of a Myxoma Virus Detected in the Italian Hare (Lepus Corsicanus). *Viruses* **2024**, *16*, 437. [CrossRef]

18. Ge, P.; Tsao, J.; Schein, S.; Green, T.J.; Luo, M.; Hong Zhou, Z. Cryo-EM Model of the Bullet-Shaped Vesicular Stomatitis Virus. *Science* **2010**, *327*, 689–693. [CrossRef] [PubMed]
19. Rogerson, T.; Xi, G.; Ampey, A.; Borman, J.; Jaroudi, S.; Pappas, D.; Linke, T. Purification of a Recombinant Oncolytic Virus from Clarified Cell Culture Media by Anion Exchange Monolith Chromatography. *Electrophoresis* **2023**, *44*, 1923–1933. [CrossRef]
20. Stachura, P.; Stencel, O.; Lu, Z.; Borkhardt, A.; Pandyra, A.A. Arenaviruses: Old Viruses Present New Solutions for Cancer Therapy. *Front. Immunol.* **2023**, *14*, 1110522. [CrossRef]
21. Lee, K.J.; Novella, I.S.; Teng, M.N.; Oldstone, M.B.A.; de la Torre, J.C. NP and L Proteins of Lymphocytic Choriomeningitis Virus (LCMV) Are Sufficient for Efficient Transcription and Replication of LCMV Genomic RNA Analogs. *J. Virol.* **2000**, *74*, 3470–3477. [CrossRef]
22. Neuman, B.W.; Adair, B.D.; Burns, J.W.; Milligan, R.A.; Buchmeier, M.J.; Yeager, M. Complementarity in the Supramolecular Design of Arenaviruses and Retroviruses Revealed by Electron Cryomicroscopy and Image Analysis. *J. Virol.* **2005**, *79*, 3822–3830. [CrossRef]
23. Kabiljo, J.; Laengle, J.; Bergmann, M. From Threat to Cure: Understanding of Virus-Induced Cell Death Leads to Highly Immunogenic Oncolytic Influenza Viruses. *Cell Death Discov.* **2020**, *6*, 48. [CrossRef]
24. Brown, E.G. Influenza Virus Genetics. *Biomed. Pharmacother.* **2000**, *54*, 196–209. [CrossRef] [PubMed]
25. Arakawa, T.; Yamasaki, H.; Ikeda, K.; Ejima, D.; Naito, T.; Koyama, A. Antiviral and Virucidal Activities of Natural Products. *Curr. Med. Chem.* **2009**, *16*, 2485–2497. [CrossRef] [PubMed]
26. Weiss, K.; Salzig, D.; Gerstenberger, J.; Röder, Y.; Cichutek, K.; Pörtner, R.; Czermak, P.; Mühlebach, M.D. Influence of Process Conditions on Measles Virus Stability. *Am. J. Biochem. Biotechnol.* **2013**, *9*, 243–254. [CrossRef]
27. Loewe, D.; Häussler, J.; Grein, T.A.; Dieken, H.; Weidner, T.; Salzig, D.; Czermak, P. Forced Degradation Studies to Identify Critical Process Parameters for the Purification of Infectious Measles Virus. *Viruses* **2019**, *11*, 725. [CrossRef]
28. Sviben, D.; Forčić, D.; Kurtović, T.; Halassy, B.; Brgles, M. Stability, Biophysical Properties and Effect of Ultracentrifugation and Diafiltration on Measles Virus and Mumps Virus. *Arch. Virol.* **2016**, *161*, 1455–1467. [CrossRef]
29. Higashikawa, F.; Chang, L.-J. Kinetic Analyses of Stability of Simple and Complex Retroviral Vectors. *Virology* **2001**, *280*, 124–131. [CrossRef]
30. Segura, M.d.l.M.; Kamen, A.; Trudel, P.; Garnier, A. A Novel Purification Strategy for Retrovirus Gene Therapy Vectors Using Heparin Affinity Chromatography. *Biotechnol. Bioeng.* **2005**, *90*, 391–404. [CrossRef]
31. Huangfu, C.; Zhang, J.; Ma, Y.; Jia, J.; Li, J.; Lv, M.; Ma, X.; Zhao, X.; Zhang, J. Large-scale Purification of High Purity A1-antitrypsin from Cohn Fraction IV with Virus Inactivation by Solvent/Detergent and Dry-heat Treatment. *Biotechnol. Appl. Biochem.* **2018**, *65*, 446–454. [CrossRef]
32. Roberts, P.L. Virus Inactivation by Solvent/Detergent Treatment Using Triton X-100 in a High Purity Factor VIII. *Biologicals* **2008**, *36*, 330–335. [CrossRef]
33. Meingast, C.; Heldt, C.L. Arginine-enveloped Virus Inactivation and Potential Mechanisms. *Biotechnol. Prog.* **2020**, *36*, e2931. [CrossRef]
34. Burns, J.C.; Friedmann, T.; Driever, W.; Burrascano, M.; Yee, J.K. Vesicular Stomatitis Virus G Glycoprotein Pseudotyped Retroviral Vectors: Concentration to Very High Titer and Efficient Gene Transfer into Mammalian and Nonmammalian Cells. *Proc. Natl. Acad. Sci. USA* **1993**, *90*, 8033–8037. [CrossRef] [PubMed]
35. Bowles, N.E.; Eisensmith, R.C.; Mohuiddin, R.; Pyron, M.; Woo, S.L.C. A Simple and Efficient Method for the Concentration and Purification of Recombinant Retrovirus for Increased Hepatocyte Transduction In Vivo. *Hum. Gene Ther.* **1996**, *7*, 1735–1742. [CrossRef] [PubMed]
36. Michalsky, R.; Pfromm, P.H.; Czermak, P.; Sorensen, C.M.; Passarelli, A.L. Effects of Temperature and Shear Force on Infectivity of the Baculovirus Autographa Californica M Nucleopolyhedrovirus. *J. Virol. Methods* **2008**, *153*, 90–96. [CrossRef] [PubMed]
37. Schimek, A.; Ng, J.K.M.; Basbas, I.; Martin, F.; Xin, D.; Saleh, D.; Hubbuch, J. An HPLC-SEC-Based Rapid Quantification Method for Vesicular Stomatitis Virus Particles to Facilitate Process Development. *Mol. Ther. Methods Clin. Dev.* **2024**, *32*, 101252. [CrossRef]
38. Eilts, F.; Labisch, J.J.; Orbay, S.; Harsy, Y.M.J.; Steger, M.; Pagallies, F.; Amann, R.; Pflanz, K.; Wolff, M.W. Stability Studies for the Identification of Critical Process Parameters for a Pharmaceutical Production of the Orf Virus. *Vaccine* **2023**, *41*, 4731–4742. [CrossRef]
39. Lesch, H.P.; Laitinen, A.; Peixoto, C.; Vicente, T.; Makkonen, K.-E.; Laitinen, L.; Pikkarainen, J.T.; Samaranayake, H.; Alves, P.M.; Carrondo, M.J.T.; et al. Production and Purification of Lentiviral Vectors Generated in 293T Suspension Cells with Baculoviral Vectors. *Gene Ther.* **2011**, *18*, 531–538. [CrossRef]
40. Flint, S.J.; Racaniello, V.R.; Rall, G.F.; Hatziioannou, T.; Skalka, A.M. *Principles of Virology*; The Biomedical & Life Sciences Collection; ASM Press: Washington, DC, USA, 2020; ISBN 978-1-683-67360-6.

41. Prentoe, J.; Jensen, T.B.; Meuleman, P.; Serre, S.B.N.; Scheel, T.K.H.; Leroux-Roels, G.; Gottwein, J.M.; Bukh, J. Hypervariable Region 1 Differentially Impacts Viability of Hepatitis C Virus Strains of Genotypes 1 to 6 and Impairs Virus Neutralization. *J. Virol.* **2010**, *85*, 2224–2234. [CrossRef]
42. Miller, C.A.; Raine, C.S. Heterogeneity of Virus Particles in Measles Virus. *J. Gen. Virol.* **1979**, *45*, 441–453. [CrossRef]
43. Lodish, H.F.; Porter, M. Heterogeneity of Vesicular Stomatitis Virus Particles: Implications for Virion Assembly. *J. Virol.* **1980**, *33*, 52–58. [CrossRef]
44. DeLong, J.P.; Al-Sammak, M.A.; Al-Ameeli, Z.T.; Dunigan, D.D.; Edwards, K.F.; Fuhrmann, J.J.; Gleghorn, J.P.; Li, H.; Haramoto, K.; Harrison, A.O.; et al. Towards an Integrative View of Virus Phenotypes. *Nat. Rev. Microbiol.* **2022**, *20*, 83–94. [CrossRef]
45. Sviben, D.; Forcic, D.; Ivancic-Jelecki, J.; Halassy, B.; Brgles, M. Recovery of Infective Virus Particles in Ion-Exchange and Hydrophobic Interaction Monolith Chromatography Is Influenced by Particle Charge and Total-to-Infective Particle Ratio. *J. Chromatogr. B* **2017**, *1054*, 10–19. [CrossRef]
46. Cantin, R.; Méthot, S.; Tremblay, M.J. Plunder and Stowaways: Incorporation of Cellular Proteins by Enveloped Viruses. *J. Virol.* **2005**, *79*, 6577–6587. [CrossRef] [PubMed]
47. Segura, M.d.l.M.; Garnier, A.; Kamen, A. Purification and Characterization of Retrovirus Vector Particles by Rate Zonal Ultracentrifugation. *J. Virol. Methods* **2006**, *133*, 82–91. [CrossRef] [PubMed]
48. Brown, G.; Aitken, J.; Rixon, H.W.M.; Sugrue, R.J. Caveolin-1 Is Incorporated into Mature Respiratory Syncytial Virus Particles during Virus Assembly on the Surface of Virus-Infected Cells. *J. Gen. Virol.* **2002**, *83*, 611–621. [CrossRef] [PubMed]
49. Hammarstedt, M.; Ahlqvist, J.; Jacobson, S.; Garoff, H.; Fogdell-Hahn, A. Purification of Infectious Human Herpesvirus 6A Virions and Association of Host Cell Proteins. *Virol. J.* **2007**, *4*, 101. [CrossRef]
50. Stegen, C.; Yakova, Y.; Henaff, D.; Nadjar, J.; Duron, J.; Lippé, R. Analysis of Virion-Incorporated Host Proteins Required for Herpes Simplex Virus Type 1 Infection through a RNA Interference Screen. *PLoS ONE* **2013**, *8*, e53276. [CrossRef]
51. Minh, A.D.; Kamen, A.A. Critical Assessment of Purification and Analytical Technologies for Enveloped Viral Vector and Vaccine Processing and Their Current Limitations in Resolving Co-Expressed Extracellular Vesicles. *Vaccines* **2021**, *9*, 823. [CrossRef]
52. Cantin, R.; Diou, J.; Bélanger, D.; Tremblay, A.M.; Gilbert, C. Discrimination between Exosomes and HIV-1: Purification of Both Vesicles from Cell-Free Supernatants. *J. Immunol. Methods* **2008**, *338*, 21–30. [CrossRef]
53. Urbanelli, L.; Buratta, S.; Tancini, B.; Sagini, K.; Delo, F.; Porcellati, S.; Emiliani, C. The Role of Extracellular Vesicles in Viral Infection and Transmission. *Vaccines* **2019**, *7*, 102. [CrossRef]
54. Cordelier, P. Unveiling the Nexus: Oncolytic Viruses, Extracellular Vesicles, and Immune Modulation. *Mol. Ther. Oncol.* **2025**, *33*, 200940. [CrossRef]
55. McCormick, W.; Mermel, L.A. The Basic Reproductive Number and Particle-to-Plaque Ratio: Comparison of These Two Parameters of Viral Infectivity. *Virol. J.* **2021**, *18*, 92–95. [CrossRef] [PubMed]
56. Bhat, T.; Cao, A.; Yin, J. Virus-like Particles: Measures and Biological Functions. *Viruses* **2022**, *14*, 383. [CrossRef] [PubMed]
57. Frensing, T.; Heldt, F.S.; Pflugmacher, A.; Behrendt, I.; Jordan, I.; Flockerzi, D.; Genzel, Y.; Reichl, U. Continuous Influenza Virus Production in Cell Culture Shows a Periodic Accumulation of Defective Interfering Particles. *PLoS ONE* **2013**, *8*, e72288. [CrossRef]
58. Tan, E.; Chin, C.S.H.; Lim, Z.F.S.; Ng, S.K. HEK293 Cell Line as a Platform to Produce Recombinant Proteins and Viral Vectors. *Front. Bioeng. Biotechnol.* **2021**, *9*, 796991. [CrossRef] [PubMed]
59. Li, Z.; Jiang, Z.; Zhang, Y.; Huang, X.; Liu, Q. Efficacy and Safety of Oncolytic Viruses in Randomized Controlled Trials: A Systematic Review and Meta-Analysis. *Cancers* **2020**, *12*, 1416. [CrossRef]
60. Minh, A.D.; Star, A.T.; Stupak, J.; Fulton, K.M.; Haqqani, A.S.; Gélinas, J.-F.; Li, J.; Twine, S.M.; Kamen, A.A. Characterization of Extracellular Vesicles Secreted in Lentiviral Producing HEK293SF Cell Cultures. *Viruses* **2021**, *13*, 797. [CrossRef]
61. Ng, J.K.M. Product-Related Impurities in Therapeutic Virus Bioprocessing. In *Bioprocess and Analytics Development for Virus-Based Advanced Therapeutics and Medicinal Products (ATMPs)*; Springer: Cham, Switzerland, 2023; pp. 277–294. ISBN 9783031284885.
62. Russell, S.J.; Federspiel, M.J.; Peng, K.-W.; Tong, C.; Dingli, D.; Morice, W.G.; Lowe, V.; O'Connor, M.K.; Kyle, R.A.; Leung, N.; et al. Remission of Disseminated Cancer After Systemic Oncolytic Virotherapy. *Mayo Clin. Proc.* **2014**, *89*, 926–933. [CrossRef]
63. Cook, J.; Peng, K.-W.; Ginos, B.F.; Dueck, A.C.; Giers, M.; Packiriswamy, N.; Brunton, B.; Patnaik, M.M.; Witzig, T.E.; Buadi, F.K.; et al. Phase I Trial of Systemic Administration of Vesicular Stomatitis Virus Genetically Engineered to Express NIS and Human Interferon Beta, in Patients with Relapsed or Refractory Multiple Myeloma (MM), Acute Myeloid Leukemia (AML), and T-Cell Neoplasms (TCL). *Blood* **2020**, *136*, 7–8. [CrossRef]
64. Burrell, C.J.; Howard, C.R.; Murphy, F.A. Virion Structure and Composition. In *Fenner and White's Medical Virology*, 5th ed.; Academic Press: Cambridge, MA, USA, 2016; pp. 27–37. [CrossRef]
65. Lothert, K.; Eilts, F.; Wolff, M.W. Quantification Methods for Viruses and Virus-like Particles Applied in Biopharmaceutical Production Processes. *Expert Rev. Vaccines* **2022**, *21*, 1029–1044. [CrossRef]
66. LaBarre, D.D.; Lowy, R.J. Improvements in Methods for Calculating Virus Titer Estimates from TCID50 and Plaque Assays. *J. Virol. Methods* **2001**, *96*, 107–126. [CrossRef]

67. Steppert, P.; Mosor, M.; Stanek, L.; Burgstaller, D.; Palmberger, D.; Preinsperger, S.; Aguilar, P.P.; Müllner, M.; Csar, P.; Jungbauer, A. A Scalable, Integrated Downstream Process for Production of a Recombinant Measles Virus-Vectored Vaccine. *Vaccine* **2022**, *40*, 1323–1333. [CrossRef] [PubMed]
68. Hochdorfer, D.; Businger, R.; Hotter, D.; Seifried, C.; Solzin, J. Automated, Label-Free TCID50 Assay to Determine the Infectious Titer of Virus-Based Therapeutics. *J. Virol. Methods* **2022**, *299*, 114318. [CrossRef] [PubMed]
69. Hotter, D.; Kunzelmann, M.; Kiefer, F.; Leukhardt, C.; Fackler, C.; Jäger, S.; Solzin, J. High-Throughput Determination of Infectious Virus Titers by Kinetic Measurement of Infection-Induced Changes in Cell Morphology. *Int. J. Mol. Sci.* **2024**, *25*, 8076. [CrossRef]
70. Lothert, K.; Pagallies, F.; Eilts, F.; Sivanesapillai, A.; Hardt, M.; Moebus, A.; Feger, T.; Amann, R.; Wolff, M.W. A Scalable Downstream Process for the Purification of the Cell Culture-Derived Orf Virus for Human or Veterinary Applications. *J. Biotechnol.* **2020**, *323*, 221–230. [CrossRef]
71. Strain, M.C.; Lada, S.M.; Luong, T.; Rought, S.E.; Gianella, S.; Terry, V.H.; Spina, C.A.; Woelk, C.H.; Richman, D.D. Highly Precise Measurement of HIV DNA by Droplet Digital PCR. *PLoS ONE* **2013**, *8*, e55943. [CrossRef] [PubMed]
72. Furuta-Hanawa, B.; Yamaguchi, T.; Uchida, E. Two-Dimensional Droplet Digital PCR as a Tool for Titration and Integrity Evaluation of Recombinant Adeno-Associated Viral Vectors. *Hum. Gene Ther. Methods* **2019**, *30*, 127–136. [CrossRef]
73. Wong, K.; Mukherjee, B.; Kahler, A.M.; Zepp, R.; Molina, M. Influence of Inorganic Ions on Aggregation and Adsorption Behaviors of Human Adenovirus. *Environ. Sci. Technol.* **2012**, *46*, 11145–11153. [CrossRef]
74. Bohren, C.F.; Huffman, D.R. *Absorption and Scattering of Light by Small Particles*; Wiley-VCH: Weinheim, Germany, 2023. [CrossRef]
75. Schimek, A.; Strebl, M.; Blech, M.; Garidel, P. Challenges at Submicron Particle Characterisation: A Case Study Using Nanoparticle Tracking Analysis (NTA). *J. Pharm. Innov.* **2024**, *19*, 29. [CrossRef]
76. Kramberger, P.; Ciringer, M.; Štrancar, A.; Peterka, M. Evaluation of Nanoparticle Tracking Analysis for Total Virus Particle Determination. *Virol. J.* **2012**, *9*, 265. [CrossRef]
77. Aguilar, P.P.; González-Domínguez, I.; Schneider, T.A.; Gòdia, F.; Cervera, L.; Jungbauer, A. At-line Multi-angle Light Scattering Detector for Faster Process Development in Enveloped Virus-like Particle Purification. *J. Sep. Sci.* **2019**, *42*, 2640–2649. [CrossRef]
78. Bousse, T.; Shore, D.A.; Goldsmith, C.S.; Hossain, M.J.; Jang, Y.; Davis, C.T.; Donis, R.O.; Stevens, J. Quantitation of Influenza Virus Using Field Flow Fractionation and Multi-Angle Light Scattering for Quantifying Influenza A Particles. *J. Virol. Methods* **2013**, *193*, 589–596. [CrossRef]
79. Zamora, J.L.R.; Aguilar, H.C. Flow Virometry as a Tool to Study Viruses. *Methods* **2018**, *134*, 87–97. [CrossRef]
80. Kiss, G.; Chen, X.; Brindley, M.A.; Campbell, P.; Afonso, C.L.; Ke, Z.; Holl, J.M.; Guerrero-Ferreira, R.C.; Byrd-Leotis, L.A.; Steel, J.; et al. Capturing Enveloped Viruses on Affinity Grids for Downstream Cryo-Electron Microscopy Applications. *Microsc. Microanal.* **2014**, *20*, 164–174. [CrossRef] [PubMed]
81. Stass, R.; Ng, W.M.; Kim, Y.C.; Huiskonen, J.T. Chapter Two Structures of Enveloped Virions Determined by Cryogenic Electron Microscopy and Tomography. *Adv. Virus Res.* **2019**, *105*, 35–71. [CrossRef] [PubMed]
82. Edeling, M.A.; Earnest, L.; Montoya, J.C.; Yap, A.H.Y.; Mumford, J.; Roberts, J.; Wong, C.Y.; Hans, D.; Grima, J.; Bisset, N.; et al. Development of Methods to Produce SARS CoV-2 Virus-Like Particles at Scale. *Biotechnol. Bioeng.* **2025**, *122*, 1118–1129. [CrossRef] [PubMed]
83. Xin, D.; Kurien, L.; Briggs, K.; Schimek, A.; Dambra, R.; Hochdorfer, D.; Arnouk, T.A.; Brgles, M.; Gautam, S.; Hotter, D.; et al. Characterization of VSV-GP Morphology by CryoEM Imaging and SEC-MALS. *Mol. Ther. Methods Clin. Dev.* **2025**, *33*, 101429. [CrossRef]
84. Rziha, H.-J.; Büttner, M.; Müller, M.; Salomon, F.; Reguzova, A.; Laible, D.; Amann, R. Genomic Characterization of Orf Virus Strain D1701-V (Parapoxvirus) and Development of Novel Sites for Multiple Transgene Expression. *Viruses* **2019**, *11*, 127. [CrossRef]
85. Willemsen, A.; Zwart, M.P. On the Stability of Sequences Inserted into Viral Genomes. *Virus Evol.* **2019**, *5*, vez045. [CrossRef]
86. Basu, R.; Dambra, R.; Jiang, D.; Schätzlein, S.A.; Njiyang, S.; Ashour, J.; Chiramel, A.I.; Vigil, A.; Papov, V.V. Absolute Quantification of Viral Proteins from Pseudotyped VSV-GP Using UPLC-MRM. *Microbiol. Spectr.* **2024**, *12*, e03651-23. [CrossRef]
87. Sviben, D.; Forcic, D.; Halassy, B.; Allmaier, G.; Marchetti-Deschmann, M.; Brgles, M. Mass Spectrometry-Based Investigation of Measles and Mumps Virus Proteome. *Virol. J.* **2018**, *15*, 160. [CrossRef]
88. Moerdyk-Schauwecker, M.; Hwang, S.-I.; Grdzelishvili, V.Z. Cellular Proteins Associated with the Interior and Exterior of Vesicular Stomatitis Virus Virions. *PLoS ONE* **2014**, *9*, e104688. [CrossRef]
89. Sousa, I.P.; Carvalho, C.A.M.; Ferreira, D.F.; Weissmüller, G.; Rocha, G.M.; Silva, J.L.; Gomes, A.M.O. Envelope Lipid-Packing as a Critical Factor for the Biological Activity and Stability of Alphavirus Particles Isolated from Mammalian and Mosquito Cells*. *J. Biol. Chem.* **2011**, *286*, 1730–1736. [CrossRef] [PubMed]
90. Wolf, T.; Calisan, K.K.; Stitz, J.; Barbe, S. The Effects of High Shear Rates on the Average Hydrodynamic Diameter Measured in Biomimetic HIV Gag Virus-like Particle Dispersions. *Front. Bioeng. Biotechnol.* **2024**, *12*, 1367405. [CrossRef]
91. Kim, S.; Lim, K. Stability of Retroviral Vectors Against Ultracentrifugation Is Determined by the Viral Internal Core and Envelope Proteins Used for Pseudotyping. *Mol. Cells* **2017**, *40*, 339–345. [CrossRef]

92. Brgles, M.; Bonta, M.; Šantak, M.; Jagušić, M.; Forčić, D.; Halassy, B.; Allmaier, G.; Marchetti-Deschmann, M. Identification of Mumps Virus Protein and Lipid Composition by Mass Spectrometry. *Virol. J.* **2016**, *13*, 9. [CrossRef]
93. Fernandes, R.P.; Escandell, J.M.; Guerreiro, A.C.L.; Moura, F.; Faria, T.Q.; Carvalho, S.B.; Silva, R.J.S.; Gomes-Alves, P.; Peixoto, C. Assessing Multi-Attribute Characterization of Enveloped and Non-Enveloped Viral Particles by Capillary Electrophoresis. *Viruses* **2022**, *14*, 2539. [CrossRef]
94. Minsker, K.; Rustandi, R.R.; Ha, S.; Loughney, J.W. Characterization of RVSVΔG-ZEBOV-GP Glycoproteins Using Automated Capillary Western Blotting. *Vaccine* **2020**, *38*, 7166–7174. [CrossRef] [PubMed]
95. Lippé, R. Flow Virometry: A Powerful Tool To Functionally Characterize Viruses. *J. Virol.* **2018**, *92*, e01765-17. [CrossRef] [PubMed]
96. Drori, P.; Mouhadeb, O.; Muñoz, G.G.M.; Razvag, Y.; Alcalay, R.; Klocke, P.; Cordes, T.; Zahavy, E.; Lerner, E. Rapid and Specific Detection of Nanoparticles and Viruses One at a Time Using Microfluidic Laminar Flow and Confocal Fluorescence Microscopy. *iScience* **2024**, *27*, 110982. [CrossRef]
97. Ricci, G.; Minsker, K.; Kapish, A.; Osborn, J.; Ha, S.; Davide, J.; Califano, J.P.; Sehlin, D.; Rustandi, R.R.; Dick, L.W.; et al. Flow Virometry for Process Monitoring of Live Virus Vaccines-Lessons Learned from ERVEBO. *Sci. Rep.* **2021**, *11*, 7432. [CrossRef]
98. Vlasak, J.; Hoang, V.M.; Christanti, S.; Peluso, R.; Li, F.; Culp, T.D. Use of Flow Cytometry for Characterization of Human Cytomegalovirus Vaccine Particles. *Vaccine* **2016**, *34*, 2321–2328. [CrossRef] [PubMed]
99. Gianchecchi, E.; Torelli, A.; Piu, P.; Bonifazi, C.; Ganfini, L.; Montomoli, E. Flow Cytometry as an Integrative Method for the Evaluation of Vaccine Immunogenicity: A Validation Approach. *Biochem. Biophys. Rep.* **2023**, *34*, 101472. [CrossRef]
100. Deng, J.Z.; Rustandi, R.R.; Swartz, A.; Shieh, Y.; Baker, J.B.; Vlasak, J.; Wang, S.; Loughney, J.W. SEC Coupled with In-Line Multiple Detectors for the Characterization of an Oncolytic Coxsackievirus. *Mol. Ther. Oncolytics* **2022**, *24*, 139–147. [CrossRef]
101. Yi, S.; McCracken, R.; Davide, J.; Salovich, D.R.; Whitmer, T.; Bhat, A.; Vlasak, J.; Ha, S.; Sehlin, D.; Califano, J.; et al. Development of Process Analytical Tools for Rapid Monitoring of Live Virus Vaccines in Manufacturing. *Sci. Rep.* **2022**, *12*, 15494. [CrossRef] [PubMed]
102. Vlecken, D.H.W.; Pelgrim, R.P.M.; Ruminski, S.; Bakker, W.A.M.; Pol, L.A. van der Comparison of Initial Feasibility of Host Cell Lines for Viral Vaccine Production. *J. Virol. Methods* **2013**, *193*, 28–41. [CrossRef]
103. Sharma, R.; Harrison, S.T.L.; Tai, S.L. Advances in Bioreactor Systems for the Production of Biologicals in Mammalian Cells. *ChemBioEng Rev.* **2022**, *9*, 42–62. [CrossRef]
104. Grein, T.A.; Loewe, D.; Dieken, H.; Weidner, T.; Salzig, D.; Czermak, P. Aeration and Shear Stress Are Critical Process Parameters for the Production of Oncolytic Measles Virus. *Front. Bioeng. Biotechnol.* **2019**, *7*, 78. [CrossRef]
105. YekrangSafakar, A.; Acun, A.; Choi, J.; Song, E.; Zorlutuna, P.; Park, K. Hollow Microcarriers for Large-scale Expansion of Anchorage-dependent Cells in a Stirred Bioreactor. *Biotechnol. Bioeng.* **2018**, *115*, 1717–1728. [CrossRef]
106. Kaiser, S.C.; Decaria, P.N.; Seidel, S.; Eibl, D. Scaling-up of an Insect Cell-based Virus Production Process in a Novel Single-use Bioreactor with Flexible Agitation. *Chem. Ing. Tech.* **2022**, *94*, 1950–1961. [CrossRef]
107. Dove, B.; Brooks, G.; Bicknell, K.; Wurm, T.; Hiscox, J.A. Cell Cycle Perturbations Induced by Infection with the Coronavirus Infectious Bronchitis Virus and Their Effect on Virus Replication. *J. Virol.* **2006**, *80*, 4147–4156. [CrossRef]
108. Zhu, Y.; Yongky, A.; Yin, J. Growth of an RNA Virus in Single Cells Reveals a Broad Fitness Distribution. *Virology* **2009**, *385*, 39–46. [CrossRef] [PubMed]
109. Weiss, K.; Salzig, D.; Mühlebach, M.D.; Cichutek, K.; Pörtner, R.; Czermak, P. Key Parameters of Measles Virus Production for Oncolytic Virotherapy. *Am. J. Biochem. Biotechnol.* **2012**, *8*, 81–98. [CrossRef]
110. Eckhardt, D.; Mueller, J.; Friedrich, J.; Klee, J.-P.; Sardlishvili, I.; Walter, L.E.; Fey, S.; Czermak, P.; Salzig, D. Production of Oncolytic Measles Virus in Vero Cells: Impact of Culture Medium and Multiplicity of Infection. *Viruses* **2024**, *16*, 1740. [CrossRef]
111. Frensing, T. Defective Interfering Viruses and Their Impact on Vaccines and Viral Vectors. *Biotechnol. J.* **2015**, *10*, 681–689. [CrossRef]
112. Thompson, K.A.S.; Yin, J. Population Dynamics of an RNA Virus and Its Defective Interfering Particles in Passage Cultures. *Virol. J.* **2010**, *7*, 257. [CrossRef] [PubMed]
113. Paillet, C.; Forno, G.; Kratje, R.; Etcheverrigaray, M. Suspension-Vero Cell Cultures as a Platform for Viral Vaccine Production. *Vaccine* **2009**, *27*, 6464–6467. [CrossRef]
114. Elahi, S.M.; Shen, C.F.; Gilbert, R. Optimization of Production of Vesicular Stomatitis Virus (VSV) in Suspension Serum-Free Culture Medium at High Cell Density. *J. Biotechnol.* **2019**, *289*, 144–149. [CrossRef] [PubMed]
115. Göbel, S.; Pelz, L.; Silva, C.A.T.; Brühlmann, B.; Hill, C.; Altomonte, J.; Kamen, A.; Reichl, U.; Genzel, Y. Production of Recombinant Vesicular Stomatitis Virus-Based Vectors by Tangential Flow Depth Filtration. *Appl. Microbiol. Biotechnol.* **2024**, *108*, 240. [CrossRef]
116. Gutiérrez-Granados, S.; Gòdia, F.; Cervera, L. Continuous Manufacturing of Viral Particles. *Curr. Opin. Chem. Eng.* **2018**, *22*, 107–114. [CrossRef]
117. Gadaleta, P.; Vacotto, M.; Coulombié, F. Vesicular Stomatitis Virus Induces Apoptosis at Early Stages in the Viral Cycle and Does Not Depend on Virus Replication. *Virus Res.* **2002**, *86*, 87–92. [CrossRef]

118. Eymieux, S.; Rouillé, Y.; Terrier, O.; Seron, K.; Blanchard, E.; Rosa-Calatrava, M.; Dubuisson, J.; Belouzard, S.; Roingeard, P. Ultrastructural Modifications Induced by SARS-CoV-2 in Vero Cells: A Kinetic Analysis of Viral Factory Formation, Viral Particle Morphogenesis and Virion Release. *Cell. Mol. Life Sci.* **2021**, *78*, 3565–3576. [CrossRef] [PubMed]
119. Haywood, A.M. Membrane Uncoating of Intact Enveloped Viruses. *J. Virol.* **2010**, *84*, 10946–10955. [CrossRef]
120. Grein, T.A.; Loewe, D.; Dieken, H.; Salzig, D.; Weidner, T.; Czermak, P. High Titer Oncolytic Measles Virus Production Process by Integration of Dielectric Spectroscopy as Online Monitoring System. *Biotechnol. Bioeng.* **2018**, *115*, 1186–1194. [CrossRef] [PubMed]
121. Petiot, E.; Jacob, D.; Lanthier, S.; Lohr, V.; Ansorge, S.; Kamen, A.A. Metabolic and Kinetic Analyses of Influenza Production in Perfusion HEK293 Cell Culture. *BMC Biotechnol.* **2011**, *11*, 84. [CrossRef]
122. Gränicher, G.; Coronel, J.; Trampler, F.; Jordan, I.; Genzel, Y.; Reichl, U. Performance of an Acoustic Settler versus a Hollow Fiber–Based ATF Technology for Influenza Virus Production in Perfusion. *Appl. Microbiol. Biotechnol.* **2020**, *104*, 4877–4888. [CrossRef]
123. Weiss, K.; Gerstenberger, J.; Salzig, D.; Mühlebach, M.D.; Cichutek, K.; Pörtner, R.; Czermak, P. Oncolytic Measles Viruses Produced at Different Scales under Serum-free Conditions. *Eng. Life Sci.* **2015**, *15*, 425–436. [CrossRef]
124. Habisch, R.; Neubauer, P.; Soza-Ried, J.; Puschmann, E. Repeated Harvest Enables Efficient Production of VSV-GP. *Front. Bioeng. Biotechnol.* **2024**, *12*, 1505338. [CrossRef]
125. Shen, C.F.; Burney, E.; Gilbert, R.; Elahi, S.M.; Parato, K.; Loignon, M. Development, Optimization, and Scale-up of Suspension Vero Cell Culture Process for High Titer Production of Oncolytic Herpes Simplex Virus-1. *Biotechnol. J.* **2024**, *19*, e2300244. [CrossRef]
126. Nikolay, A.; de Grooth, J.; Genzel, Y.; Wood, J.A.; Reichl, U. Virus Harvesting in Perfusion Culture: Choosing the Right Type of Hollow Fiber Membrane. *Biotechnol. Bioeng.* **2020**, *117*, 3040–3052. [CrossRef]
127. Vázquez-Ramírez, D.; Jordan, I.; Sandig, V.; Genzel, Y.; Reichl, U. High Titer MVA and Influenza A Virus Production Using a Hybrid Fed-Batch/Perfusion Strategy with an ATF System. *Appl. Microbiol. Biotechnol.* **2019**, *103*, 3025–3035. [CrossRef]
128. Göbel, S.; Jaén, K.E.; Dorn, M.; Neumeyer, V.; Jordan, I.; Sandig, V.; Reichl, U.; Altomonte, J.; Genzel, Y. Process Intensification Strategies toward Cell Culture-based High-yield Production of a Fusogenic Oncolytic Virus. *Biotechnol. Bioeng.* **2023**, *120*, 2639–2657. [CrossRef]
129. Gränicher, G.; Babakhani, M.; Göbel, S.; Jordan, I.; Marichal-Gallardo, P.; Genzel, Y.; Reichl, U. A High Cell Density Perfusion Process for Modified Vaccinia Virus Ankara Production: Process Integration with Inline DNA Digestion and Cost Analysis. *Biotechnol. Bioeng.* **2021**, *118*, 4720–4734. [CrossRef] [PubMed]
130. Gränicher, G.; Tapia, F.; Behrendt, I.; Jordan, I.; Genzel, Y.; Reichl, U. Production of Modified Vaccinia Ankara Virus by Intensified Cell Cultures: A Comparison of Platform Technologies for Viral Vector Production. *Biotechnol. J.* **2021**, *16*, 2000024. [CrossRef] [PubMed]
131. Schad, M.; Gautam, S.; Grein, T.A.; Käß, F. Process Analytical Technologies (PAT) and Quality by Design (QbD) for Bioprocessing of Virus-Based Therapeutics. In *Bioprocess and Analytics Development for Virus-Based Advanced Therapeutics and Medicinal Products (ATMPs)*; Springer: Cham, Switzerland, 2023; pp. 295–328. [CrossRef]
132. Rheinemann, L.; Sundquist, W.I. Virus Budding. In *Encyclopedia of Virology*, 4th ed.; Academic Press: Cambridge, MA, USA, 2021; pp. 519–528. [CrossRef]
133. Aggarwal, T.; Kondabagil, K. Poxviruses. *Adv. Exp. Med. Biol.* **2024**, *1451*, 35–54. [CrossRef]
134. Roller, R.J.; Johnson, D.C. Herpesvirus Nuclear Egress across the Outer Nuclear Membrane. *Viruses* **2021**, *13*, 2356. [CrossRef] [PubMed]
135. Payne, L.G. The Existence of an Envelope on Extracellular Cowpox Virus and Its Antigenic Relationship to the Vaccinia Envelope. *Arch. Virol.* **1986**, *90*, 125–133. [CrossRef]
136. Roberts, K.L.; Smith, G.L. Vaccinia Virus Morphogenesis and Dissemination. *Trends Microbiol.* **2008**, *16*, 472–479. [CrossRef]
137. Appleyard, G.; Hapel, A.J.; Boulter, E.A. An Antigenic Difference between Intracellular and Extracellular Rabbitpox Virus. *J. Gen. Virol.* **1971**, *13*, 9–17. [CrossRef]
138. Nguyen, H.-M.; Sah, N.; Humphrey, M.R.M.; Rabkin, S.D.; Saha, D. Growth, Purification, and Titration of Oncolytic Herpes Simplex Virus. *J. Vis. Exp.* **2021**, *171*, 10–3791. [CrossRef]
139. van Vloten, J.P.; Minott, J.A.; McAusland, T.M.; Ingrao, J.C.; Santry, L.A.; McFadden, G.; Petrik, J.J.; Bridle, B.W.; Wootton, S.K. Production and Purification of High-Titer OrfV for Preclinical Studies in Vaccinology and Cancer Therapy. *Mol. Ther. Methods Clin. Dev.* **2021**, *23*, 434–447. [CrossRef]
140. Luo, Y.; Liu, X.; Zhang, Z.; Huang, R.; Peng, Q.; Zhao, Y.; Zhong, L.; Gan, L. Efficient Production of Evolutionary Nanoparticle Newcastle Disease Virus. *J. Biomed. Nanotechnol.* **2023**, *19*, 139–145. [CrossRef]
141. Wallis, C.; Melnick, J.L. Stabilization of Enveloped Viruses by Dimethyl Sulfoxide. *J. Virol.* **1968**, *2*, 953–954. [CrossRef] [PubMed]
142. Goldberg, S. 2D PAGE: Sample Preparation and Fractionation. *Methods Mol. Biol.* **2008**, *424*, 3–22. [CrossRef] [PubMed]

143. Pförringer, D.; Braun, K.F.; Mühlhofer, H.; Schneider, J.; Stemberger, A.; Seifried, E.; Pohlscheidt, E.; Seidel, M.; Edenharter, G.; Duscher, D.; et al. Novel Method for Reduction of Virus Load in Blood Plasma by Sonication. *Eur. J. Méd. Res.* **2020**, *25*, 12. [CrossRef]
144. Mundle, S.T.; Kishko, M.; Groppo, R.; DiNapoli, J.; Hamberger, J.; McNeil, B.; Kleanthous, H.; Parrington, M.; Zhang, L.; Anderson, S.F. Core Bead Chromatography for Preparation of Highly Pure, Infectious Respiratory Syncytial Virus in the Negative Purification Mode. *Vaccine* **2016**, *34*, 3690–3696. [CrossRef] [PubMed]
145. Laposova, K.; Oveckova, I.; Tomaskova, J. A Simple Method for Isolation of Cell-Associated Viral Particles from Cell Culture. *J. Virol. Methods* **2017**, *249*, 194–196. [CrossRef]
146. Kong, B.-W.; Foster, L.K.; Foster, D.N. A Method for the Rapid Isolation of Virus from Cultured Cells. *BioTechniques* **2008**, *44*, 97–99. [CrossRef]
147. Choi, H.-J.; Ebersbacher, C.F.; Kim, M.-C.; Kang, S.-M.; Montemagno, C.D. A Mechanistic Study on the Destabilization of Whole Inactivated Influenza Virus Vaccine in Gastric Environment. *PLoS ONE* **2013**, *8*, e66316. [CrossRef]
148. O'Keeffe, R.; Johnston, M.D.; Slater, N.K.H. The Primary Production of an Infectious Recombinant Herpes Simplex Virus Vaccine. *Biotechnol. Bioeng.* **1998**, *57*, 262–271. [CrossRef]
149. Seddon, A.M.; Curnow, P.; Booth, P.J. Membrane Proteins, Lipids and Detergents: Not Just a Soap Opera. *Biochim. Biophys. Acta (BBA) Biomembr.* **2004**, *1666*, 105–117. [CrossRef]
150. Srivastava, A.; Mallela, K.M.G.; Deorkar, N.; Brophy, G. Manufacturing Challenges and Rational Formulation Development for AAV Viral Vectors. *J. Pharm. Sci.* **2021**, *110*, 2609–2624. [CrossRef]
151. Mueller, D.; Pardo Garcia, A.; Grein, T.A.; Kaess, F.; Ng, J.; Pesta, K.; Schneider, S.; Turnbull, J. Purification of Recombinant Vesicular Stomatitis Virus-Based HIV Vaccine Candidate. US20220010286A1. Filed 9 September 2021, Patent Pending. Available online: https://patents.google.com/patent/US20220010286A1/en (accessed on 17 April 2025).
152. Pagallies, F.; Labisch, J.J.; Wronska, M.; Pflanz, K.; Amann, R. Efficient and Scalable Clarification of Orf Virus from HEK Suspension for Vaccine Development. *Vaccine X* **2024**, *18*, 100474. [CrossRef]
153. Gashti, A.B.; Chahal, P.S.; Gaillet, B.; Garnier, A. Purification of Recombinant Vesicular Stomatitis Virus-Based HIV Vaccine Candidate. *Vaccine* **2023**, *41*, 2198–2207. [CrossRef] [PubMed]
154. Fernandes, R.P.; Göbel, S.; Reiter, M.; Bryan, A.; Altomonte, J.; Genzel, Y.; Peixoto, C. Streamlining the Purification of a Clinical-Grade Oncolytic Virus for Therapeutic Applications. *Sep. Purif. Technol.* **2025**, *354*, 128769. [CrossRef]
155. Mayer, V.; Steiner, F.; Jungbauer, A.; Aguilar, P.P. Highly Pure Measles Virus Generated by Combination of Salt-Active Nuclease Treatment and Heparin Affinity Chromatography. *J. Chromatogr. A* **2024**, *1738*, 465470. [CrossRef] [PubMed]
156. Hansen, J.C.; Maeshima, K.; Hendzel, M.J. The Solid and Liquid States of Chromatin. *Epigenetics Chromatin* **2021**, *14*, 50. [CrossRef] [PubMed]
157. Mayer, V.; Frank, A.; Preinsperger, S.; Csar, P.; Steppert, P.; Jungbauer, A.; Aguilar, P.P. Removal of Chromatin by Salt-tolerant Endonucleases for Production of Recombinant Measles Virus. *Biotechnol. Prog.* **2023**, *39*, e3342. [CrossRef]
158. Vincent, D.; Kramberger, P.; Hudej, R.; Štrancar, A.; Wang, Y.; Zhou, Y.; Velayudhan, A. The Development of a Monolith-Based Purification Process for Orthopoxvirus Vaccinia Virus Lister Strain. *J. Chromatogr. A* **2017**, *1524*, 87–100. [CrossRef]
159. Besnard, L.; Fabre, V.; Fettig, M.; Gousseinov, E.; Kawakami, Y.; Laroudie, N.; Scanlan, C.; Pattnaik, P. Clarification of Vaccines: An Overview of Filter Based Technology Trends and Best Practices. *Biotechnol. Adv.* **2016**, *34*, 1–13. [CrossRef]
160. Barbieri, E.; Mollica, G.N.; Moore, B.D.; Sripada, S.A.; Shastry, S.; Kilgore, R.E.; Loudermilk, C.M.; Whitacre, Z.H.; Kilgour, K.M.; Wuestenhagen, E.; et al. Peptide Ligands Targeting the Vesicular Stomatitis Virus G (VSV-G) Protein for the Affinity Purification of Lentivirus Particles. *Biotechnol. Bioeng.* **2024**, *121*, 618–639. [CrossRef]
161. Lothert, K.; Harsy, Y.M.J.; Endres, P.; Müller, E.; Wolff, M.W. Evaluation of Restricted Access Media for the Purification of Cell Culture-derived Orf Viruses. *Eng. Life Sci.* **2023**, *23*, e2300009. [CrossRef] [PubMed]
162. Gautam, S.; Xin, D.; Garcia, A.P.; Spiesschaert, B. Single-Step Rapid Chromatographic Purification and Characterization of Clinical Stage Oncolytic VSV-GP. *Front. Bioeng. Biotechnol.* **2022**, *10*, 992069. [CrossRef] [PubMed]
163. Gerster, P.; Kopecky, E.-M.; Hammerschmidt, N.; Klausberger, M.; Krammer, F.; Grabherr, R.; Mersich, C.; Urbas, L.; Kramberger, P.; Paril, T.; et al. Purification of Infective Baculoviruses by Monoliths. *J. Chromatogr. A* **2013**, *1290*, 36–45. [CrossRef] [PubMed]
164. Zhang, F.; Luo, J.; Teng, M.; Xing, G.; Guo, J.; Zhang, Y. Purification of Cell-derived Japanese Encephalitis Virus by Dual-mode Chromatography. *Biotechnol. Appl. Biochem.* **2021**, *68*, 547–553. [CrossRef]
165. Cribbs, A.P.; Kennedy, A.; Gregory, B.; Brennan, F.M. Simplified Production and Concentration of Lentiviral Vectors to Achieve High Transduction in Primary Human T Cells. *BMC Biotechnol.* **2013**, *13*, 98. [CrossRef]
166. Lotfian, P.; Levy, M.S.; Coffin, R.S.; Fearn, T.; Ayazi-Shamlou, P. Impact of Process Conditions on the Centrifugal Recovery of a Disabled Herpes Simplex Virus. *Biotechnol. Prog.* **2003**, *19*, 209–215. [CrossRef]
167. Kuroda, S.; Miyagawa, Y.; Sukegawa, M.; Tomono, T.; Yamamoto, M.; Adachi, K.; Verlengia, G.; Goins, W.F.; Cohen, J.B.; Glorioso, J.C.; et al. Evaluation of Parameters for Efficient Purification and Long-Term Storage of Herpes Simplex Virus-Based Vectors. *Mol. Ther. Methods Clin. Dev.* **2022**, *26*, 132–143. [CrossRef]

168. Baekelandt, V.; Eggermont, K.; Michiels, M.; Nuttin, B.; Debyser, Z. Optimized Lentiviral Vector Production and Purification Procedure Prevents Immune Response after Transduction of Mouse Brain. *Gene Ther.* **2003**, *10*, 1933–1940. [CrossRef] [PubMed]
169. Boroujeni, M.E.; Gardaneh, M. The Superiority of Sucrose Cushion Centrifugation to Ultrafiltration and PEGylation in Generating High-Titer Lentivirus Particles and Transducing Stem Cells with Enhanced Efficiency. *Mol. Biotechnol.* **2018**, *60*, 185–193. [CrossRef]
170. Transfiguracion, J.; Jaalouk, D.E.; Ghani, K.; Galipeau, J.; Kamen, A. Size-Exclusion Chromatography Purification of High-Titer Vesicular Stomatitis Virus G Glycoprotein-Pseudotyped Retrovectors for Cell and Gene Therapy Applications. *Hum. Gene Ther.* **2003**, *14*, 1139–1153. [CrossRef]
171. Wang, J.; Ma, J.; Wen, X. Basic Concepts of Density Gradient Ultracentrifugation. In *Nanoseparation Using Density Gradient Ultracentrifugation*; SpringerBriefs in Molecular Science; Springer: Singapore, 2018; pp. 21–36. ISBN 9789811051890.
172. Nagano, H.; Yagyu, K.; Ohta, S. Purification of Infectious Bronchitis Coronavirus by Sephacryl S-1000 Gel Chromatography. *Vet. Microbiol.* **1989**, *21*, 115–123. [CrossRef]
173. Saha, K.; Lin, Y.-C.; Wong, P.K.Y. A Simple Method for Obtaining Highly Viable Virus from Culture Supernatant. *J. Virol. Methods* **1994**, *46*, 349–352. [CrossRef] [PubMed]
174. Cui, X.-H.; Murthy, H.N.; Wu, C.-H.; Paek, K.-Y. Sucrose-Induced Osmotic Stress Affects Biomass, Metabolite, and Antioxidant Levels in Root Suspension Cultures of *Hypericum Perforatum* L. *Plant Cell, Tissue Organ Cult. (PCTOC)* **2010**, *103*, 7–14. [CrossRef]
175. Helmholz, H.F.; Bollman, J.L. The Intravenous Administration of Sucrose Solutions as a Means of Producing Intense Diuresis. *J. Lab. Clin. Med.* **1939**, *25*, 1180–1187.
176. Sandig, V.; Hofmann, C.; Steinert, S.; Jennings, G.; Schlag, P.; Strauss, M. Gene Transfer into Hepatocytes and Human Liver Tissue by Baculovirus Vectors. *Hum. Gene Ther.* **1996**, *7*, 1937–1945. [CrossRef] [PubMed]
177. Santry, L.A.; McAusland, T.M.; Susta, L.; Wood, G.A.; Major, P.P.; Petrik, J.J.; Bridle, B.W.; Wootton, S.K. Production and Purification of High-Titer Newcastle Disease Virus for Use in Preclinical Mouse Models of Cancer. *Mol. Ther. Methods Clin. Dev.* **2018**, *9*, 181–191. [CrossRef]
178. Granier, C.; Toesca, J.; Mialon, C.; Ritter, M.; Freitas, N.; Boson, B.; Pécheur, E.-I.; Cosset, F.-L.; Denolly, S. Low-Density Hepatitis C Virus Infectious Particles Are Protected from Oxidation by Secreted Cellular Proteins. *mBio* **2023**, *14*, e01549-23. [CrossRef] [PubMed]
179. Zhang, Y.; Wang, Y.; Feng, Y.; Tu, Z.; Lou, Z.; Tu, C. Proteomic Profiling of Purified Rabies Virus Particles. *Virol. Sin.* **2020**, *35*, 143–155. [CrossRef]
180. Segura, M.M.; Kamen, A.A.; Garnier, A. Viral Vectors for Gene Therapy, Methods and Protocols. *Methods Mol. Biol.* **2011**, *737*, 89–116. [CrossRef]
181. Loewe, D.; Dieken, H.; Grein, T.A.; Salzig, D.; Czermak, P. A Combined Ultrafiltration/Diafiltration Process for the Purification of Oncolytic Measles Virus. *Membranes* **2022**, *12*, 105. [CrossRef]
182. Bandeira, V.; Peixoto, C.; Rodrigues, A.F.; Cruz, P.E.; Alves, P.M.; Coroadinha, A.S.; Carrondo, M.J.T. Downstream Processing of Lentiviral Vectors: Releasing Bottlenecks. *Hum. Gene Ther. Part. B Methods* **2012**, *23*, 255–263. [CrossRef] [PubMed]
183. Labisch, J.J.; Bollmann, F.; Wolff, M.W.; Pflanz, K. A New Simplified Clarification Approach for Lentiviral Vectors Using Diatomaceous Earth Improves Throughput and Safe Handling. *J. Biotechnol.* **2021**, *326*, 11–20. [CrossRef]
184. Shoaebargh, S.; Gough, I.; Medina, M.F.; Smith, A.; van der Heijden, J.; Lichty, B.D.; Bell, J.C.; Latulippe, D.R. Sterile Filtration of Oncolytic Viruses: An Analysis of Effects of Membrane Morphology on Fouling and Product Recovery. *J. Membr. Sci.* **2018**, *548*, 239–246. [CrossRef]
185. Labisch, J.J.; Evangelopoulou, M.; Schleuß, T.; Pickl, A. Investigating Ultrafiltration Membranes and Operation Modes for Improved Lentiviral Vector Processing. *Eng. Life Sci.* **2025**, *25*, e202400057. [CrossRef] [PubMed]
186. Carvalho, S.B.; Silva, R.J.S.; Moreira, A.S.; Cunha, B.; Clemente, J.J.; Alves, P.M.; Carrondo, M.J.T.; Xenopoulos, A.; Peixoto, C. Efficient Filtration Strategies for the Clarification of Influenza Virus-like Particles Derived from Insect Cells. *Sep. Purif. Technol.* **2019**, *218*, 81–88. [CrossRef]
187. Loewe, D.; Grein, T.A.; Dieken, H.; Weidner, T.; Salzig, D.; Czermak, P. Tangential Flow Filtration for the Concentration of Oncolytic Measles Virus: The Influence of Filter Properties and the Cell Culture Medium. *Membranes* **2019**, *9*, 160. [CrossRef]
188. Jones, T.H.; Brassard, J.; Johns, M.W.; Gagné, M.-J. The Effect of Pre-Treatment and Sonication of Centrifugal Ultrafiltration Devices on Virus Recovery. *J. Virol. Methods* **2009**, *161*, 199–204. [CrossRef]
189. Wright, E.; Kawka, K.; Medina, M.F.C.; Latulippe, D.R. Evaluation of Host Cell Impurity Effects on the Performance of Sterile Filtration Processes for Therapeutic Viruses. *Membranes* **2022**, *12*, 359. [CrossRef] [PubMed]
190. Dias, D.; Bons, J.; Kumar, A.; Kabir, M.H.; Liang, H. Forever Chemicals, Per-and Polyfluoroalkyl Substances (PFAS), in Lubrication. *Lubricants* **2024**, *12*, 114. [CrossRef]
191. Mark, T.; Janice, W.; Akanksha, N. Methods for Purification of Viruses. US8785173B2, 22 July 2014.
192. Rene, A.B.; Champluvier, B.P.S. Method for Producing Virus from Cell Culture Involving Homogenization. US20120058145A1, 6 May 2010.

193. Transfiguracion, J.; Jorio, H.; Meghrous, J.; Jacob, D.; Kamen, A. High Yield Purification of Functional Baculovirus Vectors by Size Exclusion Chromatography. *J. Virol. Methods* **2007**, *142*, 21–28. [CrossRef]
194. Taylor, N.; Ma, W.J.; Kristopeit, A.; Wang, S.-C.; Zydney, A.L. Enhancing the Performance of Sterile Filtration for Viral Vaccines and Model Nanoparticles Using an Appropriate Prefilter. *J. Membr. Sci.* **2022**, *647*, 120264. [CrossRef]
195. EMA (European Medicines Agency). Guideline on the Sterilisation of the Medicinal Product, Active Substance, Excipient and Primary Container; Ref. No. EMA/CHMP/CVMP/QWP/850374/2015, 2019.
196. Valkama, A.J.; Oruetxebarria, I.; Lipponen, E.M.; Leinonen, H.M.; Käyhty, P.; Hynynen, H.; Turkki, V.; Malinen, J.; Miinalainen, T.; Heikura, T.; et al. Development of Large-Scale Downstream Processing for Lentiviral Vectors. *Mol. Ther. Methods Clin. Dev.* **2020**, *17*, 717–730. [CrossRef] [PubMed]
197. Wang, S.; Godfrey, S.; Ravikrishnan, J.; Lin, H.; Vogel, J.; Coffman, J. Shear Contributions to Cell Culture Performance and Product Recovery in ATF and TFF Perfusion Systems. *J. Biotechnol.* **2017**, *246*, 52–60. [CrossRef] [PubMed]
198. Perry, C.; Rayat, A.C.M.E. Lentiviral Vector Bioprocessing. *Viruses* **2021**, *13*, 268. [CrossRef]
199. Negrete, A.; Pai, A.; Shiloach, J. Use of Hollow Fiber Tangential Flow Filtration for the Recovery and Concentration of HIV Virus-like Particles Produced in Insect Cells. *J. Virol. Methods* **2014**, *195*, 240–246. [CrossRef]
200. van Reis, R.; Zydney, A. Bioprocess Membrane Technology. *J. Membr. Sci.* **2007**, *297*, 16–50. [CrossRef]
201. Heffron, J.; Mayer, B.K. Virus Isoelectric Point Estimation: Theories and Methods. *Appl. Environ. Microb.* **2020**, *87*, e02319-20. [CrossRef]
202. Banjac, M.; Roethl, E.; Gelhart, F.; Kramberger, P.; Jarc, B.L.; Jarc, M.; Štrancar, A.; Muster, T.; Peterka, M. Purification of Vero Cell Derived Live Replication Deficient Influenza A and B Virus by Ion Exchange Monolith Chromatography. *Vaccine* **2014**, *32*, 2487–2492. [CrossRef]
203. Eckhardt, D.; Dieken, H.; Loewe, D.; Grein, T.A.; Salzig, D.; Czermak, P. Purification of Oncolytic Measles Virus by Cation-Exchange Chromatography Using Resin-Based Stationary Phases. *Sep. Sci. Technol.* **2022**, *57*, 886–896. [CrossRef]
204. Santry, L.A.; Jacquemart, R.; Vandersluis, M.; Zhao, M.; Domm, J.M.; McAusland, T.M.; Shang, X.; Major, P.M.; Stout, J.G.; Wootton, S.K. Interference Chromatography: A Novel Approach to Optimizing Chromatographic Selectivity and Separation Performance for Virus Purification. *BMC Biotechnol.* **2020**, *20*, 32. [CrossRef]
205. Lothert, K.; Wolff, M.W. Affinity and Pseudo-Affinity Membrane Chromatography for Viral Vector and Vaccine Purifications: A Review. *Membranes* **2023**, *13*, 770. [CrossRef]
206. Nasimuzzaman, M.; Lynn, D.; van der Loo, J.C.; Malik, P. Purification of Baculovirus Vectors Using Heparin Affinity Chromatography. *Mol. Ther. Methods Clin. Dev.* **2016**, *3*, 16071. [CrossRef] [PubMed]
207. Wolff, M.W.; Siewert, C.; Lehmann, S.; Hansen, S.P.; Djurup, R.; Faber, R.; Reichl, U. Capturing of Cell Culture-derived Modified Vaccinia Ankara Virus by Ion Exchange and Pseudo-affinity Membrane Adsorbers. *Biotechnol. Bioeng.* **2010**, *105*, 761–769. [CrossRef]
208. Fortuna, A.R.; van Teeffelen, S.; Ley, A.; Fischer, L.M.; Taft, F.; Genzel, Y.; Villain, L.; Wolff, M.W.; Reichl, U. Use of Sulfated Cellulose Membrane Adsorbers for Chromatographic Purification of Cell Cultured-Derived Influenza A and B Viruses. *Sep. Purif. Technol.* **2019**, *226*, 350–358. [CrossRef]
209. Mekkaoui, L.; Parekh, F.; Kotsopoulou, E.; Darling, D.; Dickson, G.; Cheung, G.W.; Chan, L.; MacLellan-Gibson, K.; Mattiuzzo, G.; Farzaneh, F.; et al. Lentiviral Vector Purification Using Genetically Encoded Biotin Mimic in Packaging Cell. *Mol. Ther. Methods Clin. Dev.* **2018**, *11*, 155–165. [CrossRef] [PubMed]
210. Zhao, M.; Vandersluis, M.; Stout, J.; Haupts, U.; Sanders, M.; Jacquemart, R. Affinity Chromatography for Vaccines Manufacturing: Finally Ready for Prime Time? *Vaccine* **2019**, *37*, 5491–5503. [CrossRef]
211. Cheung, R.C.F.; Wong, J.H.; Ng, T.B. Immobilized Metal Ion Affinity Chromatography: A Review on Its Applications. *Appl. Microbiol. Biotechnol.* **2012**, *96*, 1411–1420. [CrossRef]
212. Moreira, A.S.; Bezemer, S.; Faria, T.Q.; Detmers, F.; Hermans, P.; Sierkstra, L.; Coroadinha, A.S.; Peixoto, C. Implementation of Novel Affinity Ligand for Lentiviral Vector Purification. *Int. J. Mol. Sci.* **2023**, *24*, 3354. [CrossRef]
213. Ma, J.; Huang, Y.; Jia, G.; Dong, X.; Shi, Q.; Sun, Y. Discovery of Broad-Spectrum High-Affinity Peptide Ligands of Spike Protein for the Vaccine Purification of SARS-CoV-2 and Omicron Variants. *Int. J. Biol. Macromol.* **2024**, *283*, 137059. [CrossRef]
214. Wolff, M.W.; Siewert, C.; Hansen, S.P.; Faber, R.; Reichl, U. Purification of Cell Culture-derived Modified Vaccinia Ankara Virus by Pseudo-affinity Membrane Adsorbers and Hydrophobic Interaction Chromatography. *Biotechnol. Bioeng.* **2010**, *107*, 312–320. [CrossRef]
215. Diogo, M.M.; Queiroz, J.A.; Prazeres, D.M.F. Chromatography of Plasmid DNA. *J. Chromatogr. A* **2005**, *1069*, 3–22. [CrossRef] [PubMed]
216. Loa, C.C.; Lin, T.L.; Wu, C.C.; Bryan, T.A.; Thacker, H.L.; Hooper, T.; Schrader, D. Purification of Turkey Coronavirus by Sephacryl Size-Exclusion Chromatography. *J. Virol. Methods* **2002**, *104*, 187–194. [CrossRef]
217. Eilts, F.; Steger, M.; Lothert, K.; Wolff, M.W. The Suitability of Latex Particles to Evaluate Critical Process Parameters in Steric Exclusion Chromatography. *Membranes* **2022**, *12*, 488. [CrossRef] [PubMed]

218. Labisch, J.J.; Wiese, G.P.; Pflanz, K. Steric Exclusion Chromatography for Purification of Biomolecules—A Review. *Separations* **2023**, *10*, 183. [CrossRef]
219. Labisch, J.J.; Kassar, M.; Bollmann, F.; Valentic, A.; Hubbuch, J.; Pflanz, K. Steric Exclusion Chromatography of Lentiviral Vectors Using Hydrophilic Cellulose Membranes. *J. Chromatogr. A* **2022**, *1674*, 463148. [CrossRef]
220. Lothert, K.; Sprick, G.; Beyer, F.; Lauria, G.; Czermak, P.; Wolff, M.W. Membrane-Based Steric Exclusion Chromatography for the Purification of a Recombinant Baculovirus and Its Application for Cell Therapy. *J. Virol. Methods* **2020**, *275*, 113756. [CrossRef]
221. Marichal-Gallardo, P.; Pieler, M.M.; Wolff, M.W.; Reichl, U. Steric Exclusion Chromatography for Purification of Cell Culture-Derived Influenza A Virus Using Regenerated Cellulose Membranes and Polyethylene Glycol. *J. Chromatogr. A* **2017**, *1483*, 110–119. [CrossRef]
222. Lothert, K.; Offersgaard, A.F.; Pihl, A.F.; Mathiesen, C.K.; Jensen, T.B.; Alzua, G.P.; Fahnøe, U.; Bukh, J.; Gottwein, J.M.; Wolff, M.W. Development of a Downstream Process for the Production of an Inactivated Whole Hepatitis C Virus Vaccine. *Sci. Rep.* **2020**, *10*, 16261. [CrossRef] [PubMed]
223. Labisch, J.; Paul, R.; Wiese, G.; Pflanz, K. Scaling Up of Steric Exclusion Membrane Chromatography for Lentiviral Vector Purification. *Membranes* **2023**, *13*, 149. [CrossRef]
224. Nestola, P.; Villain, L.; Peixoto, C.; Martins, D.L.; Alves, P.M.; Carrondo, M.J.T.; Mota, J.P.B. Impact of Grafting on the Design of New Membrane Adsorbers for Adenovirus Purification. *J. Biotechnol.* **2014**, *181*, 1–11. [CrossRef]
225. Aguilar, P.P.; Schneider, T.A.; Wetter, V.; Maresch, D.; Ling, W.L.; Tover, A.; Steppert, P.; Jungbauer, A. Polymer-Grafted Chromatography Media for the Purification of Enveloped Virus-like Particles, Exemplified with HIV-1 Gag VLP. *Vaccine* **2019**, *37*, 7070–7080. [CrossRef]
226. Connell-Crowley, L.; Nguyen, T.; Bach, J.; Chinniah, S.; Bashiri, H.; Gillespie, R.; Moscariello, J.; Hinckley, P.; Dehghani, H.; Vunnum, S.; et al. Cation Exchange Chromatography Provides Effective Retrovirus Clearance for Antibody Purification Processes. *Biotechnol. Bioeng.* **2012**, *109*, 157–165. [CrossRef] [PubMed]
227. Turnbull, J.; Wright, B.; Green, N.K.; Tarrant, R.; Roberts, I.; Hardick, O.; Bracewell, D.G. Adenovirus 5 Recovery Using Nanofiber Ion-exchange Adsorbents. *Biotechnol. Bioeng.* **2019**, *116*, 1698–1709. [CrossRef] [PubMed]
228. Vicente, T.; Fáber, R.; Alves, P.M.; Carrondo, M.J.T.; Mota, J.P.B. Impact of Ligand Density on the Optimization of Ion-exchange Membrane Chromatography for Viral Vector Purification. *Biotechnol. Bioeng.* **2011**, *108*, 1347–1359. [CrossRef]
229. Pamenter, G.; Davies, L.; Knevelman, C.; Miskin, J.; Mitrophanous, K.; Dikicioglu, D.; Bracewell, D.G. Time-dependent Sorption Behavior of Lentiviral Vectors during Anion-exchange Chromatography. *Biotechnol. Bioeng.* **2023**, *120*, 2269–2282. [CrossRef]
230. Boudeffa, D.; Bertin, B.; Biek, A.; Mormin, M.; Leseigneur, F.; Galy, A.; Merten, O.-W. Toward a Scalable Purification Protocol of GaLV-TR-Pseudotyped Lentiviral Vectors. *Hum. Gene Ther. Methods* **2019**, *30*, 153–171. [CrossRef] [PubMed]
231. Kröber, T.; Wolff, M.W.; Hundt, B.; Seidel-Morgenstern, A.; Reichl, U. Continuous Purification of Influenza Virus Using Simulated Moving Bed Chromatography. *J. Chromatogr. A* **2013**, *1307*, 99–110. [CrossRef]
232. Aust, N.; Parth, M.; Lederer, K. SEC of Ultra-High Molar Mass Polymers: Optimization of Experimental Conditions to Avoid Molecular Degradation in the Case of Narrow Polystyrene Standards. *Int. J. Polym. Anal. Charact.* **2001**, *6*, 245–260. [CrossRef]
233. Song, Y.; Yang, Y.; Lin, X.; Zhao, Q.; Su, Z.; Ma, G.; Zhang, S. Size Exclusion Chromatography Using Large Pore Size Media Induces Adverse Conformational Changes of Inactivated Foot-and-Mouth Disease Virus Particles. *J. Chromatogr. A* **2022**, *1677*, 463301. [CrossRef]
234. D'Atri, V.; Imiołek, M.; Quinn, C.; Finny, A.; Lauber, M.; Fekete, S.; Guillarme, D. Size Exclusion Chromatography of Biopharmaceutical Products: From Current Practices for Proteins to Emerging Trends for Viral Vectors, Nucleic Acids and Lipid Nanoparticles. *J. Chromatogr. A* **2024**, *1722*, 464862. [CrossRef]
235. Iyer, G.; Ramaswamy, S.; Asher, D.; Mehta, U.; Leahy, A.; Chung, F.; Cheng, K.-S. Reduced Surface Area Chromatography for Flow-through Purification of Viruses and Virus like Particles. *J. Chromatogr. A* **2011**, *1218*, 3973–3981. [CrossRef] [PubMed]
236. Wu, Y.; Simons, J.; Hooson, S.; Abraham, D.; Carta, G. Protein and Virus-like Particle Adsorption on Perfusion Chromatography Media. *J. Chromatogr. A* **2013**, *1297*, 96–105. [CrossRef] [PubMed]
237. Wu, Y.; Abraham, D.; Carta, G. Particle Size Effects on Protein and Virus-like Particle Adsorption on Perfusion Chromatography Media. *J. Chromatogr. A* **2015**, *1375*, 92–100. [CrossRef]
238. Pabst, T.M.; Thai, J.; Hunter, A.K. Evaluation of Recent Protein A Stationary Phase Innovations for Capture of Biotherapeutics. *J. Chromatogr. A* **2018**, *1554*, 45–60. [CrossRef] [PubMed]
239. Ta, D.T.; Chu, K.L.; Soonaan, N.I.B.; Chin, C.; Ng, S.K.; Zhang, W. A New and Simplified Anion Exchange Chromatographic Process for the Purification of Cell-Grown Influenza A H1N1 Virus. *Sep. Purif. Technol.* **2021**, *263*, 118412. [CrossRef]
240. Hagemann, F.; Wypysek, D.; Baitalow, K.; Adametz, P.; Thom, V.; Wessling, M. Why Device Design Is Crucial for Membrane Adsorbers. *J. Chromatogr. Open* **2022**, *2*, 100029. [CrossRef]
241. Roshankhah, R.; Pelton, R.; Ghosh, R. Optimization of Fluid Flow in Membrane Chromatography Devices Using Computational Fluid Dynamic Simulations. *J. Chromatogr. A* **2023**, *1699*, 464030. [CrossRef]

242. Picard, G.; Ajdari, A.; Bocquet, L.; Lequeux, F. Simple Model for Heterogeneous Flows of Yield Stress Fluids. *Phys. Rev. E* **2002**, *66*, 051501. [CrossRef]
243. Velali, E.; Stute, B.; Leuthold, M.; von Lieres, E. Model-Based Performance Analysis and Scale-up of Membrane Adsorbers with a Cassettes Format Designed for Parallel Operation. *Chem. Eng. Sci.* **2018**, *192*, 103–113. [CrossRef]
244. Teepakorn, C.; Fiaty, K.; Charcosset, C. Effect of Geometry and Scale for Axial and Radial Flow Membrane Chromatography—Experimental Study of Bovin Serum Albumin Adsorption. *J. Chromatogr. A* **2015**, *1403*, 45–53. [CrossRef]
245. Matos, T.; Hoying, D.; Kristopeit, A.; Wenger, M.; Joyce, J. Continuous Multi-Membrane Chromatography of Large Viral Particles. *J. Chromatogr. A* **2023**, *1705*, 464194. [CrossRef] [PubMed]
246. Fortuna, A.R.; Taft, F.; Villain, L.; Wolff, M.W.; Reichl, U. Continuous Purification of Influenza A Virus Particles Using Pseudo-Affinity Membrane Chromatography. *J. Biotechnol.* **2021**, *342*, 139–148. [CrossRef]
247. Mendes, J.P.; Bergman, M.; Solbrand, A.; Peixoto, C.; Carrondo, M.J.T.; Silva, R.J.S. Continuous Affinity Purification of Adeno-Associated Virus Using Periodic Counter-Current Chromatography. *Pharmaceutics* **2022**, *14*, 1346. [CrossRef] [PubMed]
248. Mendes, J.P.; Silva, R.J.S.; Berg, M.; Mathiasson, L.; Peixoto, C.; Alves, P.M.; Carrondo, M.J.T. Oncolytic Virus Purification with Periodic Counter-current Chromatography. *Biotechnol. Bioeng.* **2021**, *118*, 3522–3532. [CrossRef]
249. Orr, V.; Zhong, L.; Moo-Young, M.; Chou, C.P. Recent Advances in Bioprocessing Application of Membrane Chromatography. *Biotechnol. Adv.* **2013**, *31*, 450–465. [CrossRef]
250. Leinweber, F.C.; Tallarek, U. Chromatographic Performance of Monolithic and Particulate Stationary Phases Hydrodynamics and Adsorption Capacity. *J. Chromatogr. A* **2003**, *1006*, 207–228. [CrossRef]
251. Vicente, T.; Peixoto, C.; Carrondo, M.J.T.; Alves, P.M. Gene Therapy of Cancer, Methods and Protocols. *Methods Mol. Biol.* **2009**, *542*, 447–470. [CrossRef] [PubMed]
252. Koku, H.; Maier, R.S.; Czymmek, K.J.; Schure, M.R.; Lenhoff, A.M. Modeling of Flow in a Polymeric Chromatographic Monolith. *J. Chromatogr. A* **2011**, *1218*, 3466–3475. [CrossRef]
253. Podgornik, A.; Jančar, J.; Mihelič, I.; Barut, M.; Strancar, A. Large Volume Monolithic Stationary Phases: Preparation, Properties, and Applications. *Acta Chim. Slov.* **2010**, *57*, 1–8.
254. Hahn, R.; Tscheliessnig, A.; Bauerhansl, P.; Jungbauer, A. Dispersion Effects in Preparative Polymethacrylate Monoliths Operated in Radial-Flow Columns. *J. Biochem. Biophys. Meth* **2007**, *70*, 87–94. [CrossRef]
255. Brgles, M.; Sviben, D.; Forčić, D.; Halassy, B. Nonspecific Native Elution of Proteins and Mumps Virus in Immunoaffinity Chromatography. *J. Chromatogr. A* **2016**, *1447*, 107–114. [CrossRef] [PubMed]
256. Trilisky, E.I.; Lenhoff, A.M. Flow-dependent Entrapment of Large Bioparticles in Porous Process Media. *Biotechnol. Bioeng.* **2009**, *104*, 127–133. [CrossRef]
257. Kralj, Š.; Kodermac, Š.M.; Bergoč, I.; Kostelec, T.; Podgornik, A.; Štrancar, A.; Černigoj, U. Effect of Plasmid DNA Isoforms on Preparative Anion Exchange Chromatography. *Electrophoresis* **2023**, *44*, 1953–1966. [CrossRef]
258. Pavlin, N.; Černigoj, U.; Bavčar, M.; Plesničar, T.; Mavri, J.; Zidar, M.; Bone, M.; Savič, U.K.; Sever, T.; Štrancar, A. Analytical Separation of Plasmid DNA Isoforms Using Anion Exchanging Chromatographic Monoliths with 6 Mm Channels. *Electrophoresis* **2023**, *44*, 1967–1977. [CrossRef] [PubMed]
259. Schimek, A.; Ng, J.; Will, F.; Hubbuch, J. Mechanistic Modeling of the Elution Behavior and Convective Entrapment of Vesicular Stomatitis Virus on an Ion Exchange Chromatography Monolith. *J. Chromatogr. A* **2025**, *1748*, 465832. [CrossRef] [PubMed]
260. Jungreuthmayer, C.; Steppert, P.; Sekot, G.; Zankel, A.; Reingruber, H.; Zanghellini, J.; Jungbauer, A. The 3D Pore Structure and Fluid Dynamics Simulation of Macroporous Monoliths: High Permeability Due to Alternating Channel Width. *J. Chromatogr. A* **2015**, *1425*, 141–149. [CrossRef]
261. Burden, C.S.; Jin, J.; Podgornik, A.; Bracewell, D.G. A Monolith Purification Process for Virus-like Particles from Yeast Homogenate. *J. Chromatogr. B* **2012**, *880*, 82–89. [CrossRef]
262. Kadoi, K.; Iwamoto, E.; Nakama, T. Fabrication and Characterization of a Cellulose Monolith-like Particle for Virus Purification. *Biochem. Eng. J.* **2023**, *192*, 108849. [CrossRef]
263. Babanejad, N.; Mfoafo, K.; Zhang, E.; Omidi, Y.; Razeghifard, R.; Omidian, H. Applications of Cryostructures in the Chromatographic Separation of Biomacromolecules. *J. Chromatogr. A* **2022**, *1683*, 463546. [CrossRef]
264. Arvidsson, P.; Plieva, F.M.; Lozinsky, V.I.; Galaev, I.Y.; Mattiasson, B. Direct Chromatographic Capture of Enzyme from Crude Homogenate Using Immobilized Metal Affinity Chromatography on a Continuous Supermacroporous Adsorbent. *J. Chromatogr. A* **2003**, *986*, 275–290. [CrossRef]
265. Cheeks, M.C.; Kamal, N.; Sorrell, A.; Darling, D.; Farzaneh, F.; Slater, N.K.H. Immobilized Metal Affinity Chromatography of Histidine-Tagged Lentiviral Vectors Using Monolithic Adsorbents. *J. Chromatogr. A* **2009**, *1216*, 2705–2711. [CrossRef] [PubMed]
266. Williams, S.L.; Eccleston, M.E.; Slater, N.K.H. Affinity Capture of a Biotinylated Retrovirus on Macroporous Monolithic Adsorbents: Towards a Rapid Single-step Purification Process. *Biotechnol. Bioeng.* **2005**, *89*, 783–787. [CrossRef]
267. Savina, I.N.; Galaev, I.Y.; Mattiasson, B. Ion-exchange Macroporous Hydrophilic Gel Monolith with Grafted Polymer Brushes. *J. Mol. Recognit.* **2006**, *19*, 313–321. [CrossRef] [PubMed]

268. Lavoie, J.; Fan, J.; Pourdeyhimi, B.; Boi, C.; Carbonell, R.G. Advances in High-throughput, High-capacity Nonwoven Membranes for Chromatography in Downstream Processing: A Review. *Biotechnol. Bioeng.* **2024**, *121*, 2300–2317. [CrossRef]
269. Ruscic, J.; Perry, C.; Mukhopadhyay, T.; Takeuchi, Y.; Bracewell, D.G. Lentiviral Vector Purification Using Nanofiber Ion-Exchange Chromatography. *Mol. Ther. Methods Clin. Dev.* **2019**, *15*, 52–62. [CrossRef]
270. Sánchez-Trasviña, C.; Fuks, P.; Mushagasha, C.; Kimerer, L.; Mayolo-Deloisa, K.; Rito-Palomares, M.; Carta, G. Structure and Functional Properties of Capto^{TM} Core 700 Core-Shell Particles. *J. Chromatogr. A* **2020**, *1621*, 461079. [CrossRef]
271. Lothert, K.; Pagallies, F.; Feger, T.; Amann, R.; Wolff, M.W. Selection of Chromatographic Methods for the Purification of Cell Culture-Derived Orf Virus for Its Application as a Vaccine or Viral Vector. *J. Biotechnol.* **2020**, *323*, 62–72. [CrossRef] [PubMed]
272. Gencoglu, M.F.; Heldt, C.L. Enveloped Virus Flocculation and Removal in Osmolyte Solutions. *J. Biotechnol.* **2015**, *206*, 8–11. [CrossRef] [PubMed]
273. Heldt, C.L.; Saksule, A.; Joshi, P.U.; Ghafarian, M. A Generalized Purification Step for Viral Particles Using Mannitol Flocculation. *Biotechnol. Prog.* **2018**, *34*, 1027–1035. [CrossRef]
274. Hasan, T.; Kumari, K.; Devi, S.C.; Handa, J.; Rehman, T.; Ansari, N.A.; Singh, L.R. Osmolytes in Vaccine Production, Flocculation and Storage: A Critical Review. *Hum. Vaccines Immunother.* **2019**, *15*, 514–525. [CrossRef]
275. Rocha, J.M. Aqueous Two-phase Systems and Monolithic Chromatography as Alternative Technological Platforms for Virus and Virus-like Particle Purification. *J. Chem. Technol. Biotechnol.* **2021**, *96*, 309–317. [CrossRef]
276. Turpeinen, D.G.; Joshi, P.U.; Kriz, S.A.; Kaur, S.; Nold, N.M.; O'Hagan, D.; Nikam, S.; Masoud, H.; Heldt, C.L. Continuous Purification of an Enveloped and Non-Enveloped Viral Particle Using an Aqueous Two-Phase System. *Sep. Purif. Technol.* **2021**, *269*, 118753. [CrossRef]
277. Du, P.; Sun, P.; Sun, S.; Dong, J.; Dong, H.; Liu, R.; Guo, H.; Mu, K.; Liu, Z. Separation and Purification of Foot-and-Mouth Disease Virus by Multiple-Stage Aqueous Two-Phase Extraction System. *Process Biochem.* **2019**, *77*, 143–150. [CrossRef]
278. Joshi, P.U.; Turpeinen, D.G.; Schroeder, M.; Jones, B.; Lyons, A.; Kriz, S.; Khaksari, M.; O'Hagan, D.; Nikam, S.; Heldt, C.L. Osmolyte Enhanced Aqueous Two-phase System for Virus Purification. *Biotechnol. Bioeng.* **2021**, *118*, 3251–3262. [CrossRef]
279. Kim, H.; Yi, J.; Yu, J.; Park, J.; Jang, S.K. A Simple and Effective Method to Concentrate Hepatitis C Virus: Aqueous Two-Phase System Allows Highly Efficient Enrichment of Enveloped Viruses. *Viruses* **2022**, *14*, 1987. [CrossRef] [PubMed]
280. Pan, L.; Liu, X.; Fan, D.; Qian, Z.; Sun, X.; Wu, P.; Zhong, L. Study of Oncolytic Virus Preservation and Formulation. *Pharmaceuticals* **2023**, *16*, 843. [CrossRef]
281. Toniolo, S.P.; Afkhami, S.; Mahmood, A.; Fradin, C.; Lichty, B.D.; Miller, M.S.; Xing, Z.; Cranston, E.D.; Thompson, M.R. Excipient Selection for Thermally Stable Enveloped and Non-Enveloped Viral Vaccine Platforms in Dry Powders. *Int. J. Pharm.* **2019**, *561*, 66–73. [CrossRef]
282. Kumru, O.S.; Saleh-Birdjandi, S.; Antunez, L.R.; Sayeed, E.; Robinson, D.; van den Worm, S.; Diemer, G.S.; Perez, W.; Caposio, P.; Früh, K.; et al. Stabilization and Formulation of a Recombinant Human Cytomegalovirus Vector for Use as a Candidate HIV-1 Vaccine. *Vaccine* **2019**, *37*, 6696–6706. [CrossRef]
283. Homan, Y.; Rosenbloom, D.; Wong, S.; Lucchese, J.; Li, A.; Dubey, S.; Thomas, J.; Salituro, G.; Helmy, R.; Verch, T. Prediction of Frozen Virus Stability Based on Degradation Mechanisms, Real-Time Data and Modeling. *Bioanalysis* **2022**, *14*, 1177–1190. [CrossRef]
284. Shi, L.; Sanyal, G.; Ni, A.; Luo, Z.; Doshna, S.; Wang, B.; Graham, T.L.; Wang, N.; Volkin, D.B. Stabilization of Human Papillomavirus Virus-like Particles by Non-Ionic Surfactants. *J. Pharm. Sci.* **2005**, *94*, 1538–1551. [CrossRef]
285. Felix, M.N.; Waerner, T.; Lakatos, D.; Reisinger, B.; Fischer, S.; Garidel, P. Polysorbates Degrading Enzymes in Biotherapeutics—A Current Status and Future Perspectives. *Front. Bioeng. Biotechnol.* **2025**, *12*, 1490276. [CrossRef] [PubMed]
286. Chen, D.; Luo, W.; Hoffman, J.; Huang, L.; Sandefur, S.; Hall, T.; Murphy, M.; O'Donnell, S. Insights into Virus Inactivation by Polysorbate 80 in the Absence of Solvent. *Biotechnol. Prog.* **2020**, *36*, e2953. [CrossRef] [PubMed]
287. Hansen, L.J.J.; Daoussi, R.; Vervaet, C.; Remon, J.-P.; Beer, T.R.M.D. Freeze-Drying of Live Virus Vaccines: A Review. *Vaccine* **2015**, *33*, 5507–5519. [CrossRef] [PubMed]
288. Zhai, S.; Hansen, R.K.; Taylor, R.; Skepper, J.N.; Sanches, R.; Slater, N.K.H. Effect of Freezing Rates and Excipients on the Infectivity of a Live Viral Vaccine during Lyophilization. *Biotechnol. Prog.* **2004**, *20*, 1113–1120. [CrossRef]
289. Coleman, H.J.; Schwartz, D.K.; Kaar, J.L.; Garcea, R.L.; Randolph, T.W. Stabilization of an Infectious Enveloped Virus by Spray-Drying and Lyophilization. *J. Pharm. Sci.* **2024**, *113*, 2072–2080. [CrossRef]
290. Mundle, S.; Stephen, A.; Delagrave, S. Purification of Herpes Virus. US9365832B2, 14 June 2016.

4 An HPLC-SEC-Based Rapid Quantification Method for Vesicular Stomatitis Virus Particles to Facilitate Process Development

Adrian Schimek[a], Judy K.M. Ng[a], Ioannes Basbas[a], Fabian Martin[a], Dongyue Xin[b], David Saleh[c], Jürgen Hubbuch[d]

[a] ViraTherapeutics GmbH, Bundesstraße 27, 6063 Rum, Austria

[b] Boehringer Ingelheim Pharmaceuticals Inc, 900 Ridgebury Road, Ridgefield, CT 06877, USA

[c] Boehringer Ingelheim Pharma GmbH & Co. KG, Birkendorfer Str. 65, 88397 Biberach, Germany

[d] Karlsruhe Institute of Technology, Institute of Process Engineering in Life Sciences, Section IV Biomolecular Separation Engineering, Fritz-Haber-Weg 2, 76131 Karlsruhe, Germany

Corresponding authors:

(J.N.) judy.ng@boehringer-ingelheim.com

(J.H.) juergen.hubbuch@kit.edu

First author contribution (A.S.):
Conceptualization, Investigation, Formal analysis, Writing - original draft, Writing – review and editing

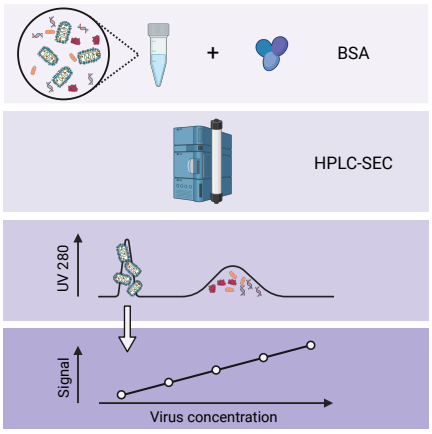

Figure 4.1: Graphical abstract

Reproduced from:
A. Schimek, J. K. M. Ng, I. Basbas, F. Martin, D. Xin, D. Saleh, and J. Hubbuch. “An HPLC-SEC-based Rapid Quantification Method for Vesicular Stomatitis Virus Particles to Facilitate Process Development”. In: *Molecular Therapy - Methods & Clinical Development* 32.2 (2024), p. 101252. DOI: 10.1016/j.omtm.2024.101252.

Molecular Therapy
Methods & Clinical Development
Original Article

An HPLC-SEC-based rapid quantification method for vesicular stomatitis virus particles to facilitate process development

Adrian Schimek,[1] Judy K.M. Ng,[1] Ioannes Basbas,[1] Fabian Martin,[1] Dongyue Xin,[2] David Saleh,[3] and Jürgen Hubbuch[4]

[1]ViraTherapeutics GmbH, Bundesstraße 27, 6063 Rum, Austria; [2]Boehringer Ingelheim Pharmaceuticals Inc, 900 Ridgebury Road, Ridgefield, CT 06877, USA; [3]Boehringer Ingelheim Pharma GmbH & Co. KG, Birkendorfer Str. 65, 88397 Biberach, Germany; [4]Karlsruhe Institute of Technology, Institute of Process Engineering in Life Sciences, Section IV Biomolecular Separation Engineering, Fritz-Haber-Weg 2, 76131 Karlsruhe, Germany

Virus particle (VP) quantification plays a pivotal role in the development of production processes of VPs for virus-based therapies. The yield based on total VP count serves as a process performance indicator for evaluating process efficiency and consistency. Here, a label-free particle quantification method for enveloped VPs was developed, with potential applications in oncolytic virotherapy, vaccine development, and gene therapy. The method comprises size-exclusion chromatography (SEC) separation using high-performance liquid chromatography (HPLC) instruments. Ultraviolet (UV) was used for particle quantification and multi-angle light scattering (MALS) for particle characterization. Consistent recoveries of over 97% in the SEC were achieved upon mobile phase screenings and addition of bovine serum albumin (BSA) as sample stabilizer. A calibration curve was generated, and the method's performance and applicability to in-process samples were characterized. The assay's repeatability variation was <1% and its intermediate precision variation was <3%. The linear range of the method spans from 7.08×10^8 to 1.72×10^{11} VP/mL, with a limit of detection (LOD) of 7.72×10^7 VP/mL and a lower limit of quantification (LLOQ) of 4.20×10^8 VP/mL. The method, characterized by its high precision, requires minimal hands-on time and provides same-day results, making it efficient for process development.

INTRODUCTION

Therapies based on virus particles (VPs) have significantly advanced over the past decades. Researchers have engineered and optimized VPs to expand their range of applications for various indications and also to enhance their safety and efficacy.[1] As a result, VP-based therapies are on their way to market with 331 active or recruiting clinical trials for gene therapies and 90 for oncolytic viruses, as listed by the US National Library of Medicine at the end of 2023.[2] For gene therapy, viruses are typically replication-incompetent and used as a vehicle to transfer genetic material to target cells. In contrast, oncolytic viruses are typically replication-competent in target cells and will multiply in the host.

Both enveloped and non-enveloped viruses are exploited for virus-based therapies. The surface of non-enveloped VPs is typically composed of a highly structured virus-encoded capsid shell consisting of multimers of protein subunits. Enveloped viruses, on the other hand, are enclosed with a lipid bilayer; its composition is directly dependent on the virus-encoded proteins, replication cycle, and host cell type. Thus, the surface of enveloped viruses is, in comparison, more complex and heterogeneous even within one production batch.

Despite the advancement of VP-based therapies, there remain significant challenges to develop manufacturing processes for such VPs. These challenges include the development of stable producer cell lines, the scalability of production, ensuring the purity and infectivity of the VPs, and maintaining the stability of the final product.[3–6] To address these challenges in process development, it is crucial to set up analytical tools to accurately quantify infectivity and particle concentration to determine yield after each step and evaluate the step and process performance.

Various quantification methods are widely used to measure different aspects of the target VPs, namely infectivity, genome copy, and particle quantification. Infectivity assays employ cell-based approaches to measure VPs that can successfully infect and replicate in host cells. Genome copy quantification is based on polymerase chain reaction (PCR) and will detect genetic material incorporated in both infectious and non-infectious VPs, as well as non-incorporated forms found in the sample. Particle quantification techniques based on physical measurement principles mostly rely on specialized devices such as nano particle tracking analysis (NTA), dynamic light scattering (DLS), tunable resistive pulse sensing (TRPS), and negative staining transmission electron microscopy (ns-TEM). A combination of some of

Received 18 December 2023; accepted 18 April 2024;
https://doi.org/10.1016/j.omtm.2024.101252.

Correspondence: Judy K.M. Ng, ViraTherapeutics GmbH, Bundesstraße 27, 6063 Rum, Austria.
E-mail: judy.ng@boehringer-ingelheim.com

these techniques is necessary to properly describe the quality and quantity of VPs in a sample. Thus, VP analysis typically requires high laboratory workload, long analysis time, low sample throughput, and high result variability.[7–9] The lack of rapid at-line analytical methods to accurately characterize and quantify VPs is an issue faced in the development of viral therapies.[5] As the fields of gene therapies and oncolytic virus therapies continue to evolve, advancement of VP analytics will be essential for the successful development and commercialization.

Quantification methods based on ultraviolet (UV) detection of entire VPs have been published for several enveloped and non-enveloped particles.[10–15] All of the referenced quantification methods employ separation techniques (such as size-exclusion chromatography [SEC], ion-exchange chromatography [IEX], or capillary electrophoresis [CE]) that influence the analyte recovery and thereby the result. Reproducible recovery values that are within specified range were shown for non-enveloped viruses with all separation techniques, but not for enveloped viruses. SEC resin based on hydrophilic polymethacrylate has previously been shown to be suitable for virus analysis,[10,15,16] and it is hypothesized it may outperform IEX resins in terms of target recovery and shape preservation upon buffer optimization to maximize recovery. When the size difference between VPs and SEC resin pore size is sufficiently large, VPs are expected to elute in the void volume, which is seen on the chromatogram as the exclusion peak. Comparatively smaller protein impurities and nucleic acids will be retained longer in the resin and be therefore separated.

The enveloped virus used in this study is a modified vesicular stomatitis virus (VSV) of the Rhabdoviridae family. Rhabdoviruses are enveloped RNA viruses with a bullet-shaped morphology measuring 70 × 196 nm.[17,18] Though wild-type VSV already has versatile application potential as an oncolytic virus and vaccine vector,[19] further engineering of the virus by substitution of its glycoprotein (GP) for that from lymphocytic choriomeningitis virus (LCMV) has resulted in VSV-GP with minimal neurotoxicity, greater potency against human cancer cells, and escape from host humoral immunity.[20,21] Infectivity assays, such as 50% tissue culture infectious dose ($TCID_{50}$), plaque assay, and laser force cytology are available and used quantification methods for VSV and its variants.[22–24] Additionally, PCR and TRPS protocols have been established. However, these methods necessitate high laboratory workload and specialized machines, thus challenges in application remain.[22,25,26]

In this study, a straightforward method for total VP count for VSV-GP was developed. The key features of the method include low hands-on time, high precision, and same-day results. The working range for quantification was tailored to process development applications. To develop a robust, versatile, and sample matrix-independent method, a label-free approach was chosen. While the method is based on SEC separation and UV detection, a downstream in-line multi-angle light-scattering (MALS) detector provided additional particle characteristics such as particle size. Each component of the setup from sample preparation to the run method itself has been optimized and characterized, and an example application for process development is presented. A standard curve based on purified reference virus material is used to interpolate absolute values. As an orthogonal method for sample characterization, ns-TEM was used as it is considered the established benchmark method for VP quantification for particle numbers.[8,27] High-performance liquid chromatography (HPLC) instruments equipped with UV detectors are ubiquitous in biopharmaceutical labs, and expertise and familiarity are typically well-established among researchers. This will facilitate wide implementation and applicability.

RESULTS

Reference material generation and characterization

Two batches of purified VSV-GP preparations were produced by sucrose cushion centrifugation followed by SEC. Both batches were analyzed using orthogonal quantification methods: ns-TEM, quantitative PCR (qPCR), and $TCID_{50}$ assay. The titers determined by ns-TEM were comparable between the two batches with 1.72×10^{11} VP/mL for the first and 1.44×10^{11} VP/mL for the second batch. The viral RNA in the sample was quantified by qPCR to be in the same magnitude as the ns-TEM, with 1.38×10^{11} genomic copies per mL (GC/mL) for the first and 2.13×10^{11} GC/mL for the second batch. Infectivity was confirmed by $TCID_{50}$ assay with 5.62×10^{10} $TCID_{50}$/mL for the first and 3.06×10^{10} $TCID_{50}$/mL for the second batch. The magnitude difference between genomic copies and infectivity is expected, as particle heterogeneity results in VPs that are unable to infect otherwise susceptible cells.[28]

Analytical separation method on the HPLC

Virus preparations are injected into the HPLC-SEC setup with an in-line MALS detector and using an SEC resin that excludes VPs from entering the bead pores and thus separating them from smaller impurities. Separation of concentrated VSV-GP VPs from impurities is shown in Figure 1A, where a sample of purified VPs spiked with impurity-rich clarified harvest material was analyzed. The chromatogram can be divided into the distinct exclusion peak at 10.2 min and a second peak region eluting between 18 and 33 min. Separate injections in Figure 1B enable peak allocation, which shows the exclusion peak originates from the VSV-GP sample. The second peak region originates from the clarified harvest material. In the light-scattering signal only the exclusion peak is observed. This indicates large, thus scattering particles in the exclusion peak; and small, thus non-, or low-scattering particles for the second peak region. An analysis of the cell culture medium of the process revealed that the second peak region mostly originates from the cell culture media itself, except for the first eluting impurity peak. This first impurity peak was depleted upon nuclease-treatment, implying its nucleic acid content (data not shown).

Virus peak identification

The presumed virus-containing exclusion peak, eluting at 10.2 min, was collected using a fraction collector, and analyzed by offline analytical methods to identify its VP identity. The presence of VPs in this fraction was confirmed by detection of viral genetic material by qPCR (showing a recovery of 63.3%) as well as by identifying virus-encoded

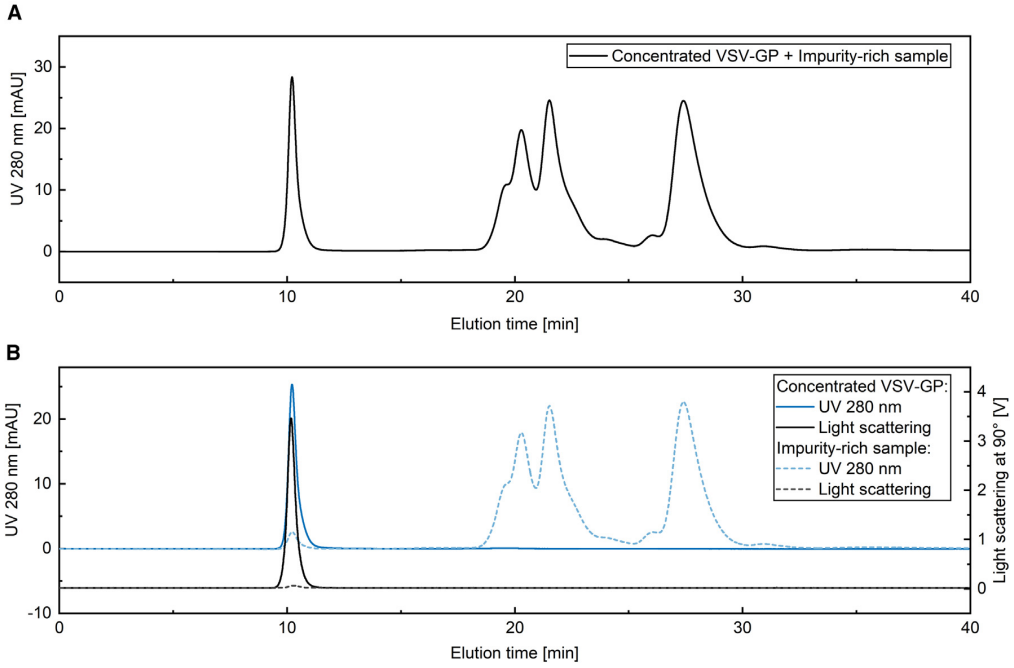

Figure 1. SEC separation chromatogram of purified VSV-GP and impurity-rich material

(A) Chromatogram of concentrated VSV-GP material (reference material) spiked into impurity-rich material (clarified harvest) on TSKgel G4000PW using optimized buffer conditions. (B) Concentrated VSV-GP material and impurity-rich material were injected separately on the SEC column using the same conditions. UV 280 nm and light-scattering signal at the 90° angle is shown.

protein bands using gel electrophoresis followed by silver staining as depicted in Figure S1 presented in the supplemental material.[28]

Method development

The initial running buffer was a Tris-based buffer with 50 mM NaCl and 150 mM Arginine (Arg) at pH 7.5. Comparing the UV 280 nm signal responses of VSV-GP injections over the column and the bypass showed VSV-GP particle recovery values of about 30%. Also, the cleaning-in-place (CIP) steps showed particles eluting from the column that could be observed in the light-scattering signal (data not shown). Buffer screening was performed to increase recovery values by reduction of non-specific interaction of the analyte with the column. Simultaneously, two different pore sizes of the Tosoh TSKgel polymethacrylate resin (50 nm, >100 nm) and two column housing materials (stainless-steel, polyetheretherketone [PEEK]) were tested for resolution improvement and sample recovery. Sample stability issues were addressed by spiking of BSA (bovine serum albumin) as a stabilizer to the samples. The aim was to increase storage duration in the system sample manager until the sample injection for analysis was performed.

Mobile phase buffer screening

Buffer screenings were performed to minimize non-specific binding of the VPs to the column resin, which are mainly due to a combination of hydrophobic and electrostatic interactions.[29] Following each buffer optimization run, two CIP steps (organic solvent and high-salt buffer) were conducted with the aim of specifically eluting bound VPs based on their interaction type. During these CIP steps, the MALS signal was qualitatively assessed to determine the residual interaction type prevailing by the buffer used.

The mobile phase was optimized in seven iteration rounds of buffer screening, each consisting of multiple runs. In each round, the buffers were adjusted based on the recovery and CIP results from the previous rounds and literature research. A detailed buffer list can be found in Table S1, the iteration rounds consisted of the following:

(I) Tris-based buffer with increasing salt content
(II) Tris-based buffer with Arginine and pH adjustments
(III) Citrate and phosphate-based buffer testing
(IV) Tris-based buffer with combined Arginine and salt content adjustment
(V) Tris-based buffer with additives (sorbitol, sucrose, dimethyl sulfoxide [DMSO])
(VI) Tris-based buffer with Arginine, salt, and DMSO content adjustments

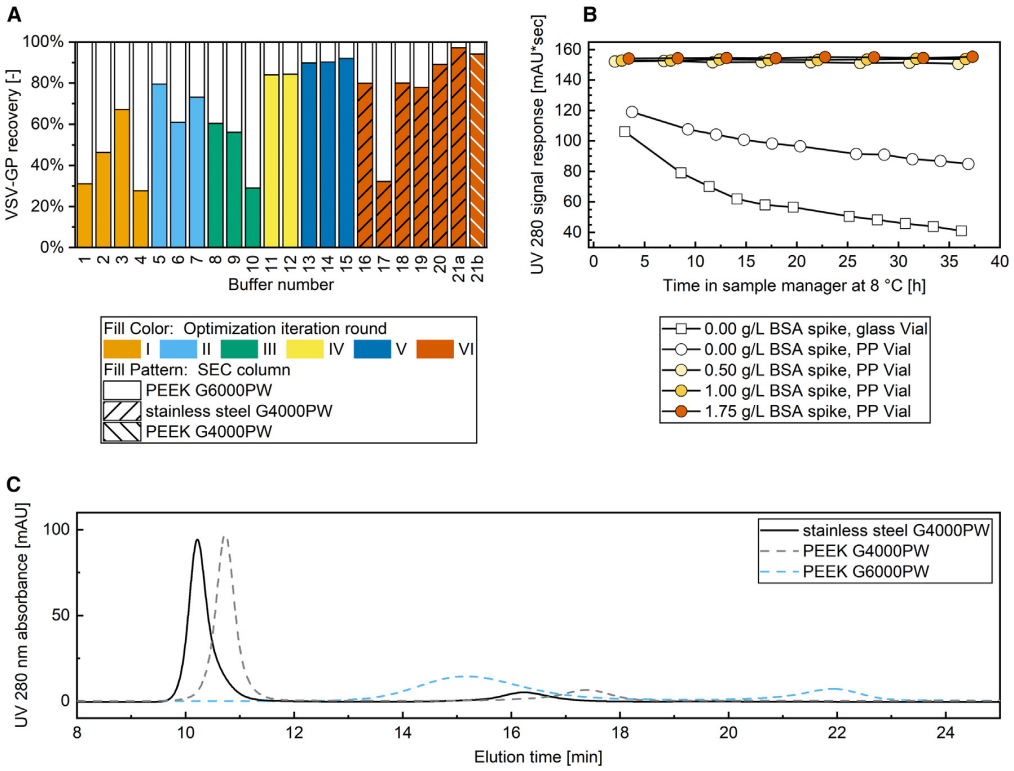

Figure 2. Buffer screening, sample stability testing, and analytical SEC column selection for method development

(A) Recovery values for virus particles upon the mobile phase optimization. Iteration rounds: I – Tris-based buffer with increasing salt content, II – Tris-based buffer with Arg and pH adjustments, III – Citrate- and phosphate-based buffer testing, IV – Tris-based buffer with combined Arg and salt content adjustment, V – Tris-based buffer with additives (sorbitol, sucrose, DMSO), VI – Tris-based buffer with Arg, salt, and DMSO content adjustments; technical replicates: $n = 1$ for buffers 1 to 20, $n = 3$ for buffer 21 (SD < 0.8%). (B) Sample stability optimization using different vials (glass and polypropylene vials) and BSA spiking. The UV 280 nm signal response is the integrated exclusion peak, identified as the virus peak. (C) SEC chromatogram comparison of BSA-spiked reference material for stainless-steel and PEEK version of G4000PW and PEEK version of G6000PW.

The initial low recovery using a non-optimized buffer could be improved by adjusting the salt and Arg content of the Tris-based buffer. A sample recovery of 84.4% could be reached after two iteration rounds as depicted in Figure 2A. The use of phosphate-based buffers and citrate as an additive did not improve recoveries. Sorbitol, sucrose, and DMSO increased recoveries, from which DMSO performed best under the tested conditions. The overall best performance of this system was achieved using a buffer composed of 50 mM Tris, 200 mM NaCl, 150 mM Arg, and 0.1% DMSO at pH 8.0: A recovery of 97.2% (SD 0.54%) on the stainless-steel version of G4000PW was reached and 94.2% (SD 0.76%) on the PEEK version. Simultaneous to the buffer screening with VSV-GP, the recoveries for BSA were determined. In the iteration rounds 1 to 4, the recovery values for BSA were much higher compared with VSV-GP with values above 70%, averaging at 87.4%. For the final buffer (number 21 Figure 2A), a BSA recovery of 96.88% (SD 0.56%) was reached for the stainless-steel version and 97.24% (SD 0.56%) for the PEEK version. (BSA recovery data not shown).

Sample stability optimization

A decrease in UV 280 nm signal response over time was observed for VSV-GP samples stored in the sample manager. This was likely due to non-specific adsorption of purified VPs to storage material surfaces. To address this issue, two different HPLC sample vial materials (glass and polypropylene [PP]) were tested as well as BSA spiking of the samples. Prior to BSA spiking, the reference material was diluted to a concentration of 9×10^9 VP/mL. Prepared samples were stored in the sample manager at 8°C over a time frame of 35 h and the signal response repeatedly determined. The results are depicted in Figure 2B. The first time point for non-spiked samples in the glass vial and the polypropylene vial resulted in 70% to 80% signal responses in comparison to the BSA-spiked sample. Over the course of the measurement, the signal response for the non-spiked samples further

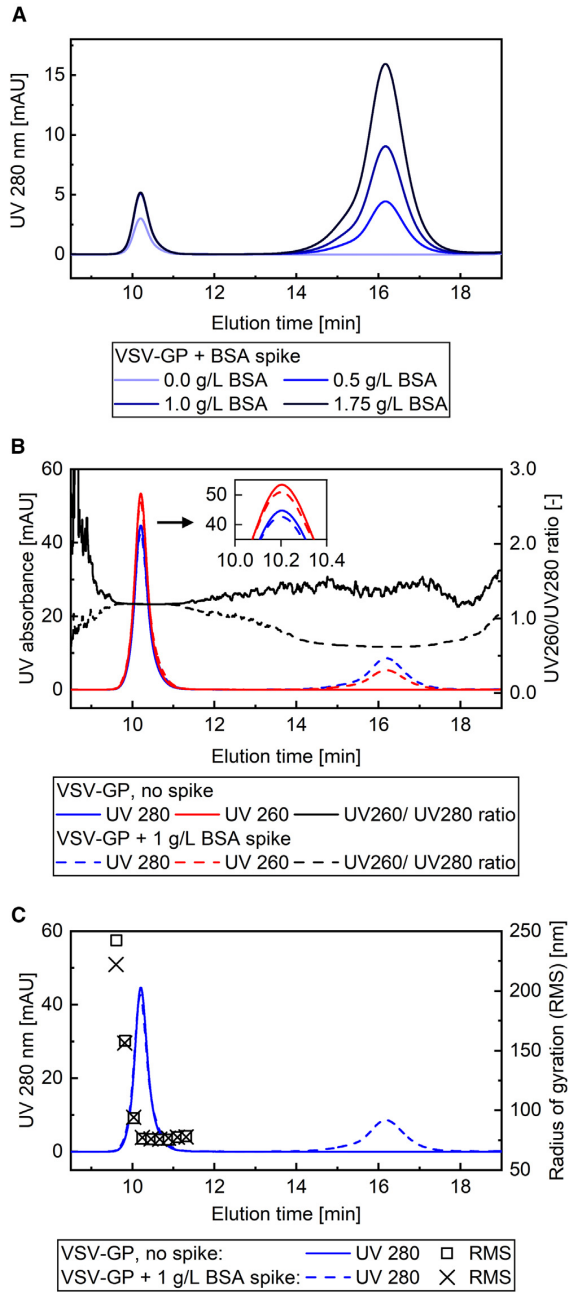

Figure 3. Exclusion peak characterization using BSA as sample stabilizer

(A) SEC chromatogram of reference material spiked with different concentrations of BSA and non-spiked. The exclusion peaks at 10.2 min of the BSA-spiked samples are entirely overlaying. The non-spiked sample has been in the sample manager for several hours before measurement. (B) UV 260 nm and UV 280 nm absorbance for non-spiked and BSA-spiked reference material and UV260/280 nm ratio; a percentile filter of 50 was used to smooth the ratio curve. (C) RMS-radii for non-spiked and BSA-spiked reference material. Radii were only evaluable for the exclusion peak due to the low light-scattering signal for the rest of the chromatogram.

decreased to 57% for the polypropylene vial and 28% for the glass vial. The UV 280-nm signal response for samples with BSA spikes were stable over the complete time frame with an RSD below 0.5%.

Column comparison

Two different pore sizes of the Tosoh TSKgel PW resin (G6000PW and G4000PW) were compared for resolution, and additionally two different column housing materials were tested for recovery. The specified mean pore sizes for the resins are 50 nm for the G4000PW and >100 nm for the G6000PW. Upon comparison of the exclusion peaks of the different columns in Figure 2C, differences in elution time and widths are observed. The PEEK G6000PW column resulted in later (4 to 4.5 min) and broader peaks (by the factor 3.3) compared with the G4000PW columns. The time shift and especially the broad peak indicates a greater retention of the VPs by the greater pore sizes. It is assumed the G6000PW resin pores are, at least partially, large enough to retard VPs, in contrast to the G4000PW resin pores that predominantly exclude them. The PEEK column housing has an inner diameter of 7.8 mm compared with 7.5 mm for the standard stainless-steel housing that results in an increased column volume of 8.2%. The PEEK version of the G4000PW retards the elution time for 31 s compared with the stainless-steel version. However, the peak shape remains comparable between the column housings.

BSA was used as sample stabilizer, and it can also be seen as a model impurity protein for column comparison as shown in Figure 2C. As expected, the BSA spike peaks elute after a longer retention time compared to the VPs. They are broadened in a similar way as the VP peaks in respective to the column used. However, the use of the G6000PW resin leads to a reduced separation efficiency without distinct baseline separation. Together with the recovery results, it was decided to continue method development using the stainless-steel version of the G4000PW.

Separation characterization using BSA as sample stabilizer

The online signals of the UV and MALS detectors were used to characterize the obtained chromatograms, focusing on the exclusion peaks. In the method setup, BSA was spiked into the samples as a stabilizing agent. Chromatograms of BSA-spiked and non-spiked reference material are shown in Figures 3. Injecting the reference VP material into the analytical SEC column results in a single peak at an elution time of 10.2 min. Different BSA spiking concentrations (0.5 to 1.75 g/L) were used in Figure 3A, resulting in a later eluting BSA peak without any effect on the elution behavior of the exclusion peak. A reduced peak area for the non-spiked sample was observed after several hours in the sample manager before injection, indicating some loss of sample during prolonged storage without addition of BSA as stabilizer. The ratio of UV 260 nm to UV 280 nm results in

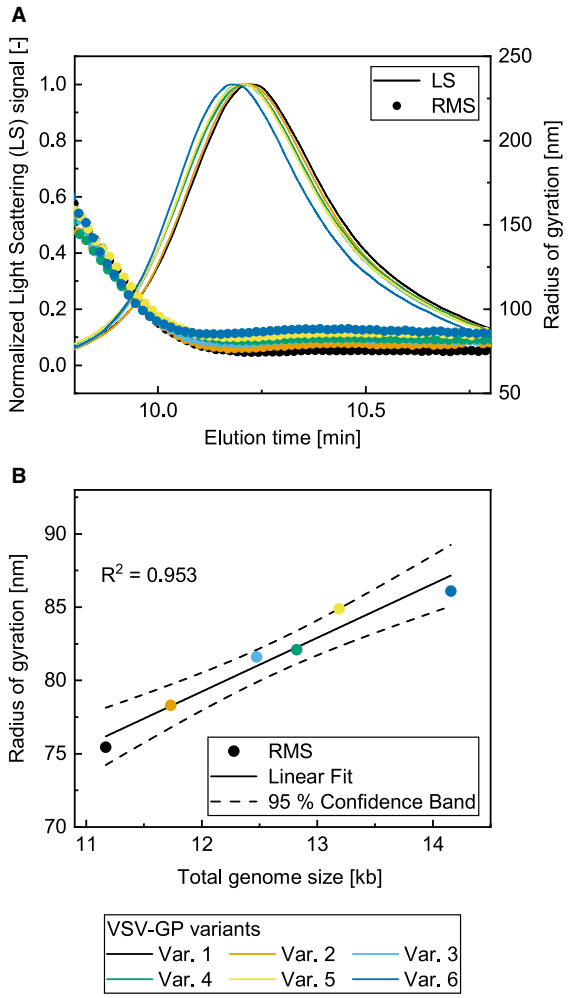

Figure 4. VP size influence on the exclusion peak and VP sizing

(A) SEC exclusion peak of VSV-GP and variants of different genome sizes. Normalized light scattering and radius of gyration. (B) Radius of gyration for VSV-GP (Variant 1) and larger size variants (Variants 2 to 6) over variant genome size. The radii were measured at the peak maximum of the exclusion peak.

a value of 1.196 (SD 0.004) for the first elution peak at 10.2 min as depicted in Figure 3B. The difference of the ratios between the BSA-spiked and non-spiked measurement lays within the standard deviation. With the addition of BSA, a second peak is observed in the UV signal at a later elution time point (16.2 min). At its peak maximum, a ratio of UV 260 nm to UV 280 nm of 0.624 is reached. In Figure 3C, size measurements based on the online light-scattering signal results in a radius of gyration of 76.4 nm (SD 0.6) for the constant region after peak fronting. The size difference between the BSA-spiked and non-spiked measurement lies within the standard deviation. In the front of the peak, larger radii are measured, with a maximum of approximately 250 nm.

Virus size variants

Virus preparations of VSV-GP variants with different total genome sizes were analyzed, and their particle sizes measured using the MALS detector signal. A shift of less than 2 s in maximum of the exclusion peak to an earlier elution time point with increasing genome size is shown in Figure 4A. The measured size of the peak maximum is plotted over the total genome size in Figure 4B. A linear regression shows the linear dependency of particle size and total genome size.

Calibration curve for VP quantification

A dilution series of the reference material containing purified VPs was analyzed by HPLC-SEC and is shown in Figure 5A. No difference in elution time and general peak shape is observed. Both online and offline analysis indicated no interference for the exclusion peak by other particles than the VPs and showed a baseline separation from smaller impurities. The reference material and the developed SEC method are deemed suitable for generating a calibration curve. The UV 280 nm signal response was defined as the integrated peak area of the exclusion peak at 10.2 min, identified as the virus peak. The signal responses of eight concentration levels of the reference material were plotted to obtain the calibration curve shown in Figure 5B. The linear regression was 1/Y-weighted due to the heteroscedasticity of the dataset and forced through the origin. The dependency of the response to the VP concentration in the sample is given by Equation 1, where y is the signal response in mAU * sec and x is the VP concentration in VP/mL. The coefficient of determination was calculated as R^2 = 0.998. The concentration range of the calibration curve reaches from 7.08×10^8 to 1.72×10^{11} VP/mL.

$$y = 1.5503 * 10^{-8} \frac{\text{mAU} * \text{sec}}{\text{VP/mL}} * x \qquad \text{(Equation 1)}$$

Method characterization

Performance

The performance of the method was tested at four concentration levels within the working range with the lowest being the lower limit of quantification (LLOQ). Based on the signal-to-noise (SN) ratio, the theoretical sensitivity of the method was calculated. A ratio of 3 was applied for the limit of detection (LOD) and a ratio of 10 for the LLOQ, resulting in an LOD = 7.72×10^7 VP/mL and an LLOQ = 2.57×10^8 VP/mL. However, sufficient accuracy was only reached for an LLOQ of 4.20×10^8 VP/mL, which was used for the performance evaluation. Accuracy, repeatability, and intermediated precision have been determined and are shown in Table 1. Recommended specifications by the Food and Drug Administration (FDA) guidelines were met or exceeded.[30]

Sample matrix influence

The influence of different sample matrices on the VP recovery was evaluated. In early downstream process (DSP) steps, the process

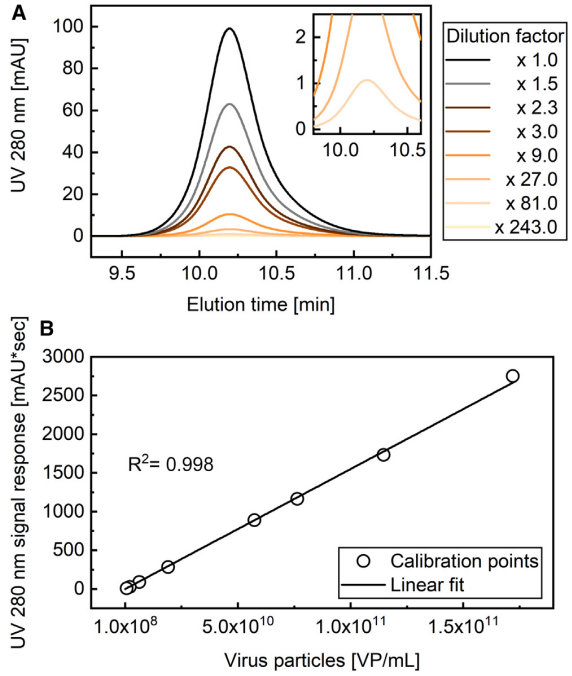

Figure 5. Calibration curve

Diluted reference material was analyzed using BSA as the sample stabilizer to obtain measurement points for the calibration curve. The UV 280 nm integrated area of the exclusion peaks was used as signal response. Three independent runs in triplicate for eight concentration levels were obtained. (A) Exemplary exclusion peaks of the concentration levels used for the calibration are shown in comparison. (B) A 1/Y-weighted linear regression was used to fit calibration curve. Only mean values are shown due to non-displayable RSD <2% and for the lowest concentration RSD <4.5%.

material matrix consists of spent cell culture media and cell-derived impurities. Nuclease is added to degrade host cell DNA and RNA. DNA and RNA fragments, as well as other residual impurities are removed throughout the process steps. Buffer compositions are changing along the process, and the total salt concentration varies and can go up to a maximum of 1 M.

For VSV-GP, cell culture media is replaced by Tris-based buffers early in the DSP and formulated with excipients such as albumin and trehalose. To examine the influence of the process sample matrices on the quantification method, samples were generated for analysis with the following method: in-process control samples from each step were filtered to deplete the VPs they originally contain, and then a defined amount of VP was spiked into each sample. The samples were first checked by HPLC-SEC (<LOD) for successful VP removal prior to spiking. The results, as presented in Table 2, show an average accuracy of 99.79% for all in-process controls (IPCs) with a standard deviation of 5.64%, indicating that the quantification method is not influenced by the sample matrices tested.

Chromatographic step mass balance

Utility of the quantification method described in this paper was demonstrated through performance of a mass balance calculation of a typical chromatographic capture step. VSV-GP was propagated in cell culture, and the conditioned clarified harvest material fed into a cation exchange chromatography (CEX) monolith column in bind-and-elute mode. VP concentration of the input feed and output flowthrough, wash, and elution were quantified by HPLC-SEC method. Fractions with expected high concentrations of VSV-GP were diluted (10× or 100×) so that the concentrations fall within the calibrated range of the method. Collected output fractions were analyzed by qPCR in parallel.

The online chromatogram signals are shown in Figure 6A and the offline fraction analysis results in Figure 6B. One liter of feed with a concentration of 2.39×10^9 VP/mL was loaded on the column, and a total of 2.76×10^{12} VPs were quantified by the HPLC-SEC method in the output fractions. Specifically, 18.8% of the total VPs in the feed was measured in the column flowthrough, VP concentration in the column wash was below LLOQ, and 66.3% was detected in the main peak with a peak width of 1.6 mL. The entire elution peak including the tailing was 9.8 mL wide and 78.8% of total input VPs was found. Additionally, the CIP peak was pH-stabilized and also collected for quantification, showing a result of 2.4% of total VPs. Overall, the total VPs quantified in the output is marginally higher than the expected total particle counts in the feed and falls within the accepted error margin of the performance runs.

The quantification results obtained from the presented HPLC-SEC method and from the established qPCR method were comparable: feed concentration 2.8×10^8 GC/mL, 5.0×10^8 VP/mL; elution peak particle count 2.03×10^{12} GC, 2.1×10^{12} VP.

DISCUSSION

Separation method and method development

In-process control samples generated from process development and production of VPs vary in buffer composition, particle concentration, and amount of process-related impurities.[31] UV-absorbing impurities need to be depleted or shown to be of neglectable concentration before target quantification by UV, thus framing the separation problem to be solved prior to the quantification. Another challenge is maintaining the integrity of the viral particles during the analytical method; all system parameters, including flow rate and resin bead size, were selected to minimize shear forces incurred. Such system parameters, once selected, remained unchanged during method development in this study.

The exclusion peak was identified as the virus peak by offline analytical methods as well as by characterization using online detectors. The online UV data show a constant ratio of UV 260 nm to UV 280 nm ratio of 1.2 over the width of the exclusion peak, indicating the presence of nucleic acids and proteins at the same time, though no more information about the sample composition can be derived. However, the consistency of the obtained value leads to the conclusion of a

Table 1. Performance evaluation

Level	Expected titer [VP/mL]	Mean [VP/mL]	Standard Dev. [VP/mL]	95% confidence interval [VP/mL]	Accuracy	Repeatability RSD	Intermediate precision RSD
H	1.44×10^{11}	1.64×10^{11}	6.31×10^{8}	1.63×10^{11} to 1.64×10^{11}	113.7%	0.63%	0.75%
M	2.06×10^{10}	2.19×10^{10}	1.88×10^{8}	2.17×10^{10} to 2.21×10^{10}	106.2%	0.09%	1.67%
L	2.94×10^{9}	2.97×10^{9}	3.28×10^{7}	2.93×10^{9} to 3.00×10^{9}	100.9%	0.59%	2.14%
LLOQ	4.20×10^{8}	4.23×10^{8}	6.44×10^{6}	4.15×10^{8} to 4.30×10^{8}	100.6%	0.49%	2.95%

Four concentration levels (High [H], Middle [M], Low [L], and LLOQ) were used to evaluate the performance of the HPLC-SEC quantification. For the concentration levels, reference material was diluted, aliquoted and stored at −80°C until usage. Measurements were done in triplicate in five independent runs.

constant ratio of nucleic acid to protein content over the width of the exclusion peak. Furthermore, it indicates no increase or decrease in light-scattering effects over the peak.[32] The in-line MALS detector can show the presence of particles in the expected size range for the target VPs. The sizing data of the MALS also reveals the presence of larger particles in the beginning of the exclusion peak with radii up to 250 nm for the start of the peak, and then constant sizes are measured throughout the rest of the exclusion peak. The larger particles eluting first may be VP aggregates still showing an unaltered UV 260 nm to UV 280 nm ratio. This observation indicates a weak separation effect of the SEC column at particle sizes much larger than its specified pore sizes, possibly induced by a broad pore size range of the SEC column or, as suspected by Vajda et al., a separation effect of the inter-particle volume.[33] This effect can also be observed when comparing the exclusion peak time points of virus variants varying in particle size. The increased particle length correlates with shift toward an earlier elution. The correlation seen with the observed separation effects and sizing data to the theoretical VP sizes indicates that the integrity of the VPs is preserved in this analytical method.

For the method characterization runs, purified VP preparations defined as reference material were used. The material was purified and concentrated by sucrose cushion centrifugation and polished using preparative SEC. However, possible impurities of similar size and density range as the VPs cannot be depleted by these steps. From analysis of previous established methods (qPCR and ns-TEM), as well as considering the lack of UV-signal and light-scattering interference signals, the preparations were deemed suitable for use as a VP standard. Similar observations for the exclusion peak in the online signal are made for IPC samples, making the peak suitable to be used for quantification purposes. A dilution series of the reference material was used to obtain a calibration curve based on the UV 280 nm signal response. The calibration curve showed good linearity in the examined range. While this approach requires an orthogonal quantified reference material, it does not require knowledge of target molecule or solute-specific optical parameters in comparison with methods based on light-scattering principles.[34]

To increase the sample recovery of the SEC method, the running buffer was optimized using a buffer screening. The rationale was to reduce suspected hydrophobic and electrostatic interactions with the column resin when altering the buffer composition. The low initial recovery could be improved by shielding electrostatic interactions by increasing the NaCl concentration until the point where the salt enhanced hydrophobic interactions leading again to a reduced recovery. Arginine proved to be a good agent to suppress both interactions as previously reported.[35] Observed recoveries for BSA were higher compared with VSV-GP for the first four iteration rounds, indicating additional or stronger interactions of the much larger VPs with the resin. Addition of sugars and organic solvents increased the recovery for VPs, of which DMSO performed best. DMSO was reported to stabilize enveloped VPs during freeze-thaw cycles,[36] but

Table 2. Results of the sample matrix influence evaluation

	IPC 1	IPC 2	IPC 3	IPC 4	IPC 5	IPC 6
Mean	3.56×10^{10}	3.58×10^{10}	3.19×10^{10}	3.58×10^{10}	3.56×10^{10}	3.13×10^{10}
Standard deviation	5.41×10^{7}	8.24×10^{7}	7.98×10^{8}	5.46×10^{6}	8.81×10^{7}	4.95×10^{8}
RSD	0.15%	0.23%	2.50%	0.02%	0.25%	1.58%
95% confidence interval	3.55×10^{10} to 3.57×10^{10}	3.57×10^{10} to 3.59×10^{10}	3.10×10^{10} to 3.28×10^{10}	3.58×10^{10} to 3.58×10^{10}	3.56×10^{10} to 3.58×10^{10}	3.08×10^{10} to 3.19×10^{10}
Accuracy	103.4%	104.0%	92.7%	104.0%	103.6%	91.0%

IPCs of a lab-scale production run were taken, the virus particles removed by filtration, and a specified virus concentration spiked in. Samples were measured in triplicate by HPLC-SEC quantification. The spike concentration in the sample was 3.44×10^{10} VP/mL. Purification stage and differences between IPCs are as follows. IPC 1: harvested cell culture including cell culture media, increased ionic strength for viral release, clarified by depth filtration; IPC 2: nuclease treated clarified harvested material; IPC 3: CEX purified material, CEX eluate consists of a Tris-based buffer containing Arginine and NaCl; IPC 4: polished material with reduced impurity content; IPC 5: buffer exchanged to a Tris-based buffer containing Arginine and excipients; IPC 6: material spiked with additives.

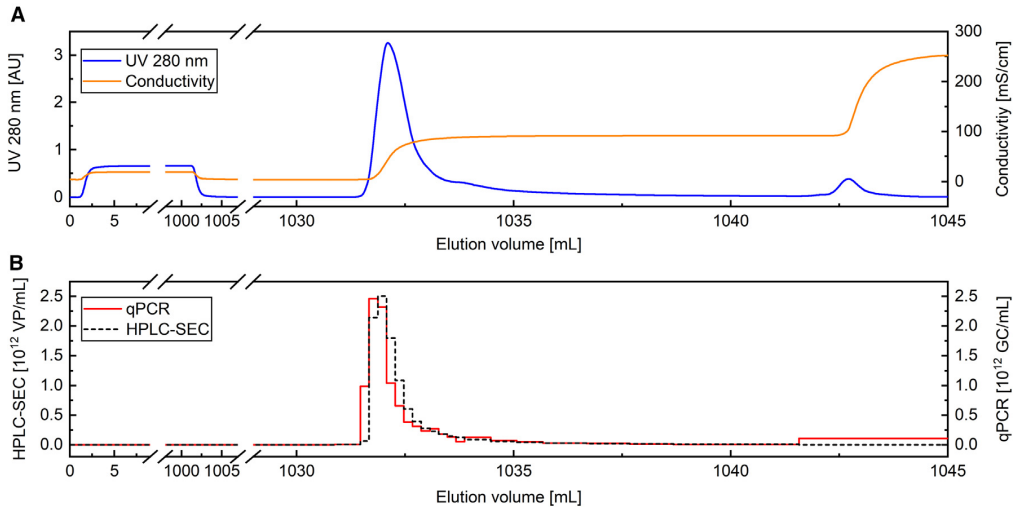

Figure 6. Offline fraction VP quantification of a CEX purification step

Clarified harvest material of a VSV-GP upstream process was applied in bind-and-elute mode on a CEX monolith column. Fractions of load, wash, elution, and CIP were collected and quantified offline by the presented HPLC-SEC method and qPCR. (A) Chromatogram of CEX run showing online UV 280 nm signal and online conductivity signal. The UV signal saturated at 3.0 AU. (B) Fraction quantification results for HPLC-SEC and qPCR. Due to low numbers for the load phase (and CIP for HPLC-SEC) and scale limitations, signals are plotted close to zero for these phases.

could also have a negative effect on VP integrity due to increased lipid bilayer permeability.[37] Thus, DMSO was reduced from 1% in first screening runs to 0.1% without impacting recovery values. For quantification purposes, a sufficiently high recovery is required, though it does not have to be 100% as stated by an FDA guideline.[30] Rather, the recovery values should be consistent and reproducible. Within the buffer screening, the final buffer was tested in triplicates with recovery RSDs below 0.6% for VSV-GP and BSA samples. The VSV-GP recoveries were later validated for four concentration levels in the performance evaluation.

Spiking BSA into the sample to act as a stabilizer enabled overnight measurements. Without BSA, UV 280 nm signal response was reduced by as much as 70% after 35 h in the temperature-controlled sample manager module. To explain and overcome this sample loss, different theories are considered. Aggregated VPs, retained by the column frit, would accumulate over injection count, leading to increased system pressure. Degraded VPs, disintegrated to fragments of smaller size, would be separated in the SEC column from the exclusion peak. However, such effects were not observed. It was thus hypothesized that VP adhered to the HPLC vial walls. To assess this hypothesis, the available wall area per VP was estimated. For 100 µL sample fill volume in the vials, the contact surface was calculated. As no technical drawings or vial interior dimensions were available, manual length measurements and surface calculations for cylinders and cones were used as geometrical approximations. A contact surface of 115 mm^2 was estimated for the glass vial, resp. 228 mm^2 for the polypropylene vial. Based on the VSV particle dimensions by Ge et al.,[17] the projected sideways rectangle for a single VP was calculated to be 1.4×10^{-8} mm^2. Based on the virus concentration in the sample and the signal reduction between the non-spiked samples and the spiked samples, the amount of presumed non-detected VPs was calculated. At the last time point of the sample stability experiment, each non-detected VP had 1.3, resp. 2.11 times more area available than its own projection on the surface. This estimation confirms the possibility of a Langmuir layer adhesion of the particles in terms of available wall area per particle. Furthermore, the declining VP concentration curves without BSA spikes observed in Figure 2B correspond to a Langmuirian adsorption kinetic.[38] The subsequent use of polypropylene vials coated with a high-performance surface did improve the sample stability but was not sufficient to enable a constant overnight signal response. BSA was reported to prevent non-specific sample binding on vial walls and the spiking of BSA to VSV-GP samples stabilized the resulting UV 280 nm response over the tested time frame of 35 h.[39] BSA spiking concentrations over the range of 0.5 to 1.75 g/L showed similar results without influencing the elution behavior of VPs or changing the rms radius. The results are in agreement with a published HPLC method development by Lorbetskie et al. in which the change from glass to polypropylene vials improved the recovery, however only the addition of an additive to the sample yielded in the sufficient reproducibility.[40]

Non-specific binding losses to HPLC vials were targeted using BSA as the sample stabilizer. Further losses could occur in other parts of the HPLC system such as the measurement chambers, tubings and connectors. These losses were minimized by the use of the "Bio" version

of the HPLC system which features bio-compatible materials for the wetted parts of the flow path up to and including the UV detector. Furthermore, the column resin and housing can induce non-specific binding. The column resin material was chosen according to manufacturer's information regarding suitability for VPs and already published applications for VPs.[10,15,16] After the above-described buffer optimization, a reproducible and high recovery of VPs from the column was achieved, showing neglectable residual interactions. Also, the column housing material was evaluated for sample recovery. Because the stainless-steel column showed high recovery and faster elution times compared with the PEEK housing, it was chosen for further method development. In case of the TSKgel G6000PW resin, the manufacturer's data of the pore size is vague with a size specification of >100 nm and the resin material has shown to produce a broad pore size distribution.[33] Diffusion effects and pore accessibility for the bullet-shaped VSV particles depend on their orientation, resulting in different possible retention behaviors for the same particle. Predominant retention effects due to pore accessibility is seen only with the G6000PW resin, resulting in a broader peak compared with the G4000PW resin with a specified mean pore size of 50 nm. However, a weak separation effect by size is also observed for the G4000PW resin. Baseline separation from protein impurities, shown for BSA as model impurity, was only achieved using the G4000PW resin, independent of the column housing.

Method characterization

The performance evaluation based on four concentration levels showed a high reproducibility and intermediate precision for all tested levels. Accuracy values decreased with increasing VP concentration. For the highest level, 13.7% deviation was observed, which is still within the FDA recommended specification of 15%, but close to the threshold.[30] Highly concentrated samples should thus be diluted for increased accuracy and extrapolation to higher levels should be omitted. This is an assumption as higher concentration levels were not tested due to the lack of well-characterized and highly concentrated material, which limited the exploration range. Theoretical sensitivity values were calculated based on the SN ratio. In order to meet performance expectations, an LLOQ concentration between the theoretical value and the lowest calibration value had to be chosen. The LLOQ measurement point, extrapolated from the calibration curve, showed good results in the method performance evaluation. It led to an established working range across 2.5 orders of magnitude from 4.20×10^8 to 1.44×10^{11} VP/mL. This range is at the upper end of published measurement ranges of other HPLC-based quantification methods for enveloped VPs.[11,13–15,41] The method's sensitivity is similar or better than the referenced quantification methods, which are all label-free methods. The use of signal-enhancing labeling dyes can increase sensitivities without reducing the measurement range.[42,43] Transfiguracion and colleagues used a fluorophore to stain viral nucleic acids without the need for VP lysis or membrane permeabilization. The labeling method reached seven times lower LLOQ compared with the herein presented method.[43] However, to develop a robust and versatile method, as well as to minimize the method's complexity, no signal enhancers were used. At the same time this approach maximizes sample recovery and reduces the probability of errors by preparational steps, thus minimizing the method's variability. A possible approach to improve the sensitivity limitation of the method is the increase of injected sample volume of currently 10 μL.

Samples from six production process steps, representing the major matrix changes in the DSP process have been analyzed to ascertain the robustness of the method in response to variations in sample matrices. Results showed a low variance (<2.5%) and an averaged accuracy of 99.79%. Sample matrix components were separated from the VPs and diluted in the SEC column, thus the matrix effect on the recovery and accuracy was low. BSA spiking seems to prevent VP adsorption in all tested sample matrices as the largest signal reductions were still below 10%.

Chromatographic step mass balance

The main objective of the developed method was a straightforward, rapid, and robust quantification method for analyzing process development samples of VSV-GP particles. This method facilitated the characterization of a chromatography run based on the collected fractions. The mass balance application shows a sufficient precision to allocate VP percentages to chromatography phases. Results were obtained the following day, due to an overnight (12 h) sample throughput for 20 samples. The results for a single sample can be determined within 1 h, enabling the immediate at-line determination of the step yield, if required. The availability of this process performance indicator enables same-day process decisions beneficial in process development. Results were confirmed by qPCR analysis, which shows comparable counts for the eluted peak. In the SEC chromatogram, the virus peak elutes in the first half and later peaks are neglected for VP quantification purposes. Consequently, a tandem column setup could be employed in order to interlace subsequent analysis runs and increase the sample throughput without altering the flow rate or the column size.[44] In the current method setup, there is broad elution time gap between the exclusion peak and the impurity peak. Thus, another approach to reduce the analysis time could be the use of a shorter SEC column. If required, smaller resin beads could improve separation efficiency in shorter columns. However, smaller beads increase backpressure and thus the shear stress on VPs, which may damage the VPs.

Summary

A robust method with rapid turnaround time for the quantification of VSV-GP particles was presented. Performance evaluation and a mass balance example using harvest material on a CEX column shows the applicability for IPCs and use for DSP process development. Absolute quantification relies on a reference VP material that was quantified by an orthogonal method; however, relative quantification can be performed in the absence of such reference material. The method was specifically established for enveloped viruses being generally more challenging in terms of physico-chemical properties and stability. The applicability to other VPs or variants of oncolytic viruses or gene therapies has yet to be shown, though it is assumed to be feasible with the suitable SEC pore size. The required knowledge about the

VPs is low and devices used are ubiquitous in biopharmaceutical laboratories. The MALS detector proved to be a useful tool for method development and can size particles, but the method application does not rely on it. For process development, the method allows determination of particle titers on the same day, enabling mass balancing and faster process decisions in the lab. Alternative methods such as PCR (qPCR or digital PCR) and $TCID_{50}$ remain essential because the additional information about genomic copies and infectious titers is beyond the scope of this method. For virus samples, multiple assays are typically required to gain the full picture of its composition and virus quality.

MATERIALS AND METHODS

Virus preparation

To generate VSV-GP, VPs were propagated by infection in mammalian cell suspension. Upon harvest at 34 h after infection, the suspension was treated with 200 mM NaCl. The harvest was clarified by centrifugation (5 min, 2 000 × *g*), filtered (0.22 μm), and then treated with nuclease. A Tris-based buffer with NaCl and 150 mM Arg at a pH of 7.5 was used in all subsequent steps. The virus-containing material was underlaid by a 20 w/v-% sucrose cushion and centrifuged at 6°C for 14 h at 5 000 rpm. The resulting pellet was resuspended and filtered (0.22 μm). A preparative SEC column comprising Sepharose 6FF (Cytiva, Marlborough, MA, USA) was used for polishing of the material. The final virus suspension was sterile-filtered (0.22 μm), aliquoted, and stored at −80°C until usage. Two batches were used for experiments to optimize and characterize the method.

For further method characterization, material generated from a different lab-scale production process was used. The upstream process (USP) is as described above, and the DSP involves an IEX step and further filtration steps as described in the process patent application.[45]

Generation of virus variants

Virus variants with varying genomic sizes were generated using the Gibson assembly NEBuilder HiFi DNA Assembly kit (New England Biolabs, Ipswich, MA, USA), adhering to the manufacturer's recommendations. In brief, synthetic DNAs (GeneArt, Thermo Fisher Scientific Inc., Rockford, IL, USA) were placed between the LCMV-GP and the VSV-L open reading frame of the VSV-GP vector backbone. Recombinant virus variants, expressing the additional gene that is not incorporated into the virion, were subsequently recovered by a helper virus-free calcium phosphate transfection in HEK293T cells using pCAG expression plasmids of T7 polymerase and VSV proteins N, P, and L, along with the respective virus construct that contained the VSV-GP vector.[46] Following detection of cytopathic effects and expansion on HEK293F cells, the virus progeny underwent two rounds of plaque purification and was further amplified on HEK293F cells.

Separation method and orthogonal analytical methods

HPLC-SEC separation

An Acquity Arc Bio HPLC system equipped with a 2998-photodiode array (PDA) detector (Waters, Milford, MA, USA) and the software Empower 3 FR 5 (Waters, Milford, MA, USA) for data acquisition and integration was used in this work. The path length of the PDA flow cell was 10 mm. An MALS DAWN detector controlled by Astra 8.1 (Wyatt Technology, Santa Barbara, CA, USA) was integrated in the HPLC detector flow path. Analytical SEC column resins with mean pore sizes of 50 nm (TSKgel G4000PW) and >100 nm (TSKgel G6000PW) were used (Tosoh Bioscience, Griesheim, Germany). Column housings made of stainless-steel and PEEK (name affix "Bio-Assist") were tested during the method development. Tosoh uses an abbreviated term for the PEEK version of the G6000PW resin, which is "BioAssist G6PW". For more clarity, we refrain from using the abbreviated term. The PEEK version of the G4000PW was custom manufactured by Tosoh. A temperature-controlled column oven was used to keep the columns at 25°C during the method. The use of Waters Fraction Manager-Analytical (WFM-A) enabled the optional collection of elution fractions. The mobile phase used after screenings consisted of 50 mM Tris-HCl, 200 mM NaCl, 150 mM Arg, and 0.1 wt-% DMSO, pH 8.0, prepared with MilliQ purified water and 0.22 μm filtered (Corning, Glendale, AZ, USA). A constant flow rate of 0.5 mL/min was used, and the column was equilibrated for at least five column volumes before sample injections. A sample volume of 10 μL was used. For the CIP of the column, a high-salt buffer and a 20% methanol step were used.

Sample preparation

Samples were measured undiluted unless stated otherwise; if dilutions were required, a Tris-buffered, NaCl and 150 mM Arg-containing solution was used. A 50 g/L BSA stock solution was prepared from a lyophilized BSA heat shock fraction (Sigma-Aldrich, Saint-Louis, MO, USA) in a Tris-buffered, 50 mM NaCl-containing solution. The stock solution was used to spike 0.98 g/L BSA into each sample. Samples were then transferred to Quan Recovery polypropylene vials with a high-performance surface (Waters, Milford, MA, USA) and kept in the HPLC sample manager at 8°C until injection. Total Recovery glass vials (Waters, Milford, MA, USA) were also tested for comparison.

Separation characterization

The exclusion peak is presumed to be the virus peak. It was characterized by online UV and MALS signals and orthogonal offline analytical methods (described in following sections). Samples with and without BSA spikes were used to investigate the influence of BSA as the stabilizing agent on the exclusion peak. Virus variants of VSV-GP with increased genome length (up to 27%), resulting in prolonged VPs,[47] were used to evaluate the influence of different-sized VPs on the exclusion peak. Also, the MALS was used to acquire sizing data of the exclusion peak.

Ns-TEM quantification

Ns-TEM experiments were performed by NanoImaging Services (San Diego, CA, USA). VSV-GP containing samples were mixed 1:1 with 100 nm Polystyrene (PS) beads of predetermined concentration. The samples were transferred on a copper grid and stained using phosphotungstic acid. At least 50 images of different areas of

the grid containing sufficient amounts of PS beads and VPs were acquired at 15 000× magnification. Visible particles were classified into PS beads, bullet-shaped VPs, deformed VPs, and empty particles, and each class was counted. The particle concentration for each class is calculated based on the known PS bead concentration and the counted number n for the virus particles VP and PS beads as shown in Equation 2. VP deformation can occur during the required sample treatment, which is why the sum of the bullet-shaped and deformed VPs class was used for subsequent calculations.

$$c(VP) = c(PS) * \frac{n(VP)}{n(PS)} \quad \text{(Equation 2)}$$

SDS-PAGE and silver staining

Collected SEC fractions were analyzed by SDS-PAGE (4%–20% Mini-PROTEAN TGX Precast Protein Gel; Bio-Rad, Hercules, CA, USA) and silver stained (Thermo Scientific Pierce Silver Stain Kit; Thermo Fisher Scientific Inc., Rockford, IL, USA), both methods were used according to the manufacturer's instructions.

qPCR

Viral RNA was extracted using Ambion's MagMAX Viral RNA isolation kit (Life Technologies Corp., Carlsbad, CA, USA) according to the manufacturer's instruction. A CFX96 Real Time Cycler (Bio-Rad, Hercules, CA, USA) and iTaq Universal Probes One-Step Kit (Bio-Rad, Hercules, CA, USA) were used for qPCR analysis with primers targeting the N-protein gene sequences as described elsewhere.[48]

$TCID_{50}$

BHK-21 cells (CLS Cell Lines Service GmbH, Eppelheim, Germany) were seeded in 96-well plates containing GMEM medium complemented with 10% fetal calf serum (FCS), 5% tryptose phosphate broth and 1% penicillin-streptomycin solution (all media components from Gibco, Thermo Fisher Scientific Inc., Rockford, IL, USA) and incubated at 37°C and 5% CO_2. 24 hours after seeding, a dilution series of the virus-containing samples was prepared. The complemented media is used to create half-log_{10} dilution steps that are then added individually to the seeded wells. The plates are incubated for 3 days and subsequently the confluence of each well is determined using an automated plate reader (Tecan, Männedorf, Switzerland). A confluence level of $\leq$95% is used as a threshold to determine cytopathic effects in wells by virus infection. The $TCID_{50}$/mL is calculated based on the number of infected wells using the Spearman-Kärber equation.[49,50]

Method development

Recovery analysis

Quantifying analyte molecules by a post-column detector requires the targeted analyte to elute with a sufficiently high and reproducible recovery. Recovery was determined by comparing analyte injections over the column and PEEK bypass tubing. Five microliters of VSV-GP reference material and, as a model protein, 5 µL of 2 g/L BSA, were applied. The post-column and post-bypass UV 280 nm signal responses were compared, and recoveries calculated.

Mobile phase screening

To improve the recovery of the SEC method, the mobile phase buffer was optimized. Various buffer components were screened: Tris, citrate, phosphate, NaCl, Arg, sorbitol, sucrose, and DMSO. Excipient concentrations as well as pH were optimized to reduce non-specific adsorption to the column resin. The initial buffer was based on Tris with NaCl and Arg at a pH of 7.5. A complete list of screened buffer compositions can be found in the supplement material, Table S1. The buffer components were iteratively optimized by single or combined adjustments of buffer components and additional additives. Buffer performance was evaluated by the above-described quantitative recovery analysis and the qualitative evaluation of the CIP peaks by the MALS detector.

Sample stability optimization

The sample stability in the sample manager was evaluated using two different sample vial materials (glass and polypropylene) and a BSA-spiking methodology. VSV-GP reference samples were diluted to a concentration of 9×10^9 VP/mL and prepared with different BSA spike concentrations. Over a time frame of 35 h, the prepared samples were stored in the sample manager at 8°C either in Quan Recovery polypropylene (Waters, Milford, MA, USA) or Total Recovery glass vials (Waters, Milford, MA, USA). During this time, samples were repeatedly drawn from the vials and analyzed by HPLC-SEC quantification.

Method characterization

The reference material for method development was used to generate a calibration curve. Eight concentration levels in the range from the undiluted reference material to the LLOQ were evaluated. For the higher concentrated range, the undiluted material and two dilutions with the factor 1.5 were used. For the lower concentrated range, a five-step dilution series with the factor 3.0 starting from the undiluted material was used. HPLC-SEC analysis was conducted in triplicates for each concentration level as previously described. The triplicate measurements were repeated in three independent runs, resulting in nine measurement points per concentration level. Independent runs on different dates and using different buffer batches ensured the robustness of the calibration curve from random influences.

For the performance evaluation, quality control samples (QCs) at four concentration levels across the working range were specified: High, Mid, Low, and LLOQ concentration level. QCs were produced by dilution of the characterization reference material, aliquoted, and stored at −80°C until usage. Every QC level was quantified by HPLC-SEC in three repetitions on five independent runs. The independent runs differed in date and mobile phase buffer batch. The performance runs were evaluated for precision and accuracy. The theoretical LOD and LLOQ were determined based on the baseline noise with an SN ratio of 3:1 and 10:1.

From a virus production run involving multiple DSP steps, IPCs were collected and frozen at −80°C until analysis. The VPs in these samples were first removed by 0.1 mm filtration (Whatman Anotop 10 Plus; Cytiva, Marlborough, MA, USA). Then, the reference virus material was spiked back into each sample. Finally, the samples were analyzed by HPLC-SEC quantification.

Chromatographic step mass balance

The VSV-GP particle quantification method described herein was applied to investigate an exemplary process development chromatography run for enveloped viruses. Clarified supernatant containing not only virus but also cell media components and cell-derived impurities was loaded on a monolithic CEX column (CIMmultus SO3 1.0 mL; Sartorius BIA Separations, Ajdovščina, Slovenia) in bind-and-elute mode. The flowthrough during sample loading and the wash phases were collected for analysis. A salt step was applied to elute bound VPs, and the peak was collected in fractions for offline quantification by HPLC-SEC and qPCR. A mass balance of the VP loading and eluting in the elution phases was conducted; 1 M NaOH + 2 M NaCl was used for the CIP step of the column as specified by the manufacturer.

DATA AND CODE AVAILABILITY

All data used to evaluate the conclusions of the article are present in the paper and/or the supplementary material. ViraTherapeutics GmbH is unable to provide raw data, protocols, or additional datasets.

SUPPLEMENTAL INFORMATION

Supplemental information can be found online at https://doi.org/10.1016/j.omtm.2024.101252.

ACKNOWLEDGMENTS

Special thanks go to Dr. Knut Elbers, ViraTherapeutics GmbH, Rum, Austria, for facilitating and supporting this work. The authors would like to thank Dr. Marija Brgles, Boehringer Ingelheim Pharma GmbH & Co.KG in Biberach a.d. Riss, Germany, and Dr. Michaela Smolle and Dr. Tobias Nolden, ViraTherapeutics GmbH, Rum, Austria, for insights into their expertise and valuable discussions. The graphical abstract was created with BioRender.com.

AUTHOR CONTRIBUTIONS

Conceptualization, A.S. and J.N.; Investigation A.S., I.B., F.M., and D.X.; Formal analysis A.S. and D.X.; Writing - original draft, A.S.; Writing – review and editing, all authors; Supervision J.N. and J.H.

DECLARATION OF INTERESTS

The authors declare no competing interests.

REFERENCES

1. Dunbar, C.E., High, K.A., Joung, J.K., Kohn, D.B., Ozawa, K., and Sadelain, M. (2018). Gene therapy comes of age. Science *359*, eaan4672. https://doi.org/10.1126/science.aan4672.
2. U.S. National Library of Medicine (2023). Oncolytic viruses in clinical trials, search terms: “gene therapies” AND “virus”, and “oncolytic virus”. clinicaltrials.gov.
3. Singh, N., and Heldt, C.L. (2022). Challenges in downstream purification of gene therapy viral vectors. Curr. Opin. Chem. Eng. *35*, 100780. https://doi.org/10.1016/j.coche.2021.100780.
4. McCarron, A., Donnelley, M., McIntyre, C., and Parsons, D. (2016). Challenges of up-scaling lentivirus production and processing. J. Biotechnol. *240*, 23–30. https://doi.org/10.1016/j.jbiotec.2016.10.016.
5. Moleirinho, M.G., Silva, R.J.S., Alves, P.M., Carrondo, M.J.T., and Peixoto, C. (2020). Current challenges in biotherapeutic particles manufacturing. Expet Opin. Biol. Ther. *20*, 451–465. https://doi.org/10.1080/14712598.2020.1693541.
6. Srivastava, A., Mallela, K.M.G., Deorkar, N., and Brophy, G. (2021). Manufacturing Challenges and Rational Formulation Development for AAV Viral Vectors. J. Pharmaceut. Sci. *110*, 2609–2624. https://doi.org/10.1016/j.xphs.2021.03.024.
7. Lothert, K., Eilts, F., and Wolff, M.W. (2022). Quantification methods for viruses and virus-like particles applied in biopharmaceutical production processes. Expert Rev. Vaccines *21*, 1029–1044. https://doi.org/10.1080/14760584.2022.2072302.
8. Parupudi, A., Gruia, F., Korman, S.A., Dragulin-Otto, S., Sra, K., Remmele, R.L., and Bee, J.S. (2017). Biophysical characterization of influenza A virions. J. Virol. Methods *247*, 91–98. https://doi.org/10.1016/j.jviromet.2017.06.002.
9. Heider, S., and Metzner, C. (2014). Quantitative real-time single particle analysis of virions. Virology *462–463*, 199–206. https://doi.org/10.1016/j.virol.2014.06.005.
10. Spitteler, M.A., Romo, A., Magi, N., Seo, M.-G., Yun, S.-J., Barroumeres, F., Régulier, E.G., and Bellinzoni, R. (2019). Validation of a high performance liquid chromatography method for quantitation of foot-and-mouth disease virus antigen in vaccines and vaccine manufacturing. Vaccine *37*, 5288–5296. https://doi.org/10.1016/j.vaccine.2019.07.051.
11. Chahal, P.S., Transfiguracion, J., Bernier, A., Voyer, R., Coffey, M., and Kamen, A. (2007). Validation of a high-performance liquid chromatographic assay for the quantification of Reovirus particles type 3. J. Pharm. Biomed. Anal. *45*, 417–421. https://doi.org/10.1016/j.jpba.2007.06.025.
12. van Tricht, E., Geurink, L., Backus, H., Germano, M., Somsen, G.W., and Sänger-van de Griend, C.E. (2017). One single, fast and robust capillary electrophoresis method for the direct quantification of intact adenovirus particles in upstream and downstream processing samples. Talanta *166*, 8–14. https://doi.org/10.1016/j.talanta.2017.01.013.
13. Transfiguracion, J., Tran, M.Y., Lanthier, S., Tremblay, S., Coulombe, N., Acchione, M., and Kamen, A.A. (2020). Rapid In-Process Monitoring of Lentiviral Vector Particles by High-Performance Liquid Chromatography. Mol. Ther. Methods Clin. Dev. *18*, 803–810. https://doi.org/10.1016/j.omtm.2020.08.005.
14. Transfiguracion, J., Coelho, H., and Kamen, A. (2004). High-performance liquid chromatographic total particles quantification of retroviral vectors pseudotyped with vesicular stomatitis virus-G glycoprotein. J. Chromatogr. B *813*, 167–173. https://doi.org/10.1016/j.jchromb.2004.09.034.
15. Steppert, P., Burgstaller, D., Klausberger, M., Tover, A., Berger, E., and Jungbauer, A. (2017). Quantification and characterization of virus-like particles by size-exclusion chromatography and nanoparticle tracking analysis. J. Chromatogr. A *1487*, 89–99. https://doi.org/10.1016/j.chroma.2016.12.085.
16. Pereira Aguilar, P., González-Domínguez, I., Schneider, T.A., Gòdia, F., Cervera, L., and Jungbauer, A. (2019). At-line multi-angle light scattering detector for faster process development in enveloped virus-like particle purification. J. Separ. Sci. *42*, 2640–2649. https://doi.org/10.1002/jssc.201900441.
17. Ge, P., Tsao, J., Schein, S., Green, T.J., Luo, M., and Zhou, Z.H. (2010). Cryo-EM Model of the Bullet-Shaped Vesicular Stomatitis Virus. Science *327*, 689–693. https://doi.org/10.1126/science.1181766.
18. Letchworth, G.J., Rodriguez, L.L., and del C Barrera, J. (1999). Vesicular Stomatitis. Vet. J. *157*, 239–260. https://doi.org/10.1053/tvjl.1998.0303.
19. Munis, A.M., Bentley, E.M., and Takeuchi, Y. (2020). A tool with many applications: vesicular stomatitis virus in research and medicine. Expet Opin. Biol. Ther. *20*, 1187–1201. https://doi.org/10.1080/14712598.2020.1787981.
20. Muik, A., Kneiske, I., Werbizki, M., Wilflingseder, D., Giroglou, T., Ebert, O., Kraft, A., Dietrich, U., Zimmer, G., Momma, S., and von Laer, D. (2011). Pseudotyping Vesicular Stomatitis Virus with Lymphocytic Choriomeningitis Virus Glycoproteins Enhances Infectivity for Glioma Cells and Minimizes Neurotropism. J. Virol. *85*, 5679–5684. https://doi.org/10.1128/jvi.02511-10.

21. Muik, A., Stubbert, L.J., Jahedi, R.Z., Geiß, Y., Kimpel, J., Dold, C., Tober, R., Volk, A., Klein, S., Dietrich, U., et al. (2014). Re-engineering Vesicular Stomatitis Virus to Abrogate Neurotoxicity, Circumvent Humoral Immunity, and Enhance Oncolytic Potency. Cancer Res. *74*, 3567–3578. https://doi.org/10.1158/0008-5472.can-13-3306.

22. Gélinas, J.F., Kiesslich, S., Gilbert, R., and Kamen, A.A. (2020). Titration methods for rVSV-based vaccine manufacturing. MethodsX *7*, 100806. https://doi.org/10.1016/j.mex.2020.100806.

23. Abdelmageed, A.A., and Ferran, M.C. (2020). The Propagation, Quantification, and Storage of Vesicular Stomatitis Virus. Curr. Protoc. Microbiol. *58*, e110. https://doi.org/10.1002/cpmc.110.

24. Hebert, C.G., DiNardo, N., Evans, Z.L., Hart, S.J., and Hachmann, A.-B. (2018). Rapid quantification of vesicular stomatitis virus in Vero cells using Laser Force Cytology. Vaccine *36*, 6061–6069. https://doi.org/10.1016/j.vaccine.2018.09.002.

25. Akpinar, F., and Yin, J. (2015). Characterization of vesicular stomatitis virus populations by tunable resistive pulse sensing. J. Virol. Methods *218*, 71–76. https://doi.org/10.1016/j.jviromet.2015.02.006.

26. Yang, L., and Yamamoto, T. (2016). Quantification of Virus Particles Using Nanopore-Based Resistive-Pulse Sensing Techniques. Front. Microbiol. *7*, 1500. https://doi.org/10.3389/fmicb.2016.01500.

27. Malenovska, H. (2013). Virus quantitation by transmission electron microscopy, TCID50, and the role of timing virus harvesting: A case study of three animal viruses. J. Virol. Methods *191*, 136–140. https://doi.org/10.1016/j.jviromet.2013.04.008.

28. McCormick, W., and Mermel, L.A. (2021). The basic reproductive number and particle-to-plaque ratio: comparison of these two parameters of viral infectivity. Virol. J. *18*, 92–95. https://doi.org/10.1186/s12985-021-01566-4.

29. Arakawa, T., Ejima, D., Li, T., and Philo, J.S. (2010). The critical role of mobile phase composition in size exclusion chromatography of protein pharmaceuticals. J. Pharmaceut. Sci. *99*, 1674–1692. https://doi.org/10.1002/jps.21974.

30. U.S. Food and Drug Administration (2018). Bioanalytical Method Validation: Guidance for Industry.

31. Lothert, K., and Wolff, M.W. (2023). Chromatographic Purification of Viruses: State of the Art and Current Trends. In Bioprocess and Analytics Development for Virus-Based Advanced Therapeutics and Medicinal Products (ATMPs), S. Gautam, A.I. Chiramel, and R. Pach, eds. (Springer), pp. 145–169. https://doi.org/10.1007/978-3-031-28489-2_7.

32. Porterfield, J.Z., Dhason, M.S., Loeb, D.D., Nassal, M., Stray, S.J., and Zlotnick, A. (2010). Full-Length Hepatitis B Virus Core Protein Packages Viral and Heterologous RNA with Similarly High Levels of Cooperativity. J. Virol. *84*, 7174–7184. https://doi.org/10.1128/jvi.00586-10.

33. Vajda, J., Weber, D., Brekel, D., Hundt, B., and Müller, E. (2016). Size distribution analysis of influenza virus particles using size exclusion chromatography. J. Chromatogr. A *1465*, 117–125. https://doi.org/10.1016/j.chroma.2016.08.056.

34. Makra, I., Terejánszky, P., and Gyurcsányi, R.E. (2015). A method based on light scattering to estimate the concentration of virus particles without the need for virus particle standards. MethodsX *2*, 91–99. https://doi.org/10.1016/j.mex.2015.02.003.

35. Ejima, D., Yumioka, R., Arakawa, T., and Tsumoto, K. (2005). Arginine as an effective additive in gel permeation chromatography. J. Chromatogr. A *1094*, 49–55. https://doi.org/10.1016/j.chroma.2005.07.086.

36. Wallis, C., and Melnick, J.L. (1968). Stabilization of enveloped viruses by dimethyl sulfoxide. J. Virol. *2*, 953–954. https://doi.org/10.1128/jvi.2.9.953-954.1968.

37. Gordeliy, V.I., Kiselev, M.A., Lesieur, P., Pole, A.V., and Teixeira, J. (1998). Lipid Membrane Structure and Interactions in Dimethyl Sulfoxide/Water Mixtures. Biophys. J. *75*, 2343–2351. https://doi.org/10.1016/s0006-3495(98)77678-7.

38. Marczewski, A.W. (2010). Analysis of Kinetic Langmuir Model. Part I: Integrated Kinetic Langmuir Equation (IKL): A New Complete Analytical Solution of the Langmuir Rate Equation. Langmuir *26*, 15229–15238. https://doi.org/10.1021/la1010049.

39. Kovalchuk, S.I., Anikanov, N.A., Ivanova, O.M., Ziganshin, R.H., and Govorun, V.M. (2015). Bovine serum albumin as a universal suppressor of non-specific peptide binding in vials prior to nano-chromatography coupled mass-spectrometry analysis. Anal. Chim. Acta *893*, 57–64. https://doi.org/10.1016/j.aca.2015.08.027.

40. Lorbetskie, B., Wang, J., Gravel, C., Allen, C., Walsh, M., Rinfret, A., Li, X., and Girard, M. (2011). Optimization and qualification of a quantitative reversed-phase HPLC method for hemagglutinin in influenza preparations and its comparative evaluation with biochemical assays. Vaccine *29*, 3377–3389. https://doi.org/10.1016/j.vaccine.2011.02.090.

41. Transfiguracion, J., Manceur, A.P., Petiot, E., Thompson, C.M., and Kamen, A.A. (2015). Particle quantification of influenza viruses by high performance liquid chromatography. Vaccine *33*, 78–84. https://doi.org/10.1016/j.vaccine.2014.11.027.

42. Murakami, P., and McCaman, M.T. (1999). Quantitation of Adenovirus DNA and Virus Particles with the PicoGreen Fluorescent Dye. Anal. Biochem. *274*, 283–288. https://doi.org/10.1006/abio.1999.4282.

43. Transfiguracion, J., Mena, J.A., Aucoin, M.G., and Kamen, A.A. (2011). Development and validation of a HPLC method for the quantification of baculovirus particles. J. Chromatogr. B *879*, 61–68. https://doi.org/10.1016/j.jchromb.2010.11.011.

44. Xia, Y.Q., Liu, D.Q., and Bakhtiar, R. (2002). Use of online-dual-column extraction in conjunction with chiral liquid chromatography tandem mass spectrometry for determination of terbutaline enantiomers in human plasma. Chirality *14*, 742–749. https://doi.org/10.1002/chir.10135.

45. Mueller, D., Pardo Garcia, A., Grein, T.A., Kaess, F., Ng, J., Pesta, K., Schneider, S., and Turnbull, J. (2022). Process for Producing a Purified Rhabdovirus from Cell Culture. U.S. Patent No. US-20220010286-A1 *1*.

46. Heilmann, E., Kimpel, J., Geley, S., Naschberger, A., Urbiola, C., Nolden, T., von Laer, D., and Wollmann, G. (2019). The Methyltransferase Region of Vesicular Stomatitis Virus L Polymerase Is a Target Site for Functional Intramolecular Insertion. Viruses *11*, 989. https://doi.org/10.3390/v11110989.

47. Soh, T.K., and Whelan, S.P.J. (2015). Tracking the Fate of Genetically Distinct Vesicular Stomatitis Virus Matrix Proteins Highlights the Role for Late Domains in Assembly. J. Virol. *89*, 11750–11760. https://doi.org/10.1128/jvi.01371-15.

48. Wilmschen, S., Schneider, S., Peters, F., Bayer, L., Issmail, L., Bánki, Z., Grunwald, T., von Laer, D., and Kimpel, J. (2019). RSV Vaccine Based on Rhabdoviral Vector Protects after Single Immunization. Vaccines *7*, 59. https://doi.org/10.3390/vaccines7030059.

49. Kärber, G. (1931). Beitrag zur kollektiven Behandlung pharmakologischer Reihenversuche. Archiv f. experiment. Pathol. u. Pharmakol. *162*, 480–483. https://doi.org/10.1007/bf01863914.

50. Spearman, C. (1908). The method of "right and wrong cases" ('constant stimuli') without Gauss formulae. Br. J. Psychol. *2*, 227–242. https://doi.org/10.1111/j.2044-8295.1908.tb00176.x.

5 Mechanistic Modeling of the Elution Behavior and Convective Entrapment of Vesicular Stomatitis Virus on an Ion Exchange Chromatography Monolith

Adrian Schimek[a], Judy Ng[a], Federico Will[b], Jürgen Hubbuch[c]

[a] ViraTherapeutics GmbH, Bundesstraße 27, 6063 Rum, Austria

[b] Boehringer Ingelheim Pharma GmbH & Co.KG, Birkendorfer Str. 65, 88397 Biberach, Germany

[c] Karlsruhe Institute of Technology, Institute of Process Engineering in Life Sciences, Section IV Biomolecular Separation Engineering, Fritz-Haber-Weg 2, 76131 Karlsruhe, Germany

Corresponding authors:

(J.N.) judy.ng@boehringer-ingelheim.com

(J.H.) juergen.hubbuch@kit.edu

First author contribution (A.S.):
Conceptualization, Investigation, Data curation, Methodology, Writing - original draft

Highlights

- Flow rate-dependent tailing effect identified as convective entrapment.
- Separation of virus populations due to convective entrapment.
- Mechanistic modeling of an enveloped virus particle ion exchange chromatography.
- Convective entrapment in a monolith is modelled using a Langmuir retention term.

Reproduced from:
A. Schimek, J. Ng, F. Will, and J. Hubbuch. “Mechanistic Modeling of the Elution Behavior and Convective Entrapment of Vesicular Stomatitis Virus on an Ion Exchange Chromatography Monolith”. In: *Journal of Chromatography A*, 1748 (2025), p. 465832. DOI: 10.1016/j.chroma.2025.465832.

Journal of Chromatography A 1748 (2025) 465832

Contents lists available at ScienceDirect

Journal of Chromatography A

journal homepage: www.elsevier.com/locate/chroma

Mechanistic modeling of the elution behavior and convective entrapment of vesicular stomatitis virus on an ion exchange chromatography monolith

Adrian Schimek [a], Judy Ng [a,*], Federico Will [b], Jürgen Hubbuch [c,**]

[a] ViraTherapeutics GmbH, Bundesstraße 27, 6063 Rum, Austria
[b] Boehringer Ingelheim Pharma GmbH & Co.KG, Birkendorfer Str. 65, 88397 Biberach, Germany
[c] Karlsruhe Institute of Technology, Institute of Process Engineering in Life Sciences, Section IV Biomolecular Separation Engineering, Fritz-Haber-Weg 2, 76131 Karlsruhe, Germany

ARTICLE INFO

Keywords:
Enveloped virus particle
Monolith
IEX
VSV
Mechanistic modeling
SMA
Convective entrapment

ABSTRACT

Developing a downstream purification process for replication-competent enveloped virus particles presents a significant challenge. This is largely due to the highly complex particle structures, as well as complexities of emerging purification modalities for such virus particles. In this study, an unexpected fluid-dynamic effect was observed during the elution of enveloped virus particles from an ion exchange chromatography monolith. This effect led to peak tailing and the separation of virus particle subpopulations. Upon considering possible causes, convective entrapment was identified as a plausible explanation. To investigate this effect, a mechanistic modeling approach representing the electrostatic resin interactions and the convective entrapment effect was implemented. The introduced Langmuir approximation of the convective entrapment showed good alignment with reference data from experiments. The model reproduced the retention effect, and furthermore suggested two virus particle populations due to the stronger retention effect on the tailing subpopulation caused by convective entrapment.

1. Introduction

Viral vector-based therapeutics have advanced significantly in the recent years, enhancing their therapeutic potential, safety, and efficacy [1,2]. This development is reflected in the current clinical landscape, highlighting the demand for suitable bioprocesses for viral vector production [3]. Virus particles (VPs) are large, complex biomolecules with unique structures, sizes, and shapes. These attributes can vary tremendously between different viruses, presenting unique challenges for process development and making it difficult to establish standard platform processes [4,5]. Enveloped viral particles tend to be susceptible to malformation and possibly degradation during bioprocessing. This necessitates the development of mild production processes with short processing times and minimal number of unit operations. A chromatographic capture step can be implemented after the clarification of harvest material, which has typically a high feed volume with low VP concentrations [6]. It is designed to concentrate VPs while reducing working volume using a positive mode (bind-and-elute, BE).

For viral vector chromatography, significant progress has been made in the development of the interacting resin surface as well as resin structure. Affinity chromatography (AC) has demonstrated good performance for some viral vectors [7], though the specificity of AC ligands limit their versatility, and harsh conditions are required for elution [8,9]. Ion exchange chromatography (IEX), on the other hand, offers greater versatility due to its lower specificity, but it requires more optimization for efficient VP purification [9]. While potential high salt elution conditions of IEX may cause osmotic stress on VPs, they are still milder than those of AC. IEX serves as the primary alternative to AC for the capture step and can also be used for polishing [7].

Large enveloped viral particles present both opportunities and challenges. While they offer a substantial gene insert capacity, their size impedes diffusional movement and obstructs pore accessibility of conventional porous bead-based resins. Convective-driven chromatographic media like monoliths, membranes, and nanofibers offers minimal mass transfer resistances and low pressure drops, facilitating high flow rates ideal for capture steps [10–12]. However, industrial

* Corresponding author at: ViraTherapeutics GmbH, Bundesstraße 27, 6063 Rum, Austria.
** Corresponding author at: Institute of Engineering in Life Sciences, Section IV: Biomolecular Separation Engineering, Karlsruhe Institute of Technology (KIT), Fritz-Haber-Weg 2, 76131 Karlsruhe, Germany.
E-mail addresses: judy.ng@boehringer-ingelheim.com (J. Ng), juergen.hubbuch@kit.edu (J. Hubbuch).

https://doi.org/10.1016/j.chroma.2025.465832
Received 14 January 2025; Received in revised form 26 February 2025; Accepted 27 February 2025
Available online 2 March 2025

experience using convective media for enveloped VPs is rather limited, and a deeper understanding of the manifold process challenges for a variety of virus vectors is needed. Monoliths are chromatographic columns comprising a continuous and homogenous structure. Polymer-based monoliths are designed to be made of convective channels, enabling a high mass transfer [13,14]. Silica-based monoliths on the other hand have a bimodal pore size distribution with convective channels and diffusional pores. The latter are inaccessible to large biomolecules, limiting their use in VP purification [15].

Modeling of chromatography purification steps for non-enveloped VP and virus-like particles (VLPs) is performed in recent years to optimize process conditions [16–19] and to gain process understanding [12]. Particularly, mechanistic chromatography models are *in silico* representations to simulate chromatographic process steps. They are based on mathematical equations to represent fluid dynamics as well as physico-chemical phenomena within a chromatographic column. The biopharmaceutical industry leverages the predictive capabilities of mechanistic models to optimize [20], simulate scale-up conditions [21], conduct root-cause investigations [22] and robustness studies [23]. Effort is initially invested to characterize and understand the phenomena within the column to effectively derive accurate mathematical equations to describe it. In the process of developing the model, process knowledge is gained.

Two examples of chromatography modeling for enveloped VPs and VLPs can be found in literature, both involving anion exchange chromatography (AEX) membrane adsorbers. Pamenter et al. observed a time-dependent irreversible sorption of lentiviral vectors, and subsequently developed a kinetic model that can predict recovery losses [24]. Vicente et al. applied the steric mass action (SMA) formalism to describe the resin interaction of Sf9-derived Baculovirus particles and to examine the impact of ligand density on impurity depletion in a gel-layered membrane adsorber [25]. They concluded that the ligands in the gel layer were inaccessible to the large virus particles, unlike the small impurities. However, this feature specific to virus particles was not represented in the model equations. Zhao et al. extended the SMA formalism to exclude ligands within bead pores inaccessible to large virus particles [26]. This extension increased the accuracy of the steric shielding SMA parameter for an enveloped and non-enveloped virus particles in bead-based chromatography systems.

In this study, we used a modified vesicular stomatitis virus (VSV) of the Rhabdoviridae family known as VSV-GP [27], an enveloped virus particle with a bullet-shaped morphology of dimensions of approximately 70 × 200 nm [28]. Production involves propagation in a mammalian cell suspension, and purification by filtration and chromatography steps [29]. Here we characterize the capture step which involves a cationic exchange chromatography (CEX) monolith. During characterization experiments, peak tailing was observed for VSV-GP eluting in a salt gradient. This tailing could not be explained by our current understanding of fluid dynamics and particle-resin interaction in the monolith. An unexpected effect, namely convective entrapment, arose from this investigation.

A convective entrapment effect has been previously described for large biomolecules trapped in constriction sites of a resin [30]. Trilisky et al. observed a flow dependent fluid-dynamic effect that impacted recovery, although dynamic binding capacity of monoliths are flow-independent [31]. Such constriction sites are convectively flown through but narrow down to a size through which large biomolecules cannot pass. Biomolecules are thereby pushed into the constriction sites by advection, thus becoming entrapped. Entrapped particles can then only be released by diffusing back through the opening, and by chance, taking a different flow path through the resin [30,32]. Trilisky et al. demonstrated this effect for monoliths with channel diameter of 2 μm and for non-enveloped human adenovirus serotype 5 of approximately 100 nm in diameter [30]. Pavlin et al. observed this effect in an analytical monolith with a 6 μm channel diameter for an open circular DNA (ocDNA) plasmid isoform [33]. Recovery reduction due to this effect was seen at flow rates of 0.5 and 1.0 mL/min. However, more compact DNA structures were not affected. In a preparative setup, this recovery reduction for ocDNA was only observed for 2 μm, but not for 6 μm channels by Kralj et al. [34]. Gabor et al. observed plasmid recovery losses due to convective entrapment on analytical monoliths as well as bead-based columns. The authors were unsuccessful in predicting the losses using the radius of gyration for different plasmid isoforms, suggesting an important role of particle geometry for the entrapment effect [35].

The retention effect due to convective entrapment is currently not accounted for in any transport term of conventional chromatographic mechanistic models. To address this gap, we incorporated the Langmuir model to approximate the particle retention by convective entrapment, in addition to the SMA formalism for the electrostatic interactions. Consequently, this study presents a mechanistic model that describes the bind-and-elute behavior of enveloped virus particles in a chromatographic monolith, taking into account the particle retention due to convective entrapment.

2. Theory and model design

A mechanistic chromatography model is an *in silico* representation of a chromatographic step utilizing mathematical equations to simulate the fluid dynamics and molecule adsorption and retention. The applied models are presented in this section, together with the implemented modifications for this study.

2.1. Equilibrium dispersive model

A monolithic structure is considered, with its porosity built up by only convective flow channels. Mass transfer is presumed to be non-limiting [13,31], and potential diffusional accessible pores and thus diffusional limitations are neglected. Therefore, the stationary phase concentration q can be directly coupled to the mobile phase concentration c.

In an axial flow column, mass transport by convection through the column is presumed to be independent of the cross-sectional position. The column geometry is thus reduced to a one-dimensional space. The equilibrium dispersive model (EDM) describes the change of the concentration c in the mobile phase (MP) at a coordinate $x \in [0, L_{\mathrm{Col}}]$ and a discrete time point $t \in [0, T]$ as shown in Eq. (1), in which u_0 is the applied flow velocity and ε the column porosity. The EDM is composed of an advection term, a dispersion term, and a term for the mass transfer to the stationary phase (SP) [36].

$$\frac{\partial c}{\partial t}(x,t) = -\frac{u_0(t)}{\varepsilon}\frac{\partial c}{\partial x}(x,t) + D_{\mathrm{ax}}\frac{\partial^2 c}{\partial x^2}(x,t) - \frac{1-\varepsilon}{\varepsilon}\frac{\partial q}{\partial t}(x,t) \tag{1}$$

In the EDM, all peak broadening effects are lumped together into the apparent dispersion factor D_{app} [36]. In general, contributing factors for chromatographic peak broadening can include: axial molecular diffusion, eddy dispersion, mass transfer limitations (film mass transfer resistance layer, pore diffusion, boundary layer) and adsorption/desorption kinetics [37]. Since mass transfer is assumed to be non-limiting and binding kinetics are accounted for in the binding isotherm, the apparent dispersion factor D_{app} can be reduced to axial effects and becomes D_{ax}.

The EDM is complemented at the inlet ($x = 0$) and outlet ($x = L_{\mathrm{Col}}$) by the Danckwerts' boundary conditions [38].

$$\frac{\partial c}{\partial x}(x = 0, t) = \frac{u(t)}{D_{\mathrm{ax}}}\left(c_i(x=0,t) - c_{\mathrm{in},i}(t)\right) \; for \; t > 0 \tag{2}$$

$$\frac{\partial c}{\partial x}(x = L_{\mathrm{Col}}, t) = 0 \; for \; t > 0 \tag{3}$$

2.2. Steric mass action isotherm

Brooks and Cramer introduced the SMA isotherm in 1992 [39], which assumes a stoichiometric exchange of ions as principle of molecule-ligand binding. The adsorption of component i on the stationary phase is described by the isotherm equation. A total of N_{comp} components including salt ($i = 0$) is considered. Eq. (4) shows the kinetic form of the SMA isotherm which considers the counter-ion concentration in the mobile phase c_0 and the ionic capacity of the stationary phase Λ [40]. The adsorption behavior is dependent on the component-specific parameters characteristic charge ν_i and steric hindrance factor σ_i. The rate of adsorption and desorption is characterized by the equilibriums parameter $K_{eq} = k_{ads}/k_{des}$ and the kinetic parameter k_{kin}. Reference concentrations ($q_{ref} = 1000\ \frac{mol}{m^3_{SP}}$, $c_{ref} = 1000\ \frac{mol}{m^3_{MP}}$) were applied to make the units of the equilibriums and kinetic parameter independent from the characteristic charge and thus decouple them. This simplifies parameter estimation and the use of reference values within the same dimension of c_0 and Λ improves numerical stability [41].

$$\frac{\partial q_i^{SMA}}{\partial t} = \frac{1}{k_{kin,i}} \left(K_{eq,i}\ c_{p,i} \left(\Lambda - \sum_{j=1}^{N_{comp}-1} (\nu_j + \sigma_j) q_j^{SMA} \right)^{\nu_i} q_{ref}^{-\nu_i} - q_i^{SMA} \left(\frac{c_0}{c_{ref}} \right)^{\nu_i} \right) \quad (i = 1, \ldots, N_{comp} - 1) \tag{4}$$

2.3. Convective entrapment effect

Convective entrapment is a fluid-dynamic effect observed in monoliths which depends on advection and the diffusional rate of affected particles. The Peclet (Pe) number was found to be a prediction parameter for convective entrapment. Pe is a dimensionless number describing the ratio of advection to diffusive transport of a physical quantity. Trilisky et al. derived and simplified an equation to estimate the Pe number for the convective entrapment of large biomolecules in monoliths, Eq. (5) [30].

$$Pe \approx \frac{u_s d_b^2}{\varepsilon D d_p} \tag{5}$$

In which u_s is the superficial flow velocity, d_b is the biomolecule diameter, ε is the porosity of the monolith, D is the diffusion coefficient of the biomolecule, and d_p the mean channel diameter of the monolith. In theory, at $Pe = 1$, advection and diffusional rate are balanced. At $Pe \ll 1$, the diffusive transport prevails and particles in constriction sites immediately diffuse out again. At $Pe \gg 1$ the advection prevails and thus particles are convectively entrapped in constriction sites.

2.4. Convective entrapment modeling

In an approach to model the convective entrapment (CE) effect, a second isotherm equation, additive to the SMA isotherm, is introduced. Fig. 1 shows the possible binding modalities for a particle in the mobile phase based on the additive isotherms shown in Eq. (6).

$$\frac{\partial q_i}{\partial t} = \frac{\partial q_i^{SMA}}{\partial t} + \frac{\partial q_i^{CE}}{\partial t} \tag{6}$$

Even though convective entrapment is a fluid dynamic effect rather than a binding modality, it can be interpreted as a binding modality due to the temporary restriction of particles in the resin's constriction sites. Entrapment-and-release is an advection- and diffusion-driven process, dependent on the flow velocity, column channel geometries and the particle diffusional rate, therefore also temperature and viscosity dependent. For reasons of simplification, the dependencies were lumped together into an entrapment (k_{trap}) and release ($k_{release}$) parameter. These parameters are thus only valid as long as the cumulated process variables are not changed.

In addition, homogenous and single-particle constriction sites were assumed. With these prerequisites, a simple Langmuir isotherm as shown in Eq. (7) was used to represent the convective entrapment effect. The total amount of constriction sites is considered using q_{max}^{CE} of which the sum of entrapped particles q_j^{CE} are subtracted to calculate the amount of available constriction sites.

$$\frac{\partial q_i^{CE}}{\partial t} = c_i\ k_{trap,i} \left(q_{max}^{CE} - \sum_{j=1}^{N_{comp}-1} q_j^{CE} \right) - q_j^{CE}\ k_{release,i} \quad (i = 1, \cdots, N_{comp} - 1) \tag{7}$$

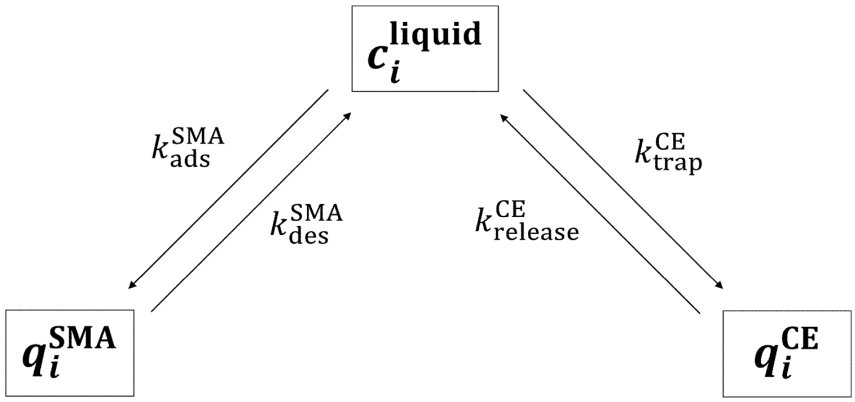

Fig. 1. Isotherm scheme Schematic representation of the isotherm setup. Particles in solution are either entrapped due to convective entrapment or bound to ligands by the SMA formalism.

3. Materials and methods

3.1. Virus preparation

VSV-GP particles were propagated by infection in a mammalian cell suspension. 37 h after infection, the suspension was treated with 200 mM NaCl for viral release. The harvest was clarified by depth filtration, sterile-filtered and treated with nuclease. VPs were captured using a CEX monolith column (CIMmultus SO3, Sartorius BIA Separations, Ajdovščina, Slovenia) and eluted using a 1 M NaCl step at pH 7.5. For polishing and buffer exchange, a preparative size exclusion chromatography column comprising Sepharose 6FF (Cytiva, Marlborough, MA, USA) was used. The mobile phase buffer consisted of a Tris-based buffer with 50 mM NaCl and 150 mM Arginine at pH 7.5. After sterile filtration (0.22 μm), the final virus suspension was aliquoted and stored at −80 °C until usage. The batch was analyzed by qPCR for genomic copies and by $TCID_{50}$ for infectivity resulting in a concentration of 2.3×10^{11} GC/mL and 1.67×10^{10} $TCID_{50}$/mL.

3.2. Chromatographic instrumentation and experimental design

Chromatographic runs were performed on an Äkta micro liquid chromatography (LC) system including an adequate fraction collector (provided by Cytiva, Munich, Germany) unless stated otherwise. PEEK tubing of 0.25 mm inner diameter were used to connect the individual LC system parts except for the column which is mounted on the UV cell. The post-column flow path of the LC system comprised of an UV and a conductivity detector, extended by a multi-angle light scattering (MALS) detector (Wyatt Technology, Santa Barbara, CA, USA).

This study focused on the chromatographic behavior of VSV-GP on a CEX monolith. For this purpose, a scale-down approach was designed. The monolith resin consisted of prototype CIMmic SO3 disks with a manufacturer-specified channel diameter of 6 μm. Three disks were stacked together into the appropriate CIMmic housing, allowing axial flow through all disks with 0.3 mL total volume. The disks and housing were kindly provided by the manufacturer Sartorius BIA Separations (Ajdovščina, Slovenia). Loading densities of virus particles on the monolith resin were kept low (<25 % of max loading capacity) to prevent additional saturation effects. An overview of runs is presented in Table 1.

A Tris-based buffer consisting of 50 mM Tris at pH 7.5 was used throughout this study. The NaCl concentration differed according to the requirements of each step. Column conditioning was conducted using 2 M NaCl for at least 10 column volumes (CVs). 50 mM NaCl were used for column equilibration, loading of virus in BE mode and subsequent wash phase of 5 CV. A linear salt gradient up to 950 mM NaCl was applied for virus particle elution. Different gradient lengths were used as presented in Table 1. In non-binding flowthrough (FT) mode, 500 mM NaCl was used for equilibration and isocratic sample application. After each run, a cleaning-in-place (CIP) step of 2 M NaCl with 1 M NaOH was applied.

Table 1
Overview of chromatographic runs. (FT – Flowthrough; CV – Column volume; BE – Bind and Elute; LGE – Linear gradient elution).

Name	Loading conditions	Run conditions
System characterization	Polystyrene beads (100 nm) 1000 mM NaCl	FT mode; 0.3 mL/min
Low load gradients for Yamamoto method	VSV-GP, <0.1 % of max. loading capacity	BE mode: 20, 40, 60, 80 CV LGE (50 to 950 mM NaCl); 0.3 mL/min
Fraction collection	VSV-GP, approx. 22 % of max. loading capacity	BE mode: 60 CV LGE (50 to 950 mM NaCl); 0.3 mL/min
Reapplication runs	VSV-GP, collected and diluted pools of fraction collection run	BE mode: 60 CV LGE (50 to 950 mM NaCl); 0.3 mL/min
Flow rate variations	VSV-GP, <0.1 % of max. loading capacity	BE mode: 40 CV LGE (50 to 950 mM NaCl) Flow rates: 0.1, 0.25, 0.3, 0.35, 0.45, 0.75 mL/min

3.3. Analytical methods

3.3.1. qPCR titer

The extraction of viral RNA was carried out using the MagMAX Viral RNA isolation kit from Ambion (Life Technologies Corp., Carlsbad, CA, USA), following the instructions provided by the manufacturer. The qPCR analysis was performed using a CFX96 Real Time Cycler from BioRad (Hercules, CA, USA) and the iTaq Universal Probes One-Step Kit, also from Bio-Rad (Hercules, CA, USA). The primers used in the analysis targeted the N-protein gene sequences, as detailed in a previously publication [42].

3.3.2. TCID50 titer

BHK-21 cells (CLS Cell Lines Service GmbH, Eppelheim, Germany) were cultured in 96-well plates using GMEM medium, which was enriched with 10 % fetal calf serum (FCS), 5 % Tryptose Phosphate Broth, and 1 % Penicillin-Streptomycin solution (all media components from Gibco, Thermo Fisher Scientific Inc., Rockford, IL, USA). The cells were then incubated at 37 °C and 5 % CO_2. 24 h post-seeding, a series of dilutions of the virus-containing samples were made. The enriched media was used to produce half-log_{10} dilution steps, which were then individually added to the seeded wells. The plates were incubated for a period of 3 days and subsequently the confluence of each well was measured using an automated plate reader (Tecan, Männedorf, Switzerland). A confluence level of ≤95 % was set as the threshold to identify cytopathic effects in wells due to infection by infectious particles (IP). The $TCID_{50}$/mL was then calculated based on the number of infected wells using the Spearman-Kärber equation [43,44].

3.3.3. Hydrodynamic radius

The hydrodynamic radius of virus samples was measured by dynamic light scattering (DLS) using a DynaPro Nanostar I (Wyatt Technology, Santa Barbara, CA, USA). Samples were diluted as required using the CEX equilibration buffer described above. The lower fit threshold of the autocorrelation function was adjusted to exclude smaller sample matrix components based on a matrix blank analysis.

3.3.4. HPLC-SEC quantification

For offline quantification of total particle count of virus particles (TP), a method based on a high performance LC (HPLC) device equipped with an analytical size exclusion chromatography (SEC) column was used as described previously [45]. An Acquity Arc Bio HPLC system including a photodiode array (PDA) detector (Waters, Milford, MA, USA) was equipped with the analytical SEC column TSKgel G4000PW (Tosoh Bioscience, Griesheim, Germany). The virus particles were separated from smaller impurities by size and the measured UV signal used for quantification against a calibration curve. The mobile phase consisted of 50 mM Tris–HCl 200 mM NaCl, 150 mM L-Arg, and 0.1 wt-% DMSO, pH 8.0. A constant flow rate of 0.5 mL/min was used. Samples were spiked with bovine serum albumin (BSA) to minimize unspecific adhesion of the VPs to the HPLC vials used.

3.4. Model application and parameter estimation

3.4.1. CADET (Chromatography analysis and design toolkit)

The mechanistic model was build using the CADET open-source framework. CADET is a chromatography-specific modeling and simulation software written in C++ which has built-in functionality for common mass transport and binding models [46]. The CADET source code for the SMA isotherm was modified to implement the convective

entrapment functionality as described in the Section 2.4. In CADET, the implicit differential–algebraic solver (IDAS) time integrator was used to discretize time steps to solve the model's differential-algebraic equation system. In this study, the required Jacobians at every time step were calculated using automatic differentiation. The CADET-Process framework was used to setup the mechanistic model. CADET-Process is an open-source python package with interfaces to external libraries such as CADET to facilitate the setup and parameter estimation of mechanistic models [47].

3.4.2. Yamamoto method

The Yamamoto method is a parameter estimation method based on low load linear gradient elution (LGE) runs to determine SMA isotherm parameters [48]. The method exploits the correlation of salt concentration c_s at the eluting peak maximum of a component with the slope g of the linear gradient applied (Eq. (8)). It thereby calculates K_{eq} and the characteristic charge ν.

$$\log(gV_{solid}) = (\nu+1)\log(c_s) - \log\left(\Lambda^{\nu}K_{eq}(\nu+1)\right) \tag{8}$$

3.4.3. Parameter calibration

An inverse parameter estimation method was applied for model parameters for which no other parameter determination method was feasible or available. The inverse method compares simulation data with reference data obtained in experiments and calculates the deviation, in this case, the normalized least square error. This enables the formulation of a minimization problem and allows the application of genetic optimization algorithms such as U-NSGA-III implemented in the pymoo Python package [49]. Within an *a posteriori* specified range, multiple start points were generated. The resulting simulations were evaluated for their error and a new generation of the genetic algorithm was derived.

4. Results and discussion

4.1. System and column characterization

The liquid chromatography system and the chromatography column were characterized for dead volumes and dispersion effects. Detector-specific tracers consisting of a NaCl solution, a dextran solution (blue dextran 2000, Cytiva, Munich, Germany) and a 100 nm polystyrene (PS) bead suspension were used to address different parts of the flow path. The peak maxima of the tracer runs were used to calculate system dead volumes. Column porosity was determined using the net retention time of NaCl and dextran in the column. The porosity determined using NaCl was 3.5 % higher than that derived from the dextran peaks. A mercury intrusion porosimetry analysis was conducted by ZetA Partikelanalytik (Mainz, Germany): the pore volume for pore sizes below 100 nm was approx. 1 % of the total determined pore volume. Based on both findings, the differences in porosities for different molecule sizes (NaCl, dextran and VPs) were regarded negligible and the porosity derived from dextran was used for the model. Dead volumes of 52 µL were considered as ideal plug flow reactors (PFRs) and dispersion was represented using ideal continuous stirred tank reactors (CSTRs) of in total 43 µL. The dispersion contribution of the tubings was expected to be minor. Hence, flow delays of tubings were modeled as ideal PFRs while residual dispersion effects were lumped together with back mixing effects of detector flow cells and other dead volumes as ideal CSTRs. This approach simplified the model setup and calibration. The tubular reactor with an axial dispersion of zero as ideal PFR, and the CSTR unit operation, both included in the CADET-Process package were utilized. The column axial dispersion value was determined by parameter fitting of the NaCl solution runs. Resulting simulations of the characterization runs are displayed in Fig. 2.

To determine ionic capacity, an acid-base-titration was conducted [50]. First, all counter-ions were displaced by protons using 0.5 M HCl.

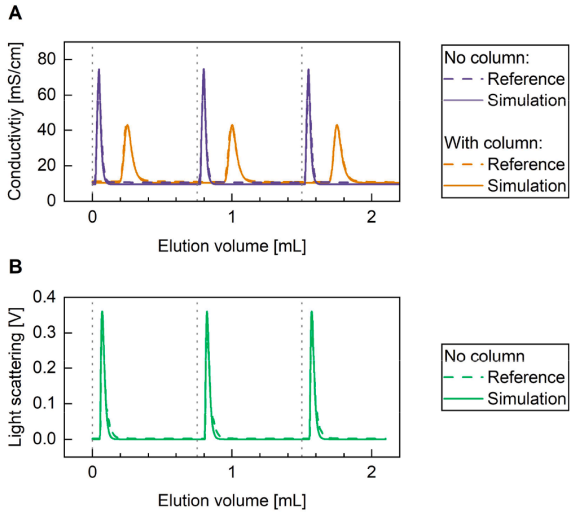

Fig. 2. System and column characterization tracer runs for system and column characterization using (A) NaCl for the conductivity detector and (B) 100 nm PS latex beads for the LS detector. Dashed lines are experimental reference data which are matched by the solid simulation data. Dotted vertical lines mark the injection times of the tracers.

Table 2
Column parameters for the CIMmic SO3 0.3 mL disk stack. Column geometry values are provided by the manufacturer.

Parameter	Symbol	Value	Unit
Column length	L_{Col}	6.3	mm
Column diameter	d_{Col}	7.9	mm
Column volume	V_{Col}	0.3	mL
Axial dispersion	D_{ax}	0.003	mm^2/s
Porosity	ε	0.636	–
Ionic capacity	Λ	0.184	mol/L

Then, a column wash was caried out using purified water. Finally, a titration using 5 mM NaOH was performed until breakthrough was observed in the conductivity signal. The applied amount of sodium ions n_{Na^+} was then used to determine the ionic capacity with Eq. (9). Variables and results are shown in Table 2.

$$\Lambda = \frac{n_{Na^+}}{V_{Col}(1-\varepsilon)} \tag{9}$$

4.2. SMA parameter estimation

SMA parameters were determined by correlating the salt concentration at peak maxima with the normalized salt gradient slope using four elution gradient lengths (20, 40, 60 and 80 CV) according to Yamamoto et al. [51]. The slope and x-intercept of the regression were used to calculate $\nu = 1000.0$ and $K_{eq} = 12.0$ according to Eq. (8). The results are shown in Fig. 3A.

The determined ν and K_{eq} were used to simulate the low load gradient runs, resulting in a good alignment of the retention times for the peak maxima as shown in Fig. 3B. Fitting of $k_{kin} = 5 \times 10^6$ s enabled the representation of the peak fronts. Additional to the main peaks where the peak maxima were used, all elution chromatograms show a strong tailing which is not represented in the simulation. The SMA approach and the assumption of a homogeneous virus particle population did not account for the observed tailing effects. Since no pore diffusion is present in the model an unaddressed phenomenon must be the cause.

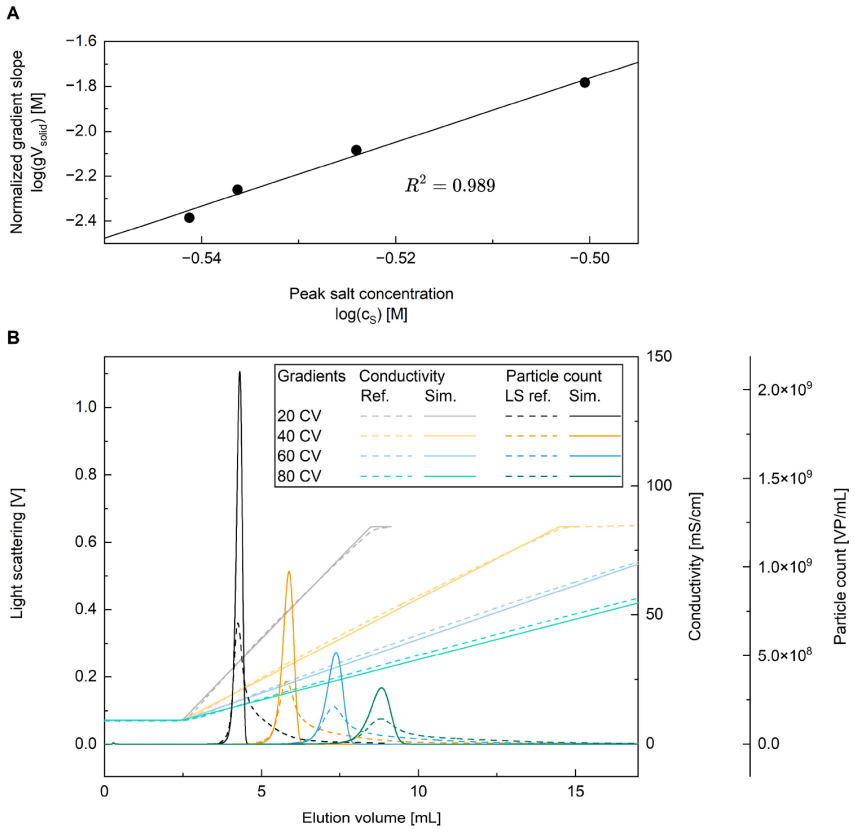

Fig. 3. SMA parameter determination and simulations of low load gradient runs. (A) SMA parameter determination based on the Yamamoto method. Log-log plot of gradient slope and salt concentration at elution maximum yielding in K_{eq} and ν using given equation. (B) Yamamoto LGE runs, conducted at 20, 40, 60 and 80 CV gradient lengths and low loading densities. Experimental reference data and simulations which are based on the SMA parameter determined in A and a fitted kinetic parameter.

4.3. Causes for peak tailing

A variety of factors can contribute to tailing in an elution peak for IEX chromatography: Mass transfer limitations, (extra-column) dispersion effects, sample heterogeneity and secondary particle-resin interactions [37]. These potential causes were considered, using both experimental and theoretical approaches. The findings are presented in this section, and potential contributing factors are discussed.

4.3.1. Peak height and tailing are flow rate dependent

To investigate potential influences from fluid dynamics, the bind-and-elute run using a 40 CV NaCl-gradient (Fig. 3) was repeated at various flow rates. In the tested range of flow rates between 0.1 to 0.75 mL/min, the elution peak showed changes in the extent of peak tailing as well as peak height depending on the flow rate as shown in Fig. 4. For the previously used flow rate of 0.3 mL/min, the tailing is most pronounced (Fig. 4B, blue line). Deviations of 0.05 mL/min in either direction reduced the tailing. A minimal tailing in the set is reached for the highest flow rate deviations in both direction (Fig. 4A+C) for which the increased flow rates also show a reduced peak height (Fig. 4C). Due to these findings, the influence of flow rate on dispersion was evaluated as presented in the following section.

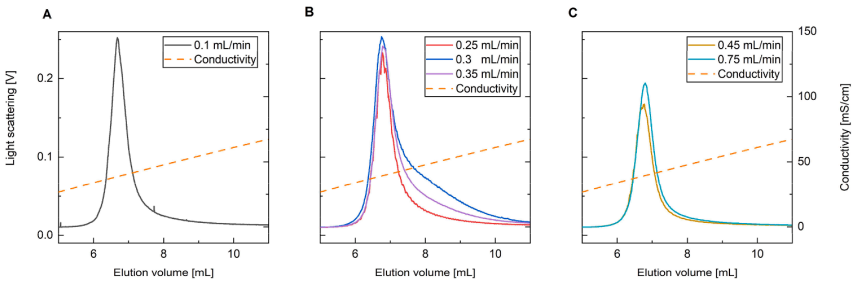

Fig. 4. The impact of flow rate on the elution profile was analyzed by deviating the flow rate between 0.1 and 0.75 mL/min for 40 CVs LGE runs at low loading densities. (A) 0.1 mL/min, (B) (0.3 ± 0.05) mL/min and (C) 0.45 mL/min, 0.75 mL/min.

4.3.2. Possible dispersion effects

Dispersion effects in the column and LC system were characterized and considered as shown in Fig. 2. Furthermore, the influence of flow rate and thus potential impact on the chromatogram was investigated. Acetone pulses were applied on the column at different flow rates. Overlying peaks are observed for higher flow rates between 0.5 to 1.0 mL/min while slightly broader peaks are observed for lower flow rates between 0.1 to 0.25 mL/min (supplemental Figure S1).

From a theoretical point of view, dispersion effects in chromatography can be categorized as either column-originated or extra-column effects. Within the column, the hydrodynamic dispersion due to the resin geometry is a constant parameter according to van Deemter and is independent of the flow rate [52]. The longitudinal (axial) molecular diffusion is dominant for very low flow rates, which is seen using the acetone pulses at very low flow rates in Figure S1 [52]. However, with lower residence times at elevated flow rates and low inherent diffusional rates of large biomolecules, its influence is considered negligible. Thus, it is unlikely that flow rate-induced dispersion effects is responsible for the observed tailing variations in Fig. 4.

For monoliths in disk formats used in this study, observed dispersion is dominated by extra-column effects [14] such as system dead volumes. Tubings, column housing and detector flow cells contribute to the dead volume which becomes more important when using low volumetric columns [53]. In a similar chromatographic setup, Yamamoto et al. observed a fronting and slight tailing which was assumed to originate from dispersion in the column housing [54]. In comparison, tailing effects observed in the results presented here are much more dominant. The setup used for this study was optimized for minimal dispersion effects: the chromatographic system used features small internal volumes, and the axial flow CIM disks exhibit lower dispersion compared to the radial flow monoliths [13]. In the presented study, no relevant peak broadening influence of the flow rate was determined. Observed dispersion effects were constant within the tested flow rate and accounted for in Fig. 2.

4.3.3. Fractions of main peak and tailing show distinct elution behavior

To examine the behavior of virus particles in the main and tailing part of the elution peak separately, the elution peak was fractionated accordingly. The column was loaded to approximately 22 % of its capacity with purified virus particles, and then a 60 CV NaCl-elution gradient at 0.3 mL/min was performed. With this higher loading density, the elution profile (Fig. 5A) remains the same as for the low load runs (Fig. 3B), comprising a main peak and a strong tailing.

Fractions collected throughout the run were quantified by offline HPLC-SEC analysis. The overlay of the light scattering signal at 90° and the offline quantification matches except for the peak maxima where the scatter signal was saturated even though the laser power was reduced to 10 %. The ratio of offline measured VP concentration to the scatter signal of this run was used as measurement factor for this study. The measurement factor of $1.9 \times 10^{9} \frac{VP}{mL} / V$ was applied in all plots to visualize the scatter signal of experiments, the reference data, together with simulated virus particle count data at a constant ratio between them.

The fractions at the peak maximum and the mid part of the tailing (indicated in Fig. 5A) were pooled and conditioned (diluted) to adjust the NaCl concentration to the initial binding conditions. The pools were individually reapplied on the regenerated column using the same conditions as for the initial fraction collection run. Reapplication of the two pools resulted in completely different behaviors compared to the initial application and also between the two pools (Fig. 5B). Specifically, the main pool elutes as a sharp peak with minor tailing at the same retention

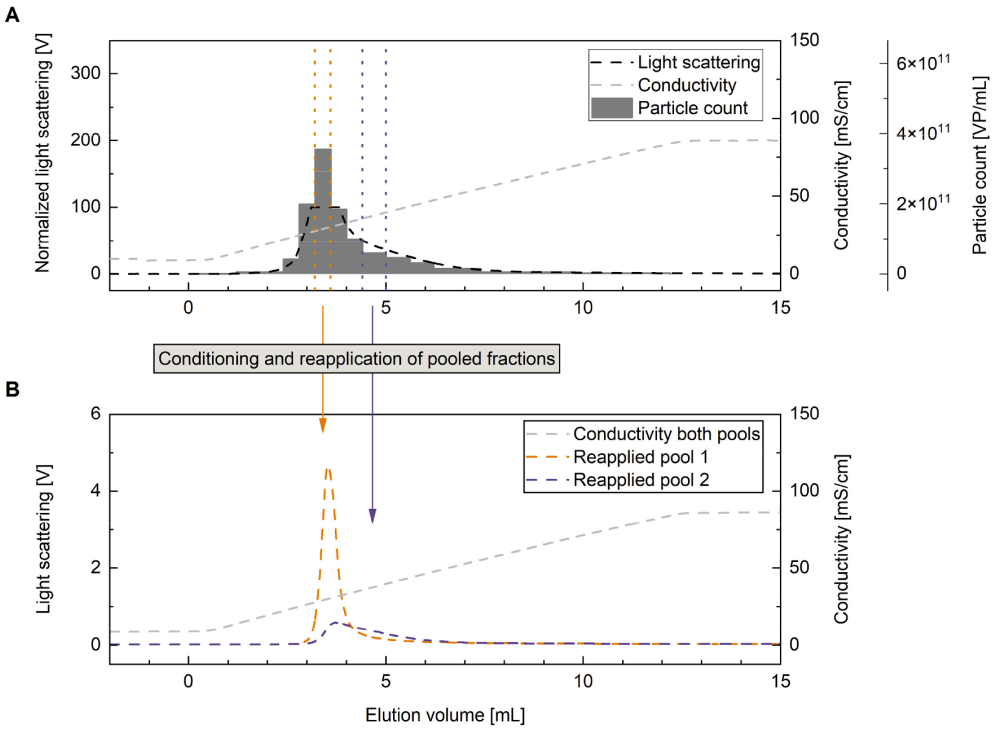

Fig. 5. Main peak and tailing fraction collection and reapplication. (A) Fraction collection of a 60 CVs LGE run with purified VSV-GP. Laser power was reduced to 10 % to prevent saturation which still occurred at peak maxima. The scatter signal shown was normalized to 100 % laser power for comparability. Fractions were colllected and VPs quantified offline by HPLC-SEC. (B) Pools of the main and tailing peak region (marked in A) were reapplied onto the same column using the same bind-and-elute parameters as in A. NaCl concentrations of the pool loads were adjusted by dilution to meet initial sample loading conditions of A.

time as the pool collection. On the contrary, the reapplied tailing pool starts eluting with a small delay compared to the main peak and exhibits a dominant tailing. In this case, however, no distinct peaks can be discriminated. This phenomenon of different elution behaviors of collected fractions was observed also in a scaled-up setup using the same run conditions: 1 mL CIMmultus SO3 column (Sartorius BIA Separations, Ajdovščina, Slovenia) on an Äkta avant150 (Cytiva, Munich, Germany) at 1 CV/min. A different batch of purified virus particles was used which was produced in the same way as the virus material applied to the original experiment. The scaled column uses a radial flow pattern instead of an axial flow in the scale-down approach. Even in this scaled setup and changed flow pattern, the same distinctive elution behavior of virus particles in the main and tailing peak part were observed (Figure S2). In the next sections possible causes which could explain observed effects are discussed.

4.3.4. Charged subspecies and kinetic effects

When multiple peaks or shoulders are observed in an IEX elution gradient, the first logical assumption is that there is a diverse population of subspecies or impurities with different charges. Effio et al. showcased an example where a single target component had to be separated from a complex feed stock. [17] In their highly complex LGE chromatogram, many overlapping peaks are observed which could be deconvoluted into individual components. In their derived model, all components were modeled individually with different and independent SMA parameters [17]. In contrast, the chromatograms observed in this study show a different behavior: no individual distinct peaks are revealed in any of the utilized gradients (Fig. 3B). Instead, a flow rate dependency for the tailing was observed in Fig. 4. The strongest effects were seen at the flow rate of 1 CV/min = 0.3 mL/min. Deviations in both directions decreased the tailing. These observations strongly oppose the tailing effect being originated from charged species.

Another influence on the chromatogram are time-dependent kinetics of the particle-resin-interaction. These effects are amplified in bead-based chromatographic resins due to mass transfer resistances which are considered negligible in this study setup using a monolith. By increasing the kinetic parameter in the kinetic form of the SMA equation, the actual kinetics decrease due its reciprocal form. This results in slowed desorption of components and peak tailing [55]. Decreased kinetics also impact the adsorption term in the SMA equation, leading to a slowed adsorption until breakthrough during loading occurs. The kinetic parameter was fitted to be aligned with the front of the LGE peaks. A further increase of the parameter in the model lead to an early breakthrough of components during the loading phase (data not shown) which is not seen in the reference data set. Slow kinetics were thus excluded as a tailing cause.

4.3.5. Hydrophobic interaction chromatography (HIC) effects

Residual hydrophobic interactions of the polymethacrylate backbone of the monolithic resin may slow down the desorption process of bound particles, especially with salt ions being present. The salting out effect should increase potential hydrophobic interactions, thus a steeper salt gradient for elution should increase effects as observed by Altern et al. for mixed-mode columns [56]. This is not observed in Fig. 3. Moreover, a potential HIC effect would not exhibit a flow rate dependency as observed for the tailing in Fig. 4.

4.3.6. Binding modalities

The shape of VSV particles resembles a bullet with its cylindrical structure, with one flat end and the other one convex. Thus, different binding strengths of the particle facets to the resin surface could be assumed. If so, a certain proportion of the different binding modalities is expected to be established. This proportion would then be observed as the ratio of the peak areas eluting from the column. And the ratio should be re-established when any elution peak fractions are reapplied on the column. Fractions of the main peak and the tailing were collected and reapplied on the same column using the same process conditions at two different scales (Fig. 5 and Figure S2). Upon reapplication of the pools, the resulting chromatograms show a very different ratio of the main and tailing part. This observation indicates that different binding modalities are most likely not the main contributor to the observed tailing.

4.3.7. On-column particle alterations

Morphological differences in VSV-GP particles were previously described to occur in the preparative process [57] and enveloped virus particles are typically sensitive to environmental stress such as high ionic strength [58] and shear rates [59]. Possible morphological on-column alterations could result in a variety of elution behaviors, thus the broad tailing peak. The reapplication of the main peak does not support this hypothesis. The tailing upon reapplication is reduced to a minimum (Fig. 5B), so no on-column alterations result in an extended tailing behavior. Furthermore, no significant difference in infectivity was determined between the pooled fractions: $\text{ratio}_{\text{IP/TP}}\ (\text{Main peak}) = 14\ \pm 7\%\ \text{TCID}_{50}/\text{VP}$; $\text{ratio}_{\text{IP/TP}}\ (\text{Tailing}) = 20\ \pm 12\%\ \text{TCID}_{50}/\text{VP}$.

4.3.8. Convective entrapment

The observed peak tailing may be caused by fluid-dynamic effects rather than particle-resin-interactions. The convective entrapment effect as described by Trilisky et al. [30,32] and Koku et al. [60] is a fluid-dynamic effect leading to partial or complete particle retention. Particles are entrapped in narrowed channels by convective pressure and released by chance due to diffusional movement. This leads to a retention effect observed as a peak delay, tailing effect or peak area reduction.

Convective entrapment can be classified by the Peclet number (*Pe*), a dimensionless number dependent on process parameters such as the flow rate but also on particle characteristics such as the diffusional rate. The Peclet number is used as a predictor for recovery losses due to the convective entrapment effect ($Pe \gg 1$), but convective entrapment was also observed for $Pe < 1$ [30,33]. In the bind-and-elute runs presented here, the determined Peclet numbers of the utilized flow rate range were $Pe < 1$ (Figure S3). Peclet numbers were estimated based on diffusional rate measurements of VPs using DLS. At the flow rate of 0.3 mL/min for which the strongest tailing effect was observed (Fig. 4B), a $Pe_{0.3} \approx 0.14$ was estimated. At lower flow rates (Fig. 4A), Peclet numbers are lower ($Pe_{0.1} \approx 0.04$) and diffusional transport becomes more dominant: particles would have a higher chance of a fast release from constriction sites by diffusion. Conversely, at higher flow rates the advection compared to diffusional transport becomes dominant, and particles in constriction sites remain entrapped until the conditions change. This leads to a reduced peak height as observed in Fig. 4C. However, this is not represented in the estimated Peclet numbers which are $Pe < 1$ ($Pe_{0.45} \approx 0.2$, $Pe_{0.75} \approx 0.34$) and demonstrates the estimative character of the Peclet number. The correct interpretation of Peclet numbers in the dimension of 1 is difficult due to the equilibrium of advection and diffusional rate. It thus remains unclear at which Peclet value tailing effects due to convective entrapment are most prominent.

The reapplication runs using the main and tailing fractions in Fig. 5 and Figure S2 indicate the presence of at least two populations in the feed material. These are weakly separated due to their different behaviors in terms of the convective entrapment effect. Since the salt-gradient alone cannot effectively separate these populations, it is presumed that there is a morphological difference between them. Particle analysis of the two pools by DLS reveals a difference in the hydrodynamic diameter by 14 nm, with pool 1 measuring 156 nm and pool 2 measuring 170 nm. Based on these findings, we conclude that there are at least two distinct populations within the feed material exhibiting different convective entrapment behaviors. We further suspect that the convective entrapment is likely highly sensitive to even minor differences, which may originate from upstream production conditions and/or alterations from downstream processing. Heterogeneity in functional

and structural properties of VSV particles can arise from the timepoint of budding from the infected host cell [61]. Morphological changes may be further introduced throughout the preparative process due to environmental stress on particles [57]. Differences in VSV particles were observed in this study, however the root cause analysis for the variations is out of scope. It remains unclear if particle heterogeneity originate from the cell culture or is later introduced, eg. during clarification. Particles alterations occurring in the CEX column were excluded as discussed in Section 4.3.7.

Additional runs in non-binding conditions at elevated salt concentrations ($c_{NaCl} = 950$ mM) were conducted. These runs used an initial flow rate of 0.75 mL/min. Subsequently the flow rate was either paused (Figure S4A) or stepwise reduced (Figure S4B). After the initial flow-through peaks, subsequent 'eluting' peaks were detected every time the flow rate conditions changed. 7.5 % of the total peak area was measured after the flow rate pauses while 2.5 % was seen with flow rate reduction. When conducting blank runs without virus particle application or without a column, no subsequent peaks were observed upon flow rate changes (data not shown). Low flow rates are impractical in preparative applications as monoliths are specifically chosen to be used at high flow rates, eg. for high volumetric feeds in initial capture steps. A flow rate reduction after preparative runs can help to evaluate recovery losses due to entrapment effects. Furthermore, CIP steps might be improved by flow rate adjustments to increase the diffusional movement out of constriction sites.

Koku et al. showed a near complete entrapment of Adenovirus particles at high Peclet numbers [60]. In the study presented here, no complete entrapment was observed. Instead, a strong tailing effect was attributed to the entrapment effect already at Peclet numbers below 1. In this range, the impact on recovery might be low, nevertheless for analytical applications it could be important. Loading densities are usually low to start with and retained particles might lead to misinterpreted chromatograms.

4.4. Modeling of convective entrapment effect

Particle retention due to convective entrapment was implemented additionally to the SMA isotherm through an approximation by a Langmuir term. Model parameter estimation and calibration, as well as model insufficiencies due to simplifications are presented.

To estimate the amount of constriction sites of the monolith resin, a pore size distribution analysis was performed. The mercury intrusion porosimetry analysis shown in Figure S5 shows a generally narrow pore size distribution. A pore volume of $V_{Pore} = 1255.0$ mm^3/g and a modal pore diameter of 5.47 μm was determined in the analyzed pore size range between 10 nm and 100 μm. The pore volume of pore sizes between 10 nm and 100 nm was considered ($V_{CE} = 12.55$ mm^3 /g) for an estimation of the convective entrapment constriction site capacity. A cylindrical approximation using the particle geometry of 70 nm x 200 nm [28] was utilized to determine the single virus particle volume and derive a theoretical maximum number of virus particles fitting in the convective entrapment capacity. The density of the dried monolith resin was determined to be $\rho = 0.491$ g/mL (mean of 4). Using these values, a theoretical convective entrapment capacity of $q_{max}^{CE}(VSV) = 8.01 \times 10^{12}$ particles/mL was calculated. This estimated capacity exceeds the amount of virus particles applied in a single run of this study by a factor of at least 10. The pore size population considered represents only the end volume of presumed funnel-shaped constriction sites whereas virus particles would most likely be stuck above in more spacious geometries. The result is thus a low estimate which still exceeds the number of viral particles applied.

Based on the findings described in Section 4.3, two virus particle populations were assumed. The same SMA parameters, previously determined, were used for both populations which means that the same electro-chemical interaction with the resin is presumed. The convective entrapment parameters k_{trap} and $k_{release}$ were calibrated together with the ratio of populations by parameter estimation based on the low load gradient runs. Table 3 summarizes the determined population specific parameters. The difference in the determined convective entrapment parameters reflects their different convective entrapment behavior.

Table 3
Resulting parameters from model calibration of the two particle populations.

Parameter	Symbol and unit	Population 1	Population 2
Population share	[−]	0.65	0.35
SMA specific parameters			
Equilibriums constant	K_{eq} [−]	1.0×10^3	1.0×10^3
Kinetic	k_{kin} [s]	5.0×10^{-6}	5.0×10^{-6}
Characteristic charge	ν [−]	12.0	12.0
Steric factor	σ [−]	1.0×10^6	1.0×10^6
CE specific parameters			
Entrapment factor	k_{trap} [m$^3_{MP}$/mol s]	2.150×10^4	2.168×10^5
Release factor	$k_{release}$ [1/s]	3.587×10^{-2}	1.613×10^{-1}

4.5. Predicted chromatograms

The predicted gradient runs using the combined isotherm, Eq. (6), are shown in Fig. 6A. The simulations exhibit a strong peak tailing for all gradient slopes which represents the tailing of the reference data. Individual population signals are shown in Fig. 6B for the 40 CV gradient run: the second population is mainly responsible for the tailing though the first population slightly tails as well. The start of elution for the second population is delayed by approx. 60 s, which can be explained by the retention effect due to convective entrapment after eluting at the same time as the first population. For the steeper gradients, the simulated tailing is observed as a distinct shoulder which differs from the rapidly decreasing tailing in the reference data. The elution of population 2 is simulated as strongly retained which is not the case in the reference data.

The predicted simulations of the fraction collection and reapplication of collected pools are shown in Fig. 7. The simulations of the fraction collection are well aligned to the reference data (Fig. 7A). Based on the simulation, a virtual pooling of eluted material was conducted at the marked volume points. The concentrations of both populations (P1, P2) were determined and the purity in the collected fractions derived by Eq. (10): $purity_{P1}(\text{Main peak}) = 0.89$, $purity_{P2}(\text{Tailing}) = 0.69$.

$$purity_{Pi} = c_{Pi}/(c_{P1} + c_{P2}),\ i \in (1,2) \tag{10}$$

The results were used as feed properties for the subsequent simulations of the reapplied runs (Fig. 7B). The dilution factors to reduce the salt concentration and re-establish initial feed conditions were considered. The consecutive simulations show a good representation of the reference data, even though the tailing of pool 1 is overrepresented compared to the reference.

4.6. Model simplifications

The entrapment model based on the Langmuir-approximation and the presumption of 2 populations distinguished by different entrapment behavior is a simplified approach. There are likely some unaccounted properties or entrapment effects leading to the observed deviations from the reference data and are discussed in the following.

A steep gradient leads to a fast desorption of particles and a locally high concentration of particles in the mobile phase. These concentration differences between the gradients could induce a changed entrapment behavior, especially for population 2, which is not considered in the model. The contrary is observed for the fraction collection run (Fig. 7). The loading density is much higher compared to the LGE runs (approx. 1400-fold) and thus the number of particles desorbing at the same time. Nevertheless, no concentration related fast elution of population 2 is observed. The separation from population 2 is sufficient enough to

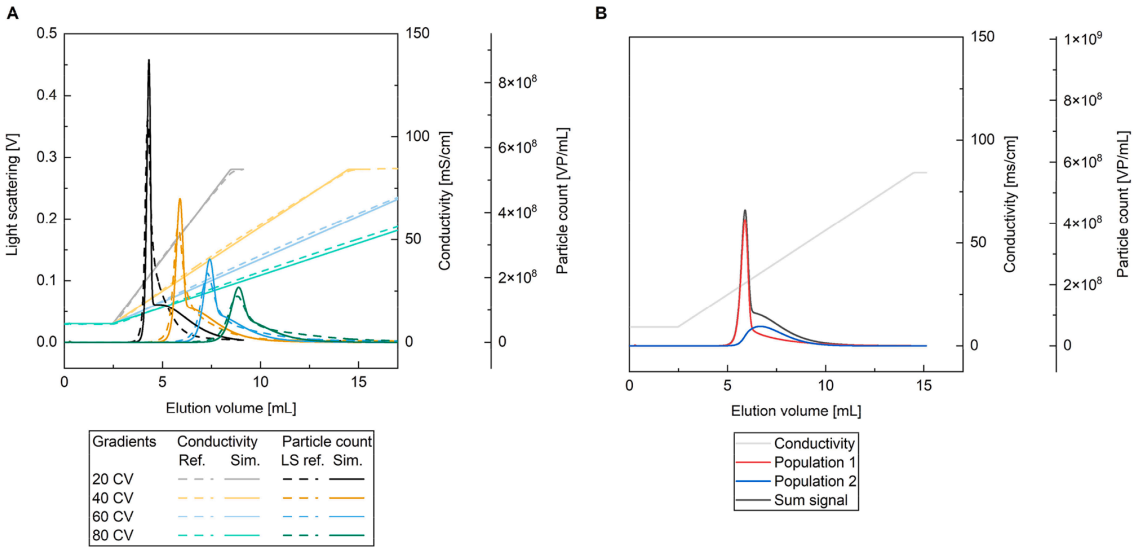

Fig. 6. CE + SMA isotherm simulations of low load gradient elution runs. (A) Simulations of Yamamoto LGE runs, conducted at 20, 40, 60 and 80 CV gradient lengths and low loading densities. Simulations use the combined isotherm (SMA + CE) and two assumed populations. (B) Deconvoluted view of the 40 CVs Yamamoto LGE run displayed in A, showing the individual population signals.

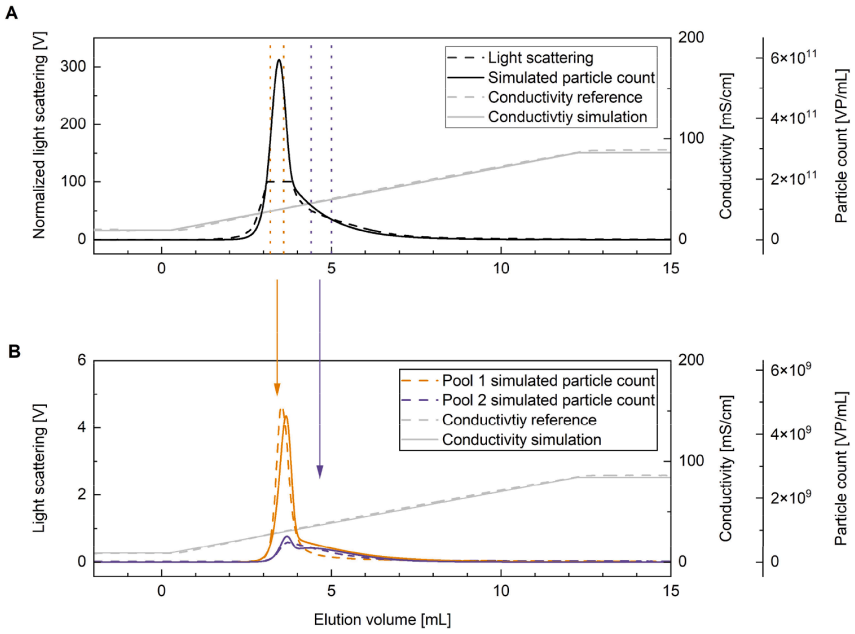

Fig. 7. CE + SMA isotherm simulation of fraction collection and reapplication run. (A) Simulation and experimental reference data of the fraction collection run shown in Fig. 5. Marked fractions were used for pooling of main and tailing peak regions. (B) Simulation and experimental reference data of reapplied pools. Virtual pooling of marked fractions in A yielded in feed properties for the subsequent simulation of reapplication. Simulations in A and B use the combined isotherm (SMA + CE) and two assumed populations.

reduce the tailing of the reapplied pool 1 drastically.

Further simplifications originated from the use of the Langmuir approximation for the convective entrapment effect might result in additional errors. The classic Langmuir model has three preconditions: monolayer adsorption, no particle-particle interaction and homogenous binding sites. Applied to the convective entrapment effect, these preconditions are transformed to: Single particle convective entrapment per constriction site and homogenous constriction sites. Constriction sites are convective channels which taper off to a narrow passage blocking particles from passing through. This funnel-shaped structure depends on the polymerization conditions and cannot be evaluated in detail. Looking at the structure of polymethacrylate monoliths in scanning electron microscopy (SEM) pictures [62], homogeneous constriction sites cannot be assumed. In regard to multiple particle entrapment in one

constriction site, Trilisky et al. presumed a low probability [30]. They argued that an entrapped particle would reduce the convective flow and reduce the characteristic distance for diffusive release, thus reducing the likelihood of other particles being entrapped after the initial one.

Lastly, the additive setup of SMA and convective entrapment equations in the isotherm considers both effects distinctly without interdependencies. Therefore, particle-ligand-interaction is not considered for particles being entrapped in the constriction sites. However, ligands within constrictions sites can contribute to the binding of particles. Considering the limitation in suitable analytical methods, it is not feasible to determine if the misalignment observed in the simulation compared to reference data is due to insufficient characterization of the feed material or lack of representation of the model of the actual effects.

5. Conclusion

Downstream process development of enveloped virus particles is complex due to the structure of the virus particles and new technologies. This can lead to unforeseen effects that are not well understood. Mechanistic modeling can help identify knowledge gaps and improve our understanding of the process.

In this study, a fluid-dynamic effect was observed during the chromatographic purification of an enveloped virus using a CEX monolith resin. This effect was found to be independent of virus batch, column scale and LC equipment. Standard mechanistic modeling approaches were used to understand the effect, but the models could not accurately represent the observed effect, leading to misalignment. Potential contributing factors were examined and discussed.

The convective entrapment effect was identified as plausible factor. This fluid-dynamic effect results in a retention of large biomolecules dependent on the convective flow and the biomolecules diffusional parameters. To the best of our knowledge, the entrapment was not yet simulated in a chromatographic model. Thus, we extended the SMA isotherm by a Langmuir term to include the retention of bioparticles resulted from convective entrapment. It was shown that the introduced approach with the combined isotherm was capable of representing tailing effects and consequently separation of population due to different convective entrapment behaviors. This allowed to investigate the effect in silico without an analytical panel which is not yet available. However, the presented isotherm approximates the entrapment and neglects dependencies e.g. flow rate, particle diffusion rate, resin channel geometries and concentration dependencies. Together with the simplification inherent in the Langmuir equation, some misalignments are still observed. The model application must be considered limited.

The observed convective entrapment effect has implications for both, preparative runs and analytical methods using resins with convective channels and large biomolecules. Polymerization processes of monoliths are intended to keep channel sizes constant across scales [63]. It is expected that scaled-up columns should behave like the scaled-down columns, and this was shown for lab scale columns. Tailing effects are to be expected across all scales at characteristic flow rates. Recovery losses due to entrapment should be evaluated, and CIP steps adjusted accordingly (e.g. low flow rate steps or flow rate pauses during CIP phases can be incorporated). For analytical applications, the impact of entrapment may be more significant due to shifted retention times and tailings. Flow rate effects should be investigated and considered during method development. The separation of populations which was shown might be exploited for analytical purposes. More orthogonal analytical methods are necessary to understand the biophysical correlates leading to this separation.

In this study, the relevance to consider the entrapment effect was demonstrated. Although the proposed modeling approach was able to describe this effect, further studies and suitable analytical methods are necessary to gain more knowledge about this effect and its consequences.

Data availability

All data used to evaluate the conclusions of the article are present in the paper and/or supplementary material. ViraTherapeutics GmbH is unable to provide raw data, protocols or additional datasets.

Funding

This research did not receive any specific grant from funding agencies in the public, commercial, or not-for-profit sectors.

CRediT authorship contribution statement

Adrian Schimek: Writing – original draft, Methodology, Investigation, Data curation, Conceptualization. **Judy Ng:** Writing – review & editing, Conceptualization. **Federico Will:** Writing – review & editing, Data curation. **Jürgen Hubbuch:** Writing – review & editing, Supervision.

Declaration of competing interest

The authors declare the following financial interests/personal relationships which may be considered as potential competing interests:

Adrian Schimek reports equipment, drugs, or supplies was provided by Sartorius BIA Separations doo. Adrian Schimek reports equipment, drugs, or supplies was provided by Cytiva Europe GmbH. Adrian Schimek and Judy Ng report a relationship with ViraTherapeutics GmbH that includes: employment. Federico Will reports a relationship with Boehringer Ingelheim Pharma GmbH & Co KG that includes: employment. Judy Ng has patent #US20220010286A1 pending to Boehringer Ingelheim International GmbH. If there are other authors, they declare that they have no known competing financial interests or personal relationships that could have appeared to influence the work reported in this paper.

Acknowledgements

Special thanks go to Dr. Knut Elbers, ViraTherapeutics GmbH, Rum, Austria for facilitating and supporting this work. The authors would like to thank David Saleh (formerly employed at Boehringer Ingelheim Pharma GmbH & Co.KG) for insights into his expertise and valuable discussions. The authors wish to acknowledge the IBG-1 Modeling and Simulation group, especially Johannes Schmölder (Forschungszentrum Jülich, IBG-1: Biotechnology, Jülich, Germany) for the often rapid support, bug fixes and feature implementations regarding the CADET-Process Python package. The authors are grateful to Matthias Schimek for coding support.

Supplementary materials

Supplementary material associated with this article can be found, in the online version, at doi:10.1016/j.chroma.2025.465832.

References

[1] C.E. Dunbar, K.A. High, J.K. Joung, D.B. Kohn, K. Ozawa, M. Sadelain, Gene therapy comes of age, Science 359 (2018), https://doi.org/10.1126/science.aan4672.

[2] Q. Lan, S. Xia, Q. Wang, W. Xu, H. Huang, S. Jiang, L. Lu, Development of oncolytic virotherapy: from genetic modification to combination therapy, Front. Med. 14 (2020) 160–184, https://doi.org/10.1007/s11684-020-0750-4.

[3] Q. Ji, Y. Wu, A. Albers, M. Fang, X. Qian, Strategies for advanced oncolytic virotherapy: current technology innovations and clinical approaches, Pharmaceutics. 14 (2022) 1811, https://doi.org/10.3390/pharmaceutics14091811.

[4] A. Srivastava, K.M.G. Mallela, N. Deorkar, G. Brophy, Manufacturing challenges and rational formulation development for AAV viral vectors, J. Pharm. Sci. 110 (2021) 2609–2624, https://doi.org/10.1016/j.xphs.2021.03.024.

[5] N. Singh, C.L. Heldt, Challenges in downstream purification of gene therapy viral vectors, Curr. Opin. Chem. Eng. 35 (2022) 100780, https://doi.org/10.1016/j.coche.2021.100780.

[6] G.-A. Junter, L. Lebrun, Polysaccharide-based chromatographic adsorbents for virus purification and viral clearance, J. Pharm. Anal. 10 (2020) 291–312, https://doi.org/10.1016/j.jpha.2020.01.002.

[7] R. Kilgore, A. Minzoni, S. Shastry, W. Smith, E. Barbieri, Y. Wu, J.P. LeBarre, W. Chu, J. O'Brien, S. Menegatti, The downstream bioprocess toolbox for therapeutic viral vectors, J. Chromatogr. A (2023) 464337, https://doi.org/10.1016/j.chroma.2023.464337.

[8] B. Lins-Austin, S. Patel, M. Mietzsch, D. Brooke, A. Bennett, B. Venkatakrishnan, K. V. Vliet, A.N. Smith, J.R. Long, R. McKenna, M. Potter, B. Byrne, S.L. Boye, B. Bothner, R. Heilbronn, M. Agbandje-McKenna, Adeno-associated virus (AAV) capsid stability and liposome remodeling during endo/lysosomal pH trafficking, Viruses. 12 (2020) 668, https://doi.org/10.3390/v12060668.

[9] R. Rieser, J. Koch, G. Faccioli, K. Richter, T. Menzen, M. Biel, G. Winter, S. Michalakis, Comparison of different liquid chromatography-based purification strategies for adeno-associated virus vectors, Pharm 13 (2021) 748, https://doi.org/10.3390/pharmaceutics13050748.

[10] J. Turnbull, B. Wright, N.K. Green, R. Tarrant, I. Roberts, O. Hardick, D. G. Bracewell, Adenovirus 5 recovery using nanofiber ion-exchange adsorbents, Biotechnol. Bioeng. 116 (2019) 1698–1709, https://doi.org/10.1002/bit.26972.

[11] M. Krajacic, M. Ravnikar, A. Štrancar, I. Gutiérrez-Aguirre, Application of monolithic chromatographic supports in virus research, Electrophoresis 38 (2017) 2827–2836, https://doi.org/10.1002/elps.201700152.

[12] T. Vicente, M.F.Q. Sousa, C. Peixoto, J.P.B. Mota, P.M. Alves, M.J.T. Carrondo, Anion-exchange membrane chromatography for purification of rotavirus-like particles, J. Membrane Sci. 311 (2008) 270–283, https://doi.org/10.1016/j.memsci.2007.12.021.

[13] R. Hahn, A. Tscheliessnig, P. Bauerhansl, A. Jungbauer, Dispersion effects in preparative polymethacrylate monoliths operated in radial-flow columns, J. Biochem. Bioph. Meth. 70 (2007) 87–94, https://doi.org/10.1016/j.jbbm.2006.09.005.

[14] A. Jungbauer, R. Hahn, Polymethacrylate monoliths for preparative and industrial separation of biomolecular assemblies, J. Chromatogr. A 1184 (2008) 62–79, https://doi.org/10.1016/j.chroma.2007.12.087.

[15] F.C. Leinweber, U. Tallarek, Chromatographic performance of monolithic and particulate stationary phases hydrodynamics and adsorption capacity, J. Chromatogr. A 1006 (2003) 207–228, https://doi.org/10.1016/s0021-9673(03)00391-1.

[16] P. Nestola, R.J.S. Silva, C. Peixoto, P.M. Alves, M.J.T. Carrondo, J.P.B. Mota, Robust design of adenovirus purification by two-column, simulated moving-bed, size-exclusion chromatography, J. Biotechnol. 213 (2015) 109–119, https://doi.org/10.1016/j.jbiotec.2015.01.030.

[17] C.L. Effio, T. Hahn, J. Seiler, S.A. Oelmeier, I. Asen, C. Silberer, L. Villain, J. Hubbuch, Modeling and simulation of anion-exchange membrane chromatography for purification of Sf9 insect cell-derived virus-like particles, J. Chromatogr. A 1429 (2016) 142–154, https://doi.org/10.1016/j.chroma.2015.12.006.

[18] J.P. Mendes, M. Bergman, A. Solbrand, C. Peixoto, M.J.T. Carrondo, R.J.S. Silva, Continuous affinity purification of adeno-associated virus using periodic counter-current chromatography, Pharm 14 (2022) 1346, https://doi.org/10.3390/pharmaceutics14071346.

[19] W.R. Keller, A. Picciano, K. Wilson, J. Xu, H. Khasa, M. Wendeler, Rational downstream development for adeno-associated virus full/empty capsid separation – a streamlined methodology based on high-throughput screening and mechanistic modeling, J. Chromatogr. A 1716 (2024) 464632, https://doi.org/10.1016/j.chroma.2024.464632.

[20] S.M. Pirrung, L.A.M. van der Wielen, R.F.W.C. van Beckhoven, E.J.A.X. van de Sandt, M.H.M. Eppink, M. Ottens, Optimization of biopharmaceutical downstream processes supported by mechanistic models and artificial neural networks, Biotechnol. Prog. 33 (2017) 696–707, https://doi.org/10.1002/btpr.2435.

[21] J.M. Mollerup, T.B. Hansen, S. Kidal, L. Sejergaard, A. Staby, Development, modelling, optimisation and scale-up of chromatographic purification of a therapeutic protein, Fluid Phase Equilib. 261 (2007) 133–139, https://doi.org/10.1016/j.fluid.2007.07.047.

[22] G. Wang, T. Briskot, T. Hahn, P. Baumann, J. Hubbuch, Root cause investigation of deviations in protein chromatography based on mechanistic models and artificial neural networks, J. Chromatogr. A 1515 (2017) 146–153, https://doi.org/10.1016/j.chroma.2017.07.089.

[23] E.J. Close, J.R. Salm, D.G. Bracewell, E. Sorensen, A model based approach for identifying robust operating conditions for industrial chromatography with process variability, Chem. Eng. Sci. 116 (2014) 284–295, https://doi.org/10.1016/j.ces.2014.03.010.

[24] G. Pamenter, L. Davies, C. Knevelman, J. Miskin, K. Mitrophanous, D. Dikicioglu, D.G. Bracewell, Time-dependent sorption behavior of lentiviral vectors during anion-exchange chromatography, Biotechnol. Bioeng. (2023), https://doi.org/10.1002/bit.28483.

[25] T. Vicente, R. Fáber, P.M. Alves, M.J.T. Carrondo, J.P.B. Mota, Impact of ligand density on the optimization of ion-exchange membrane chromatography for viral vector purification, Biotechnol. Bioeng. 108 (2011) 1347–1359, https://doi.org/10.1002/bit.23058.

[26] H. Zhao, X. Lin, L. Wang, Y. Yang, H. Zhu, Z. Li, Z. Su, R. Yu, S. Zhang, Pore-blocking steric mass-action model for adsorption of bioparticles, J. Chromatogr. A 1726 (2024) 464968, https://doi.org/10.1016/j.chroma.2024.464968.

[27] A. Muik, I. Kneiske, M. Werbizki, D. Wilflingseder, T. Giroglou, O. Ebert, A. Kraft, U. Dietrich, G. Zimmer, S. Momma, D. von Laer, Pseudotyping vesicular Stomatitis virus with lymphocytic Choriomeningitis virus glycoproteins enhances infectivity for glioma cells and minimizes neurotropism, J. Virol. 85 (2011) 5679–5684, https://doi.org/10.1128/jvi.02511-10.

[28] P. Ge, J. Tsao, S. Schein, T.J. Green, M. Luo, Z. Hong Zhou, Cryo-EM model of the bullet-shaped Vesicular stomatitis virus, Science (1979) 327 (2010) 689–693, https://doi.org/10.1126/science.1181766.

[29] D. Mueller, A. Pardo Garcia, T.A. Grein, F. Kaess, J. Ng, K. Pesta, S. Schneider, J. Turnbull, Process for producing a purified rhabdovirus from cell culture, 2022.

[30] E.I. Trilisky, A.M. Lenhoff, Flow-dependent entrapment of large bioparticles in porous process media, Biotechnol. Bioeng. 104 (2009) 127–133, https://doi.org/10.1002/bit.22370.

[31] R. Hahn, M. Panzer, E. Hansen, J. Mollerup, A. Jungbauer, Mass transfer properties of monoliths, Separ Sci. Technol. 37 (2007) 1545–1565, https://doi.org/10.1081/ss-120002736.

[32] E.I. Trilisky, A.M. Lenhoff, Effect of bioparticle size on dispersion and retention in monolithic and perfusive beds, J. Chromatogr. A 1217 (2010) 7372–7384, https://doi.org/10.1016/j.chroma.2010.09.040.

[33] N. Pavlin, U. Černigoj, M. Bavčar, T. Plesničar, J. Mavri, M. Zidar, M. Bone, U. K. Savič, T. Sever, A. Štrancar, Analytical separation of plasmid DNA isoforms using anion exchanging chromatographic monoliths with 6 μm channels, Electrophoresis 44 (2023) 1967–1977, https://doi.org/10.1002/elps.202300031.

[34] Š. Kralj, Š.M. Kodermac, I. Bergoč, T. Kostelec, A. Podgornik, A. Štrancar, U. Černigoj, Effect of plasmid DNA isoforms on preparative anion exchange chromatography, Electrophoresis 44 (2023) 1953–1966, https://doi.org/10.1002/elps.202300035.

[35] B. Gabor, U. Černigoj, M. Barut, A. Štrancar, Reversible entrapment of plasmid deoxyribonucleic acid on different chromatographic supports, J. Chromatogr. A 1311 (2013) 106–114, https://doi.org/10.1016/j.chroma.2013.08.075.

[36] S. Golshan-Shirazi, G. Guiochon, Theoretical advancement in chromatography and related separation techniques. The Equilibrium-Dispersive Model of Chromatography, 1992, pp. 35–59, https://doi.org/10.1007/978-94-011-2686-1_2.

[37] G. Guiochon, D.G. Shirazi, A. Felinger, A.M. Katti, Fundamentals of preparative and nonlinear chromatography, 2006. doi:10.1016/b978-012370537-2/50034-5.

[38] P.V. Danckwerts, Continuous flow systems distribution of residence times, Chem. Eng. Sci. 2 (1953) 1–13, https://doi.org/10.1016/0009-2509(53)80001-1.

[39] C.A. Brooks, S.M. Cramer, Steric mass-action ion exchange: displacement profiles and induced salt gradients, AIChe J. 38 (1992) 1969–1978, https://doi.org/10.1002/aic.690381212.

[40] T. Hahn, T. Huuk, A. Osberghaus, K. Doninger, S. Nath, S. Hepbildikler, V. Heuveline, J. Hubbuch, Calibration-free inverse modeling of ion-exchange chromatography in industrial antibody purification, Eng. Life Sci. 16 (2015) 107–113, https://doi.org/10.1002/elsc.201400248.

[41] J. Diedrich, W. Heymann, S. Leweke, S. Hunt, R. Todd, C. Kunert, W. Johnson, E. von Lieres, Multi-state steric mass action model and case study on complex high loading behavior of mAb on ion exchange tentacle resin, J. Chromatogr. A 1525 (2017) 60–70, https://doi.org/10.1016/j.chroma.2017.09.039.

[42] S. Wilmschen, S. Schneider, F. Peters, L. Bayer, L. Issmail, Z. Bánki, T. Grunwald, D. von Laer, J. Kimpel, RSV vaccine based on rhabdoviral vector protects after single immunization, Vaccines (Basel) 7 (2019) 59, https://doi.org/10.3390/vaccines7030059.

[43] G. Kärber, Beitrag zur kollektiven Behandlung pharmakologischer Reihenversuche, Naunyn-Schmiedebergs Arch. Für Exp. Pathol. Pharmakol 162 (1931) 480–483, https://doi.org/10.1007/bf01863914.

[44] C. Spearman, The method of "right and wrong cases" ('constant stimuli') without Gauss formulae, Br. J. Psychol. 2 (1908) 227–242, https://doi.org/10.1111/j.2044-8295.1908.tb00176.x, 19041920.

[45] A. Schimek, J.K.M. Ng, I. Basbas, F. Martin, D. Xin, D. Saleh, J. Hubbuch, An HPLC-SEC-based rapid quantification method for vesicular stomatitis virus particles to facilitate process development, Mol. Ther. - Methods Clin. Dev. (2024) 101252, https://doi.org/10.1016/j.omtm.2024.101252.

[46] S. Leweke, E. von Lieres, Chromatography analysis and Design toolkit (CADET), Comput. Chem. Eng. 113 (2018) 274–294, https://doi.org/10.1016/j.compchemeng.2018.02.025.

[47] J. Schmölder, M. Kaspereit, A modular framework for the modelling and optimization of advanced chromatographic processes, Processes 8 (2020) 65, https://doi.org/10.3390/pr8010065.

[48] S. Yamamoto, Plate height determination for gradient elution chromatography of proteins, Biotechnol. Bioeng. 48 (1995) 444–451, https://doi.org/10.1002/bit.260480506.

[49] J. Blank, K. Deb, Pymoo: multi-objective optimization in Python, IEEe Access. 8 (2020) 89497–89509, https://doi.org/10.1109/access.2020.2990567.

[50] T.C. Huuk, T. Briskot, T. Hahn, J. Hubbuch, A versatile noninvasive method for adsorber quantification in batch and column chromatography based on the ionic capacity, Biotechnol. Prog. 32 (2016) 666–677, https://doi.org/10.1002/btpr.2228.

[51] T. Ishihara, T. Kadoya, H. Yoshida, T. Tamada, S. Yamamoto, Rational methods for predicting human monoclonal antibodies retention in protein A affinity chromatography and cation exchange chromatography structure-based chromatography design for monoclonal antibodies, J. Chromatogr. A 1093 (2005) 126–138, https://doi.org/10.1016/j.chroma.2005.07.077.

[52] J.J. van Deemter, F.J. Zuiderweg, A. Klinkenberg, Longitudinal diffusion and resistance to mass transfer as causes of nonideality in chromatography, Chem. Eng. Sci. 5 (1956) 271–289, https://doi.org/10.1016/0009-2509(56)80003-1.

[53] G. Desmet, K. Broeckhoven, Extra-column band broadening effects in contemporary liquid chromatography: causes and solutions, TrAC Trends Anal. Chem. 119 (2019) 115619, https://doi.org/10.1016/j.trac.2019.115619.
[54] S. Yamamoto, T. Okada, M. Abe, N. Yoshimoto, Peak spreading in linear gradient elution chromatography with a thin monolithic disk, J. Chromatogr. A 1218 (2011) 2460–2466, https://doi.org/10.1016/j.chroma.2011.03.013.
[55] T. Fornstedt, G. Zhong, G. Guiochon, Peak tailing and slow mass transfer kinetics in nonlinear chromatography, J. Chromatogr. A 742 (1996) 55–68, https://doi.org/10.1016/0021-9673(96)00323-8.
[56] S.H. Altern, J.P. Welsh, J.Y. Lyall, A.J. Kocot, S. Burgess, V. Kumar, C. Williams, A. M. Lenhoff, S.M. Cramer, Isotherm model discrimination for multimodal chromatography using mechanistic models derived from high-throughput batch isotherm data, J. Chromatogr. A 1693 (2023) 463878, https://doi.org/10.1016/j.chroma.2023.463878.
[57] D. Xin, L. Kurien, K. Briggs, A. Schimek, R. Dambra, D. Hochdorfer, T.A. Arnouk, M. Brgles, S. Gautam, D. Hotter, J. Solzin, T. Kriehuber, J. Ashour, A. Vigil, M. Hawley, X. He, Characterization of VSV-GP morphology by CryoEM imaging and SEC-MALS, Mol. Ther. Methods Clin. Dev. (2025) 101429, https://doi.org/10.1016/j.omtm.2025.101429.
[58] M. de las M. Segura, A. Kamen, P. Trudel, A. Garnier, A novel purification strategy for retrovirus gene therapy vectors using heparin affinity chromatography, Biotechnol. Bioeng. 90 (2005) 391–404, https://doi.org/10.1002/bit.20301.
[59] D. Sviben, D. Forčić, T. Kurtović, B. Halassy, M. Brgles, Stability, biophysical properties and effect of ultracentrifugation and diafiltration on measles virus and mumps virus, Arch. Virol. 161 (2016) 1455–1467, https://doi.org/10.1007/s00705-016-2801-3.
[60] H. Koku, R.S. Maier, M.R. Schure, A.M. Lenhoff, Modeling of dispersion in a polymeric chromatographic monolith, J. Chromatogr. A 1237 (2012) 55–63, https://doi.org/10.1016/j.chroma.2012.03.005.
[61] H.F. Lodish, M. Porter, Heterogeneity of vesicular stomatitis virus particles: implications for virion assembly, J. Virol. 33 (1980) 52–58, https://doi.org/10.1128/jvi.33.1.52-58.1980.
[62] I. Mihelič, D. Nemec, A. Podgornik, T. Koloini, Pressure drop in CIM disk monolithic columns, J. Chromatogr. A 1065 (2005) 59–67, https://doi.org/10.1016/j.chroma.2004.10.054.
[63] A. Podgornik, M. Barut, A. Štrancar, D. Josić, T. Koloini, Construction of large-volume monolithic columns, Anal. Chem. 72 (2000) 5693–5699, https://doi.org/10.1021/ac000680o.

6 Discussion

6.1 A Comprehensive View on Viral Integrity in Virus Particle Bioprocessing

The inherent fragility of enveloped VPs, due to their labile lipid envelope, makes them susceptible to damage from various environmental factors and processing conditions. This fragility mandates the development of mild production processes with short processing times and minimal number of unit operations to ensure infectivity, safety, and efficacy of the final therapeutic product. The majority of conventional bioprocessing methods are unsuitable for VPs due to the fundamental differences to conventional protein-based biopharmaceuticals. New methods have been specifically developed for these large and labile particles. E.g., convective-driven approaches are often applied, being suitable for high flow rates and advantageous for low particle concentrations and high processing volumes. However, many methods have only recently found application in industry while others are novel or still in development. The review presented in chapter 3 delves into bioprocessing purification methods for enveloped VPs and provides guidance for researchers tasked with the process development of enveloped VP. A sequential evaluation of purification steps based on published study results (and patent descriptions) is performed, covering all bioprocessing steps, from cell culture to formulation and storage. Special focus is set on viral integrity which is required for effective and safe therapeutic application of replication-competent VPs. A general purification scheme is drawn, however it contains some variability showcasing the need for process adaptations depending on the virus strain processed. Different initial purification steps might be required, depending on cell culture parameters, such as cell disruption, nuclease treatment and viral release from cell debris. In further process steps various technical possibilities are available: filtration, centrifugation and chromatography. While centrifugation is only suitable for small scale productions, filtration and chromatography methods are generally scalable.

Experience and knowledge in bioprocessing accumulate over time through testing and application of methods which improves the bioprocess. However, for VP purification methods, generating knowledge is cumbersome due to the heterogeneity of applied virus strains resulting in different processing requirements and parameters. Hence, transferability of methods between strains is not always possible. E.g., perfusion cell cultures enable continuous or repeated harvesting strategies which shows increased productivity [1, 2], however not for all virus species [3, 4]. The IEP of VPs is not predictable, nonetheless it is generally negative and therefore AEX application is the first choice. While AEX works well for some strains [5, 6], other strains show a very strong surface charge leading to a non-recoverable binding of particles [7, 8].

In terms of chromatographic stationary phases, convective-driven media such as membrane adsorbers and monoliths show beneficial properties and outcomes compared to conventional purification technologies. Due to their convection-based approach, these methods offer high mass transfer rates and low back pressure, ideal for processing large particles exhibiting a low diffusive mobility and high volumetric feeds. The size of viruses, particularly enveloped VPs influences binding strength on the stationary phase depending on ligand and spacer design. Multipoint binding of particles increases binding strength of particles, making the process robust against salt concentrations, however can also negatively impact recoveries through irreversible binding [9]. Further, conformational changes are assumed to occur e.g. for lentiviruses, further strengthening irreversible binding to ligands [10]. Another effect of particle size is the entrapment of particles due to advection in constriction sites of monoliths [11]. This flow-rate dependent entrapment is influenced by monolith channel sizes. While smaller channels increase theoretical column capacity, it may also lead to convective entrapment and increased shear stress. Other stationary phases like monolith-like particles (MLPs), cryogels, and (nano-) fibers are being explored, aiming to combine the benefits of convective flow with other unique properties. RAM are specifically

designed for polishing in flow-through mode, effectively binding small impurities while allowing VPs to pass through due to steric differences.

The importance of maintaining viral integrity throughout the bioprocess is emphasized as key element to achieve a safe and functional therapeutical product. A relevant factor impeding viral integrity during bioprocessing is mechanical stress, typically encountered during agitation in bioreactors, (peristaltic) pumps of filtration systems, as well as sonication and centrifugation processes. The induced shear stress on particles can degrade whole particles or the envelope leading to loss of infectivity. Other integrity impeding factors are environmental conditions such as pH, elevated temperatures (e.g, in bioreactors), osmolarity and ionic strength (e.g., in high salt chromatographic conditions) and other physical stressors encountered e.g., during freeze thaw cycles (FT-cycles), vortexing and overcompaction in centrifugation. Besides particle degradation through these factors, the loss or degradation of virus glycoproteins can also occur, leading to inactivation.

A detailed understanding of the bioprocess impact on particle quality can often not be assessed due to analytical challenges. To gain the full analytical view of particle quality, a high laborious effort is required. Also, a high amount of samples needs to be analyzed to reach detailed process characterizations. This is typically not feasible due to low throughput of available methods. Analytical methods focus on specific particle properties, which can often not be correlated with the infectious property, the key quality attribute of interest. Flow virometry utilizing a multiplexing approach analyzing multiple properties at once, while being able of generating rapid results, holds the potential of a useful process development analytical method. However, specialized equipment and highly skilled personnel is required for its establishment. Process development necessitates fast and reliable analysis of sample attributes, such as particle count to facilitate mass balances. This enables yield calculations and same-day decisions required for rapid development iterations. It can support the identification particle losses in the process, e.g., due to non-specific interactions. Quantification methods such as quantitative polymerase chain reaction (qPCR) and tissue culture infectious dose 50 ($TCID_{50}$) are typically not suitable due to their high variability, sample preparation bias or slow turn over times. Analytical separation methods such SEC or field flow fractionation (FFF), coupled with online detector (e.g., UV, FLR or MALS) have proven to be applicable for fast mass balances. However, methods might not always be established for the VP of interest and transferability of methods is not straightforward. Methods must be sufficiently precise, of high and robust particle recovery for quantification by the online detector and validated for in-process controls (IPCs) differing in sample matrices. Such method was not available for VSV particles, hindering efficient process development. Also, advanced technological methods for process optimization such as mechanistic modeling could not be applied due to the lack of suitable process characterization methods. To address this analytical gap and enable the application of mechanistic models, a quantification method was developed, as discussed in the next section.

6.2 Advancing Analytical Quantification for Efficient Process Development

Optimized bioprocesses are essential for the economic production of high quality therapeutical biomolecules. Especially the purification process has a high impact on overall process yield and product quality. The absence of reliable and rapid analytical methods for quantification and VP characterization impedes efficient process development and optimization. Property variations between virus strains hinders quick method transferability, necessitating characterization and validation of analytical methods regardless if newly developed or transferred.

For quantification purposes of a specific analyte, the measurement principle must be either specific to the analyte of interest or the analyte must be separated prior to the measurement from potential interfering sample components. Specificity for viral particles is typically reached through distinct labeling techniques or visual single particle analysis such as EM. Even though EM provides pictures of countable particles, sample preparation might alter the particle concentrations and thus a known standard as comparison is added. This renders it to a relative quantification method [12, 13].

Labeling techniques include nucleic acid stains which require a membrane permeabilization step introducing additional dependencies such as incubation time and temperature, as well as the amount of permeabilization compound and staining dye [14]. In case of enveloped VPs, lipid dyes and antibodies which are targeting accessible surface antigens can be used for targeted labeling. Methods are often realized in a ELISA approach, however viral antigens can also be incorporated in cell debris impeding an accurate measurement [15]. Flow virometry employs a multiplexing staining approach on a single particle level and thus acquires additional information and theoretically enables detection of subpopulations [16]. However, specialized equipment and experienced operators are required. While labeling techniques might offer increased specificity, at the same time method complexity is increased through additional steps and longer sample preparation. Although automation approaches can help reduce required hands-on time, the complexity of labeling methods also increases the possibility for errors which needs be evaluated and validated.

The separation of the analyte from impeding impurities is generally the same task as for the preparative purification process, however with increased requirements regarding purity and recovery to establish a precise method. HPLC devices are ubiquitously available as an analytical method platform in biopharmaceutical laboratories and offer flexibility in the chromatographic separation principles applied and detectors used. While bind-and-elute chromatographic principles such as IEX offer specificity, the interaction with the stationary phase can result in lowered recoveries [14].

SEC operates on a straightforward size-based separation principle, but its applicability is limited for large VPs due the exclusion of large particles. The diffusional pores used for separation are generally inaccessible to large particles, resulting in a single eluting exclusion peak including all particles larger than the exclusion limit. Nevertheless, SEC is a gentle separation technique that allows for the characterization of intact particles using MALS following chromatographic separation [17]. High recovery rates are anticipated due to the absence of analyte-resin interactions, however secondary interactions must be minimized through buffer optimization [18]. The simplicity of SEC, along with its high recovery rates and potential for whole VP characterization, were relevant factors for the decision to use SEC as separation principle before quantification. Smaller impurities were successfully separated and no impeding particles were observed in the VP exclusion peak. During development, emphasis was placed on achieving high recoveries and ensuring sample stability, resulting in reliable quantification and enabling overnight measurements. Further validation confirmed its applicability to process samples from various matrices.

The modular HPLC approach enables the use of different detectors for particle quantification and characterization such as FLR, UV, RI, and MALS. RI and MALS detectors are both very sensitive detectors, however require knowledge of the specific refractive index increment for accurate quantification [19]. MALS theoretically allows for absolute quantification of particles, but obtaining refractive index increment values (dn/dc) particularly for enveloped VPs is challenging if not unfeasible with current methods. Nonetheless, the MALS detector has proven effective for particle detection during CIP steps in method development and particle characterization, e.g., for particle sizing.

Fluorescence is emitted by fluorophores as present in aromatic amino acids of proteins. Quantification application of FLR signal is shown for VPs [20], however fluorescence intensity depends on local environment of fluorophores [21]. Even though the influence of the local environment on fluorescence intensity in peptide is modest [22], it was decided against FLR for quantification due to the methods intended use for varying sample matrices and method robustness. UV-based quantification is widely applied for the qualification of nucleic acids [23] and peptides [24]. It is a straightforward method, demonstrating a linear correlation when properly calibrated, even for large VPs [25, 26, 27]. For calibration, an orthogonally quantified reference material is required. Non-linear light scattering interferences were not observed, potentially due to general low concentration ranges of VP suspensions.

Virus variants of different lengths showed a slight size separation of particles within the exclusion peak. Vajda et al. presumed the intra- and inter-particle volume would be relevant for size-based separation of influenza VPs, although the theory is not further detailed [17]. Xin et al. observed a separation of different VSV particle morphologies in an analytical SEC column and suggested a size and shape-based separation principle [28]. The exact origin of the slight size separation within the exclusion peak remained unclear.

In the characterization of the SEC exclusion peak, presence of viral proteins and absence of other proteins were verified through SDS-page. Also, the UV ratio of 260 nm to 280 nm remained constant over the whole peak, indicating a constant ratio of present nucleic acids to proteins. EVs are empty or nucleic-acid filled lipid vesicles of various sizes, generally overlapping with the VP size range. EVs are expressed by cells, especially by infected cells and are of concern as same-sized impurities potentially impacting quantification. However, with current technologies, the assessment of EV content in a VP sample is very difficult to impossible [29]. Thus, drawn conclusions regarding EVs content are pre-dominantly based on presumptions. A size and protein/nucleic-acid composition difference to the VSV particles is assumed, resulting in different signals from UV and MALS. However, the UV ratio remained constant throughout the peak suggesting an absence or non-relevant influence of same sized impurities such as EVs.

Greater particle sizes were measured by MALS in the beginning of the exclusion peak which might point to aggregated VSVs. In theory, larger particles scatter more light, resulting in an increased UV absorption. However, the UV peak area from detected potential aggregates was limited, and most samples were taken from filtered material. The influence on quantification by potential particle aggregates was regarded minimal. VPs were successfully separated from smaller impurities and no interfering components were detected in the virus containing exclusion peak. Method validation was conducted to ensure reliable performance utilizing an independent validation reference material as recommended in current guidelines [30]. Further, applicability to the intended range of process samples was validated using IPCs samples. The assessment of recovery efficiency showed already reliable results during buffer optimization and evaluation of column housing materials. The performance validation showed sufficient repeatability and reproducibility according to guidelines [31]. The comparison of quantification results to orthogonal measurements, however also relative, showed sufficient accuracies according to guidelines [31]. The absence of absolute quantification methods precludes a definitive assessment of accuracy.

The applicability to different batches and variants necessitates a new calibration curve for each variant, primarily due to size differences affecting scattering behavior and slight variations in retention time. Variations in surface proteins on the viral envelope, which can be features of virus variants, may require re-evaluation of particle recovery. However, incorporating arginine and dimethyl sulfoxide (DMSO) in the buffer matrix is expected to robustly suppress secondary interactions [32, 33].

The linear concentration range for quantification spans over 2.5 orders of magnitude, from 7.08×10^8 to 1.44×10^{11} $\frac{\text{VPs}}{\text{mL}}$. While at the upper linearity limit the accuracy was reduced, the lower concentration range showed low precision. As indicated in the HPLC based quantification method overview (Table 1.2 on page 10), the upper limits of approximately same sized VPs are within the same magnitude of 1×10^{11} $\frac{\text{VPs}}{\text{mL}}$. For smaller VPs, higher linearity limits are exhibited. Non-linearities exist for high analyte concentrations in UV [34] and in light scattering [35], both due to inter-particle interactions. Similar effects could impact the quantification of VPs at high concentrations, however non-linearities have not been addressed in similar studies. The maximum linearity threshold typically corresponds to the highest available concentration for characterized VP material. In the future, due to further optimized bioprocesses, higher particle titers might be reached for which UV absorption quantification might not be applicable anymore. However, sample dilution is a simple solution. At very low concentrations, performance quality criteria were not met when the LLOQ was calculated based on the signal-to-noise ratio. LLOQ had to be defined at 4.2×10^8 $\frac{\text{VPs}}{\text{mL}}$ which is still lower than the calibration range, thus denoting the start of the working range.

A quantification method was developed with sufficient throughput, reliability and robustness for application within process development. The at-line characterization is independent of co-eluting impurities which impede online detectors and thus enables process understanding related to VPs. The utilization of the HPLC device allows for automated analysis with low hands-on efforts. Analyte losses in the HPLC system, in specific in the sample containers and in the SEC column were addressed and sufficiently minimized to ensure high recoveries. The automated sample handling and validated robust recoveries enabled overnight measurements and sufficiently increased sample throughput to achieve detailed characterizations of fractionated processes. The information could thus being used to generate process knowledge and develop a mechanistic model as described in the next section.

6.3 Unravelling Purification Complexities through Mechanistic Modeling

The development of preparative purification processes for enveloped VPs is challenging due to their complex and labile structures and the novelty of purification methods while lacking analytical methods for process characterization. The previously described quantification method was utilized to characterize a CEX purification on a monolith for an enveloped VP. The goal was to establish a mechanistic model for process optimization, however an unexpected phenomenon occurred that highlighted the lack of process understanding. The effect leading to peak tailing and separation of subpopulation was identified as convective entrapment. Other causes were experimentally falsified or excluded by extensive discussion. For example, axial dispersion potentially leading to peak tailing was shown to be minimal for small monolithic columns [36] and dispersion effects of the system and column were assessed and considered. Convective entrapment was identified as phenomenon in monoliths influencing the elution of large particles such as enveloped VPs. For VSV particles, the effect was observed independent of virus batches, monolith scale and LC equipment. In order to understand the effect, it was characterized and described in a mechanistic model, however within limitations.

Mechanistic modeling approaches for VPs on IEX adsorbers have been explored in limited settings and mainly for process understanding. For non-enveloped rotaviruses VLPs, the SMA formalism was applied in 2008 by Vicente et al. This first proof-of-principle showed the successful application of SMA for large particles and was used to gain process knowledge for an AEX membrane process step [37]. Pamenter et al. developed a kinetic model for lentivirus particles, representing the time-dependent sorption behavior of these enveloped VPs on an AEX membrane. Observed conformational changes after sorption lead to irreversible binding which reduced recoveries [10]. In a study by Vicente et al. in 2011, the SMA formalism was employed to evaluate the elution conditions for baculovirus separation [9]. The study focused on the influence of ligand density on impurity reduction using AEX membranes. However, the model did not account for variations in spacer length, which affects the number of VP inaccessible ligands. Recently, a pore blocking extension for the SMA formalism was published which considers VP inaccessible ligands due to VP blocked pores [38]. In recent years, mechanistic models for non-enveloped VPs have been established also for process optimization such as full/empty particle separation in AAV purification processes. Both, the Langmuir isotherm and the SMA formalism have been used to evaluate the influence of process parameters such as salt concentration and pH to optimize full AAV product yield at specified purities [39, 40].

The mechanistic model presented in this thesis incorporates electrostatic interactions using the SMA formalism and accounts for convective entrapment through an additive Langmuir isotherm. It thereby describes both retention effects individually and was used to gain process knowledge. The span of application is limited due to the simplified system which does not consider relevant system parameters. E.g., the calibrated chromatography column is an axial flow column which shows low dispersion, but the geometry cannot be used at larger scales due to manufacturability limitations. Scale up columns utilize an inward radial flow which results in flow velocity variations. Radial flow column models have been applied which considered the flow rate increase in radial direction [41]. For the convective entrapment, the flow rate has a direct influence which is not accounted for in the presented model due to the applied constant flow in the axial column. The implementation of a radial column model would prerequisite the evaluation and representation of the flow rate parameter.

Further model limitations of the convective entrapment implementation include the particle size, fluid temperature and viscosity, all influencing diffusive mobility. Evaluating these factors and finding correlations to the entrapment phenomena could result in detailed models for the convective entrapment parameters k_{trap} and k_{release}, which are currently lumped parameters for the calibrated system. The Langmuir isotherm also assumes homogeneous constriction sites and single particle entrapment, neglecting structural parameters of the stationary phase geometry and varied pore geometries.

Within prevailing limitations the model reproduced retention effects occurring during elution in the monolith chromatography column and aided in process understanding. Through the identification and separated mechanistic description the individual effects could be better understood. The utilization of the Langmuir isotherm for the convective entrapment allowed for a description of the additional retention effect and peak tailing through entrapment. Combined with the SMA formalism, gradient elution runs were successfully

reproduced. It demonstrated the model's capability to investigate the effect in silico even when suitable analytical panels are not yet available.

Two distinct VP populations were identified, with fractions from the main peak and the tailing part of the elution peak demonstrating different elution behaviors upon re-application. Model simulations showed differences in entrapment behavior resulting in a subpopulation being responsible for the peak tailing, separating itself partially from the other subpopulation. A measurable difference in hydrodynamic diameter was observed between the two populations, with the main peak at 156 nm and the tailing at 170 nm. However, the biophysical correlate for this separation remains unclear. Practical implications for bioprocess development and analytical methods include evaluating recovery losses during preparative runs and adjusting CIP phases for low flow rates to enhance efficiency. The impact of flow rates should be considered especially in analytical applications. Additionally, the separation and analysis of particle subpopulations should be explored to identify their origins.

6.4 Conclusion and Outlook

The therapeutic application of replication-competent VPs is a cutting-edge area in modern medicine with high potential in cancer treatment. However, an obstacle to market readiness is the development of safe and cost-efficient bioprocesses for these therapeutic particles. Especially in the case of enveloped VPs, the manufacturability faces numerous challenges. These particles are highly sensitive if subjected to environmental and mechanical stressors such as pH, ionic strength, temperature, and shear forces. Their complex and non-rigid lipid envelope, derived from the host cell, makes them vulnerable to degradation, leading to a loss of infectivity and therapeutic effect. The particle variability and heterogeneity complicate purification, often necessitating virus-specific process development rather than universal platform approaches. Their inherent lability, complex structures and size necessitates meticulous control and deep understanding of all manufacturing stages, from initial cell culture harvest to final product formulation. Precise and rapid analytical methods are indispensable for assessing VP quality and integrity and thus evaluation of process performance to iteratively optimize processes. Conventional virology methods like $TCID_{50}$ and plaque assays are time-consuming and prone to variability, while PCR-based methods can overestimate total VPs due to non-incorporated genetic material. The development of HPLC-SEC-based quantification methods offers a label-free approach for total VP count with same-day results and low laborious effort. This method, which uses UV for quantification and a MALS detector for particle characterization, has proven robust across various sample matrices and significantly reduces hands-on time. It enables in-depth process characterizations and fast process iterations based on knowledge generated from same-day analytical results. Process understanding can be generated, ultimately achieving improvements in titer and quality of processed VPs. The facilitation of mass balances supports the development and application of advanced tools such as mechanistic modeling of chromatographic steps.

Chromatography is a cornerstone of VP purification, with IEX, HIC, and SEC commonly used. The choice of chromatographic modality and stationary phase is critical. Convective-driven stationary phases, such as monoliths and membrane adsorbers, are favored due to their low mass transfer resistances and thus suitability for processing large volumes at high flow rates. Despite these benefits, their application for enveloped VPs encompasses challenges. Multipoint binding of large VPs to chromatography ligands increase binding strength and process robustness, however can also lead to conformational changes and irreversible strong binding. Properties of grafted polymer layers have a direct influence on binding strength and thus impact recovery and infectivity, and also purity. Empirical studies suggest that the low ligand densities, e.g. due to a shallow polymer graft, yield the highest recovered infectious titers and help reduce co-purification of smaller impurities. Membrane adsorbers face additional challenges in device design and flow distribution, where the low bed height to frontal area ratio can lead to dispersion, local particle concentration, early breakthrough, and low resolution, with flow velocity heterogeneities also inducing shear stress. The intrinsic binding kinetics of some VPs might also become flow rate limiting, independent of the resin type. Monoliths exhibit heterogeneity of channel sizes, leading to flow variances and reduced resolution, while smaller channels, despite offering higher binding capacity, might induce increased shear stress. Another concern is the phenomenon of convective

entrapment so far only reported occurring in monolithic stationary phases. VP are temporarily retained in the resin's constriction sites due to advection. It is the current understanding of research that this occurs due to VPs being pushed into narrow constriction sites, with their release relying on chance of diffusional movement. This phenomenon depends on characteristic Peclet number of the system and leads to undesirable outcomes such as peak tailing, peak delay, and peak area reduction and the separation of subpopulations.

Faced with such complexities, mechanistic modeling has emerged as a tool to deepen understanding and potentially predict VP elution behavior. The developed model presented in this thesis extends the SMA formalism to include a Langmuir approximation for particle retention due to convective entrapment. The individual description of retention phenomena, separated from other system effects such as dispersion, enabled detailed process understanding. A key outcome of this study is the identification of two distinct VP populations with varying convective entrapment behaviors, accounting for the complex elution profiles observed. The differences in hydrodynamic diameter between fractions show the inherent heterogeneity of the VPs. Morphological variations or alterations introduced during upstream production or downstream processing, such as the timing of viral budding, significantly affect elution.

The characteristic Peclet number can be used for an estimation of entrapment impact, however also at low Peclet numbers entrapment has been observed. Assessment of recovery losses and flow rate influence should be conducted experimentally, in particular in analytical applications of monoliths in which the entrapment can skew results. CIP steps may be adjusted to lower flow rates or flow rate pauses included to enhance diffusional movement and release entrapped particles. Conversely, the demonstrated separation of VP populations due to differing entrapment behaviors may even be exploited for analytical purposes. However, the influence of additional process parameters, such as flow rate and viscosity, need to be evaluated. The utilization of standardized beads to explore the behavior of individual size categories might be useful, although typical bead materials such as polystyrene might exhibit secondary interactions with chromatographic resin material.

This PhD thesis addresses challenges in preparative and analytical methods of enveloped VP processing and consolidates research efforts to overcome them. Specific obstacles are associated with the size and fragile envelope structure of these VPs, which integrity is essential for maintaining infectivity and replication competency, both needed to ensure a safe and effective medicinal application. The overview of current process knowledge and analytical methods reveals impeding factors on viral integrity throughout the bioprocess and identifies an analytical gap hindering efficient process development. The development of a straight-forward, fast and robust quantification method addressed the gap and provides a tool for informed same-day process decisions as well as in-depth process characterizations. The latter is used to gain process knowledge of the CEX capture step for VSV which revealed the fluid dynamic CE effect leading to peak retention and tailing. Through mechanistic modeling the effect was better understood and the impact of the effect evaluated, however further model extension is required for model based optimizations. This thesis contributes through presented advancements to the overarching goal of producing replication-competent enveloped VPs at a high quality suitable for medicinal application.

References

[1] E. Petiot, D. Jacob, S. Lanthier, V. Lohr, S. Ansorge, and A. A. Kamen. "Metabolic and Kinetic Analyses of Influenza Production in Perfusion HEK293 Cell Culture". In: *BMC Biotechnology* 11.1 (2011), p. 84. DOI: 10.1186/1472-6750-11-84.

[2] S. Göbel, K. E. Jaén, M. Dorn, V. Neumeyer, I. Jordan, V. Sandig, U. Reichl, J. Altomonte, and Y. Genzel. "Process Intensification Strategies toward Cell Culture-based High-yield Production of a Fusogenic Oncolytic Virus". In: *Biotechnology and Bioengineering* 120.9 (2023), pp. 2639–2657. DOI: 10.1002/bit.28353.

[3] G. Gränicher, F. Tapia, I. Behrendt, I. Jordan, Y. Genzel, and U. Reichl. "Production of Modified Vaccinia Ankara Virus by Intensified Cell Cultures: A Comparison of Platform Technologies for Viral Vector Production". In: *Biotechnology Journal* 16.1 (2021), p. 2000024. DOI: 10.1002/biot.202000024.

[4] R. Habisch, P. Neubauer, J. Soza-Ried, and E. Puschmann. "Repeated Harvest Enables Efficient Production of VSV-GP". In: *Frontiers in Bioengineering and Biotechnology* 12 (2024), p. 1505338. DOI: 10.3389/fbioe.2024.1505338.

[5] T. Rogerson, G. Xi, A. Ampey, J. Borman, S. Jaroudi, D. Pappas, and T. Linke. "Purification of a Recombinant Oncolytic Virus from Clarified Cell Culture Media by Anion Exchange Monolith Chromatography". In: *ELECTROPHORESIS* 44.24 (2023), pp. 1923–1933. DOI: 10.1002/elps.202200270.

[6] M. Banjac, E. Roethl, F. Gelhart, P. Kramberger, B. L. Jarc, M. Jarc, A. Štrancar, T. Muster, and M. Peterka. "Purification of Vero Cell Derived Live Replication Deficient Influenza A and B Virus by Ion Exchange Monolith Chromatography". In: *Vaccine* 32.21 (2014), pp. 2487–2492. DOI: 10.1016/j.vaccine.2014.02.086.

[7] D. Sviben, D. Forcic, J. Ivancic-Jelecki, B. Halassy, and M. Brgles. "Recovery of Infective Virus Particles in Ion-Exchange and Hydrophobic Interaction Monolith Chromatography Is Influenced by Particle Charge and Total-to-Infective Particle Ratio". In: *Journal of Chromatography B* 1054 (2017), pp. 10–19. DOI: 10.1016/j.jchromb.2017.04.015.

[8] D. Eckhardt, H. Dieken, D. Loewe, T. A. Grein, D. Salzig, and P. Czermak. "Purification of Oncolytic Measles Virus by Cation-Exchange Chromatography Using Resin-Based Stationary Phases". In: *Separation Science and Technology* 57.6 (2022), pp. 886–896. DOI: 10.1080/01496395.2021.1955267.

[9] T. Vicente, R. Fáber, P. M. Alves, M. J. Carrondo, and J. P. Mota. "Impact of Ligand Density on the Optimization of Ion-exchange Membrane Chromatography for Viral Vector Purification". In: *Biotechnology and Bioengineering* 108.6 (2011), pp. 1347–1359. DOI: 10.1002/bit.23058.

[10] G. Pamenter, L. Davies, C. Knevelman, J. Miskin, K. Mitrophanous, D. Dikicioglu, and D. G. Bracewell. "Time-dependent Sorption Behavior of Lentiviral Vectors during Anion-exchange Chromatography". In: *Biotechnology and Bioengineering* 120.8 (2023), pp. 2269–2282. DOI: 10.1002/bit.28483.

[11] E. I. Trilisky and A. M. Lenhoff. "Flow-dependent Entrapment of Large Bioparticles in Porous Process Media". In: *Biotechnology and Bioengineering* 104.1 (2009), pp. 127–133. DOI: 10.1002/bit.22370.

[12] H. Malenovska. “Virus Quantitation by Transmission Electron Microscopy, TCID50, and the Role of Timing Virus Harvesting: A Case Study of Three Animal Viruses”. In: *Journal of Virological Methods* 191.2 (Aug. 2013), pp. 136–140. DOI: 10.1016/j.jviromet.2013.04.008.

[13] A. Parupudi, F. Gruia, S. A. Korman, S. Dragulin-Otto, K. Sra, R. L. Remmele, and J. S. Bee. “Biophysical Characterization of Influenza A Virions”. In: *Journal of Virological Methods* 247 (Sept. 1, 2017), pp. 91–98. DOI: 10.1016/j.jviromet.2017.06.002.

[14] J. Transfiguracion, J. A. Mena, M. G. Aucoin, and A. A. Kamen. “Development and Validation of a HPLC Method for the Quantification of Baculovirus Particles”. In: *Journal of Chromatography B* 879.1 (Jan. 1, 2011), pp. 61–68. DOI: 10.1016/j.jchromb.2010.11.011.

[15] K. Lothert, F. Eilts, and M. W. Wolff. “Quantification Methods for Viruses and Virus-like Particles Applied in Biopharmaceutical Production Processes”. In: *Expert Review of Vaccines* 21.8 (Aug. 3, 2022), pp. 1029–1044. DOI: 10.1080/14760584.2022.2072302.

[16] R. Lippé. “Flow Virometry: A Powerful Tool To Functionally Characterize Viruses”. In: *Journal of Virology* 92.3 (2018), e01765–17. DOI: 10.1128/jvi.01765-17.

[17] J. Vajda, D. Weber, D. Brekel, B. Hundt, and E. Müller. “Size Distribution Analysis of Influenza Virus Particles Using Size Exclusion Chromatography”. In: *Journal of Chromatography A* 1465 (Sept. 23, 2016), pp. 117–125. DOI: 10.1016/j.chroma.2016.08.056.

[18] P. Steppert, D. Burgstaller, M. Klausberger, A. Tover, E. Berger, and A. Jungbauer. “Quantification and Characterization of Virus-like Particles by Size-Exclusion Chromatography and Nanoparticle Tracking Analysis”. In: *Journal of Chromatography A* 1487 (Mar. 3, 2017), pp. 89–99. DOI: 10.1016/j.chroma.2016.12.085.

[19] W. C. Knol, B. W. J. Pirok, and R. A. H. Peters. “Detection Challenges in Quantitative Polymer Analysis by Liquid Chromatography”. In: *Journal of Separation Science* 44.1 (Jan. 2021), pp. 63–87. DOI: 10.1002/jssc.202000768.

[20] J. Transfiguracion, A. P. Manceur, E. Petiot, C. M. Thompson, and A. A. Kamen. “Particle Quantification of Influenza Viruses by High Performance Liquid Chromatography”. In: *Vaccine* 33.1 (Jan. 1, 2015), pp. 78–84. DOI: 10.1016/j.vaccine.2014.11.027.

[21] F. Sun, W. Zong, R. Liu, J. Chai, and Y. Liu. “Micro-Environmental Influences on the Fluorescence of Tryptophan”. In: *Spectrochimica Acta Part A: Molecular and Biomolecular Spectroscopy* 76.2 (July 1, 2010), pp. 142–145. DOI: 10.1016/j.saa.2010.03.002.

[22] J. D. Russell, R. T. Hilger, D. T. Ladror, M. A. Tervo, M. Scalf, M. R. Shortreed, J. J. Coon, and L. M. Smith. “Parallel Detection of Intrinsic Fluorescence from Peptides and Proteins for Quantification during Mass Spectrometric Analysis”. In: *Analytical Chemistry* 83.6 (Mar. 15, 2011), pp. 2187–2193. DOI: 10.1021/ac103023q.

[23] A. O. Nwokeoji, P. M. Kilby, D. E. Portwood, and M. J. Dickman. “Accurate Quantification of Nucleic Acids Using Hypochromicity Measurements in Conjunction with UV Spectrophotometry”. In: *Analytical Chemistry* 89.24 (Dec. 19, 2017), pp. 13567–13574. DOI: 10.1021/acs.analchem.7b04000.

[24] J. E. Noble and M. J. A. Bailey. “Chapter 8 Quantitation of Protein”. In: *Methods in Enzymology*. Ed. by R. R. Burgess and M. P. Deutscher. Vol. 463. Guide to Protein Purification, 2nd Edition. Academic Press, Jan. 1, 2009, pp. 73–95. DOI: 10.1016/S0076-6879(09)63008-1.

[25] P. S. Chahal, J. Transfiguracion, A. Bernier, R. Voyer, M. Coffey, and A. Kamen. "Validation of a High-Performance Liquid Chromatographic Assay for the Quantification of Reovirus Particles Type 3". In: *Journal of Pharmaceutical and Biomedical Analysis* 45.3 (Nov. 2007), pp. 417–421. DOI: 10.1016/j.jpba.2007.06.025.

[26] M. A. Spitteler, A. Romo, N. Magi, M.-G. Seo, S.-J. Yun, F. Barroumeres, E. G. Régulier, and R. Bellinzoni. "Validation of a High Performance Liquid Chromatography Method for Quantitation of Foot-and-Mouth Disease Virus Antigen in Vaccines and Vaccine Manufacturing". In: *Vaccine* 37.36 (Aug. 23, 2019), pp. 5288–5296. DOI: 10.1016/j.vaccine.2019.07.051.

[27] J. Transfiguracion, M. Y. Tran, S. Lanthier, S. Tremblay, N. Coulombe, M. Acchione, and A. A. Kamen. "Rapid In-Process Monitoring of Lentiviral Vector Particles by High-Performance Liquid Chromatography". In: *Molecular Therapy Methods & Clinical Development* 18 (Sept. 11, 2020), pp. 803–810. DOI: 10.1016/j.omtm.2020.08.005.

[28] D. Xin, L. Kurien, K. Briggs, A. Schimek, R. Dambra, D. Hochdorfer, T. A. Arnouk, M. Brgles, S. Gautam, D. Hotter, J. Solzin, T. Kriehuber, J. Ashour, A. Vigil, M. Hawley, and X. He. "Characterization of VSV-GP Morphology by CryoEM Imaging and SEC-MALS". In: *Molecular Therapy Methods & Clinical Development* 33.1 (2025), p. 101429. DOI: 10.1016/j.omtm.2025.101429.

[29] A. D. Minh and A. A. Kamen. "Critical Assessment of Purification and Analytical Technologies for Enveloped Viral Vector and Vaccine Processing and Their Current Limitations in Resolving Co-Expressed Extracellular Vesicles". In: *Vaccines* 9.8 (2021), p. 823. DOI: 10.3390/vaccines9080823.

[30] FDA. *M10 Bioanalytical Method Validation and Study Sample Analysis*. 2022.

[31] FDA. *Bioanalytical Method Validation Guidance for Industry*. 2018.

[32] T. Arakawa, K. Tsumoto, K. Nagase, and D. Ejima. "The Effects of Arginine on Protein Binding and Elution in Hydrophobic Interaction and Ion-Exchange Chromatography". In: *Protein Expression and Purification* 54.1 (July 2007), pp. 110–116. DOI: 10.1016/j.pep.2007.02.010.

[33] D. Cubrilovic and R. Zenobi. "Influence of Dimehylsulfoxide on Protein–Ligand Binding Affinities". In: *Analytical Chemistry* 85.5 (Mar. 2013), pp. 2724–2730. DOI: 10.1021/ac303197p.

[34] D. A. Skoog, D. M. West, F. J. Holler, and S. R. Crouch. "Introduction to Spectrochemical Methods". In: *Fundamentals of Analytical Chemistry*. 10th ed. Boston, MA: Cengage, 2022.

[35] M. Printz, D. S. Kalonia, and W. Friess. "Individual Second Virial Coefficient Determination of Monomer and Oligomers in Heat-Stressed Protein Samples Using Size-Exclusion Chromatography-Light Scattering". In: *Journal of Pharmaceutical Sciences* 101.1 (Jan. 1, 2012), pp. 363–372. DOI: 10.1002/jps.22749.

[36] R. Hahn, A. Tscheliessnig, P. Bauerhansl, and A. Jungbauer. "Dispersion Effects in Preparative Polymethacrylate Monoliths Operated in Radial-Flow Columns". In: *Journal of Biochemical and Biophysical Methods* 70.1 (2007), pp. 87–94. DOI: 10.1016/j.jbbm.2006.09.005.

[37] T. Vicente, M. F. Sousa, C. Peixoto, J. P. Mota, P. M. Alves, and M. J. Carrondo. "Anion-Exchange Membrane Chromatography for Purification of Rotavirus-like Particles". In: *Journal of Membrane Science* 311.1–2 (Mar. 2008), pp. 270–283. DOI: 10.1016/j.memsci.2007.12.021.

[38] H. Zhao, X. Lin, L. Wang, Y. Yang, H. Zhu, Z. Li, Z. Su, R. Yu, and S. Zhang. "Pore-Blocking Steric Mass-Action Model for Adsorption of Bioparticles". In: *Journal of Chromatography A* 1726 (July 2024), p. 464968. DOI: 10.1016/j.chroma.2024.464968.

[39] J. Gomis-Fons, B. Zee, D. Hurwit, J. Woo, J. Moscariello, and B. Nilsson. "Mechanistic Modeling of Empty-full Separation in Recombinant Adeno-associated Virus Production Using Anion-exchange Membrane Chromatography". In: *Biotechnology and Bioengineering* 121.2 (Feb. 2024), pp. 719–734. DOI: 10.1002/bit.28595.

[40] W. R. Keller, A. Picciano, K. Wilson, J. Xu, H. Khasa, and M. Wendeler. "Rational Downstream Development for Adeno-Associated Virus Full/Empty Capsid Separation – A Streamlined Methodology Based on High-Throughput Screening and Mechanistic Modeling". In: *Journal of Chromatography A* 1716 (Feb. 2024), p. 464632. DOI: 10.1016/j.chroma.2024.464632.

[41] C. Ladd Effio, T. Hahn, J. Seiler, S. A. Oelmeier, I. Asen, C. Silberer, L. Villain, and J. Hubbuch. "Modeling and Simulation of Anion-Exchange Membrane Chromatography for Purification of Sf9 Insect Cell-Derived Virus-like Particles". In: *Journal of Chromatography A* 1429 (Jan. 2016), pp. 142–154. DOI: 10.1016/j.chroma.2015.12.006.

7 Appendix A: Supplementary Material of Chapter 4

OMTM, Volume *32*

Supplemental information

An HPLC-SEC-based rapid quantification method for vesicular stomatitis virus particles to facilitate process development

Adrian Schimek, Judy K.M. Ng, Ioannes Basbas, Fabian Martin, Dongyue Xin, David Saleh, and Jürgen Hubbuch

Table S1: Buffer compositions for mobile phase optimization.

Buffer 1	50 mM Tris, 50 mM NaCl, 150 mM Arg, pH 7.5
Buffer 2	50 mM Tris, 100 mM NaCl, 150 mM Arg, pH 7.5
Buffer 3	50 mM Tris, 200 mM NaCl, 150 mM Arg, pH 7.5
Buffer 4	50 mM Tris, 300 mM NaCl, 150 mM Arg, pH 7.5
Buffer 5	50 mM Tris, 200 mM NaCl, 300 mM Arg, pH 7.5
Buffer 6	50 mM Tris, 200 mM NaCl, 300 mM Arg, pH 8.0
Buffer 7	50 mM Tris, 200 mM NaCl, 150 mM Arg, pH 8.0
Buffer 8	50 mM Tris, 50 mM NaCl, 50 mM Arg, 100 mM Citrate, pH 8.0
Buffer 9	25 mM Phosphate, 250 mM NaCl, 150 mM Arg, pH 8.0
Buffer 10	25 mM Phosphate, 250 mM NaCl, 300 mM Arg, pH 8.0
Buffer 11	50 mM Tris, 200 mM NaCl, 400 mM Arg, pH 7.5
Buffer 12	50 mM Tris, 250 mM NaCl, 300 mM Arg, pH 7.5
Buffer 13	50 mM Tris, 200 mM NaCl, 150 mM Arg, pH 8.0, 100 mM Sorbitol
Buffer 14	50 mM Tris, 200 mM NaCl, 150 mM Arg, pH 8.0, 100 mM Sucrose
Buffer 15	50 mM Tris, 200 mM NaCl, 150 mM Arg, pH 8.0, 1% DMSO
Buffer 16	50 mM Tris, 200 mM NaCl, 150 mM Arg, pH 8.0, 1% DMSO
Buffer 17	50 mM Tris, 200 mM NaCl, 1% DMSO, pH 8.0
Buffer 18	50 mM Tris, 250 mM NaCl, 1% DMSO, pH 8.0
Buffer 19	50 mM Tris, 200 mM NaCl, 0.1% DMSO, pH 8.0
Buffer 20	50 mM Tris, 200 mM NaCl, 150 mM Arg, pH 8.0
Buffer 21	50 mM Tris, 200 mM NaCl, 150 mM Arg, pH 8.0, 0.1% DMSO

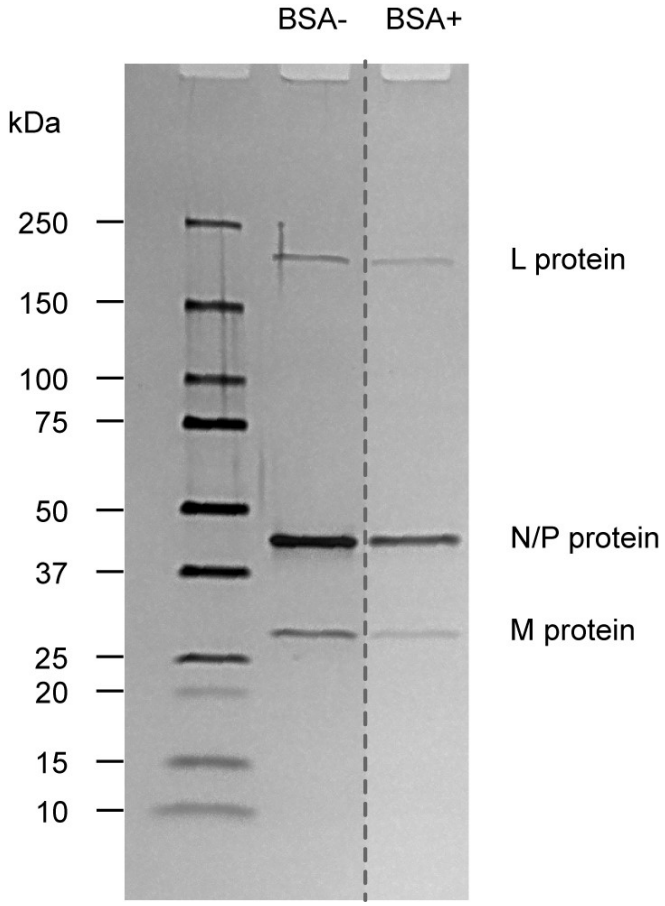

Figure S1: SDS-PAGE of the exclusion peak
BSA-spiked and non-spiked VSV-GP reference material was injected on the TSKgel G4000PW column and the exclusion peak collected. The peak was then applied on a SDS-PAGE gel and silver-stained for the identification of viral proteins. Irrelevant lanes were removed from the picture at the dashed line. L – large subunit of polymerase, N – nucleocapsid, P – phosphoprotein, M – matrix protein.

8 Appendix B: Supplementary Material of Chapter 5

Supplementary material

Mechanistic Modeling of the Elution Behavior and Convective Entrapment of Vesicular Stomatitis Virus on an Ion Exchange Chromatography Monolith

Adrian Schimek[a], Judy Ng[a,*], Federico Will[b], Jürgen Hubbuch[c,*]

a – ViraTherapeutics GmbH, Bundesstraße 27, 6063 Rum, Austria

b – Boehringer Ingelheim Pharma GmbH & Co.KG, Birkendorfer Str. 65, 88397 Biberach, Germany

c – Karlsruhe Institute of Technology, Institute of Process Engineering in Life Sciences, Section IV Biomolecular Separation Engineering, Fritz-Haber-Weg 2, 76131 Karlsruhe, Germany

*Corresponding authors.

J.N. (judy.ng@boehringer-ingelheim.com)

J.H. (juergen.hubbuch@kit.edu)

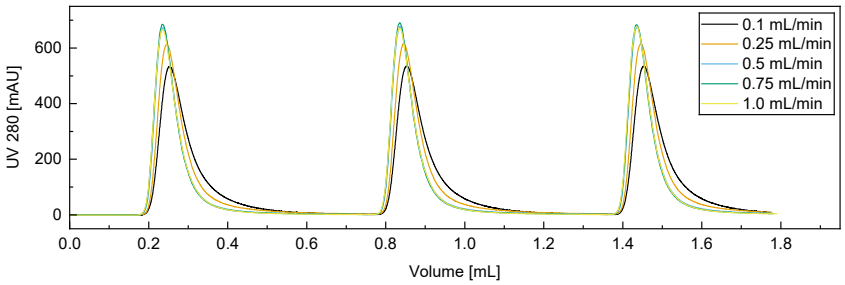

Figure S1: Dispersion analysis using acetone pulses
Acetone pulses (10 %) were injected to determine flow rate induced dispersion effects. Flow rates of 0.5 to 1.0 mL/min are overlapping.

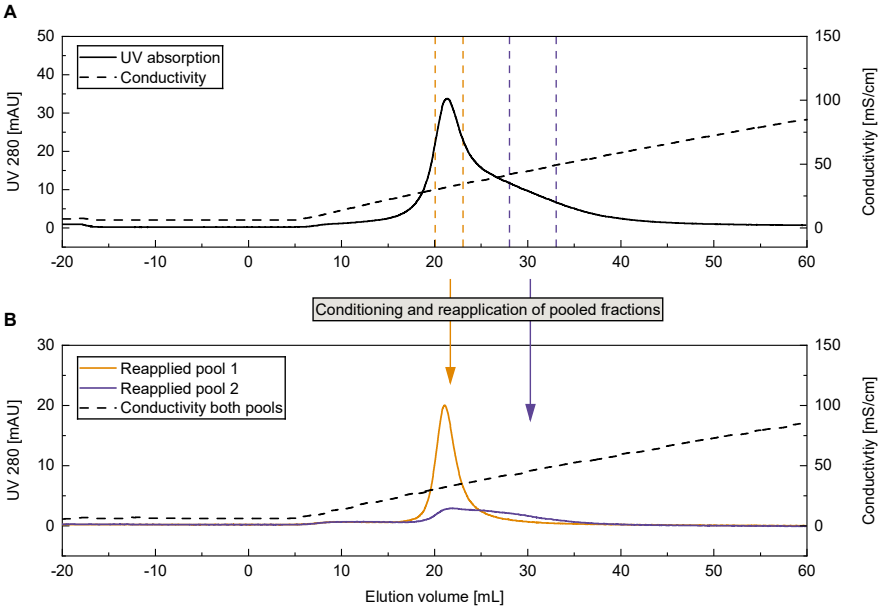

Figure S2: Fraction collection and reapplication on 1 mL column scale
A 1 mL (axial) CEX monolith column was used for repetition of fraction collection and reapplication. This run was conducted on an Äkta avant150 (cytiva, Munich, Germany) using a different virus batch. (A) Fraction collection. Marked peak regions were used to pool main and tailing fractions. (B) Reapplication of main and tailing pools column using the same bind and elute parameters as in A. NaCl concentrations of the pool loads were adjusted by dilution to meet sample loading conditions.

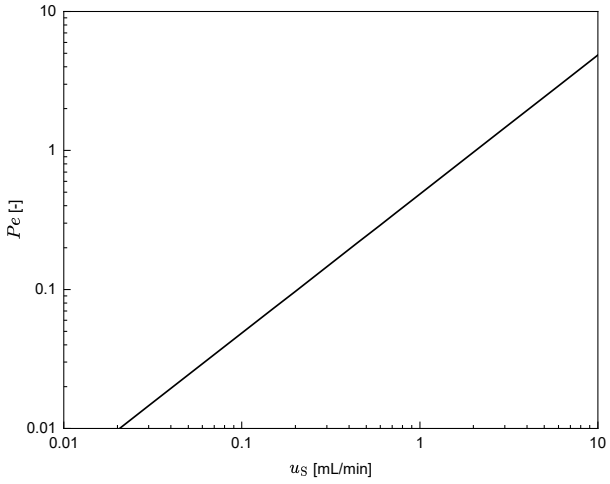

Figure S3: Estimated Peclet numbers.

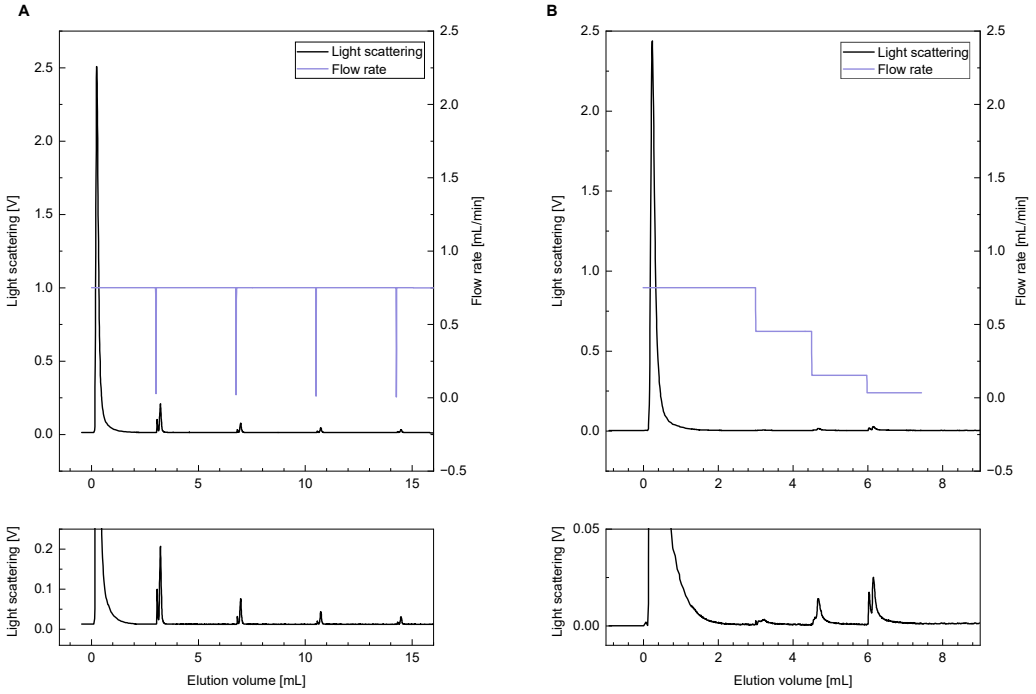

Figure S4: Non-binding flowthrough peaks indicate convective entrapment effect
Non-binding conditions were established using 950 mM NaCl in the running buffer. (A) Flowthrough peak and 5 min flow pauses; subsequent peaks after flow rate pauses sum up to 7.5 % peak area. (B) Flowthrough peak and stepwise flow rate reduction; subsequent peaks after flow rate reductions sum up to 2.5 % peak area. A detailed view of the y-axis is provided below corresponding graphs.

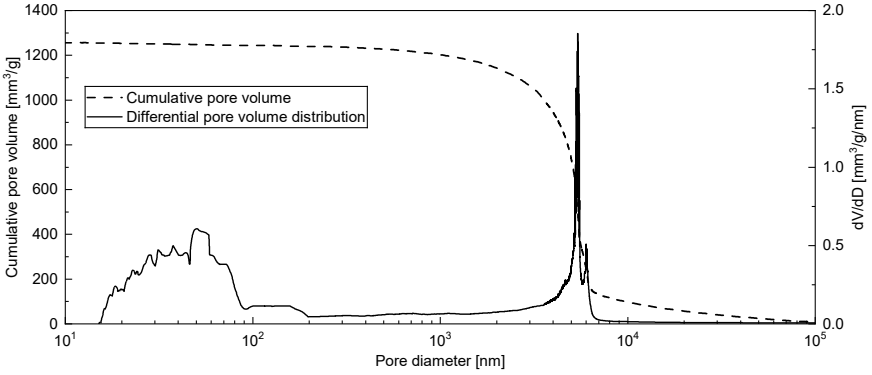

Figure S5: Monolith mercury porosimetry

The used 6 µm monolith resin was analyzed for pore sizes using monolith mercury porosimetry. The logarithmic x-axis was chosen for improved visualization of the size distribution over the whole size range. In this presentation, smaller pore diameters are overrepresented compared to larger pore sizes. The pore population between 10 and 100 nm is about 1 % of the total measured pore volume (up to 100 µm). For the differential pore volume distribution, a Savitzky-Golay filter of the order 1 and window size 30 was applied.